5-24-1991

High precision laser radar tracking device

V. P. Raghavan

HIGH PRECISION LASER RADAR TRACKING DEVICE

by

V. P. Raghavan

A Thesis Submitted
in
Partial Fulfillment
of the
Requirements for the Degree of

MASTER OF SCIENCE

in
Electrical Engineering

Approved by:

Dr. Roger E. Heinz - Thesis Advisor

Dr. Joe DeLorenzo

Robert E. Pearson

Dr. Paul E. Petersen - Dean of Engineering

DEPARTMENT OF ELECTRICAL ENGINEERING

COLLEGE OF ENGINEERING

ROCHESTER INSTITUTE OF TECHNOLOGY

ROCHESTER, NEW YORK

May 24th 1991

Dedicated with Reverence

to

the ***Rajarajeswari Peedam*** *of Rochester, New York*

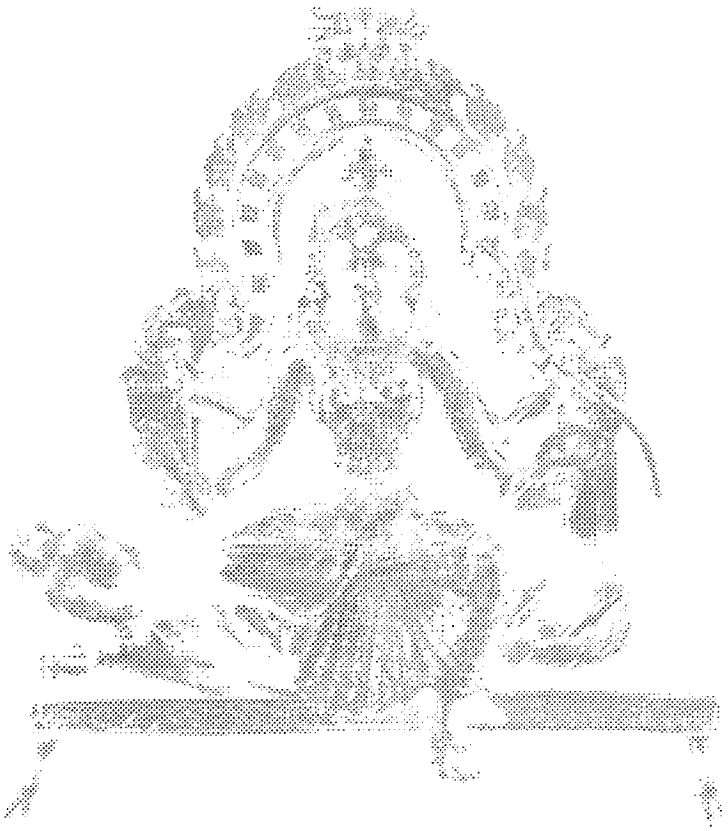

and

Rajan marma & Sakuntala marmi

Copy Protection

Preface

The purpose of this thesis was to design a process and fabricate a High Precision Laser Radar Tracking device. The device was perceived by Dr. Walter Kahn working for ANRO Engineering Consultants Inc., and was part of the Small Business Innovative Research program (SBIR). It was managed and funded by the Army Strategic Defense Command which represent SDIO, and thereby the Department of Defense. Fabrication of this device has been accomplished at the Rochester Institute of Technology, Microelectronic Engineering facility, and is presented here in partial fulfillment of the Master of Science degree.

Results of the theoretical analysis are presented here in order to give the reader an understanding of the mathematics involved. This section begins with the basics of Integrated Optics and leads to device operation. Also covered, is a brief on hetrodyne detection, which is needed at the output stage of the device.

Fabrication of this device covers all aspects of processing leading to Integrated Optics. Some of the processing is an adaptation of techniques used in the microelectronic industry, while other steps involve novel ideas specifically needed for Integrated Optics. Bulk of the thesis is on this section. Also presented, are some results of ion exchange simulations which were the subject of an independent study dedicated to the understanding of this process. As seen later, ion exchange results in the formation of integrated optic devices in glass substrates.

This project initially started in 1987 as phase 1, and investigated a Fiber Optic Multimode Feed for monopulse LIDAR, or light radar. The principal investigator as defined by SDI, was Dr. Gerald F. Ross, president of ANRO Engineering consultants. Theoretical analysis were performed by Dr. Kahn and Dr. DeLorenzo who are also attached to ANRO. Dr. Kahn is a faculty member at George Washington University and a fellow of IEEE. Dr. DeLorenzo, a faculty member of the RIT EE department, has been instrumental in obtaining device parameters via simulations and test vectors.

Phase 1 of this project, comprised of a feasibility study undertaken by ANRO and RIT. Robert Pearson, a faculty member of the RIT Microelectronic Engineering department, was involved with the processing aspect. Some devices were fabricated by Mr. Pearson using a melt process. However, due to the butt coupling scheme which requires a polished, microscopic chip free, surface edge and precision optics, these were not tested. During phase 2, some were cut back and polished, and found to function as waveguides. The ability to make wave guides, was the first objective of the second phase.

Phase 1, also tested a commercially available coupler which was made utilizing fiber optic technology. The tests were done by Dr. David A. Sumberg. Results of this tests and other aspects of phase 1, are presented in the final report document submitted by ANRO to SDI, on the 30th of September 1987.

Collaboration of ANRO and RIT, saw implementation of phase 2 of this project in June 1989. ANRO involvement was through Dr. Kahn, Dr. Ross and Dr. DeLorenzo. RIT was contracted to fabricate and demonstrate the High Precision Laser Radar Tracking device.

Research at RIT was headed by Dr. Roger E. Heintz. Prof. Heintz is a faculty member of the EE department, and is well known for his experimental abilities. The group headed by him comprises of three sections: fabricating, testing and polishing. The semi automated testing process involving precision optics and noise free electronics, was performed by graduate student, Gene Kulp. Pertinent results namely the V curve, is shown where appropriate. Some of the initial equipment characterization was also performed by another graduate student, Tim German.

The device has an input beam which is butt coupled into the front face. The individual guides have a depth of about 30um and a width of 50um, while the input Gaussian beam is 10 to 15um in diameter. This requires the front face to have a chip free edge. As the project was to discover, this stringent specification could not be met by commercial glass polishers. Therefore, this highly specialized process had to be developed in-house, and saw deployment of an undergraduate student, Steve Ciccarelli. Steve, also associated with the EE department, was successful in implementing a process that yielded the required edge with chips less than 1um. Some of the SEM photos show his work, and the importance of this edge.

Fabrication of this device involves processes commonly used in the microelectronic industry such as thin film deposition by evaporation, lithography, mask making, pattern transfer etc. Since device dimensions are in the micron range, a cleanroom facility was needed for most of the steps. The fabrication was accomplished by the author, a graduate of the BS Microelectronic Engineering curriculum at RIT, in class 100 and class 1000 clean room facilities which are part of the Microelectronic Engineering department.

SEM analysis of photos involving the polishing process, and Microprobe profiles giving gradient index profiles, were done at the New York Center for Imaging Science located at the University of Rochester, Institute of Optics.

Abstract

This thesis explores a relatively new Solid Silver Thin Film Source technology, for the implementation of a novel High Precision Laser Radar Tracking device. The process which consists of a Ag^{+}-Na^{+} ion exchange, is designed in two steps. It utilizes an initial electric field-aided ion exchange step for a predeposition, and a subsequent second diffusion step to force the profile latitude necessary for optimization of the device. While the entire project of implementing this device, consists of analyzing, processing, polishing and testing, this thesis covers only the process aspect in detail. The success achieved by obtaining the required Power Coupling Ratio curve on a Simple Coupler, demonstrates a novel integrated optic multimode feed for a Monopulse LIDAR application.

Acknowledgments

My sincere thanks are due to Prof. Heintz, Prof. DeLorenzo and the Dean of engineering, Dr. Peterson, who over the past two years have encouraged and supported this project in every way possible.

The following people have been a great help and encouragement with respect to the actual processing. I would like to thank Prof. Robert Pearson for his helpful insight, Dr. Lynn Fuller for the use of the cleanroom facility, and Gary and Scott without whose help the CVC would never have run. I would also like to thank Dr. Richard L. Lane, Mike Jackson, Bruce W. Smith, Dr. Santosh K. Kurinec and Dr. Turkman for their advise.

A special thanks is also due to Brian Macintire of the New York Center for Imaging Science, without whose help the Microprobe profiles could not have been obtained, and Marianna O'Brien of Apple Computer, Inc. whose computing expertise was invaluable.

After two years of research, it has to be said that many people in different departments at RIT, have contributed in some way or another, towards the successful completion of this project. Thanks to the Mechanical Engineering department, the Physics and Chemistry departments, and the American School of Craftsman. Special thanks go overseas to A. Thervonen from the Finish Institute of Research based in Finland.

Last, but not least, a big thank you to the Integrated Optics group, the Facilities Manager, Technicians and Secretaries of the EE department at RIT, and my friends who have helped in numerous ways. It has been a great pleasure, and a privilege, knowing and working with professionals like you.

Table of contents

		page
	Dedication	i
	Copyright	ii
	Preface	iii
	Abstract	vii
	Acknowledgments	viii
	Table of contents	x
	List of figures	xiii
	List of flow charts & flow diagrams	xiv
	List of tables & symbols	xv
Chapter I	**Introduction**	1
	A. Precision Tracking Radar	1
	1. Identification of the problem	1
	2. Solution methodology	2
	B. Analytical Technique	5
	1. Mathematical model	5
	2. Output detection	11
Chapter II	**Integrated Optics**	14
	A. A review	14
	B. Ion Exchange	17
	1. Process	17
	2. Ion exchange model	18
	3. Different ion exchange techniques	20
	4. Ag^+-Na^+ exchange	26
	5. Attenuation	28
	6. Characterization	29
Chapter III	**Fabrication Technology**	32
	A. Process selection	32
	1. Melt vs. Solid Silver Thin Film process	32
	2. Substrate choice	34
	3. Masking material	37

Table of contents

		page
	B. Basic ion exchange process	39
	1. Patterning of silver - without a diffusion mask	41
	2. Al mask for selective ion exchange	43
Chapter IV	**Device Process**	46
	A. Mask making	52
	1. Pattern generator program	52
	2. Mask processing	59
	B Substrate Identification	62
	C. Preprocessing	66
	D. Al mask evaporation	68
	E. Photoresist coating	71
	F. Pattern transfer	73
	1. Alignment and exposure	73
	2. Development	74
	3. Etching of the Al mask	75
	4. Stripping of photoresist	76
	G. Deposition of silver	77
	H. Predeposition	80
	I. Stripping of layers	87
	J. Polishing process	89
	K. Second diffusion	91
	L. Testing	96
Chapter V	**Discussion**	99
	A. Microprobe profiling	99
	B. Profile simulation	101
	C. Changes in process parameters	106
	D. Recommendations	112
	E. Conclusion	116

Table of contents

	page
References	117
Bibliography	121
Appendix	122
A1. Old coupler PCR test	123
A2. Simulated V curve	124
A3. Simulated V curve	125
A4. Phase 1 scan	126
A5. Phase 1 scan	127
A6. Phase 2 scan	128
A7. Balanced output configuration curve	129
B1. Manufacturer information on 0211	130
C1. Lot follower	135
C2. Source code of the Vax program	146
C3. Compound coupler design	153
C4. Al & Ag pallet data from MRC	154
C5. Silver thickness graph	156
C6. SEM photos of polished edges (drawings)	157
D1. Independent study	158

List of Figures

Figure	*page*
1. Coupler in a monopulse LIDAR feed	1
2. Index profile	5
3. Index profile of the coupler	10
4. Step index waveguide	15
5. (a) Melt process, (b) Solid Thin Film process	22
6. Field assisted ion exchange (Melt process)	23
7. Two schemes for Ag^+-Na^+ ion exchange	38
8. Photoresist removal schemes	42
9. Ion exchange profiles	47
10. S curve waveguides	52
11. S curve computation	53
12. Mask with different widths	54
13. Simpler coupler	55
14. Registration marks	60
15. Old method of identification	62
16. Cross section of the guide	63
17. New method of identification	64
18. CVC evaporator dimensions	68
19. Substrate alignment marks	70
20. KTI 820 data sheet	71
21. Hot plate diffusion	80
22. Unsuccessful diffusion apparatus	81
23. The VP clamp	82
24. Modified Heintz diffusion clamp	83
25. Diffusion power supply	84
26. Prediffusion program	85
27. Current during ramp up	86
28. Thermal ion exchange	92
29. Sample profiles	93
30. Second diffusion programs	94

List of Figures

Figure	*page*
31. Simplified power detection scheme	96
32. 90 minute second diffusion	97
33. 60 minute second diffusion	98
34. Prediffusion peak concentration	102
35. Peak concentration	103
36. Contour profiles	104
37. Prediffusion vs. Second diffusion	105
38. Dark band (drawing of the SEM photo)	106
39. Asymmetric guide (drawing of the SEM photo)	107
40. Bubbles (drawing of the SEM photo)	108
41. Simulated current flow	110
42. Actual current flow	111
43. Flat bottom V curve	112
44. Profile merger	113
45. PCR sensitivity	115

List of flow charts

Flow chart	
1. Process flow for the melt source	43
2. Solid source process	44
3. Process flow	49
4. Polishing process	90

List of flow diagrams

Flow diagram	*page*
1. Silver patterning process	39
2. Al masking process	40

List of tables

Table	
1. Comparison of M^+ ion properties	26
2. Diffusion coefficients & activation energies	27
3. Substrate properties	34

List of symbols

x	displacement from bore sight
N_0	peak waveguide index
N_s	substrate index
X	axis
Y	axis
Z	axis
X_c	center of guide
X_1	half width of guide
∇	laplacian

List of symbols

ko	free space wave number
$\psi(x,z)$	wave function
$\frac{\partial^2\psi(x,z)}{\partial z^2}$	second derivative with respect to z
U_{xx}	second derivative with respect to x
n!	orthornormal polynomial
ICE	integrated circuit design tool
SPLIT	program
CVC	evaporator
MRC	Materials Research Corporation
RPM	revolutions per minute
SEM	Scanning Electron Microscope
WKB	index profiling technique
EDS	Energy Dispersive Spectrometry
IC	integrated circuit
V_T	threshold voltage
torr	pressure unit
erfc	complimentary error function
PCR	Power Coupling Ratio
P_{CF}	Power output of the coupled guide
Σ	sum channel
Δ	difference channel
T	pulse width
η_c	index of air
η_f	index of guide
η_s	index of glass
θ_c	critical angle

List of symbols

Cr	chromium
Al	aluminum
Ag	silver
Ag^+	silver ion
Na^+	sodium ion
Li^+	lithium ion
Tl^+	thulium ion
Cs^+	cesium ion
Fe^+	ferrous ion
e^-	electron
Ld_{50}	dosage lethal to 50% of the animals tested
CN	coordination number of the ion
mg	milligram
kg	kilogram
nm	nanometer
um	micrometer
cm	centimeter
O_2	oxygen
UV	ultra violet
A	angstrom
kA	kiloanstrums
dB/cm	decibels per centimeter

Chapter I

Introduction

A. Precision Tracking Radar

1. Identification of the problem

Precision as defined in terms of angular tracking, is the ability to detect small changes in the target which translate to fractions of a beam width in angle. Normally a target acquired at distances of 1000km, would require a shift of a hundredth of a beamwidth.[1,2] This would require optics with apertures of the order of meters. Undoubtedly, such large aperture high cost systems, will find dedicated use and be deployed in tracking. However, this fine resolution can also be obtained with aperture optics of only a few centimeters when utilized in monopulse radar.[3] The reduction in size, and at least two orders of magnitude reduction in cost, makes this device very attractive. Although not useful for acquisition purposes, this resolution is needed for aiming kinetic energy weapons.

Monopulse microwave radar trackers are currently being used in multiple target tracking and discrimination applications. Present LIDAR or light wave radar, is limited to a four sectoral tracker head system. These tracker heads use a local oscillator beam from one driver to obtain coherent hetrodyne detection. Mechanical dimensions limit the precision of these systems.

Target characteristics and the difficulty of obtaining identical performance from the four detector heads, points to a major error in the system. At microwave frequencies, these errors are controlled by using passive circuitry to separate the sum and difference signals before hetrodyne detection.

Current experimental systems utilize hetrodyne detection as it takes place on the quadrant surface. In conventional systems, it is performed after the formation of the sum and difference signals. Detailed analysis of these schemes is given in Reference 4.

2. Solution methodology

The monopulse radar device proposed here, has the required fine angular accuracy, the advantage of passive circuitry and gains the size reduction resulting from the use of the optical region of the spectrum. The sum and difference signals are obtained by a feed configuration employing a waveguide. This, is a multimode waveguide diffused into a glass substrate, and is termed the driven guide. Another guide known as the coupled guide, similar to the driven guide, is also fused into the substrate in close proximity to the first. The lens - antenna system used for focusing the input beam remains conventional. This configuration is shown in figure 1.

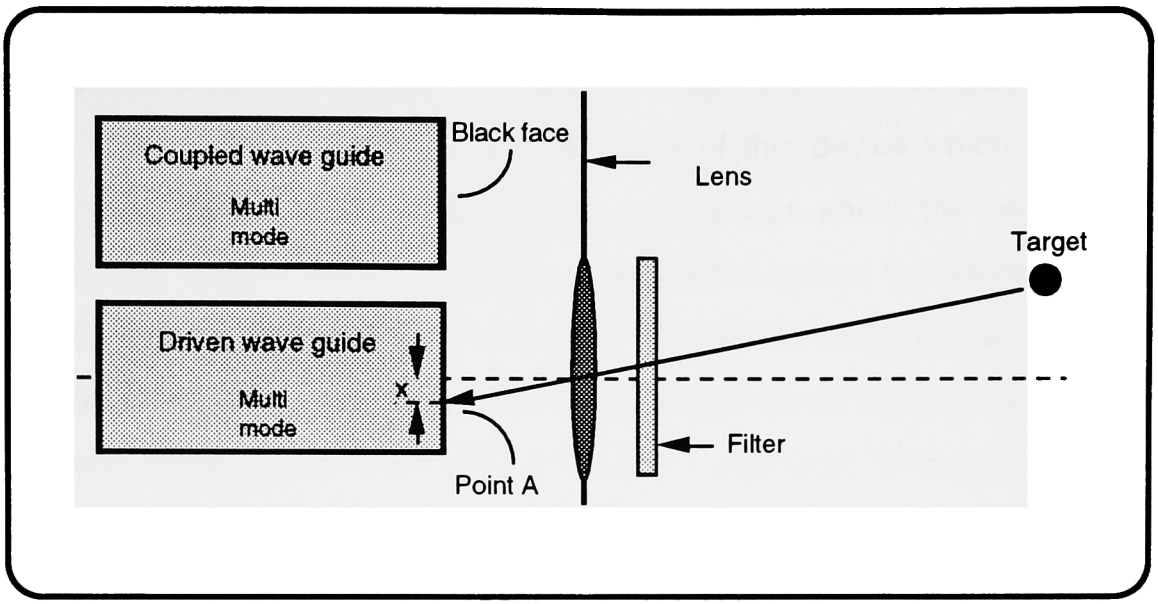

Figure 1: Coupler in a monopulse LIDAR feed

The multi mode guides act as mode filters separating out into the coupled guide, the higher mode content of the driven guide. The lower order modes propagate down the driven guide with little or no coupling into the coupled guide. Higher order modes are excited by larger x values. The converse also holds. This direct function of deviation corresponding to displacement of point A, furnishes the monopulse sum and difference signals as outputs from the guides.

During phase 1, a commercially available fiber optic coupler was used to confirm these expectations. Appendix A1, shows the results of these tests which are theoretically in the form of a V curve. The results show that multimode gradient index couplers partially exhibit the required phenomenon.

Commercially available couplers which are used in the telecommunication industry, are specifically designed for non selective coupling of all modes. This defeats the very purpose of this device which is highly dependent on selective mode coupling, and brings about the need for a specialized coupler.This coupler is also designed to reduce the effects of fiber defects and the residual effects, in order to improve the quality of the minimum. The quality of the minimum translates to a near zero power value for zero target deviation (drives the minimum point of the V to a near zero). Steep side walls of the V are also highly desirable. This would lead to greater shift in power for a small variation in input position x, or greater sensitivity of the device.

The success of this research would demonstrate an important new application, for multimode graded index couplers in monopulse LIDAR. As stated, the main attraction would be its inexpensive manufacturing capability, while still yielding high precision tracking.[4]

B. Analytical Technique

During phase 1, an analytical model was developed to simulate the coupler slab fiber performance. This section briefly describes this analysis as given in the phase 1 final report.[4]

1. Mathematical model

The slab fiber is a rectangular region formed in an optically transparent substrate, about 1.5 inches in length and 50um in width. The peak index of refraction within it has to be greater than that of the substrate, for this channel to act as a waveguide. The index of refraction, has a maximum value at the center and tapers to the substrate index at the boundary, and is uniform along its length and depth. Figure 2, shows this profile.

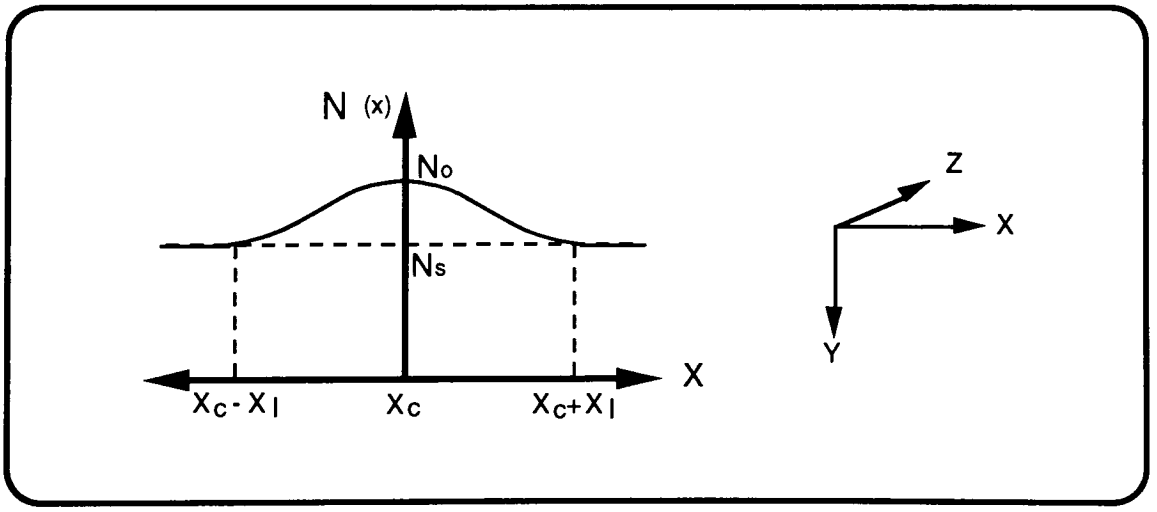

Figure 2: Index profile

The profile shown in figure 2, is independent of depth, y, and length, z. The z independence is physically accurate. However, the actual wave guide does have a depth profile, dependent on y. The y invariance is justified by noting that the energy propagation is in the z direction, and the salient properties of the coupler are due to the transverse index variation. This, greatly reduces the complexity involved in the analysis.

The y component of the electric field in the guide has to satisfy the time reduced wave equation

$$\nabla^2 E_y + k_o^2 N^2(x) E_y = 0 \qquad \text{.....(1)}$$

where k_o is the free space wave number and e^{-jwt}, is the assumed time dependence. With negligible reflections at the end of the guide, the field Ey is given by

$$E_y = \psi(x,z)\, e^{jN_o k_o z} \qquad \text{.....(2)}$$

where $\psi(x,z)$, is the wave function and e^{jkz}, denotes propagation in the positive z direction.

Substitution of (2) into (1), with

$$\frac{\partial^2 \psi(x,z)}{\partial z^2} \approx 0 \qquad \text{and} \qquad \left|\widehat{N}(x)\right|^2 \approx 0$$

gives the equation:

$$j\frac{1}{k_o}\frac{\partial\psi(x,z)}{\partial z} = -\frac{1}{2k_o^2 N_o}\frac{\partial^2\psi(x,z)}{\partial x^2} + N_o\,\widehat{N}(x)\,\psi(x,z) \qquad \text{.....(3)}$$

The function $\psi(x,z)$ provides solutions to equation (3), and the information required to predict coupler performance. Equation (3), represents a single fiber profile. This is formally identical to the harmonic oscillator equation of quantum mechanics which is given below:

$$j\,h\frac{\partial\psi}{\partial t} = -\frac{h^2}{2m}\frac{\partial^2\psi}{\partial x^2} + \frac{1}{2}kx^2\,\psi \qquad \text{.....(4)}$$

The solution given by Shiff[5] for equation (4), is

$$\psi(x,t) = \sum_{n=0}^{\infty} An\,Un(x)\,e^{-jEn\,t/h} \qquad \text{.....(5)}$$

or

$$\psi(x,t) = e^{-(j\omega_c t)/2}\sum_{n=0}^{\infty} An\,Un(x)\,e^{-jn\omega_c t} \qquad \text{.....(6)}$$

where Un(x), are solutions to the equation:

$$-\left(h^2/2m\right)U_{xx} + \frac{1}{2}kx^2U = EU \qquad \text{.....(7)}$$

Using perturbation analysis, the harmonic oscillator problem is used to obtain solutions to other problems. If a square law index profile is assumed, this technique can also be used for the waveguide.

The square law index profile is given by:

$$\widehat{N}(x) = \eta x^2 \qquad \text{.....(8)}$$

Using this, the solutions are obtained as

$$\Psi(x,z) = e^{-j(1/2\lambda_c)} \sum_{n=0}^{\infty} A_n U_n(x) e^{-j(nz/\lambda_c)} \qquad \text{.....(9)}$$

with

$$U_n(x) = N_n H_n(\alpha x) e^{-(\alpha^2 x^2)/2} \qquad \text{.....(10)}$$

where

$$\alpha = \frac{N_0}{\lambda_0 \lambda_c} \quad ; \quad N_n = \frac{\sqrt{\alpha}}{(\sqrt{\pi}\, 2^n\, n!)^{1/2}}$$

Changing variables to

$$\xi = \alpha x \quad \text{and} \quad \zeta = z / \lambda_c$$

gives:

$$H_n(\alpha x) = H_n(\xi) = (-1)^n e^{\xi^2} \frac{\partial^n}{\partial \xi^n}\left(e^{-\xi^2}\right) \qquad \text{.....(11)}$$

If we let

$$\phi_n(\xi) = \frac{H_n(\xi) e^{-\xi^2/2}}{(\sqrt{\pi}\, 2^n\, n!)^{1/2}}$$

the solution (equation 9), is in the form:

$$\Psi(\xi,\zeta) = e^{-j(\zeta/2)} \sum_{n=0}^{\infty} A_n \phi_n(\xi) e^{-jn\zeta} \qquad \text{.....(12)}$$

or

$$\Psi(\xi,\zeta) = e^{-j(\zeta/2)} \sum_{n=0}^{\infty} \zeta_n(\xi)\, \phi_n(\xi) \qquad \text{.....(13)}$$

where

$$A_n = \int_{-\infty}^{\infty} \Psi(\xi,0)\, \phi_n^*(\xi)\, d\xi$$

and

$$\zeta_n(\zeta) = A_n\, e^{-jn\zeta}$$

The orthogonal expansion for

$$\psi(\xi,\zeta)$$

allows computation of the wave function at all locations down the guide provided the input illuminating beam profile,

$$\psi(\xi,0)$$

is known at z=0.

By introducing an index profile that consists of a pair of adjacent parabolic shapes (that may overlap), the solution is extended to the coupler.

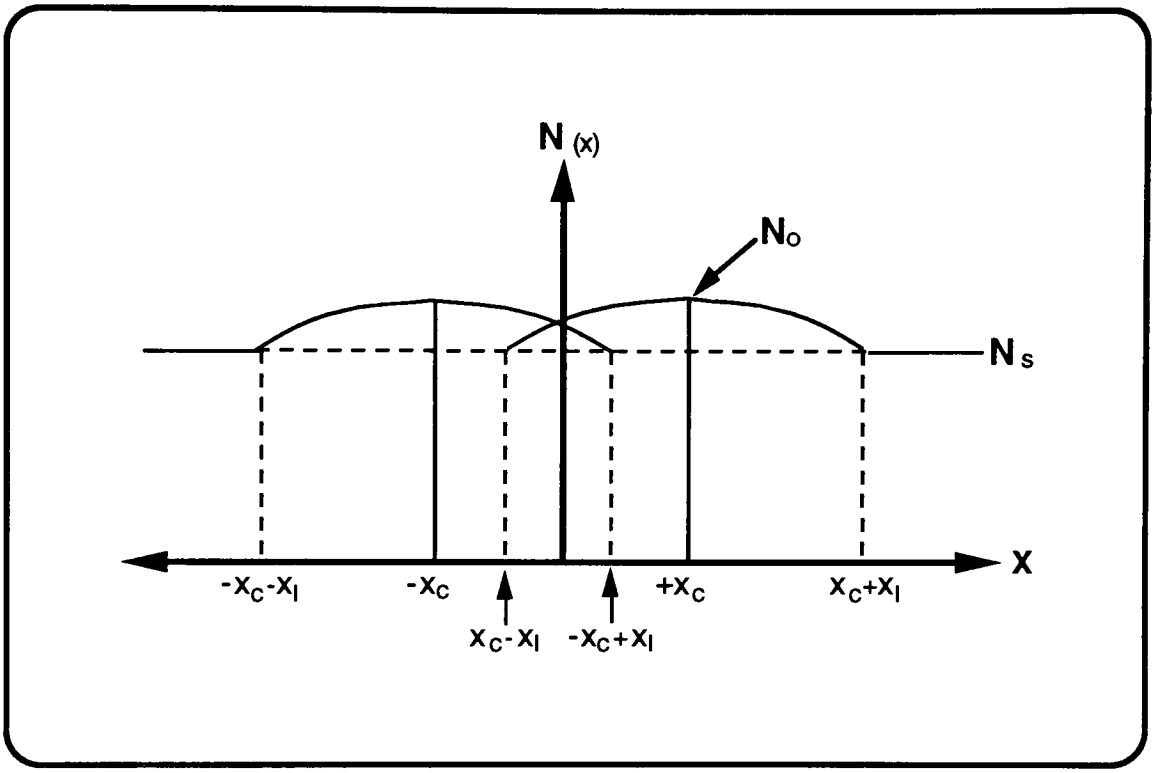

Figure 3: Index profile of the coupler

The analysis beyond this point gets extremely complicated, and solutions are obtained via matrix manipulations. Interested readers are again referred to reference 4 which carries the complete solutions. One of the key elements of these computations is the Power Coupling Ratio, and is defined as follows:

$$PCR = \sqrt{\frac{P_{CF}}{\text{Total power}}}$$

where P_{CF}, is the power output of the coupled guide, while the total power is the sum of the driven and coupled guide outputs.

The PCR provides the amplitude information necessary for tracking. Some of the computer simulations are given in Appendix A1 through A3. The pair of guides is fully described by the three parameters, x_c - half the center to center spacing, N_x - peak fractional increase in the index of refraction over the index of the substrate N, and z - the coupling length.

Experimental verification of the device feasibility was obtained by performing a scan across the polished face of the driven guide. The PCR curves thus obtained are given in Appendix A4-A6. A4 and A5 were scans obtained during phase 1. A6 was obtained during the beginning of phase 2. Even though an optimized spot was not used during the manual scan process, the data clearly shows the desired effect for the monopulse feed system.

It should be noted that while the position information is obtained via the amplitude plots, some other scheme is required to produce the sense information. This information containing left or right of bore sight, is obtained by analyzing the phase changes taking place at the outputs as the input varies. The phase analysis leads to coherent detection or homodyne detection.

2. Output detection

When comparing microwave radar to LIDAR, the difference and sum signals in the former, are found to be equivalent to the coupled and driven guide outputs of the latter. In the LIDAR case the input signal is coherent. This produces output signals related in phase and can be assumed if the amplitude and phase ratios are preserved in the channels.

As the target crosses bore sight from left to right, the coupled guide phase angle flips 180°. This shift, can be detected by an interference pattern between a stable reference and the coupled guide output. A pattern reversal would indicate the input beam crossing the center.

The detection of output optical signals is usually performed with Avalanche Photo Diodes or PIN diodes. APDs are inherently high gain detectors producing high noise levels which are undesirable for the application at hand. The PIN diodes produce one electron for every photon and thereby are low noise, low gain detectors. However, the low noise factor of the PIN diode is usually offset by noise generating post detection electronic amplifier circuits.

This is eliminated by using PIN diodes with a strong local oscillator signals in a homodyne scheme. The configuration provides near optimum detection performance. The coupled guide output is given by either

$$|\Delta| \cos(\omega_o t) \quad \text{or} \quad -|\Delta| \cos(\omega_o t)$$

The driven guide output is large, and therefore taken to be the strong local oscillator signal. It is given by:

$$|\Sigma| \cos(\omega_o t)$$

The addition of these signals on the face of the PIN diodes, produce a voltage proportional to:

$$(|\Sigma| + |\Delta|)^2 T \quad \text{or} \quad (|\Sigma| - |\Delta|)^2 T$$

where T is the pulse width. The large sum signal when compared to the noise introduced by the post detection electronic circuits, provides a large signal to noise ratio. The detection problem of a small difference signal riding on the large sum signal, is avoided by using two PIN diodes in a balance output configuration. One diode detects the addition of the sum and difference channels, while the other detects the difference. The outputs of the two diodes are subtracted, producing a voltage proportional to:

$$+2\,|\Sigma|\,|\Delta|\,T \quad \text{or} \quad -2\,|\Sigma|\,|\Delta|\,T$$

It is seen that the error probability decreases as the amplitude of the sum signal increases.

As shown in Appendix A7, the $+2\,|\Sigma|\,|\Delta|\,T$ term provides one half of the V curve, while the $-2\,|\Sigma|\,|\Delta|\,T$ term provides the horizontally flipped second half. It is believed that this curve alone will provide both, the amplitude information gathered from the V curve, and the sense information obtained from the shifting interference pattern.

Chapter II

Integrated Optics

This section begins with a literature search which covers Integrated Optics from a historical perspective. It covers the need, requirements and different processes applicable to the technology, and is designed to bring the reader up to date.

A. A review

From a historical perspective the basic design of optical systems did not change for many years. Such systems consisted of bulky, heavy components mounted on an air table, and required careful alignment and protection against vibration, moisture and temperature drift. The concept of integration of these optical components was motivated during the early 1970's, by a desire to minimize these problems and make it more compatible with advancing technology.

Integrated optics is basically guided wave optics, where light is constrained within the guide by total internal reflection while propagating in discreet modes. Problems such as atmospheric conditions associated with light transmission through air, are thereby eliminated. Many textbooks and papers carry indepth theoretical analysis of light wave propagation in wave guides.[1-8] Basics of the theory is given here.

Figure 4, shows a step index wave guide.

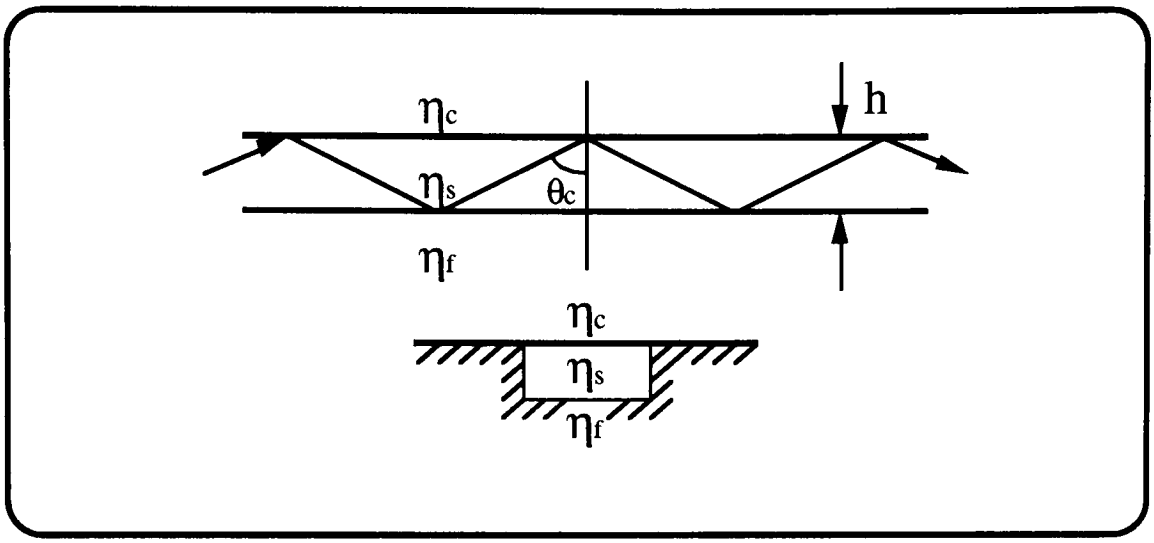

Figure 4: Step index waveguide

Conditions required for the ray to propagate within the guide are as follows:

$$\eta_f \supset \eta_s , \eta_c$$

$$\sin \theta_c = \eta_s / \eta_f$$

The condition for this ray to be the lowest order mode depends on wave length lambda, and is given by:

$$h \approx \lambda / \left(2 \sqrt{\eta_f^2 - \eta_s^2}\right)$$

where, h is the height of the guides.

If h is allowed to increase, other discreet modes can also propagate. While the guide described above has a step index profile, the tracking devise has waveguides which have Gaussian profiles. The theory of operation varies very little between the two, and as before, the key concept is the increase in index of refraction between the guide and substrate.

Another important concept with regard to the coupler, is the evanescent field which extends outside the boundaries of the guide. It is this phenomenon which allows coupling to occur. Using this, the index profile and the number of allowable modes in a given waveguide can also be calculated.[9,10]

B. Ion Exchange

1. Process

As mentioned above, the selective increase in the index of a substrate forms a waveguide. This section describes the basic ion exchange process and some of the techniques used to achieve this.

The possibility of changing the optical properties in the surface combined with low attenuation in the working wavelength, makes glass the substrate of choice. Furthermore, it has low thermal expansion and high mechanical strength. Dielectric crystals and semi conductors have also been investigated for this purpose. However, low process cost and simplicity, favor glass and the ion exchange process.

The glass substrates used, consist of a mixture of SiO_2 and metal oxides such as Li_2O, Na_2O, Al_2O_3 and K_2O. The refractive index of glass is related to the density and electronic polarizability of constituent ions. The electric field component of light, as it is propagating through the glass, interacts with its polarizable species and causes displacement of the electronic charge with respect to the nuclei. This creates a dipole which lowers the phase velocity of light, and hence gives rise to an increase in the index of refraction of glass.

The diffusion of externally introduced monovalent ions such as Ag^+, Tl^+ and K^+ into the glass, replaces and exchanges with ions such as Na^+ and Li^+. Ions with higher valency are closely linked to the glass network, and therefore have very low diffusion coefficients. Hence they do not partake in the exchange process.[11]

2. Ion exchange model

The increase in substrate index is caused by two factors:[12]

a) Difference in the ionic polarizability.

b) Change in molar volume of the glass caused by the difference in ionic radii.

A simple model predicts the value of the change in index, and is given by:

$$\Delta n = \frac{X}{V_0}\left(\Delta R - R_0 \frac{\Delta V}{V_0}\right)$$

where X is the fraction of cations replaced by the incoming ion, V_o is the volume per mole of oxygen atoms, R_o is the refraction per mole of oxygen atoms and delta R and delta V are the changes in these quantities as a result of cation exchange. The first term in the equation represents the difference in ionic polarizability, while the last term is the result of the difference of ionic radii.

Consider the following cases:

Case 1 The first term is negative. The second term is also negative, but dominant. The result is a positive or increase in index and resembles an Li^+-Na^+ exchange. The model works well for this case.[13]

Case 2 As seen with a Ag^+-Na^+ exchange, the polarizability of silver is larger than that of the sodium in glass. The first term dominates since the second term is not very large. Model representation of this case is also fairly accurate.

Case 3 A K^+-Na^+ exchange constitutes an intermediate case. The modal predicts a value which is smaller by an order of two.[12] Inaccuracy is due to the large stress induced index of refraction which is ignored by the model.

Stress induced index of refraction - The difference in the radii of K^+ and Na^+ causes residual compressive stress in the guide which is balanced by tensile stress in the substrate. This increases the index of refraction in the compressive layer while reducing it in the tensile region.[14] The mismatch between the thermal expansion coefficients of the guide and substrate also causes stress induced changes, but are usually negligible.[15]

3. Different ion exchange techniques

The monovalent ions are introduced into the glass substrate using the following techniques:

a) Melt

b) Solid source

c) Ion implant

d) Photo chemical

The **photo chemical** process uses a class of photosensitive organometalic compounds that impregnates into the porous glass. Corning glass 7920 has such a porous structure, and thus provides a good substrate.

When exposed to light, the photosensitive organometalic compound decomposes into photoproducts. These bind tenaciously to active sites of the highly porous surface. Subsequent heating oxidizes these bound photoproducts to their metallic states. The refractive index is proportional to the amount of metal oxide produced. As a final step, the porous glass is consolidated to form dense silica rich glass.[16] The photosensitive organometalic compound is Titanocene Dichloride, and is spin or spray coated. This is excited by an Argon ion laser source, utilizing a direct write approach and the lithographic step is eliminated. The process although appearing simple, is far more complicated.

The **Melt process**, is the most common technique. The substrate coated with a suitable masking material is immersed in molten salt solutions such as $AgNO_3$ or KNO_3. Inside the lattice of the substrate, Na^+ ions remain in the vicinity of monobonded oxygen atoms. Under the influence of an electric field or thermal agitation, these ions move within the glass. When immersed in the molten bath of M^+, A^- salt, the Na^+ ions from the glass escape into the melt and are replaced by the M^+ metallic ions of the bath. The salt melt can contain the monovalent ions in any desired concentration. This has a big advantage in tailoring the index change. For example, the addition of Na^+ or K^+ ions to the melt, dilutes the concentration of exchanging monovalent ions, and thus facilitates the formation of single mode guides.

During this process, the number of monovalent ions such as Ag^+ or Cs^+ diffusing from the melt into the glass, is negligible when compared to the total ions in the melt. The thermal diffusion of these ions can take place over a very long period of time and the process is never, source limited or controlled. A non field aided purely thermal diffusion, is also possible because the Na^+ ions out diffusing from the glass are reduced as they enter the melt.[17]

The speed of ion exchange can be considerably enhanced by using an electric field to assist in the diffusion process. Applied voltage and heat, reduces diffusion times by a factor 5 to 3000.[18] A schematic version of this, and the purely thermal process is shown in figure 5.

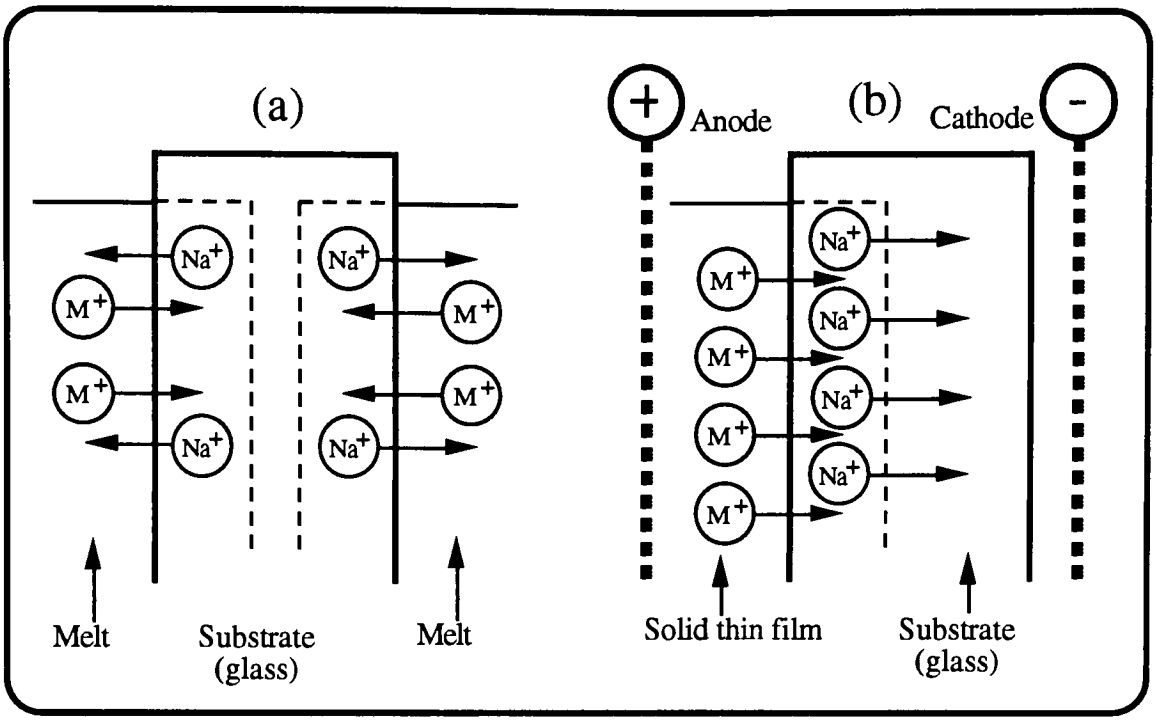

Figure 5: (a) Melt process; (b) Solid Thin Film process
(Field assisted)

While the scheme of this electric field assisted melt process looks simple, its implementation is not practical. This is compounded by the fact that the melting point of the salts is anywhere from 200°C to 300°C. The salts if allowed to cool below this with the substrate immersed, forms a solid, placing high stress on the glass. This easily cracks substrates that are only a few millimeters thick. In addition the fumes released from the melt are usually toxic, and have to be handled in a safe manner. Figure 6, shows a configuration that uses an electric field assisted ion exchange to form light guiding structures on sheet glass substrates.[19]

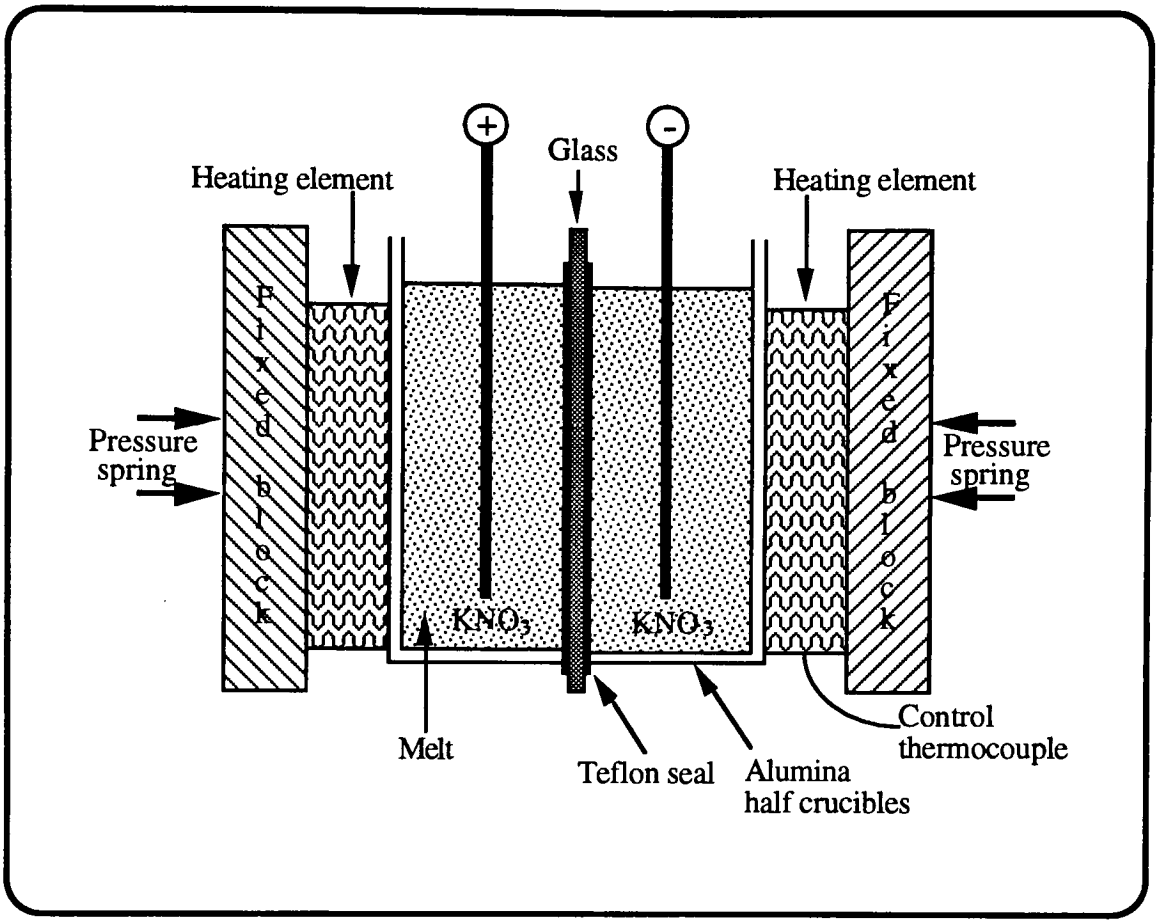

Figure 6: Field assisted ion exchange (Melt process)

The two halves of the crucible are brought together with the substrate placed in between. KNO_3 crystals are put in the two halves and the temperature ramped up (if placed directly in a hot oven the glass substrate shatters due to thermal shock). After the exchange is complete, the halves have to be separated while the temperature is still above the melting point of the salt and allowed to drain. Any melt on the substrate has to be removed before it is allowed to cool.

Even if this scheme was to be implemented without the electric field, immersion of sheet glass in a melt causes considerable irreversible warpage of the substrate. As will be seen later, this does not facilitate in the polishing process to follow. The polishing process is unavoidable for devices requiring the Butt Coupling technique.

During processing, some steps like the pattern transfer process require thin (1mm) substrates. Thick block type substrates are useful only for planner diffusions as they are very hard to work with. Many of the suitable substrates are also sold in the form of sheet glass by manufacturers like Corning and Scott Glass Works, and are not commercially available in the form of blocks.

Even though a number of devices have been made using the melt process, it is a cumbersome technology. While it is still being used extensively for planner diffusions, the problems associated with selective diffusion call for a simpler approach.

The **Solid Silver process** is a technology which eliminates the practical problems associated with a melt process and is thus more suited for selective diffusion. The two processes are similar, except that the M^+ ions are now obtained from a solid thin film which is in intimate contact with the glass substrate.

The behavior of ions in the glass does not depend on the source. However, the nature of the source affects ion transaction into the substrate. A basic difference between melt and solid thin film process, is that the latter does not contain Ag^+ ions. These are released in an electrochemical reaction in which silver is oxidized.

$$Ag \text{ ----------> } Ag^+ + e^-$$

Since the Na^+ ions need to be reduced as they leave the glass, the metal thin film is not able to accept them unlike the melt. This rules out any purely thermal diffusion without an electric field.[20]

Experiments show that a large temperature variation has only a slight effect on the profile.[17] Even though exchange time depends strongly on temperature, the entire process can be monitored by the currant flow between the anode and cathode. A steep reduction in current, would indicate an exhausted thin film ion supply. Hence, instead of time and temperature, the thickness of the film can be used to control the process. This parameter alone determines the depth of diffusion as long as an electric field exists.

The lack of obtaining Cs^+, Tl^+ or K^+ in metallic thin film form, severely limits the solid source process to an Ag^+-Na^+ exchange.

4. Ag^+ - Na^+ exchange properties

Ag^+-Na^+ constitutes a one to one ion exchange; they posses the same charge, occupy similar sites and diffuse by the same mechanisms. Table 1, is a comparison of the M^+ ion properties.[21]

Ion	Ionic Radius / CN ** (pm)	Δn_d	LD * / Salt (mg / kg)
Li^+	59 / 4 76 / 6	0.02	710 / Li_2CO_3
Na^+	99 / 4 102 / 6	-0.02 0.002	1955 / $NaNO_3$
K^+	138 / 6	0.009	1894 / KNO_3
Rb^+	152 / 6	0.01	1200 / RbCl
Cs^+	167 / 6	0.04	1200 / $CsNO_3$
Ag^+	126 / 6	0.10	2820 / Ag_2O
Tl^+	150 / 6	0.10	25 / Tl_2SO_4

Table 1: Comparison of M^+ ion properties

* Ld_{50}: Dose which is lethal to 50% of the animals tested.

** CN: Coordination number of the ion.

The ionic radius of Ag^+ is close to that of Na^+, when compared to that of Cs^+, Tl^+ or Rb^+ as evident from Table 1. The lower stress differential produces lower losses and less of a tendency for substrate cracking which is reported with the Cs^+ exchange.[23] It should be mentioned that Ag^+-K^+ exchange performed in a potassium rich glass, produces the least amount of stress.[24]

Silver in its ionic form, has the highest LD_{50} index. This means that the solid silver process causes the least health hazards. Table 2, lists the diffusion coefficients and activation energies for these cations.[13]

Cation	Glass	Temperature C	D 10^{-14} m^2/s	Q 10^4 J/mole
Tl^+	Borosilicate	530	20	
Li^+	Soda-lime	575	64	14.2
Ag^+	Soda-lime	374	0.7	9.1
	Borosilicate	615	0.26	9.1
	Soda-lime	215	0.01	
	BK - 7	320	0.02	9.8
	Soda-lime	330	0.01	8.9
			0.03	
K^+	Soda-lime	385	0.11	12.5
	BK - 7		0.14	
	Pyrex		0.06	
Cs^+	BGG21	407	0.32	20
Na^+	Soda-lime	371	12	16

Table 2: Diffusion coefficients & activation energies

An important point is that the mobility of K^+ ions at temperatures used is at least two orders of magnitude smaller than the mobility of either Na^+ or Ag^+ ions. Thus when all these ions are present, the Ag^+-Na^+ exchange is dominant.

The biggest drawback with Ag^+-Na^+ ion exchange as reported by various references is attenuation, and is the topic of the next section.

5. Attenuation

The total attenuation of a given mode propagating along a wave guide, has two components.[26]

a) Surface scattering originating from roughness on the surface.
b) Volume losses caused by diffusants such as Ag^+ ions in the guide.

At a wave length less than or equal to 550nm, surface scattering is dominant, and absorption is attributed to Fe^{3+} originally present in most substrates as Fe^{2+}. The absorption of Fe^{2+} at 1.1um causes the greenish color in cheap glass.[27]

During an Ag^+-Na^+ ion exchange, a small fraction of silver ions are neutralized by the oxidation of Fe^{2+} to Fe^{3+}.[24] Other polyvalent impurities like Arsenic, also have this neutralizing effect.[28]

Volume scattering is thus due to the tendency of Ag^+ ions to neutralize and form atomic silver within the glass. Absorption is caused by these sub microscopic particles. Neutralizing of silver can be reduced, by limiting the blocking anode current at the glass surface.[29]

Blocking anode: The mobility of Na^+ is greater than that of Ag^+ ions.[30] This results in a potential which tends to increase the indiffusion of silver while retarding the sodium ion outdiffusion. Since the exchange is one to one, any excessive Ag^+ ions in the glass resulting from Na^+ ion depletion, will be reduced and deposited in the substrate as metallic silver. This is enhanced at elevated temperatures.[22]

6. Characterization

This final and important stage covers index or ion profile, attenuation and device characterization.

There are two different approaches for the measurement of refractive index profiles in glass substrates fabricated by ion exchange.

a) Measurement of dopant profile: This is done by using an electron or ion microprobe[31], analysis of back scattered electrons in a Scanning Electron Microscope[32], or Atomic Absorption Spectrophotometry.[33]

b) Optical measurements of parameters such as surface reflectivity or mode indices: The profile is derived by using WKB approximation.[34]

An electron microprobe can be used to measure the profile of the diffusing ion. High energy electrons are collected and analyzed for the concentration of the specific ion. Even though any ion can be analyzed, the output can be very noisy as the sensitivity strongly depends on the species. It can be difficult to draw definite conclusions, specifically if the ion concentration is low.[35]

The Scanning Electron Microscope has two uses;

a) Analysis of X-rays or energy dispersive spectrometry - EDS.
b) Analysis of the back scattered electrons from the ions.

Both approaches have been used successfully in many references. It should be noted that scattering efficiency for ions of large atomic number, is greater. This method is therefore more accurate in detecting Cs^+ and Ag^+ ions.

Concentration measurement of any element can be obtained via Atomic Absorption Spectrophotometry. A layer of the substrate is etched by using Hydrofloric acid. The resulting solution is analyzed for ionic concentration. Subsequent etching steps are performed and the analysis repeated. Even though his technique is destructive it is capable of giving absolute concentration.

For planner guides, attenuation can be measured by the Three Prism Method. This technique measures both, the contribution due to scattering and that due to absorption. The former can be measured independently by probing a fiber tip along the face and capturing the scattered signal.

Chapter III

Fabrication Technology

Process discussion from now on is device specific. The fabrication of the High Precision Laser Radar Tracking Device is described in detail . An attempt has been made to walk a process engineer through the simple but delicate steps. While all process related information has been recorded here, the operation of the machines is limited to special points of interest with regards to the device, and the reader is periodically referred to the operations manual. References are also made to information given in previous chapters.

A. Process selection

The section describes the reasoning behind most process steps chosen. A reader specifically interested in the process aspect could omit this section.

1. Melt vs. Solid Silver Thin Film process

The solid silver thin film process was originally chosen as the M^+ ion source and has proven its worth over the past two years. The advantages of this process have been described in previous sections and are reiterated on the following page.

(a) The process is controlled by the thickness of the film as opposed to temperature or time, and is therefore more repeatable.

(b) Since there are no fumes present that are usually associated with a melt, this process posses no health hazards; precautionary steps are not needed.

(c) Unlike the melt process that requires handling of substrates at the elevated exchange temperature, the solid film process requires only current monitoring.

(d) Multiple substrate ion exchanges are made easier.

(e) The melt process needs monitoring of the silver ion concentration. For the sake of repeatability, it is required to be kept at a constant from diffusion to diffusion. The silver thin film is always fixed at the purity of the evaporating pallets.

(f) Since the electric field is produced between two metal plates, the clamping of the substrates in between, ensures no warpage of the glass. A flat surface is very important for the polishing process that is to follow.

(g) The silver ion has better electron back-scattering capability. This is ideal for microprobe detection.

2. Substrate choice

Corning 0211 glass was chosen for a substrate. Its composition along with that of others is listed in Table 3.

	SiO_2	B_2O_3	Na_2O	K_2O	Al_2O_3	TiO_2
Corning 0211 glass	64.4	10.3	6.2	6.9	4.1	3.1
Corning 0317 glass	61.2		12.9	3.4	17.0	0.8
Low iron soda lime glass	70.0		14.0		1.8	
BK 7 glass	69.6	9.9	8.4	8.4		
Pyrex 7740 glass	81.0	13.0	4.0		2.0	
Fisher glass slides	72.2		14.31	1.2	1.2	
Soda lime glass	70.0		14.0		1.8	

Table 3: Substrate properties

Cont.

	As_2O_3	SO_3	Fe_2O_3	ZnO	CaO	MgO
Corning 0211 glass				5.4		
Corning 0317 glass	0.8				0.4	3.4
Low iron soda lime glass	1.8	0.3			7.3	3.8
BK 7 glass						
Pyrex 7740 glass	2.0					
Fisher glass slides	1.2	0.3			6.4	4.3
Soda lime glass		0.3	0.1		8.6	4.0

Table 3 *Cont.*: **Substrate properties**

Note:

Corning 0211[25] - Optical quality.

Corning 0317[38] - Rapid diffusion. - Few Alkaline earth ions.

Low ion soda lime[38]

BK 7[39] - Low loss channel guides.

Pyrex 7740[39] - Not optical quality

Fisher slides[40] - Sodium content too high: Silver colloids.

The following points influenced the choice of substrate.

(a) Glass free of fining agents - Arsenic, Antimony. These ions neutralize the Ag^+ ion:- formation of silver colloids.

(b) Moderate content of Na^+ ions:- to prevent excessive Ag^+ diffusion which forms silver residues.

(c) Optical quality:- good transmission properties.

(d) Glass which has not been subjected to an ion exchanging strengthening process performed by the manufacturer.

(e) Inexpensive and available.

Background information on Corning 0211 glass as provided by the manufacturer, is made available in Appendix B1.

3. Masking material

99.9995% pure Aluminum was chosen for a mask. This is used as a metal interconnect in the semiconductor industry. For selective ion exchange of Ag^+-Na^+ ions, two schemes were experimented with. Figure 7, describes these two processes.

Process (a), involves the patterning of silver. As will be seen later, this scheme provides tricky in the making of guides that are inches rather than centimeters in length.

Process (b), has a masking layer which is deposited on the substrate and patterned. A blanket layer of silver is then put down on top of it. Ag^+ ions diffuse into the glass only where the silver and glass are in contact. Since there is no ion exchange taking place between aluminum ions and sodium ions, the layer of Al effectively prevents the silver coming into contact and diffusing into the glass substrate.

Chromium was also tried as a mask. According to reference 20, a Cr layer of only 90nm is needed to prevent silver diffusion. However, the evaporation of Cr is tricky. The stress differential between the different layers results in peeling. It should be mentioned that a Cr mask cannot be used with the melt process because chromium dissolves in salts.[20]

The Cr mask is most useful when IC lithography masks are used as substrates for the ion exchange. This fabrication process is suitable for cheap mass production. The patterning of these mask plates can be done by the manufactures with a high degree of accuracy. It is therefore useful in the formation of single mode waveguides that require fine geometry.

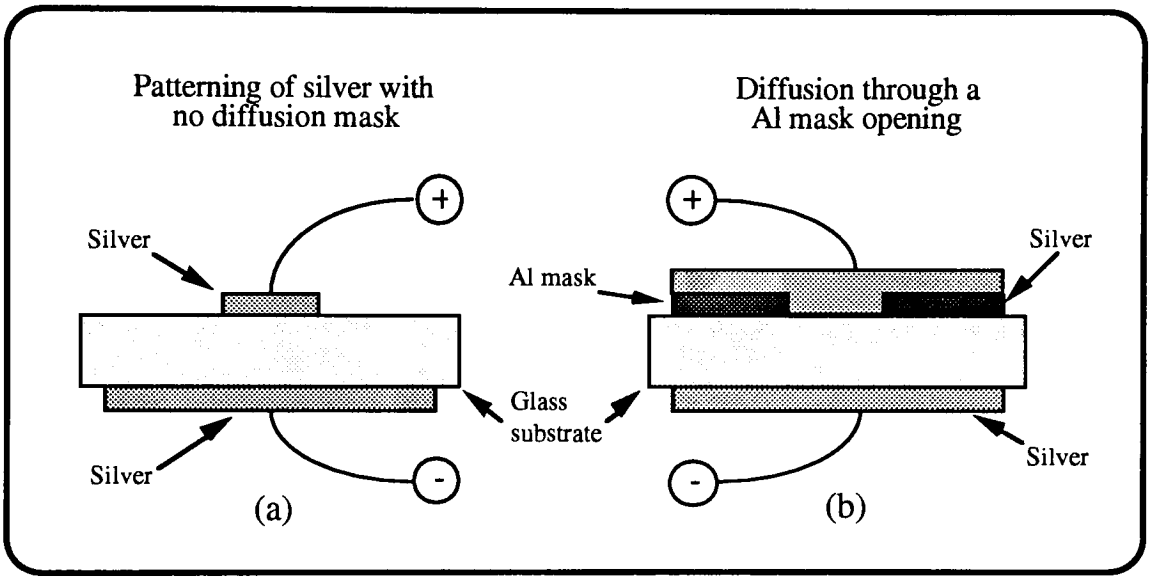

Figure 7: Two schemes for Ag^+-Na^+ ion exchange

B. Basic ion exchange process

This section describes the very basic process involved with obtaining a glass substrate containing embedded glass waveguides. Details of steps such as substrate marking, diffusion, etc. are covered in a later section. Flow diagram 1 describes the silver patterning process given in figure 7a.

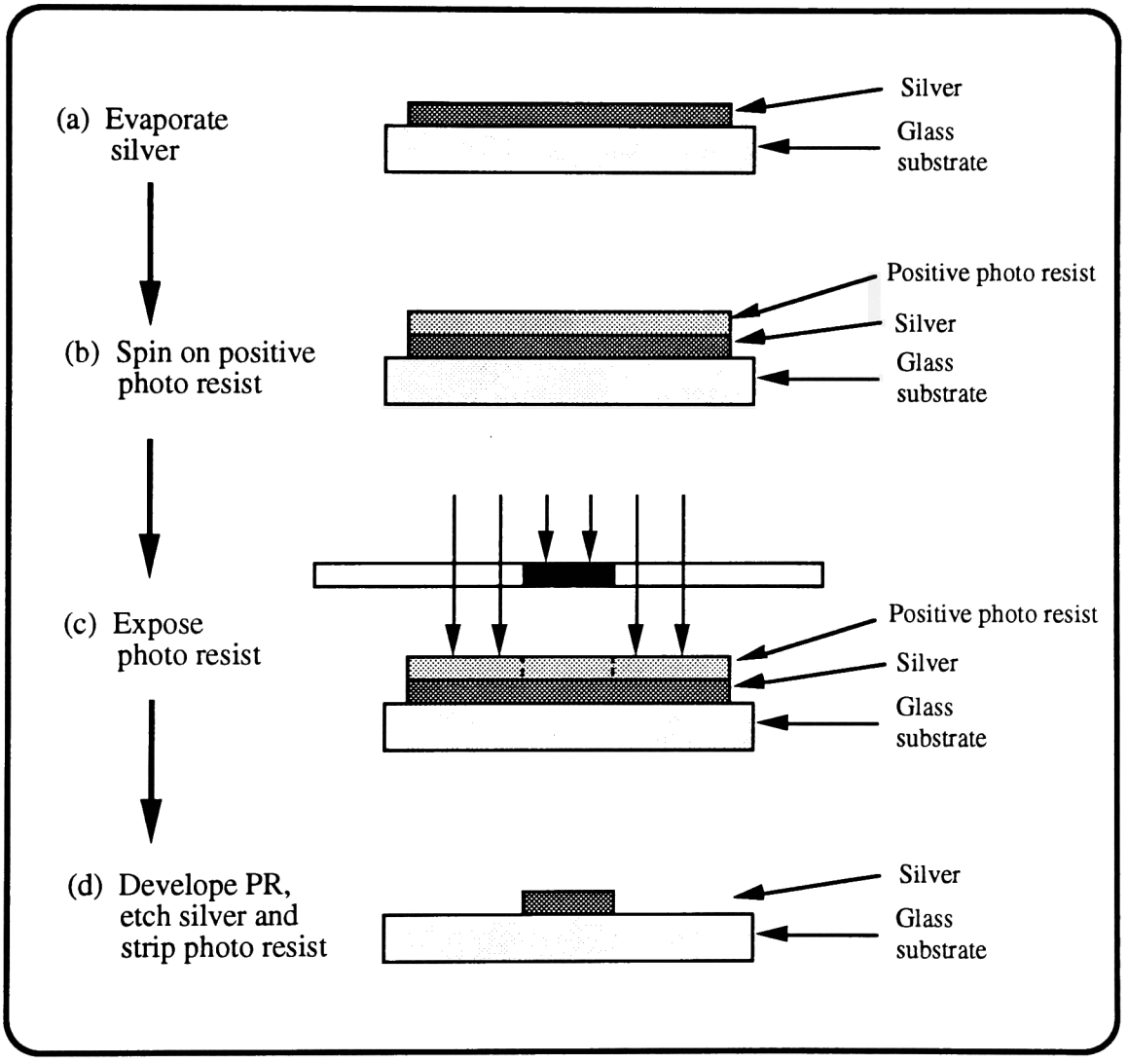

Flow diagram 1: Silver patterning process

Silver diffusion through a patterned mask as described in figure 7b, is given in flow diagram 2.

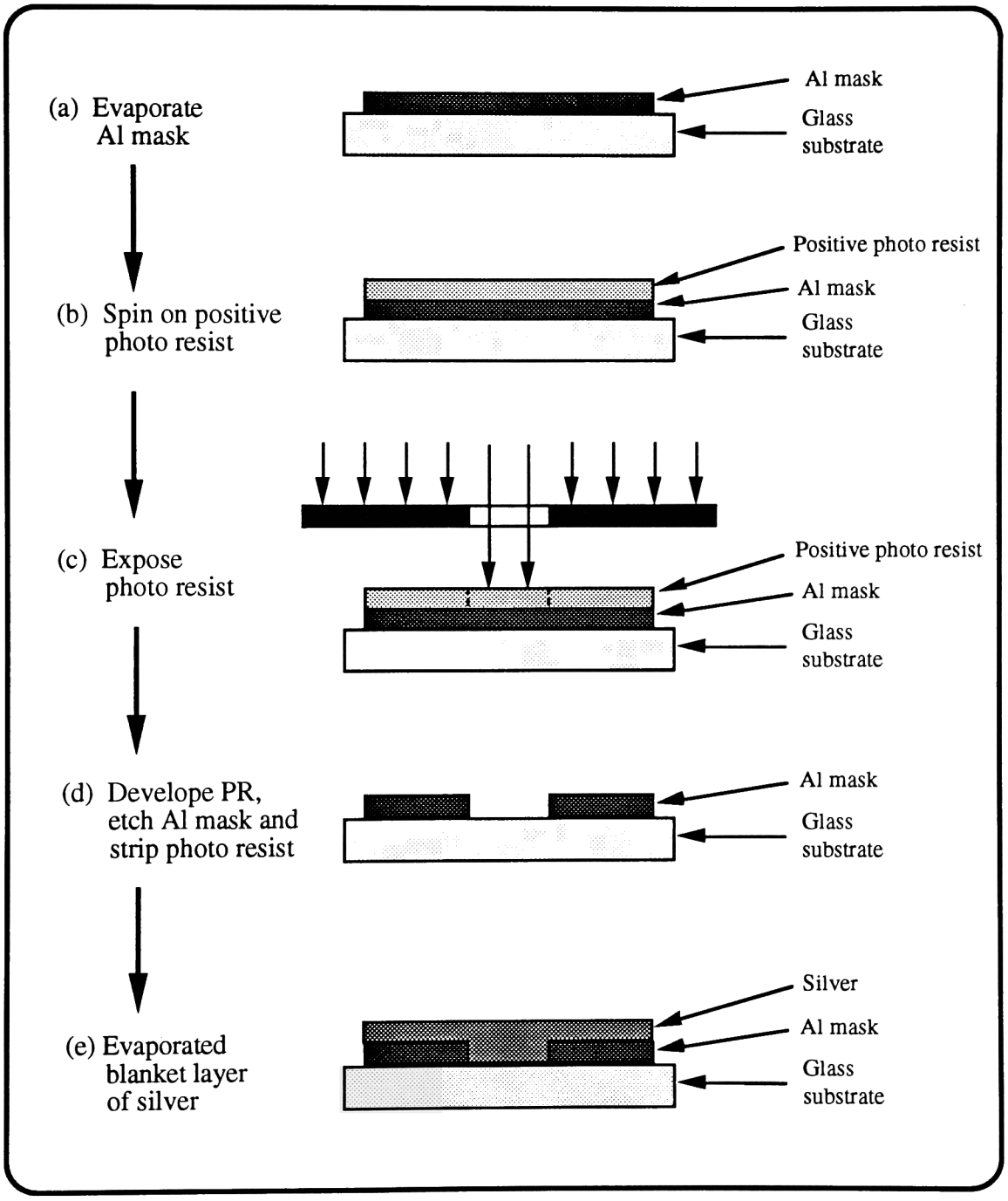

Flow diagram 2: Al masking process

1. **Patterning of silver** - without a diffusion mask

After the substrates are prepared, silver is evaporated onto the glass. The evaporation process is a thermal one where a silver pallet is placed on a heating element and evaporated in vacuum. The hot particles deposit on the cool substrates and form a thin film. Positive photoresist is spun on the silver coated substrates. The pattern of the waveguides is then transferred on to the substrate. The subsequent development process yields exposed silver regions that are removed via an etchant solution.

The photoresist that remains on the silver has to be stripped before the diffusion step: Figure 8. This is usually performed in an O_2 plasma. The highly reactive Oxygen species reacts with the organic photoresist and removes it. However, it is well known that silver oxidizes when exposed to atmosphere. The process is greatly enhanced in the presence of the O_2 plasma. This plasma not only removes the photoresist, but also oxidizes the silver to the point of a brown dust which easily wipes off.

Another technique used is to strip the photoresist by using an Acetone solution. Due to poor adhesion between the layer of silver and the substrate, the stripes of Ag that provide cations for the ion exchange process float off. This is also due to the length of these stripes (2in. x 30um with no interconnections to other parts of the silver film).

Yet a third technique tried, was the removal of photoresist by a flood exposure method. The remaining photoresist is subjected to a flood of exposing UV which is then developed. Again as before, the same problem with adhesion resulted in lift-off. It should also be noted that while patterning of the silver can be accomplished to some degree with a very thin film of silver (less than 1000 A), it is nearly impossible with a thicker film (3000 A or more).

This processing technique was thus abandoned in favor of the Al mask process. Most of the processing steps discussed are dealt with in detail in the following sections.

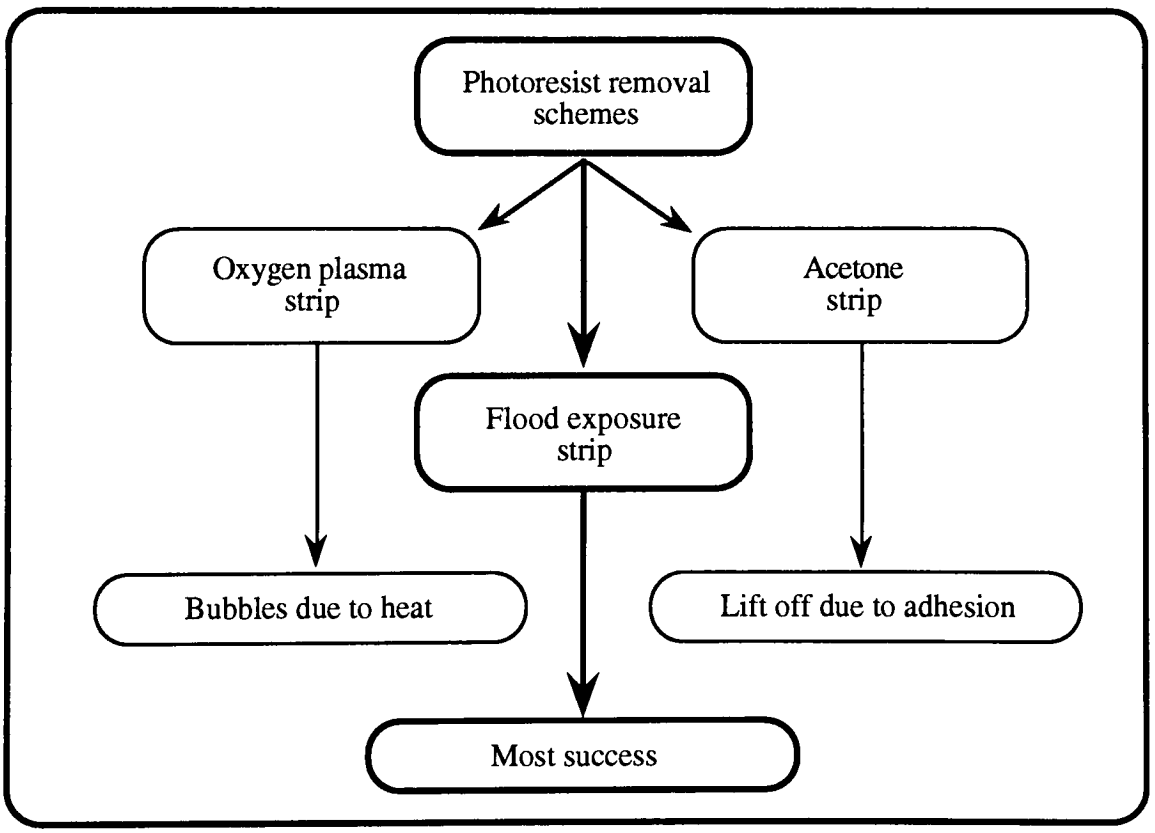

Figure 8: Photoresist removal schemes

2. Al mask for selective ion exchange

This process by far has seen the most widespread use with the melt and solid source methods. The section gives a brief account of this technique before going into details in the next chapter.

A typical process flow for the melt technique using an Aluminum mask, is given in flow chart 1.

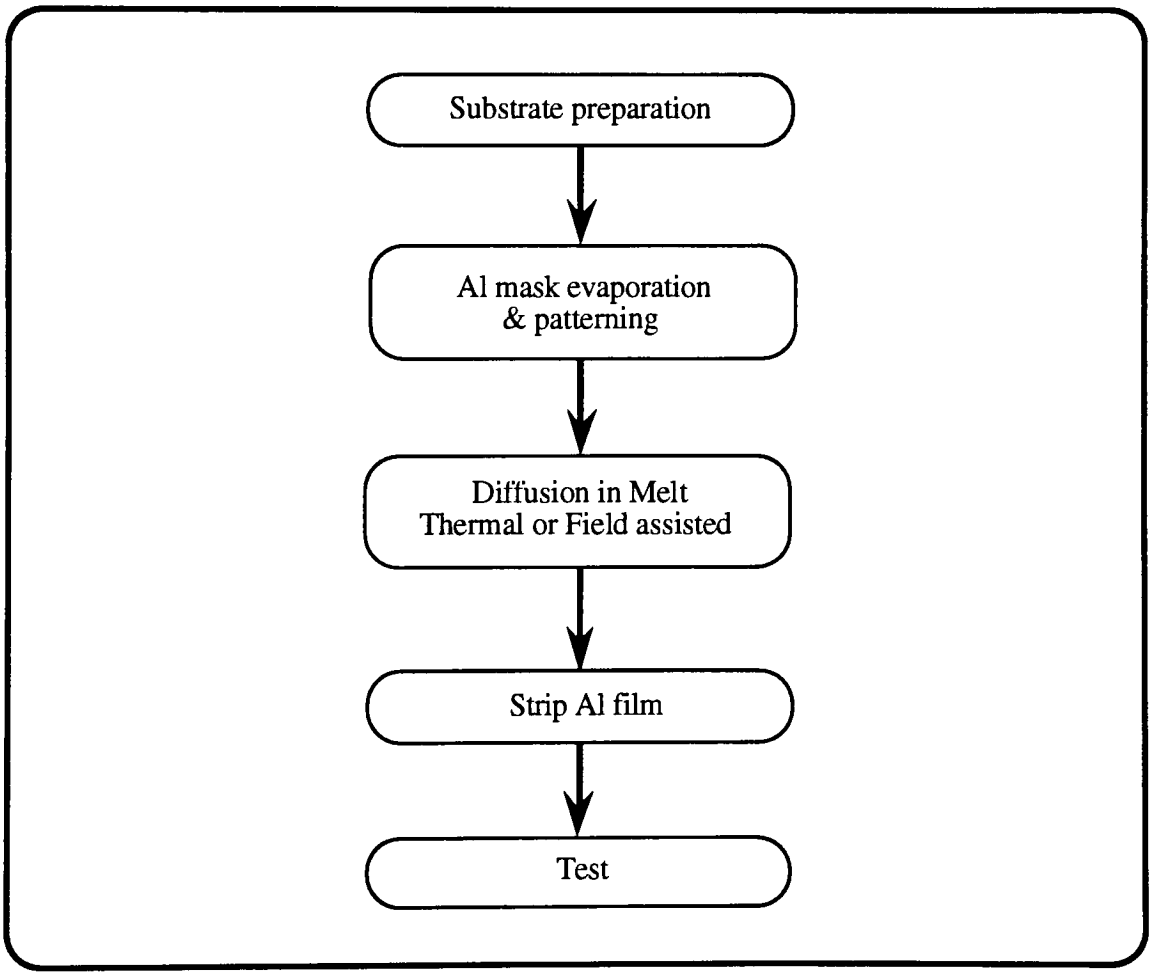

Flow chart 1: Process flow for the melt source

The Al pallets used for the evaporation are 99.9995% pure. It is important that this film is free of contaminating ions such as Fe or As, as these ions could also diffuse into the glass. The substrate should also be void of any adsorbed atoms. This reduces adhesion between the glass and the Al film, and results in blistering of the mask during any subsequent temperature step.

The solid source process flow is given in flow chart 2.

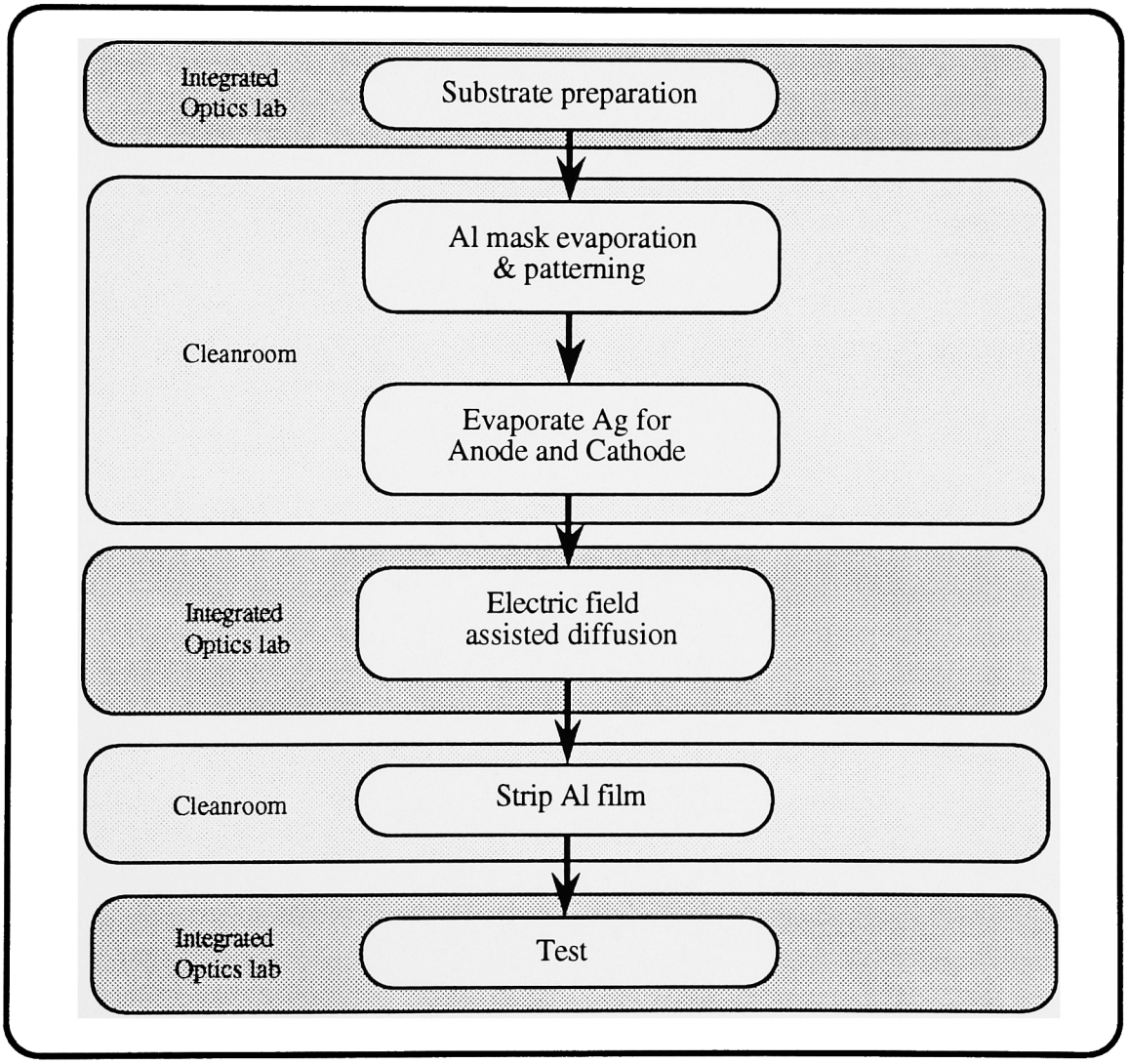

Flow chart 2: Solid source process

The areas marked cleanroom, require a microelectronic fabrication facility or its equivalent. It is important that the evaporation and patterning processes be kept void of dust and other particles, as this greatly increases yield. Steps requiring this environment were carried out in the RIT cleanroom facility.

Chapter IV

Device Process

This chapter describes selective ion exchange through a patterned Al mask. It leads up to the final product, the High Precession Laser Radar Tracking Device. The following two points are to be taken note of:

1) The substrate used is rich in sodium. A cleanroom such as the RIT facility, is kept strictly void of sodium. Beakers, wafer handling equipment, etc. are sodium free. This type of alkali metal atoms (Na^+, K^+) are extremely mobile in SiO_2 (gate oxide) and cause long term changes in the device threshold voltage V_T. A value of $10^{12}cm^{-2}$ will result in V_T shifts of several volts. The interest in keeping sodium contamination within acceptable levels has resulted in process steps designed to minimize any contact with the regular process of microchips.

2) The glass substrates used in integrated optics are square with dimensions of 4in. x 4in. Typically wafers used in microelectronics are circular having a radius of 3 to 4in.. The glass substrates are also a lot thicker and therefore heavier. This makes it impossible to use the wafertrack for photoresist coating. The pattern transfer process is also made more complicated. Customized steps are needed to overcome these problems.

The process described here, consist of a field assisted ion exchange and a thermal ion exchange. The first field assisted step, is needed to oxidize the silver and drive the ions into the glass while forcing the sodium ions out of the substrate. As to be shown, this produces an erfc profile characteristic of such a diffusion. The depth of penetration of the ions is about 10um. A simulated profile is shown in figure 9a. However, the device simulations call for a Gaussian profile in order to achieve the desired result.

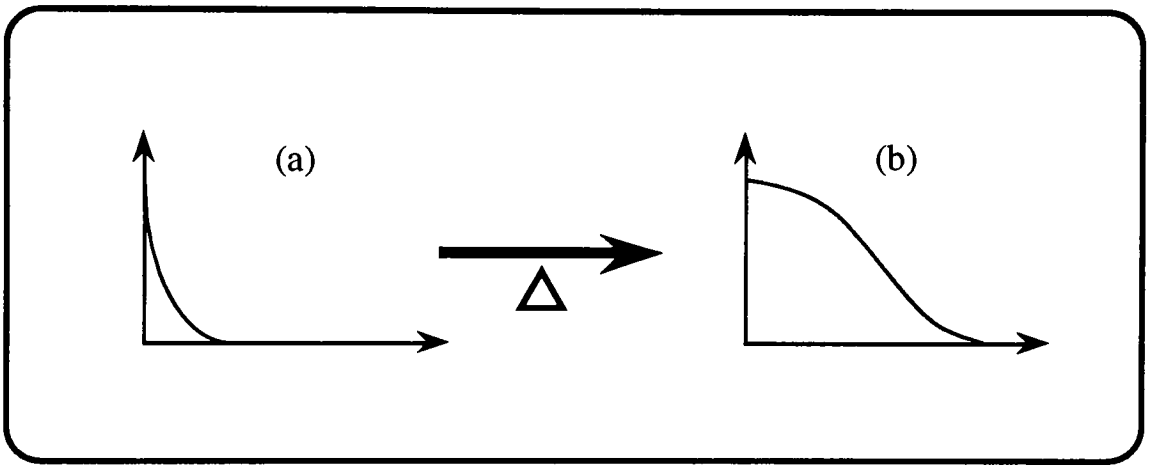

Figure 9: Ion exchange profiles

The second non field aided thermal diffusion step was designed with this purpose in mind. The simulation shown in figure 9b, is typical of this final profile and is proven by microprobing of second diffused substrates.

Note: Even though subtle differences exist between a diffusion process and an ion exchange process, the terminology has been used interchangeably.

The purpose of this second diffusion step is two-fold. It helps in tailoring of the final profile as desired. This is done by varying the diffusion time or temperature and has been utilized very effectively. Further diffusion of the silver into the glass more completely oxidizes the Ag^+ ions. Scattering due to silver colloids formed during the field assisted exchange is thus greatly reduced. This step, which can also be considered an anneal, is reported to produce waveguides with losses of less than 0.1 dB/cm.[36]

Flow chart 3, describes the entire process in detail.

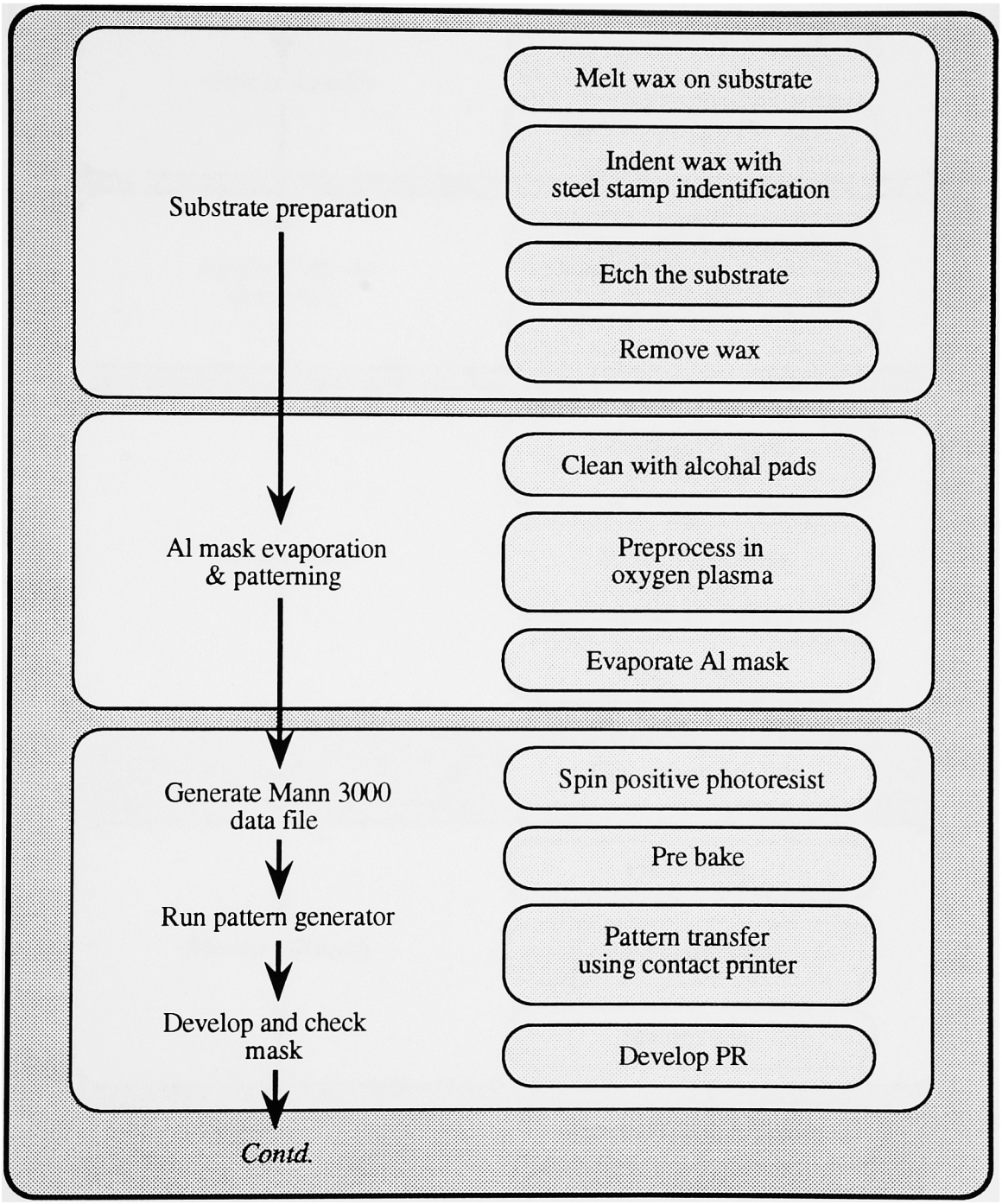

Flow chart 3: Process flow

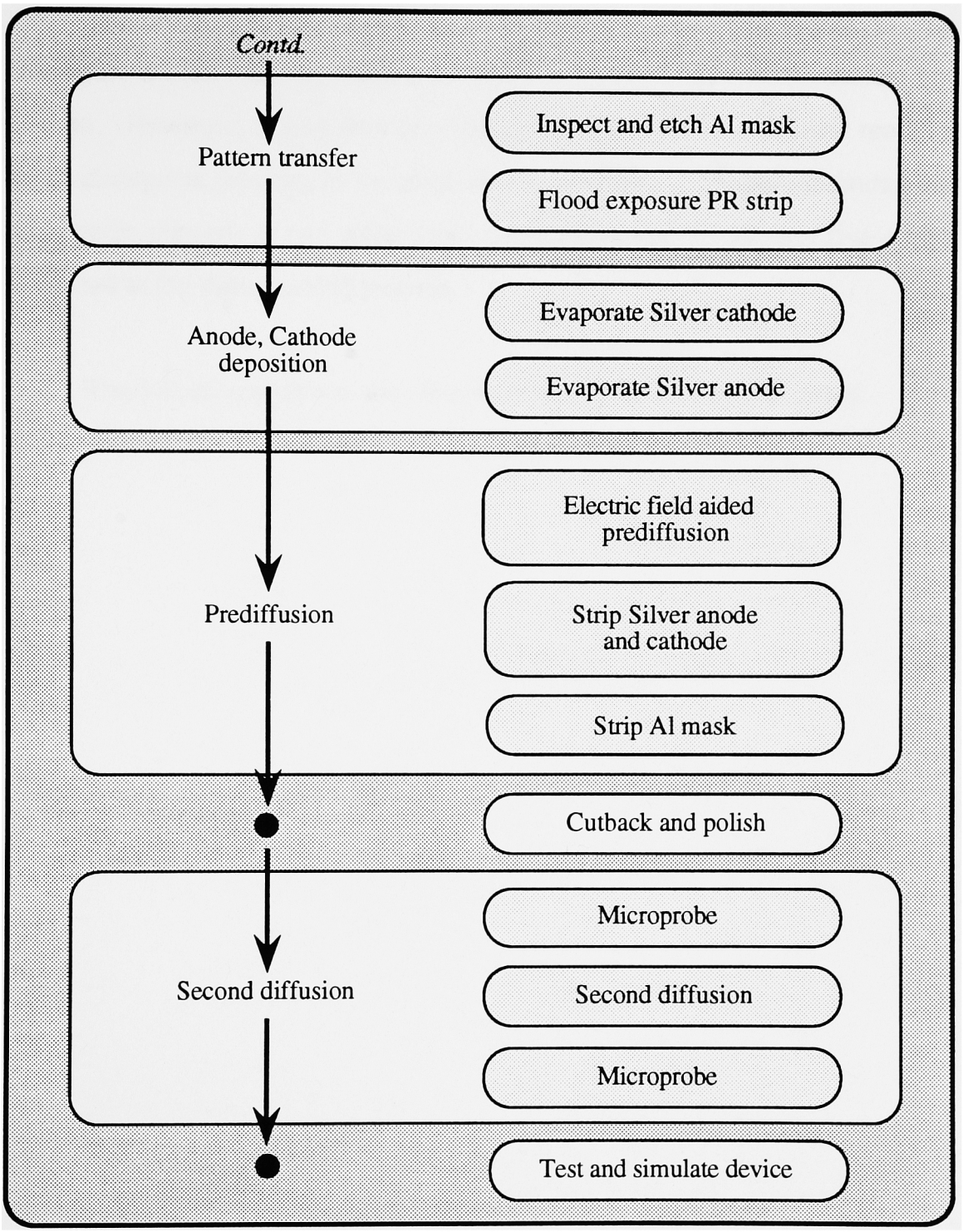

Flow chart 3 *contd.*: **Process flow**

The process steps are also given in the lot follower: Appendix C1. This has been written step by step with recommended times, temperatures and dosage. However, it also has provisions for comments and actual readings taken during the process, to be used later for analysis. It is recommended that each batch consists of two substrates and has its own lot follower. This greatly facilitates in the data tracking process.

The following sections describe each step of flow chart 3 in detail.

A. Mask making

The making of the required mask is probably the first step associated with any process. At the beginning of the project the most important goal to be met, was the demonstration of light guiding action or the formation of waveguides. It was decided that this could be best demonstrated by designing a S curve: Figure 10.

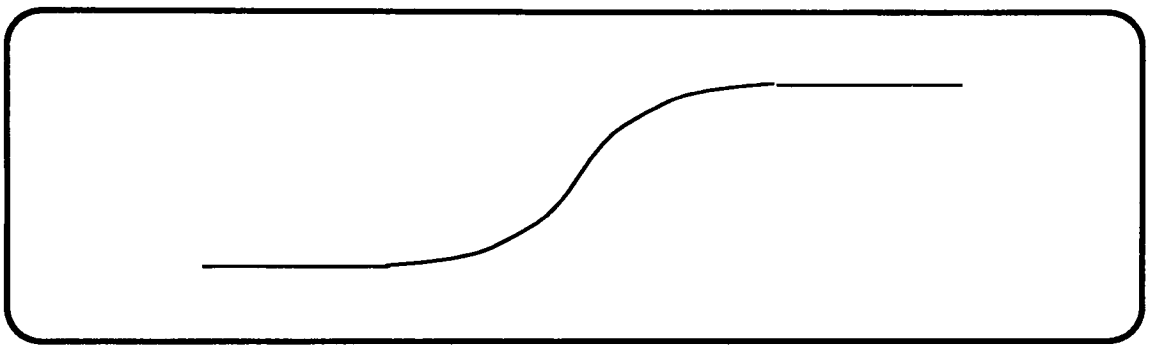

Figure 10: S curve waveguide

At RIT, mask patterns are usually generated by students and faculty using the inhouse Integrated Circuit Design tool, ICE. Unfortunately ICE does not posses the capability of rotating boxes even though this capability exists with the pattern generator. The solution required a program to output a Mann 3000 pattern generator formatted data file.

1. **Pattern Generator program** - The design

This program contains Fortran 77 source code and was run directly on the Vax. The radius of curvature was calculated as shown in figure 11.

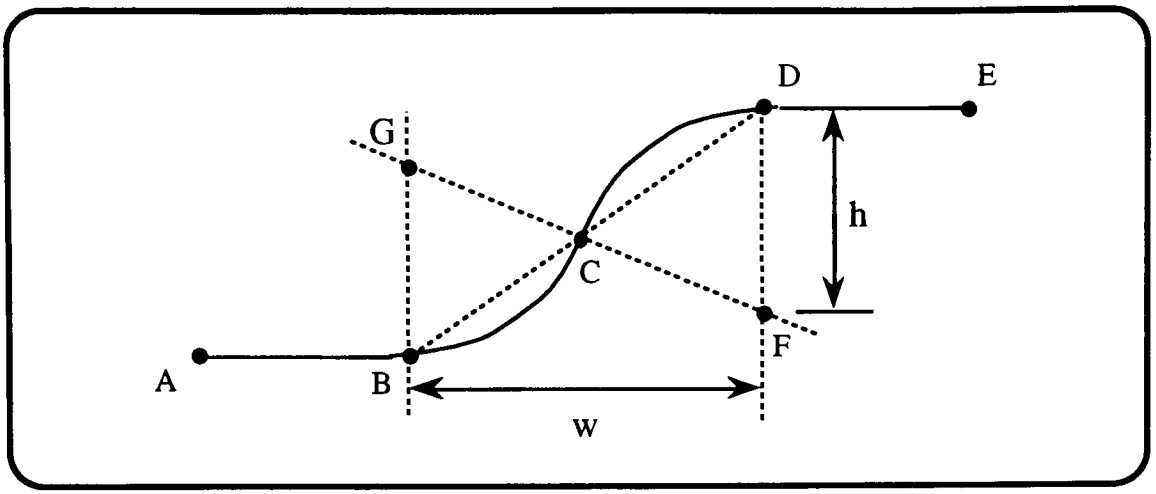

Figure 11: S curve computation

The manual on the Pattern Generator has the requirements for the input file. The reader is referred to this for further information. Calculations of the center points of the individual boxes were performed as follows.

AB and DE represent the straight portions of the guide. C is the mid point of BD. Straight line GCB was picked such that CG = CF. Points along the arc BC and CB are computed by the program using G as a center point for the former and F as a center point for the later. The X coordinate, Y coordinate, length, height, and angle of rotation of each box is written into the output file after the program request the height, h, length, l, and the width of the guide, W. An example of the source code is given in Appendix C2.

Initially wave guides of different widths were put down on the mask: Figure 12.

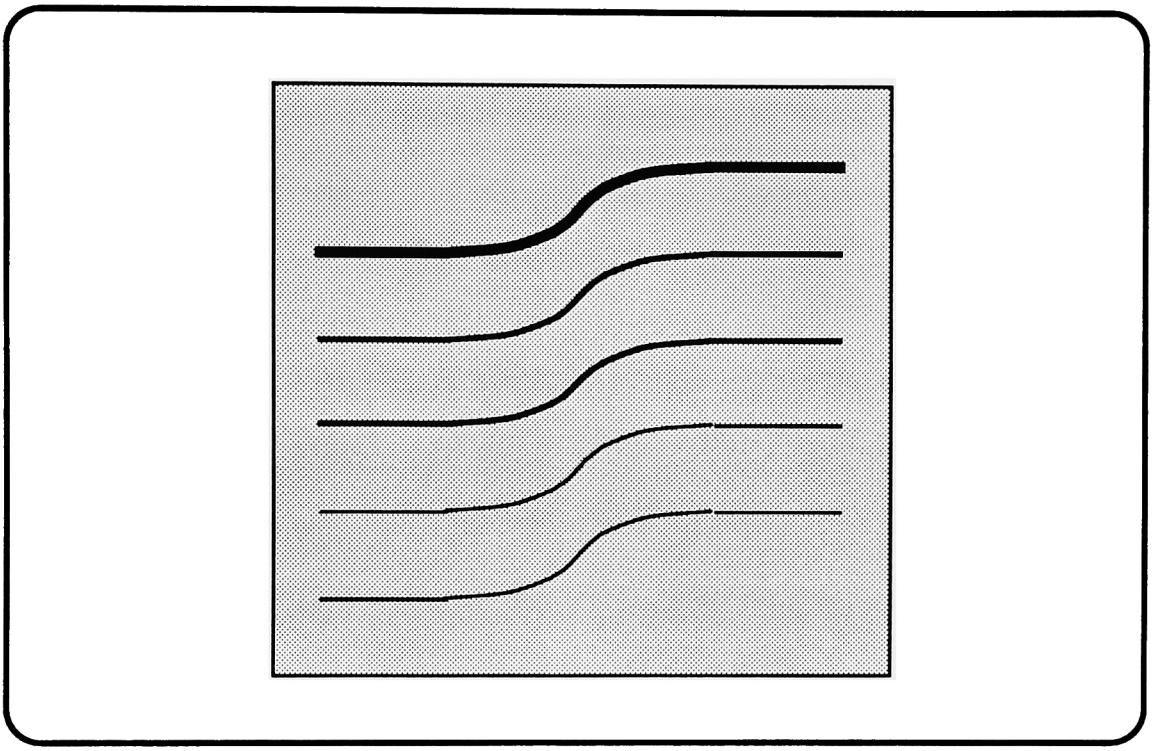

Figure 12: Mask with different widths

Once light guiding action had been demonstrated, the next goal was to optimize coupling in a Simple Coupler. A Simple Coupler consists of two straight line waveguides placed next to one another: Figure 13.

There are approximately 24 couplers on a mask. The first few masks contained 50um width waveguides with a wide range of separations in order to cover the required latitude. However, this approach was abandoned due to the following reasons.

1) Difficulty in keeping track of the guides.

2) The number of edge chips at the time was overwhelming, and most of the guides could not be tested.

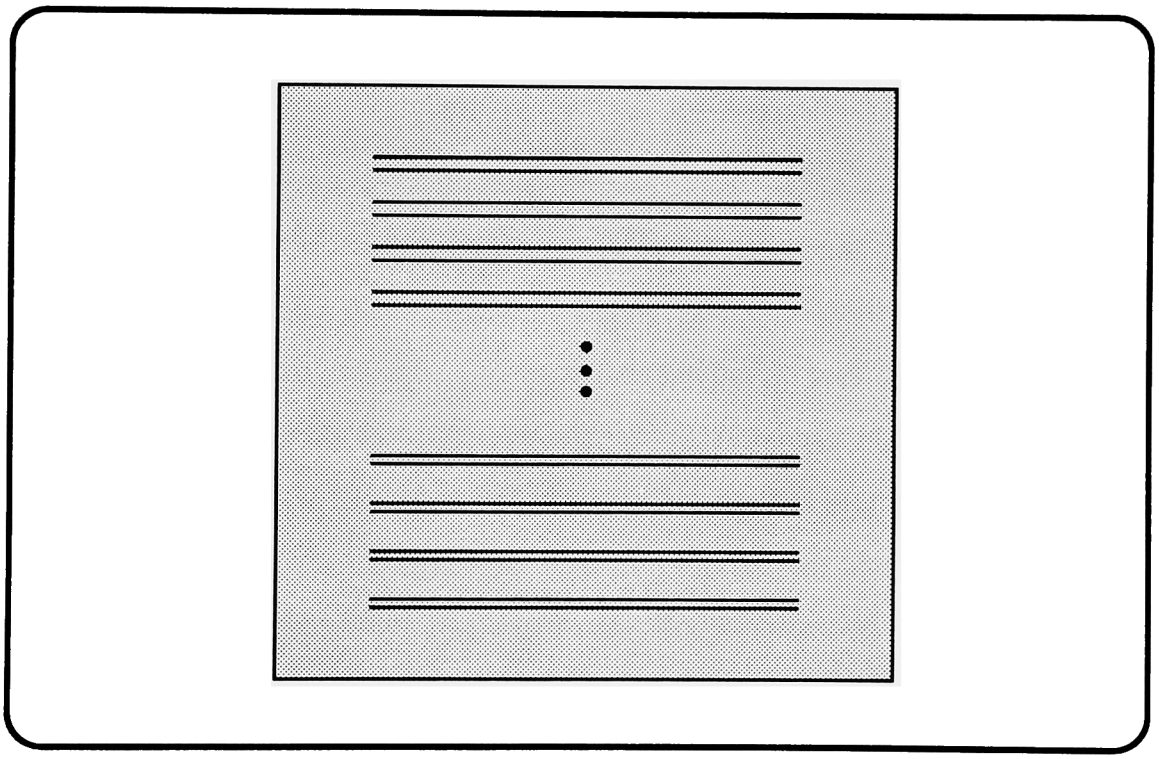

Figure 13: Simple coupler mask

The solution to this, was to pick a couple of best guesstimate separation values and make a mask consisting of only these two values. Different values were tried; 12um and 14um spacings seemed to yield the best design profiles.

It should be said that at this stage of the project no Microprobe data was available to indicate the profile shape. The only profile indicator was from back lighting the guides. This produced a hazy unclear picture. An important point to note, is that at this point of time only the initial field aided ion exchange step was being used.

The main problem seemed to be that the profile fell away sharply giving no latitude for coupling. This profile is typical of an erfc, but was not clearly understood due to the inability to index profile. Even though coupling was evident, the required V shape could not be obtained.

The pressing need for greater latitude, gave rise to the idea of a second thermal diffusion. By now, the requirements for the initial diffusion were also fairly well understood. It was apparent that while the silver lay on the surface in the form of a thin film, the only way to achieve diffusion was by using an electric field. It was also understood that changing the thickness of the film controlled the depth, and not the shape of the profile. The second thermal diffusion, gave the increase in latitude necessary to fine tune the profile, and thus the required V curve for the High Precession Laser Radar Tracking device.

The second diffusion greatly increases the depth of ion penetration. This increase translates to a greater need in guide separation. The mask opening was made smaller and the lateral diffusion allowed to make up the difference.

The mask designed to incorporate the second diffusion process, consisted of 30um waveguides separated by 30 to 40um separations. Again, only two widths were put on each mask due to the polishing problem reported previously.

The success with the Simple Coupler saw implementation of the Compound Coupler design: Appendix C3. Multiple guides were again put down on each mask. The only difference being that all the guides were identical.

Note: While the masks shown in these figures consist of opaque guides, the actual mask consists of its negative image.

Once the data file has been created, two things need to be done. All the blank spaces in the file have to be replaced with zeros because of formatting requirements. While the program can be modified to perform this task, another easy method of accomplishing this is given as follows.

Type: EVE, file name, on the Vax.
Once the data file is brought up, hit the command key, and type: Replace
At the prompt, Old string, type:<space bar>
At the prompt, New string, type:<0>
At the next prompt, type:<all>

This command sequence replaces all blank spaces in the program with zeros. The same task can be performed using any other editor too. The data file should now be run through the program SPLIT which is available in microlib. Since the memory capacity of the pattern generator is limited, this program divides the data file into sections as required.

2. Mask processing

Usually the lithography mask made by the pattern generator is used as the radical in the step and repeater. The product of the step and repeater is the final mask which is then used by the contact or projection printers in the Microelectronic industry. The radical made by the pattern generator is also used by the steppers.

However, the radical itself is used as the final transfer mask during our process. This is because the waveguides are 3 inches in length. The width of the guides are also not small enough to justify any photo reduction or photo repeating.

Two data files need to be run separately in order to produce this radical or the final mask. Since it is the larger of the two, the data file containing the waveguide information should be run first. A second file containing registration marks, is run subsequently. It puts down registration marks as shown in figure 14.

The process involves the exposure of boxes in the waveguide region. However, if this was to be developed using direct processing, the exposed regions or the guides would remain opaque while the background clears out. While this is acceptable for the silver patterning process, the negative of this is needed to produce the proper polarity required for our process. The required mask is generated by first exposing the boxes and then subjecting it to a reversal developing process.

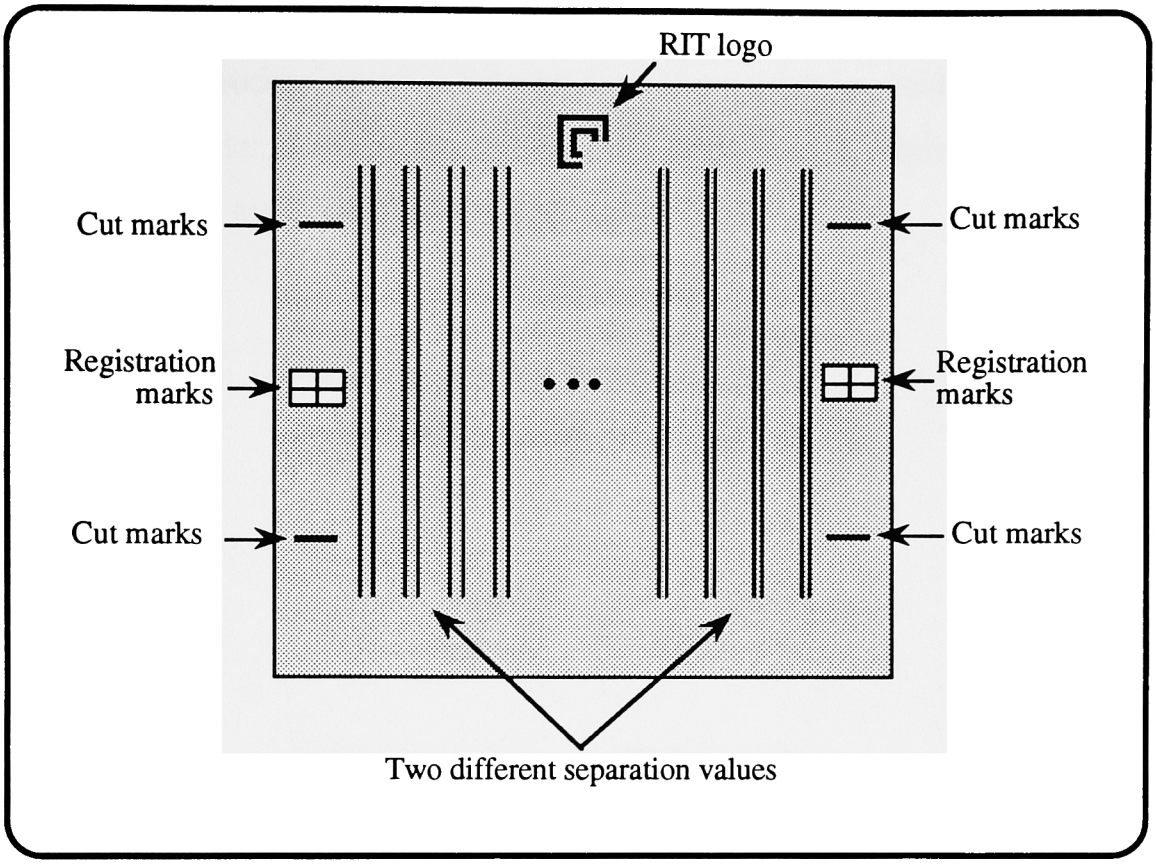

Figure 14: Registration marks

During reversal processing, the mask is first developed in the regular manner. It is then placed in a bleaching solution which clears out the already developed guide regions. The subsequent blanket exposure exposes the remaining areas. The development step which follows, produces an opaque mask which contains transparent guides. This is the polarity needed for our positive image transfer step.

The comparatively larger image dimensions, require a fine tuned development process which is different from the normal reversal process used at RIT. The order of processing remains the same but the required processing times vary, and are given bellow.

Platen holder - 309561 B - 4X4 mask
Focus setting - 4.75
Intensity setting - B2

1st Development time - 14.0 minutes
Bleaching time - 5.0 minutes
Clearing time - 5.0 minutes

2nd Exposure time - 20.0 seconds

2nd Development time - 2.0 minutes
Stop time 30.0 seconds
Fixer time 2.0 minutes

After blow drying the mask, the intensity level has to be checked on the Nanoline. The readings have to be in the region of 5.0 : 0.4, transparent : opaque, with the 100X objective. The transparent intensity has to be at least 3 times greater than that of the opaque region. This ensures clearing of photoresist within the required time frame, and thereby gives limited repeatability. This term is appropriate, as that is the best that can be achieved by hand processing. The line widths should be measured using the appropriate program on the Nanoline.

B. Substrate identification

Even though this step appears deceivingly simple, it has posed a problem in the past. Initially, alignment marks and identification numbers were scribed on the surface of the glass substrate with a diamond scribe: Figure 15.

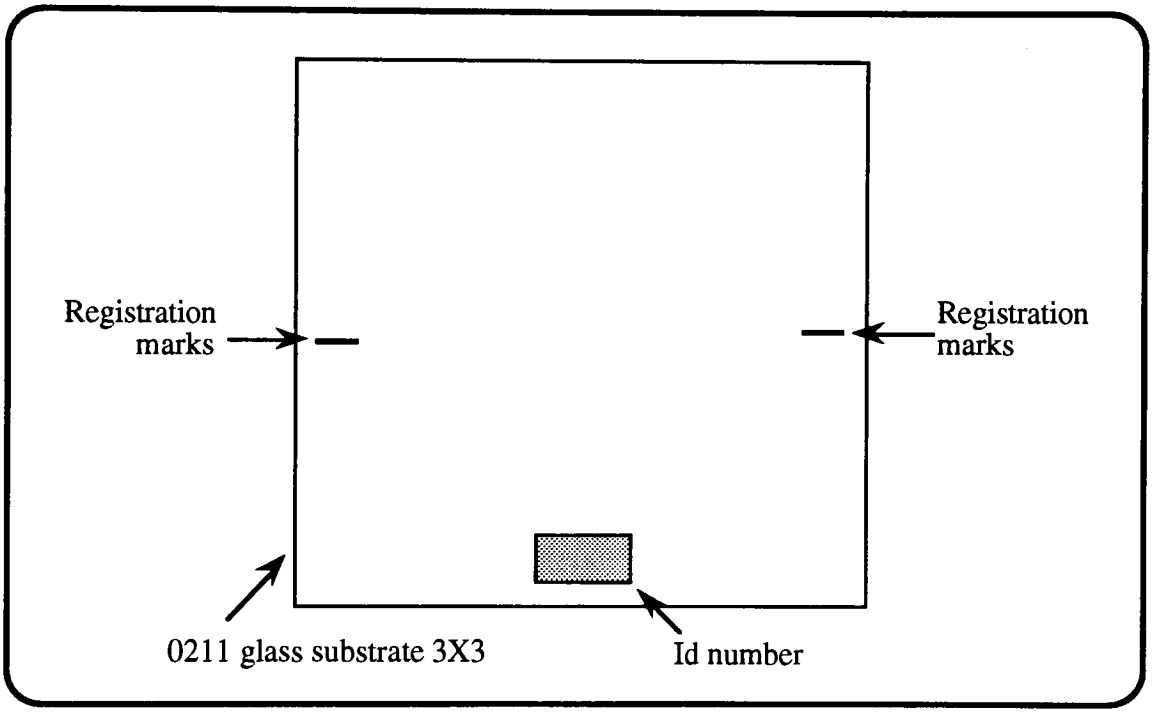

Figure 15: Old method of identification

The alignment marks are needed to keep the waveguides parallel to the sides of the substrate, so that the cutback and polish step would yield a face cross section perpendicular to the longitudinal axis of the guides: Figure 16. This is needed to ensure maximum coupling efficiency during the butt coupling process.

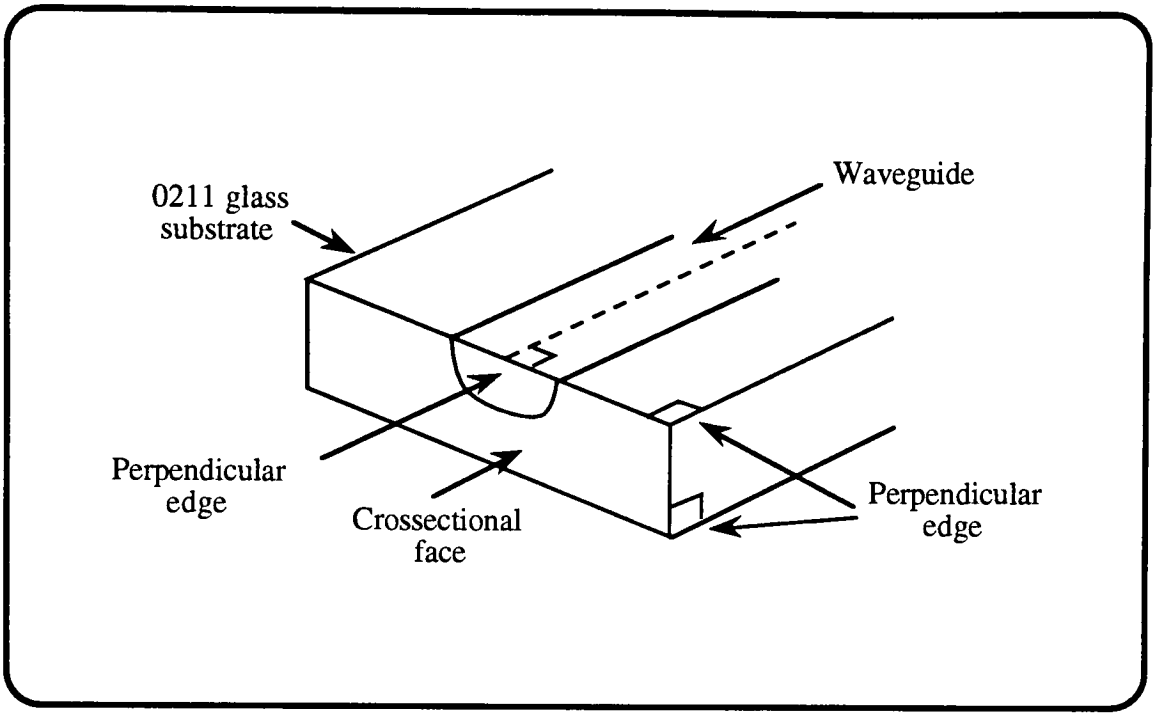

Figure 16: Cross section of the guide

However, these substrates have to be placed under moderate pressure during the diffusion and blocking steps. At this point of time, the scribes propagate cracks which then shatters the glass.

A fancy identification process was devised in order to prevent scribing of the surface. Ordinary wax chips were placed on the glass substrate and heated until the melt coated the surface: Figure 17. They are then removed from the oven and allowed to cool. During this period, identification numbers are imprinted on the wax film with a steel stamp.

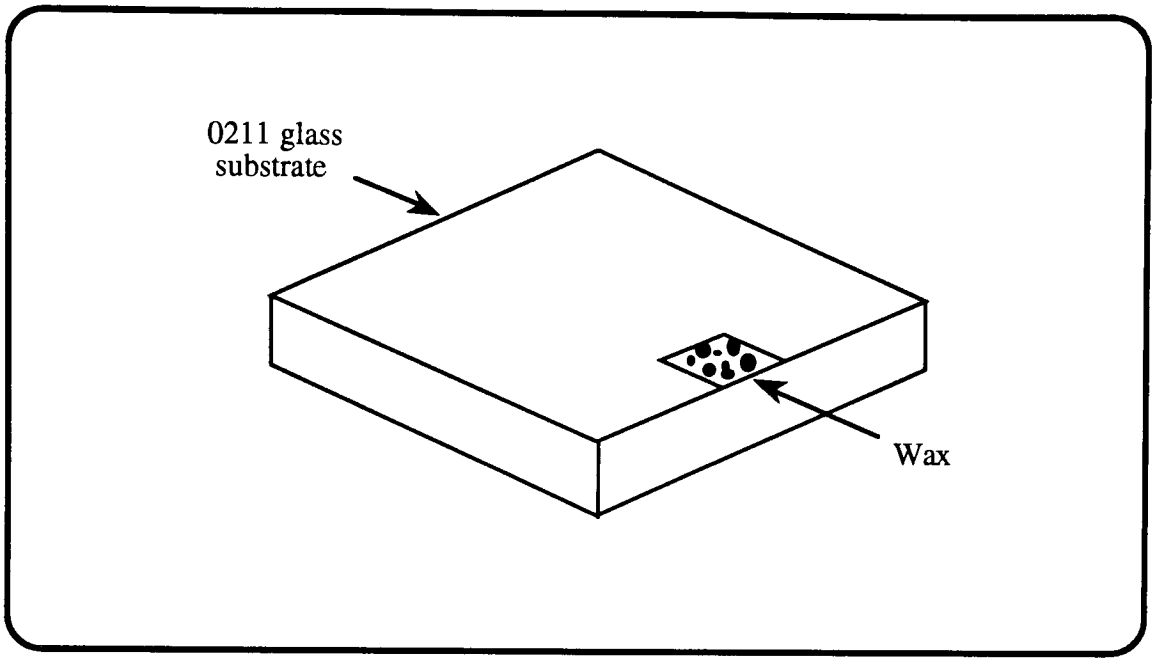

Figure 17: New method of identification

A glass frosting compound* is applied to the indentation on the wax and allowed to etch for 10 minutes. The compound is then washed out in water and the wax scrapped off with a blade.

Care should be taken so that water does not come in contact with the glass in regions other than the waxed areas. Water molecules stick to the surface as adatoms. They then tend to blister the aluminum mask and result in the formation of bubbles on the glass surface. For this reason, it is strongly recommended that only the mentioned solvents are used in contact with the substrates during the entire process.

* Armour etch, The original Glass Etching Cream - Armour products, Midland Park, NJ 07432.

Any remaining wax can be removed with paraffin. Dusting of the substrates should be done with an air brush which is free of oil vapor and condensed water molecules. These could also cause blisters in the Al mask.

It should be noted that no alignment marks are put on at this time. The above mentioned marking process can be done in a non cleanroom environment as long as the substrates are handled by the edges. Any oils deposited from the fingers should be kept at a minimum by the use of gloves. Note that due to the weight of the glass, tweezer handling is not recommended as the substrates tend to slip.

C. Preprocessing

This is a very important step in ensuring good contact between substrate and the different film layers that are to be deposited. It should be mentioned that this step was introduced as a measure to reduce the formation of surface bubbles on the Al mask.

At the start of this project, the substrates were cleaned with a mild soapy rinse solution. They were then air-blown dry and placed in the CVC evaporator. The evaporation appeared to produce a smooth film of Al. However, this deteriorated and a few days later bubbles appeared on the Al mask. This has been attributed to the adatoms being released from the surface.

A heat step was also tried. The substrates were placed in an oven at 85°C for 30 minutes. This also failed to curtail the bubble phenomena. Still a third technique which was tried, was the Argon plasma clean in the CVC evaporator just prior to an evaporation. The ionic bombardment of the surface was supposed to knock off adatoms. Due to the lack of success and hardware related problems, this technique too was discontinued.

The most current technique and one which seemed to provide reasonable reduction in the formation of bubbles, was an O_2 plasma clean. This is used commonly in the microelectronic industry to remove organic photoresist material.

The plasma consists of pure oxygen at moderate pressures and contains reactive species that attack organic materials to form CO, CO_2 and H_2O. These volatile by-products are then carried away by the flow of gas. The plasma is selective in the sense that it does not etch the underlying glass substrate.

The O211 substrate is supposed to be produced by an unique drawn process which produces flawless, firepolished surfaces. While the information is proprietary, it is possible that there is certain amount of oil involved, especially in the cutting process which is cooled by a liquid. The success experienced with the O_2 plasma, could be attributed to the fact that these surface contaminants are removed by the process.

A 20minute clean in the O_2 plasma is very strongly recommended in order to increase yield. The timing associated with the CVC and the plasma clean, should be such that the substrates are placed directly in the CVC ready for evaporation at the end of the 20minute period.

Note: The concern here is that: (1) CVC bell jar is not kept open to atmosphere for any length of time, and (2) substrate transfer time from the O_2 plasma boat to the CVC platen is minimal (heat associated with the O_2 plasma helps in the adhesion process).

Caution: The reader is referred to the O_2 plasma strip operator manual for operational details. Process values given in the lot follower should be adhered too.

D. Al mask evaporation

The substrates are placed on a specially designed platen (used with the CVC) as they are removed from the O_2 plasma.

Caution: Substrates removed from the O_2 plasma contain heat. Care should therefore be exercised in handling.

The platen is designed to hold two 4x4 glass substrates. Another glass substrate, a 4x4 Corning 7059 is placed above the 0211 glass on the holder. This is done to prevent deposition of any back streamed oil; another possible cause that could be attributing to blisters on the Al mask.

Although not critical for this step, it is important that the distance between the coil and the platen remains the same: Figure 18. The crystal monitor has been calibrated for this distance. A deviation from this would require recalibration.

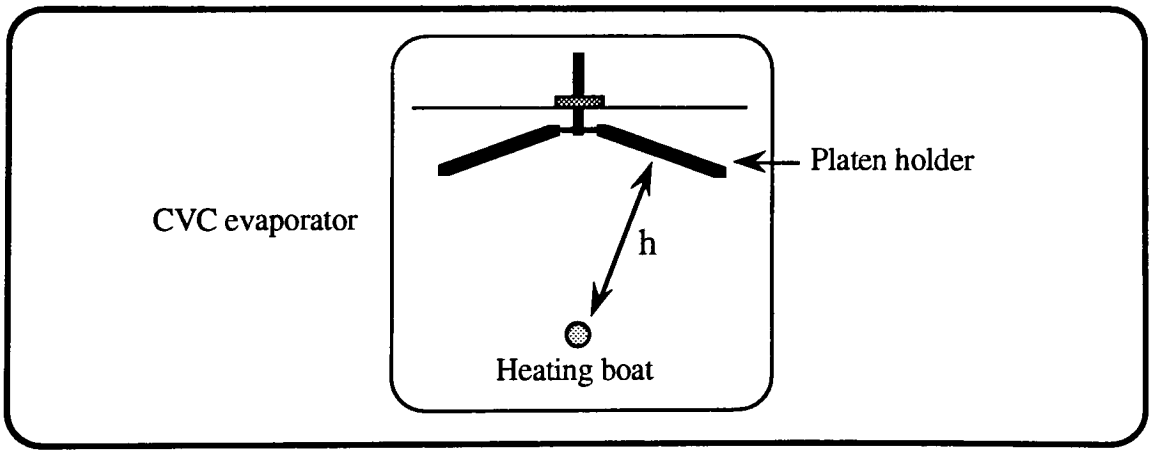

Figure 18: CVC evaporator dimensions

The aluminum pallet used is 99.9995% pure and is available from MRC.* Appendix C4 gives the required data. At least two pallets have to be evaporated to obtain the required thickness of 1.2um. The regularly used helical heating coil** was good enough to hold the Al pallets.

Caution: The CVC requires careful operation. The reader is referred to the operating manual.

The evaporation should be performed at a 170 volts on the Variac. This voltage setting translates to heat applied to the pallets and is therefore proportional to the rate of evaporation. With regards to this, the aluminum mask evaporation did not posed a problem, but has to be taken very seriously during silver evaporations.

Note: The CVC pumps down a lot faster if the cold trap is **filled** with liquid Nitrogen. Partial filling is inadequate. This also helps stem the back flow of oil.

Putting alignment marks is the next step. For this, the substrate is placed on figure 19. Using a blade (not a diamond scribe) and a ruler, the approximate portions indicated in the diagram are marked. This diagram is also available on the lot follower sheets and should be used in the proper sequence during processing.

* Al pallet,MRC, product # 29-13-499-380 MARZ grade (99.9995%)

** Al coil, R.D.Mathis Company, Long Beach CA, product # B1-3X.025W

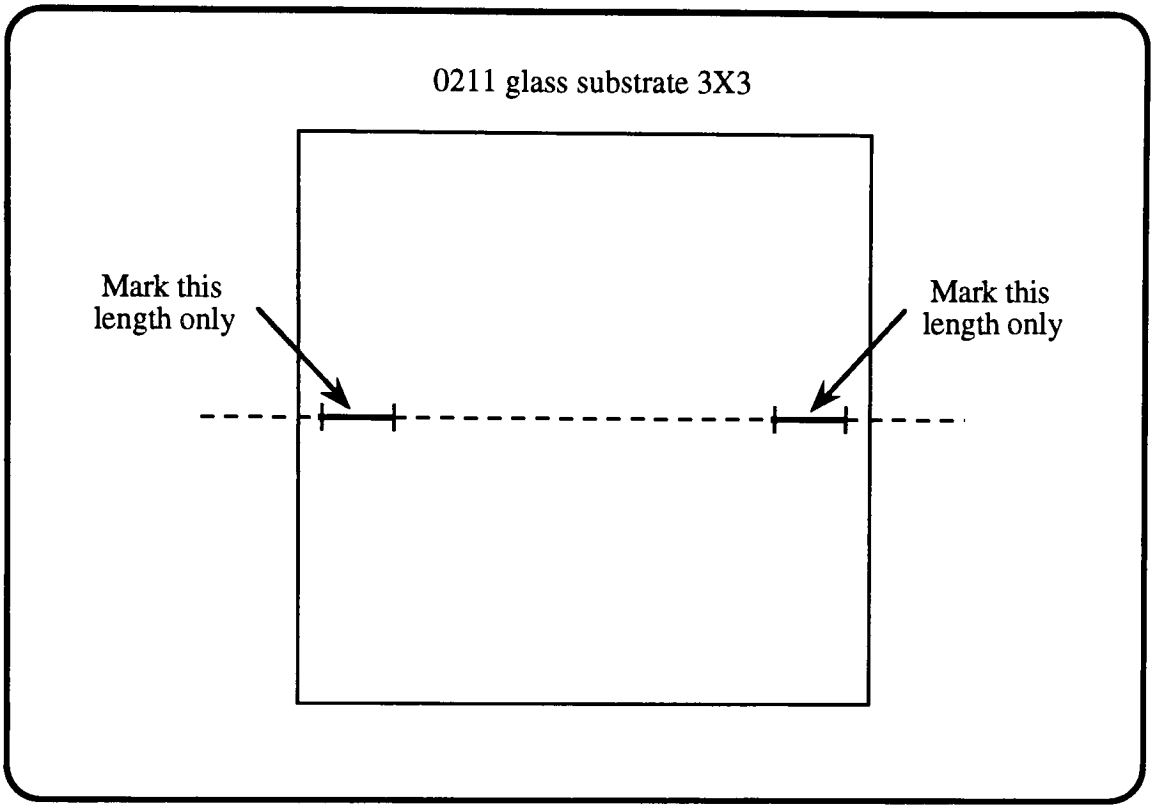

Figure 19: Substrate alignment marks

Post evaporation examinations: The film should show a highly polished surface. The amount of distortion in the back reflection is a direct result of the stress and provides a quantitative means for guesstimation. Minimization is desirable, but has not caused major concern.

Viewing the coated substrates under a microscope with back lighting, shows the presence of any pinholes. Pinholes are not anticipated at this stage of the processing. Viewing the substrate under dark field brings out any topography such as bubbles that are otherwise invisible. This check is important in ensuring a bubble-free starting film.

E. Photoresist coating

The photoresist that was used for coating of the substrates in preparation for the pattern transfer, is KTI 820, and contains 32.5% solids. Due to the weight and square shape of the glass, it is not possible to send them through the wafer track. The spin coating process has to be performed on the manual spinners. According to the data sheets provided for KTI 820, a spin speed of 4500 RPM provides a resist coating of 1.3um. The curve used to extract this data is given in figure 20.

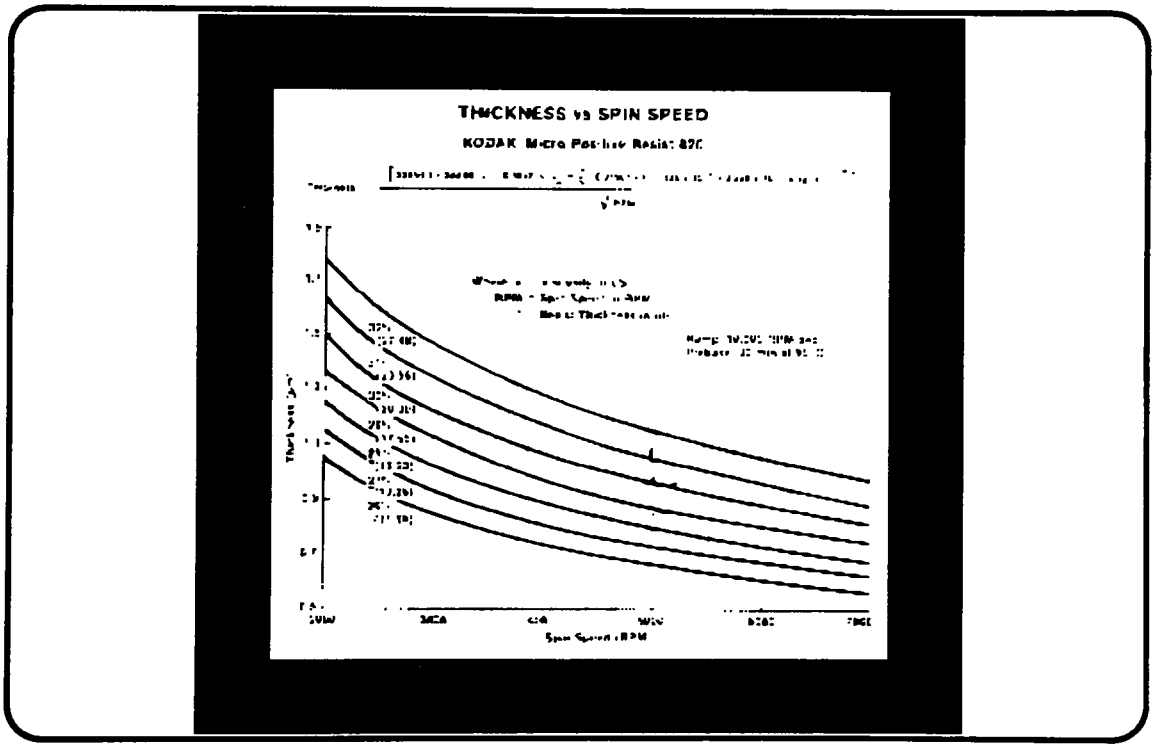

Figure 20: KTI 820 data sheet

An HMDS primer is strongly recommended prior to the coating of resist. This acts as an adhesion promoter between the photoresist and the metal film.

Note: It is important that no particles are present in the pipettes as the liquids are dispensed. These tend to form streaks during the spinning process. They also damage the mask by reducing its useful life, and can be avoided by exercising care during the opening of the bottle.

Once the substrates have been coated, it is necessary to drive out the excess solvents from the photoresist. This is done via a pre bake step at 85°C in the appropriate oven. It is important that this temperature is not exceeded as the photoresist becomes insensitive to exposing UV light, and therefore affects the flood exposure stripping technique.

F. Pattern transfer

1. Alignment and exposure

Now that the masks have been made and the substrates coated, the transfer process can take place via the contact printer.

The shape and size of the substrate require a manual exposure process. The reader is referred to the Aligner operations manual for information regarding this. After the substrates have been brought into the separation mode, the alignment mark on it has to be lined up with the cross hairs on the lithography mask. Note that this alignment is only in one dimension. Care should be taken to prevent scratches on the mask during this step.

A manual exposure using the manual override switch at the back of the machine is recommended. Use of the exposure button on the front panel, causes automatic ejection after the exposure and is not desirable. The time of expose is calculated in the standard manner by first obtaining an irradiance reading from the exposure source.

$$\text{Time of exposure T, in seconds} = 60 / \text{Irradiance}$$

where, 60 is the dosage used.

2. Development

The development again is a manual process. Developer 934 and DI water are used in a 1 : 1 ratio. It is desirable to mix these using 300ml of each in a 500ml beaker. This quantity is needed specifically if two or more batches are worked concurrently. Even though this step by itself needs very little developer solution, it can also be used for the flood exposure photoresist strip step, which requires a lot of developer.

The development time is related to the concentration of the developer solution used. The substrates are processed until all the photoresist is removed, usually about 30 seconds. The time is also affected by the method of agitation. Some agitation is required.

A visual inspection is done to check for complete removal of photoresist. If inadequacies exist, the substrates can be reworked (this is not a recommended procedure).

Note: A post bake is not needed and should not be done in order to facilitate the stripping of photoresist via a flood exposure step, implemented after etching of the Al mask.

3. Etching of the Al mask

This is done in regular Al etchant used in the Microelectronic industry. However, a separate bottle of the solution is recommended to be kept aside for the processing needs of the sodium rich glass. This can be reused and should be stored away with proper labeling.

The recommended operating temperature of the etchant is 55°C. This temperature is recommended in order to achieve the proper etch rate. Etch time is around 45seconds or complete clearing of the guide regions. Care should be taken not to over etch or undercut the aluminum. This causes a rough jagged edge which is undesirable for a diffusion mask.

A post etch inspection is recommended to check for the deterioration of the Al mask. The line widths should be measured using the Nanoline and recorded on the lot follower.

4. Stripping of photoresist

A few different techniques have been experimented with in order to facilitate the removal of photoresist.

During the processing of microchips, photoresist is usually stripped by an oxygen plasma. As explained previously, this plasma contains reactive species that react with photoresist to form heat and volatile products. The gaseous state of reactance and by-products, make this a clean processing technique. However, the use of a plasma strip for our purpose was seen to aggravate the blister phenomena. Bubbles are particularly noticeable after this step. The heat released during the process seemed to be the likely cause.

The flood exposure removal technique was tried in order to avert this situation. The avoidance of a post bake step makes the over laying resist layer still sensitive to an exposure. A flood exposure exposes all regions of the remaining material which is then developed out.

The contact printer can be used for this purpose with an exposure dose of 80mJ. The developer solution of the previous process can now be reused. Unlike the O_2 plasma strip step, this process does not increase the concentration of bubbles.

The substrates are now ready for deposition of the silver films.

G. Deposition of silver

Deposition of the cathode as a first step is recommended. This tends to even out the bow caused by the Al masking film. As long as extensive contact with the substrate has been avoided, a predeposition cleaning step is not needed. The silver used is available from MRC in pallet form and is 99.9995% pure.* The data sheets are given in Appendix D4.

The filament coil that serves the aluminum evaporation was a cause of problems for the silver deposition. As the silver melts, it falls right through the coils and was lost before any significant evaporation could take place. An evaporation boat was the solution to this problem. A plain boat with no interior coatings was first tested.** It was found that while the silver melted and remained on the surface, it had a tendency to work its way up to the electrodes. After a few minutes of evaporation the rate of deposition would fall. An increase in heat via the Variac would only cause the boat to burn out.

The problem was successfully overcome with an Alumina coated boat.*** The barrier of Alumina effectively kept the silver from wetting the boat and thus running back up to the electrodes.

* Ag pallet, MRC, Product # 29-47-499-380, MARZ grade (99.9995%)

** Evaporation boat, R.D.Mathis, Product # S9C-.010W

*** Evaporation boat, R.D.Mathis, Product # S38B-AO

The clamping of these boats to these electrodes was a problem which was overcome by drilling.

Note: Since oil is used in the cooling of the drill bits, the boat has to receive an initial burn-in. Holding the boat at a white hot temperature for 30 seconds is adequate. Careful handling of the boat during installation and removal ensures an extended life.

The singularly most important parameter during silver evaporation is temperature control via the Variac. The cathode deposition does not pose a problem since the evaporation is on a plain substrate. However, it is critical during the subsequent source evaporation. A higher temperature producing a high rate of deposition, causes extensive peeling of the film. This is due to the sudden stress exerted by the hot evaporating molecules on a cool film of Al.

The cathode side of the substrate is placed on the platen and covered with the dummy glass as before. The evaporation is done at 2.5×10^{-5} torr with a Variac setting of 200 volts. The crystal monitor is reset to zero before the evaporation and is monitored up to 3 on the 10 scale. This gives a thickness reading of 1.7 kA: Appendix C5. As stated the cathode silver thickness is not a critical step.

Note: Al was used as a cathode unsuccessfully. Refer to the next section.

Thickness is the most important parameter that determines the depth of diffusion with regards to the source. After completion of the cathode deposition, the substrates are placed with the aluminum mask facing down or towards the boat. As explained previously a slow rate of evaporation is initially done at a pressure of $1.5x10^{-5}$ torr, and a Variac setting of 170 volts. The deposition is temporarily stopped when the crystal monitor reads 3 on the 10 scale, and the substrates and boat are allowed to cool for about 3 minutes. The evaporation is resumed with a setting of 190 volts on the Variac (the increase in temperature allows for a faster deposition rate). It is terminated at a reading of 6.2 on the 10 scale. From Appendix D5, the thickness of deposition is noted to be 3.0 kA:.

It should be noted that since the depth of diffusion is controlled by the film thickness during predeposition, it is possible to vary the depth of ion penetration by changing this parameter.

H. Predeposition

This step is commonly known as the electric field aided ion exchange, and until completely mastered has been a cause of anxiety. To understand the significance and the need for the elaborate apparatus used, we backtrack to the beginning stages.

Initially a hot plate was used. The surface served as a thermal source and a cathode.

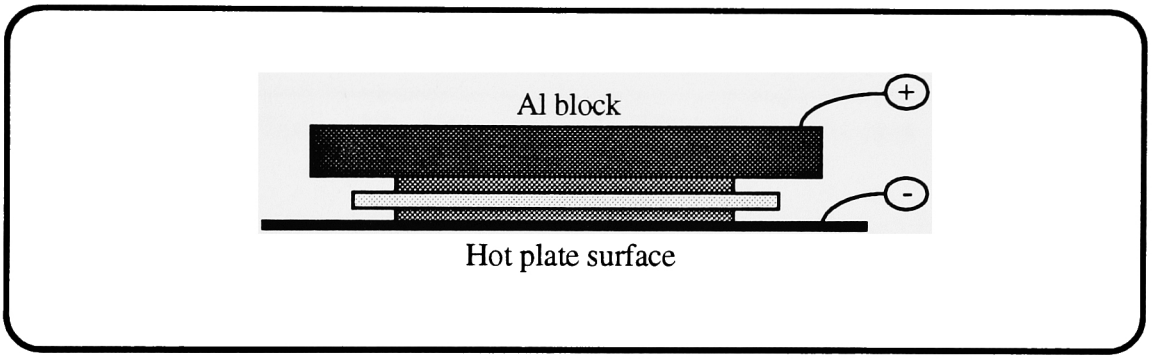

Figure 21: Hot plate diffusion

An Al film was used for the cathode and the substrate set up as shown in figure 21. The anode comprised a block of aluminum which was placed above the substrate and connected to a voltage source. The flow of current was to be detected by an ammeter. As the substrate was heated up the current initially increased, but then fell and remained erratic: Figure 22a. Subsequent stripping of films revealed no visible waveguide formation.

During this phase of the project, a Fisher Oven* was purchased and dedicated for the ion exchange process. The diffusion apparatus initially used with the oven is given in figure 22b. While being similar to the previous apparatus, this too produced no success regarding diffusion.

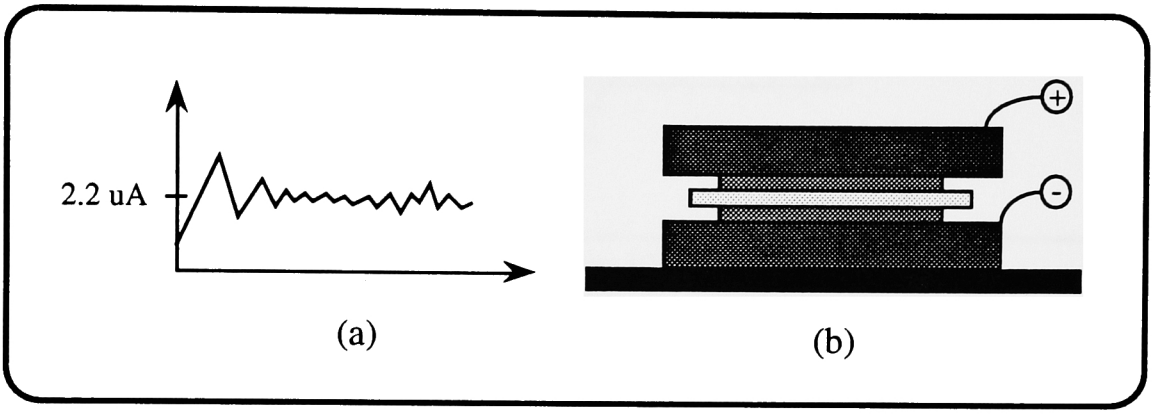

Figure 22: Unsuccessful diffusion apparatus

It was thought that the silver layer oxidized as the temperature was being raised. The erratic behavior of current seemed to indicate breaking contact between the aluminum blocks and the films. Diffusions were attempted for six hours without any success. This consolidates the fact that no appreciable purely thermal diffusion is possible when using the solid thin film technique.

In order to test this postulate the anode and cathode blocks were bolted together in a configuration shown in figure 23. Immediate success was evident in that it was able to provide the current necessary to drive the thermally ionized Ag^+ ions into the glass, and provide waveguiding capabilities within the substrate.

* FisherScientific, Isotemp, programmable furnace, model 497.

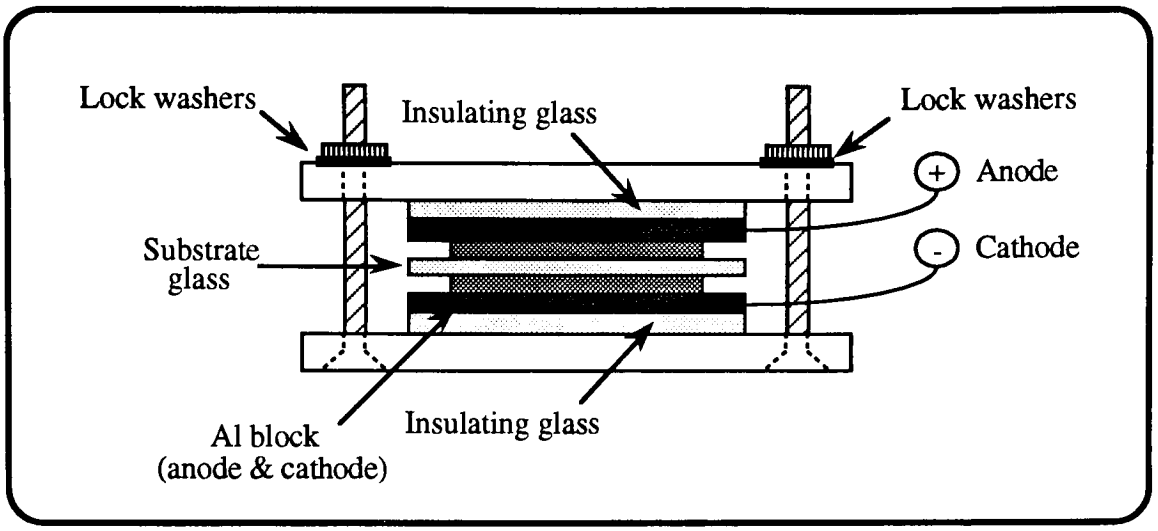

Figure 23: The VP clamp

This provided the breakthrough, but the diffusion itself had other problems. The Al film evaporated for a cathode provided unpredictable diffusions. The out diffusing highly reactive sodium ions attacked the Al cathode film and caused a brownish deposit. This form of electrode deterioration is also reported by Ramaswamy and Najafi.[37].

The use of noble metals like gold or platinum is reported to serve as better electrodes. Since no thermal diffusion had been noted, it was decided to try an Ag film for a cathode too. The success with this film, combined with the ease of process has seen its permanent implementation.

In order to minimize the concentration and achieve better process control, the modified field aided ion exchange apparatus is given in figure 24.

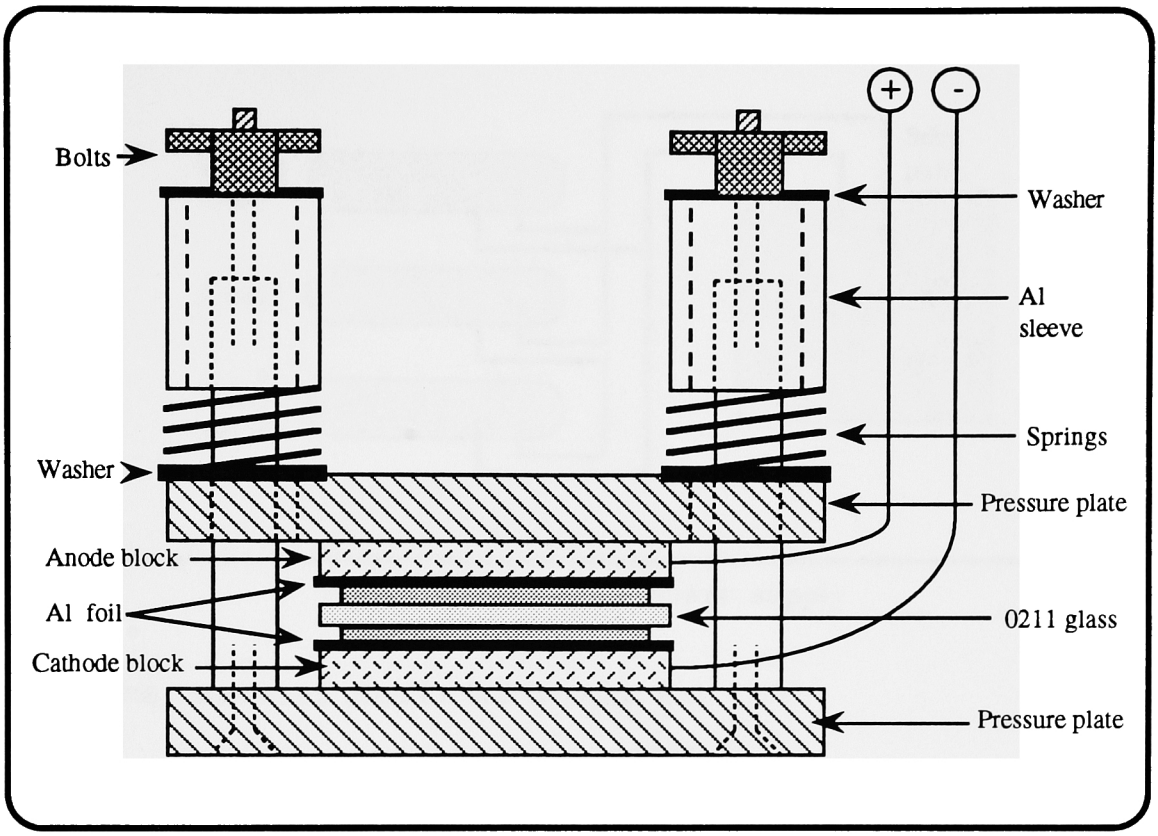

Figure 24: Modified Heintz diffusion clamp

The coil springs are of a special make and are capable of withstanding thermal stress without losing their characteristic.* The cables connecting the apparatus to the power supply are also heat resistant. The voltage supply is wired in, as shown in figure 25.

* Wave springs, Smalley,Steel Ring Company, Product # CO75-L7-S17

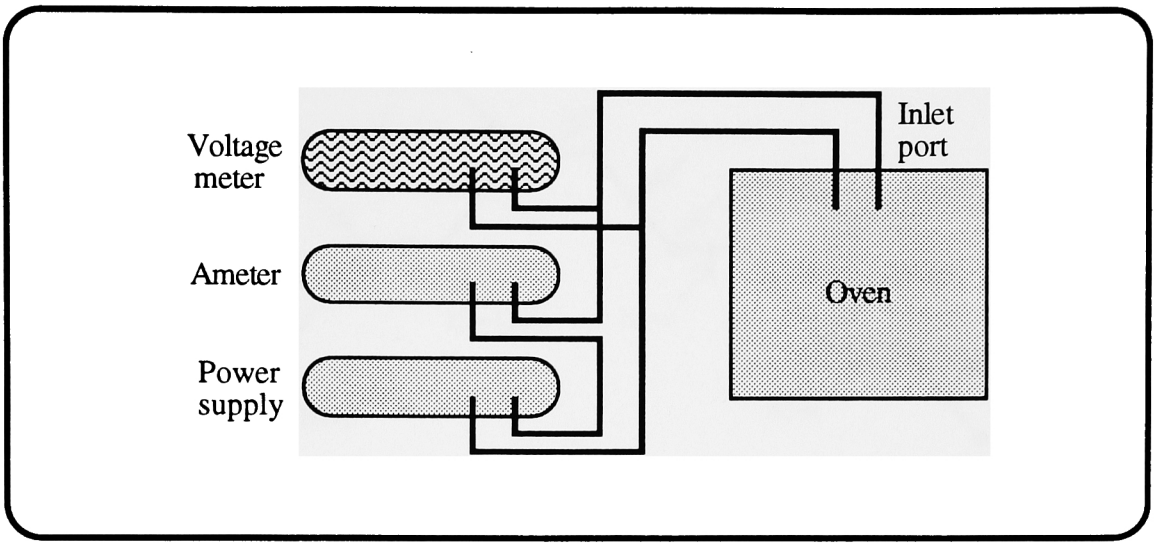

Figure 25: Diffusion power supply

The parameters used for first diffusion are:

Temperature = 270°C

Voltage = 100 volts

Time = 1/20th the maximum current

The oven requires a program which incorporates ramp up, hold and ramp down steps. The ramp up is designed to produce minimum time to achieve a diffusion temperature while preventing thermal shocking. The Fisher Isotemp is a high temperature (1200°C) oven, and has therefore inadequate control in the lower temperature ranges. The overshoot problem was overcome by programing a lower set point and a hold time. The excess heat is converted to an increase in temperature which then stabilizes at the required value. Figure 26, gives the oven program.

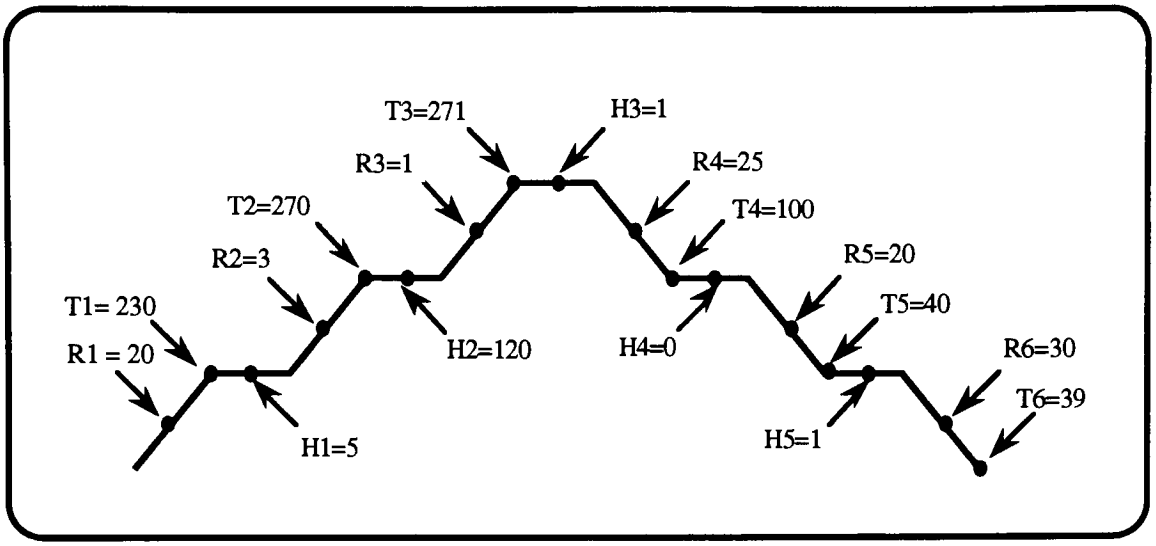

Figure 26: Prediffusion program

It has been suggested by some references that turning on the electric field after reaching the final exchange temperature produces better uniformity. It was found that this was unnecessary:

1) It is better to monitor the current through the ramp up step. This helps in early detection of a short. As the temperature is ramped up, the aluminum foil tends to curl up and cause the short.

2) The following graph shows no appreciable current flow indicating a lack of diffusion during this ramp up step: Figure 27.

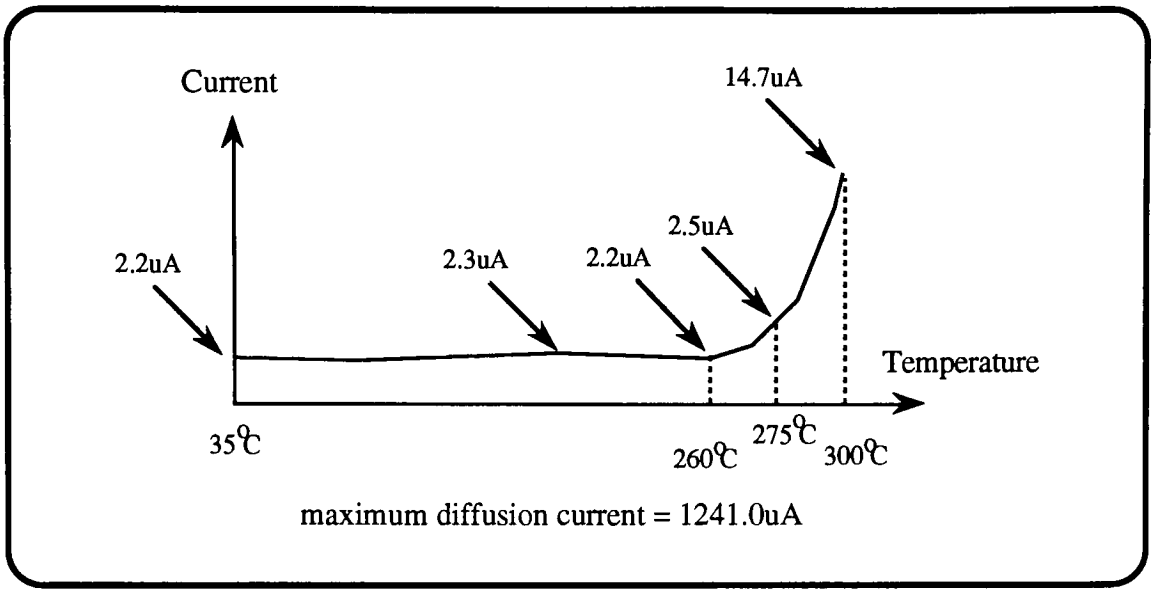

Figure 27: Current during ramp up

As can be seen, very little change in current occurs during the entire ramp up cycle.

I. Stripping of layers

After the completion of the electric field aided ion exchange, all the films need to be stripped off. The silver film is initially stripped in the following solution.

1 liter of H_2O (DI water)

9.5gm of $K_2Cr_2O_7$

12.0ml of H_2SO_4

This solution is mixed and kept in a properly labeled bottle for reuse. The substrates are soaked in it for a few minutes until all the silver has dissolved. This solution does not etch the Al mask.

Potential places where the silver film has given way to pinholes, due to bubbles on the Al mask, can now be viewed by back lighting. The broken bubbles appear as specks of light on an otherwise black background. Dark field illumination shows the bubbles that have not been affected by the process steps and still provide an adequate mask.

The Al mask is then stripped using the bottle of Al etchant.

The process so far, yields glass substrates that are embedded with waveguides which are visible to the naked eye. At this point of time colloidal silver formation due to the reduction of Ag^{+} ions, can be seen as occasional silver speckles. This, as reported by many of the references, is what causes lossy waveguides. It is of no concern to us as the second diffusion step further oxidizes and diffuses these colloidal formations into extinction.

These processing steps do not facilitate the formation of waveguides up to the edges of the glass. Due to the butt coupling technique used to excite the propagating modes, the edges have to be cut back and polished, and is the topic of the next section.

J. Polishing process

This process is not part of this thesis. All the development work was done by Steve M. Ciccarelli, an undergraduate student attached to the Electrical Engineering Department at RIT.

Initially, commercial glass polishing houses were approached with the request to cut back and polish. However, since these places could not meet the spec. requirement of providing an edge with chips less than 1.0um, the process had to be developed inhouse. Flow chart 4, provides these steps and has been reprinted with permission from Steve.

Appendix D6, provides SEM photos of some of the polished surfaces. As a final note, it should be stated that this chip free surface is important in providing uniform injection without loss.

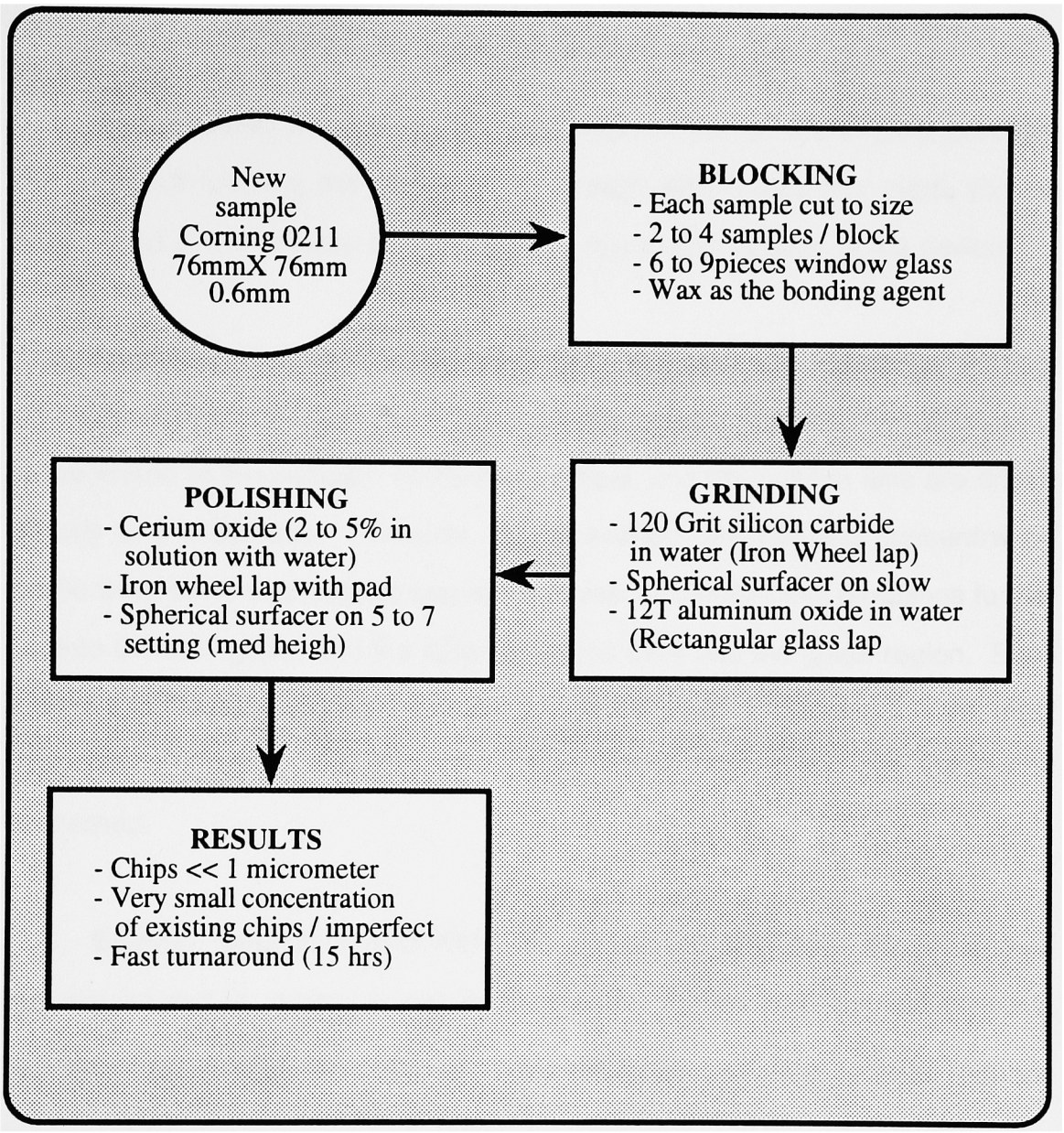

Flow chart 4: Polishing process*

* Reprinted with permission from Steve Ciccarelli.

K. Second diffusion

As previously mentioned, this step was not part of the original process. The need for tailoring the shape of the prediffusion profile has made this an integral part of the process and plays a key role in optimization of the device.

One of the main features of a field assisted ion exchange without appreciable thermal diffusion, is the negligible lateral diffusion. The diffusion is concentrated in the direction of the electric field, and the sodium ions are driven directly to the cathode. However, during second diffusion the concentration gradients of silver and sodium cause the former to diffuse in all directions further out into the bulk glass, and the latter to diffuse back into the guide region. Even though it is the easiest step in comparison to the other processes, it is the most important as far as the High Precision Laser Radar tracking device is concerned.

Eguchi, Maunders and Naik have reported this step as an anneal technique used to reduce losses in waveguides.[36] The heat applied converts any silver atoms back to Ag^+ ions . This reoxidation of silver colloids reduces losses . Attenuation less than 0.1dB / cm is reported.

The second diffusion step serves a dual purpose for this process.

1) Reduces attenuation by redistributing silver colloidals.
2) Converts the profile shape from an erfc with little process latitude, to the required Gaussian with more latitude for design and process.

The purely thermal diffusion step is now made possible by the already predeposited Ag^+ ions: Figure 28.

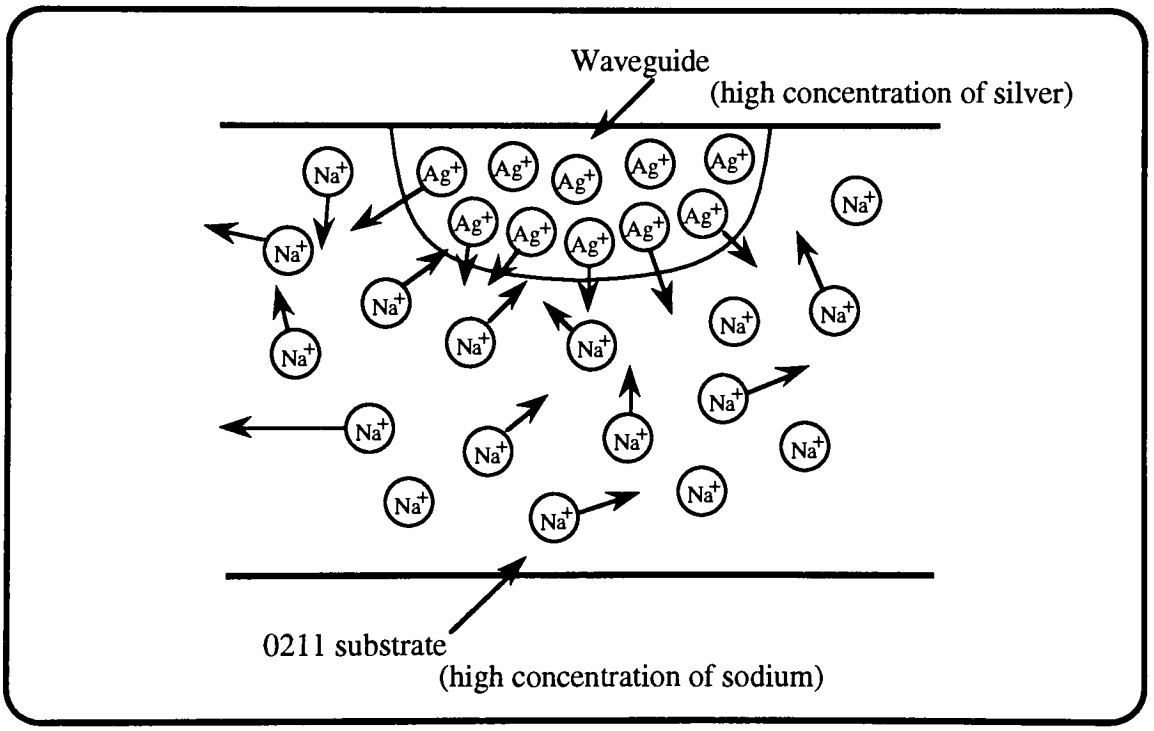

Figure 28: Thermal ion exchange

Except for negligible out diffusion of Ag^+ and Na^+, the total number of ions remain a constant. The redistribution reduces the peak concentration of Ag^+ in the guide region while changing the profile shape: Figure 29.

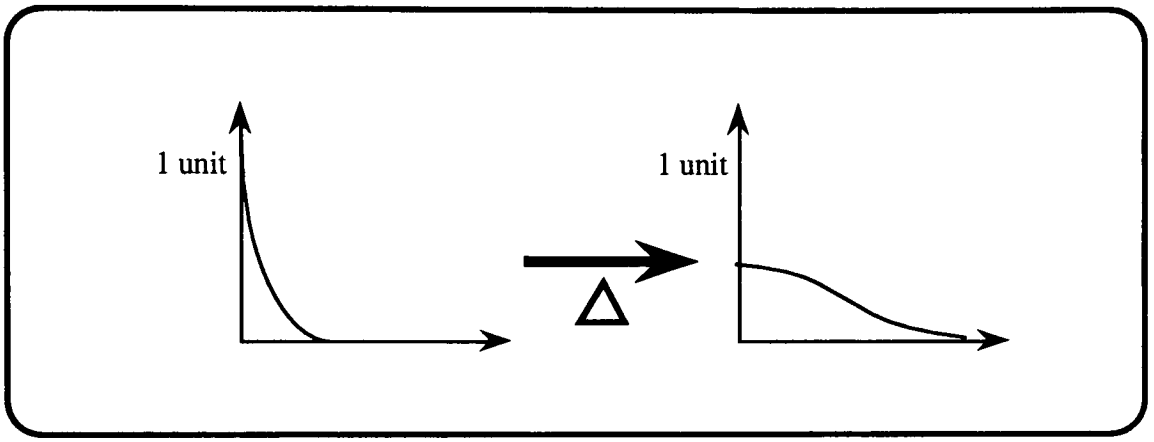

Figure 29: Sample profiles

Simulation of this process tracks this change, and is presented in the next chapter.

Since metallic films are present during the field aided diffusion, the temperature cannot be arbitrarily increased. Aluminum has a melting point of 660°C. However, significant atom movement is evident around 2/3 the melting point temperature or 440°C. The processing temperature has to be kept low because of the bubble phenomena too.

The only upper limit on the second diffusion step is the softening point of glass itself (800°C). Since all metallic films have been stripped off and the substrate cut back and polished, they can be simply placed on a flat block and second diffused. The processing temperature of 400°C for second diffusion was seen to give a moderate processing time of 90 minutes.

The oven program used for second diffusion is given in figure 30.

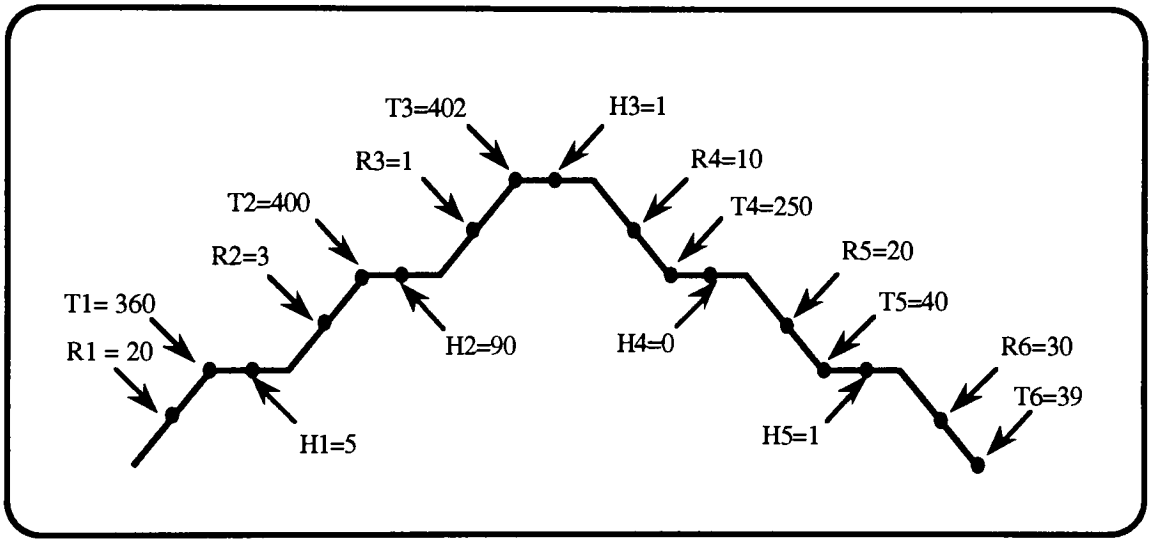

Figure 30: Second diffusion program

While the prediffusion program given in figure 26, contained no anneal step during the cool down cycle, this program does. This is a procedure performed to release thermal stress built up as a result of the elevated diffusion temperatures. It is designed to reduce subsequent cracking and chipping of the substrate which are stress induced. The parameters used were recommended by 0211 glass process engineers at Corning Glassworks.

Selection of the hold time in figure 30, is a parameter purely defined by the performance of the High Precision Laser Radar tracking device. The simulations performed gave an idea of the suitable time window with regards to process, and was incorporated into the original lithography mask design.

L. Testing

The testing process is also not part of this thesis. Readers are referred to the thesis written by Gene Kulp, which covers the entire testing process. A brief discussion follows.

Testing consists of noise limited detector circuitry and computer controlled electronics with data acquisition capability. A highly simplified schematic is given in figure 31.

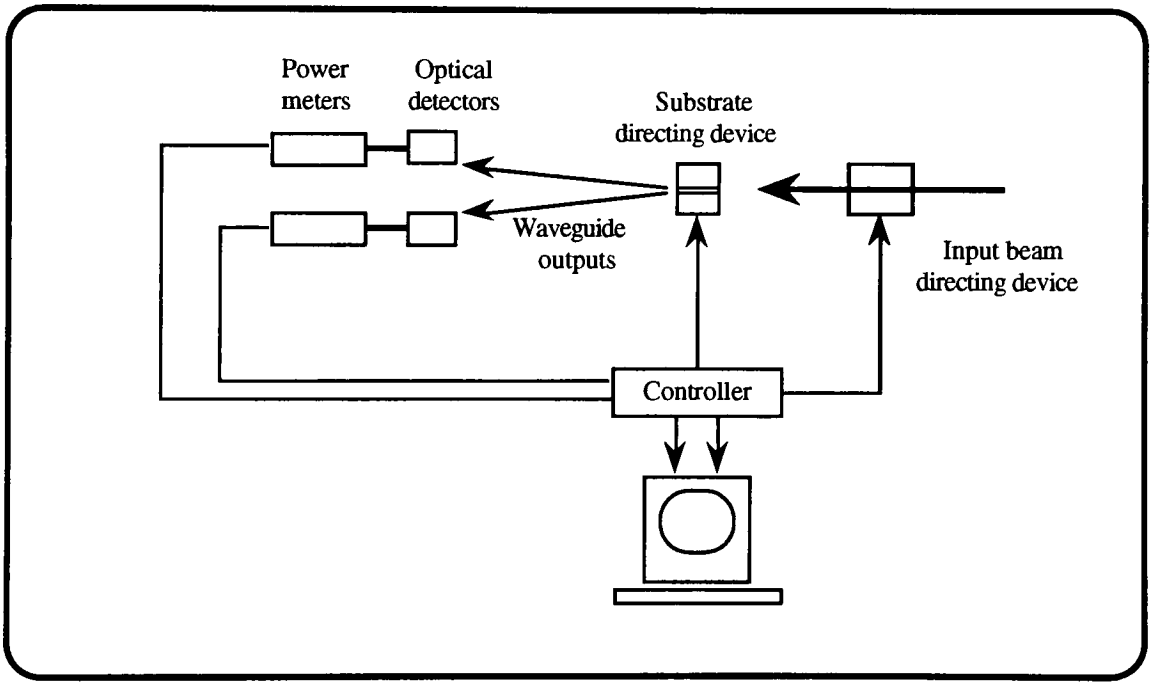

Figure 31: Simplified power detection scheme

A typical power coupling ratio curve, requires a two dimensional scan of the input beam across the front face of the driven guide. The curves in figure 32, are reprinted with permission from Gene Kulp.

As can be seen, tailoring of the second diffusion time yields the optimum power coupling ratio curve: Figure 32a.

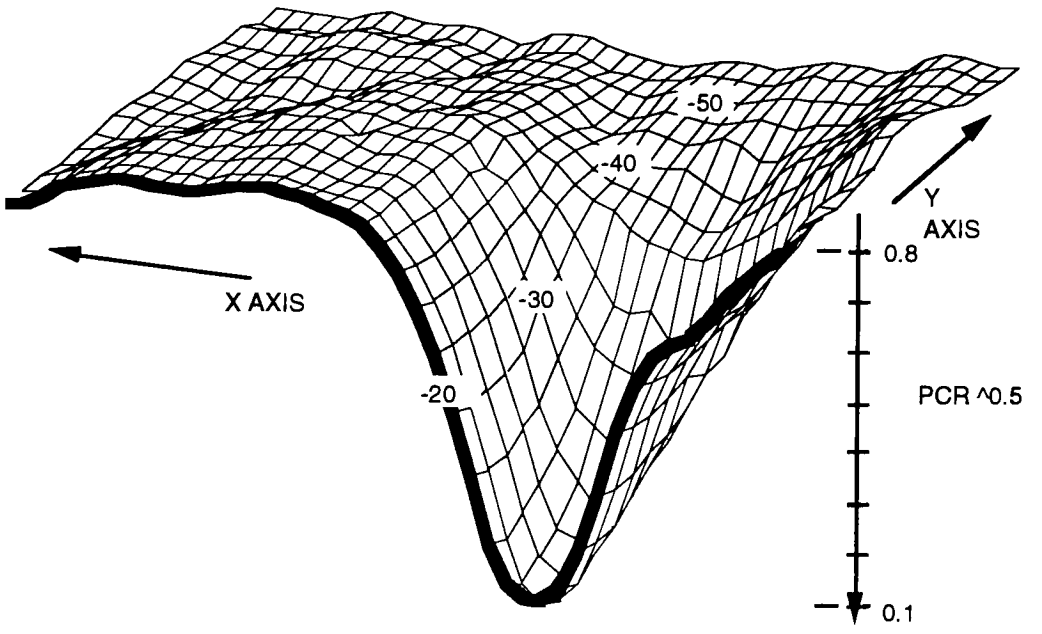

Graph of Power Coupling Ratio ^0.5
At Y Depths below Substrate Surface from -50 to -20 microns
X Position varies from -80 to 0 microns

Steps of 2 microns for X and Y direction
spot size 15 microns diameter

Coupler 15/16 inch long

Figure 32a: 90 minute second diffusion V curve*

* Reprinted with permission from Gene Kulp.

The 60minute second diffusion provided inadequate profile coupling which resulted in a flat bottomed U curve: Figure 32b.

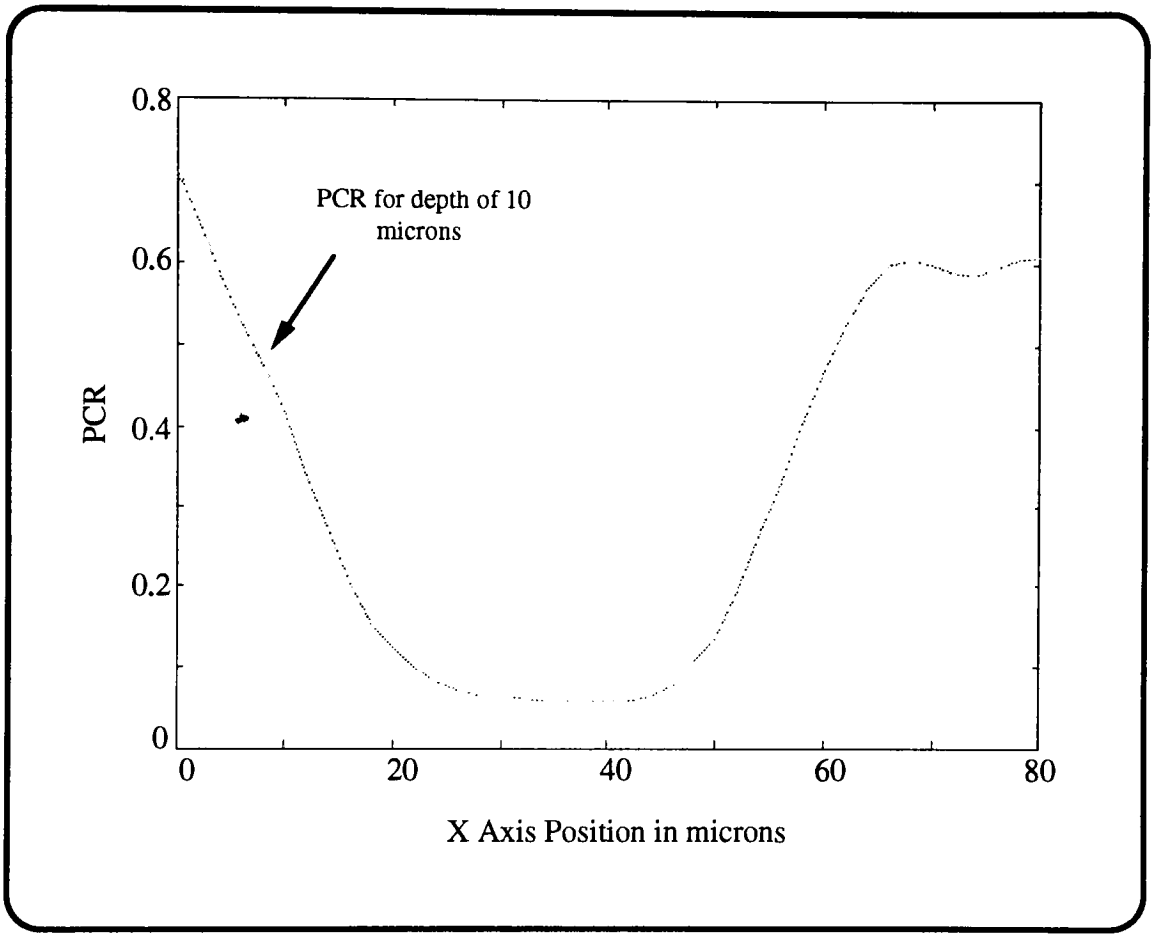

Figure 32b: 60 minute second diffusion U curve*

* Reprinted with permission from Gene Kulp.

Chapter V

Discussion

Most of the process discussion was covered in the previous chapter. This chapter covers the profiling technique used. This leads to a section on profile simulations, and finally to a general discussion on process specifics.

A. Microprobe profiling

While most of the process related problems were solved, the one question that remained unanswered, was index profiling. The inability to determine the shape of the diffused ions, remained a major drawback for the bulk of the project. An erfc profile was postulated for the field aided ion exchange step. However, there seemed to be no means of verifying this. The prediffusion step provided a semi defined shape which was visible. The second diffusion step however, has no defined edge at all. It was impossible to detect the merger point between the two guides.

The back reflection technique was briefly pursued, but dropped due to the complexity involved. The microprobing technique seemed the easiest to implement even though it consisted of a destructive method.

Microprobing was done on the SEM. Backscattered electrons are detected by the machine, which then separates out the concentrations due to the different atoms resident in the glass. This process is made more accurate by the choice of Ag^+ ions. The concentration data gathered is then plotted vs. depth of the electron beam. RS1 curve fitting was done inorder to obtain a profile with the least square error. Profiles obtained from prediffusion and second diffusion are given in the following section.

B. Profile simulations

This section attempts to understand and model the Ag^{+}-Na^{+} ion exchange process in 0211 Coning Glass substrates. The task was primarily undertaken as an independent study. The unbridged version of this report is given in Appendix D1.

The study explains the basic diffusion equation as it relates to field assisted ion exchange. Also explained is the numerical program which was run on a Macintosh Computer. Some extracts of the graphs are given here as they provide valuable information with regards to process windows.

Concentration Vs. Time plots provide interesting information. Figure 33, shows the peak concentration as it varies with time for the 60 min. prediffusion sample. The graph indicates that a prediffusion time of at least 50 min. would be required before 90% of the silver is diffused into the sample. Figure 34, is the peak concentration as it varies with time for the 240 min. second diffused sample. The graph is an indication of time dependence of this diffusion.

A short second diffusion time indicates greater change in concentration resulting in critical control of this parameter. On the other hand, longer diffusion times show less of a gradient, giving rise to a more controlled process. The parameters are designed around the optimum second diffusion time of 90 min.: Figure 35.

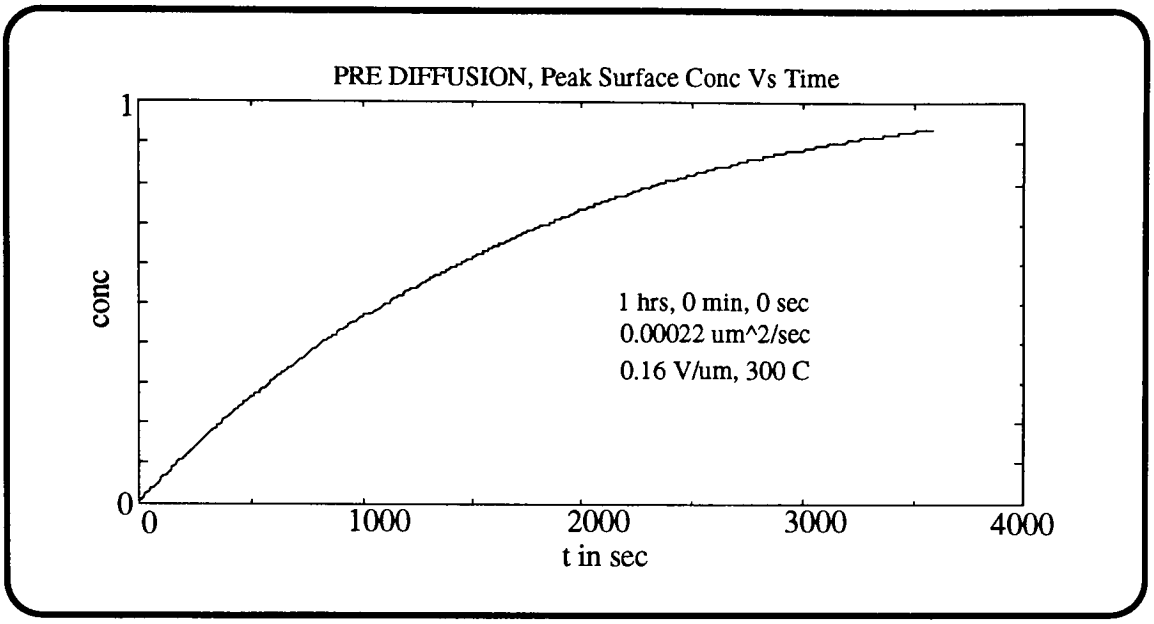

Figure 33: Prediffusion peak concentration

As noted before, merger of the two coupling guides is critical for the device performances. This information is obtained from figure 36, which is a profile plot at different depths into the guide. The inability to understand or accurately simulate the tail regions of the microprobe profiles was a major draw back. The simulation of the 90min profile indicates the merger point to be at a depth of about 30um. This is due to the Gaussian tail (extended tail). However, the short tail of the microprobe profiles would indicate a merger at a depth of about 10um.

It should be noted that the simulated profiles do give a good indication as to its shape.

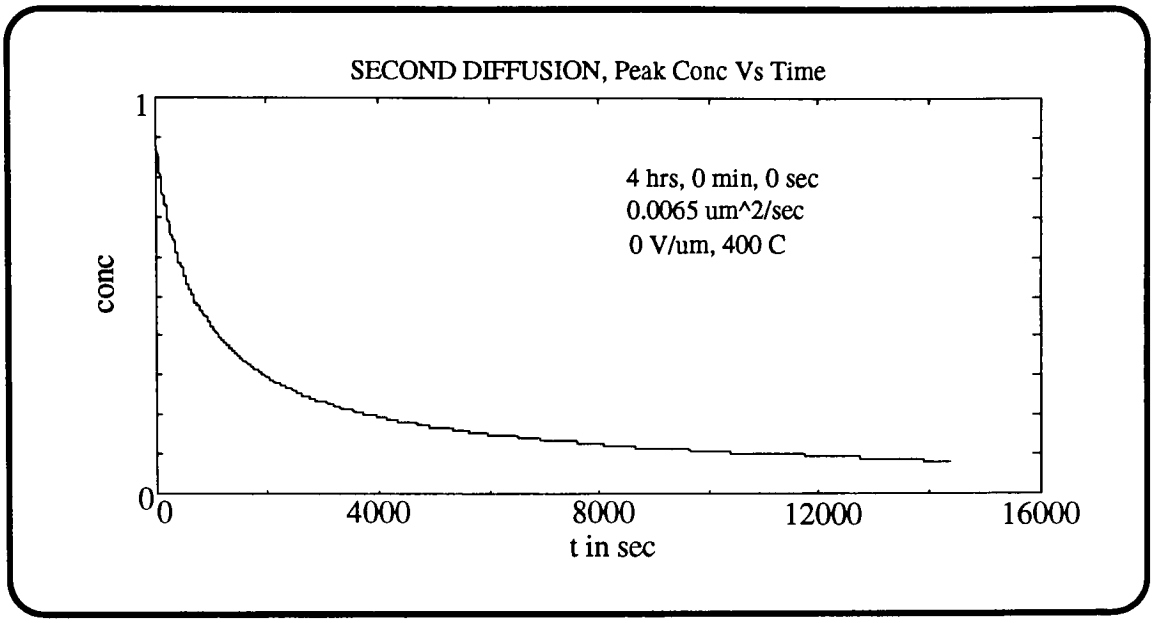

Figure 34: Second diffusion peak concentration

Figure 37, is an unnormalized plot of the 90min sample. Peak concentration of the source is taken to be one. Surface concentration after pre deposit is seen to approach this value. As a result of the source controlled second diffusion process, it then drops to 2%.

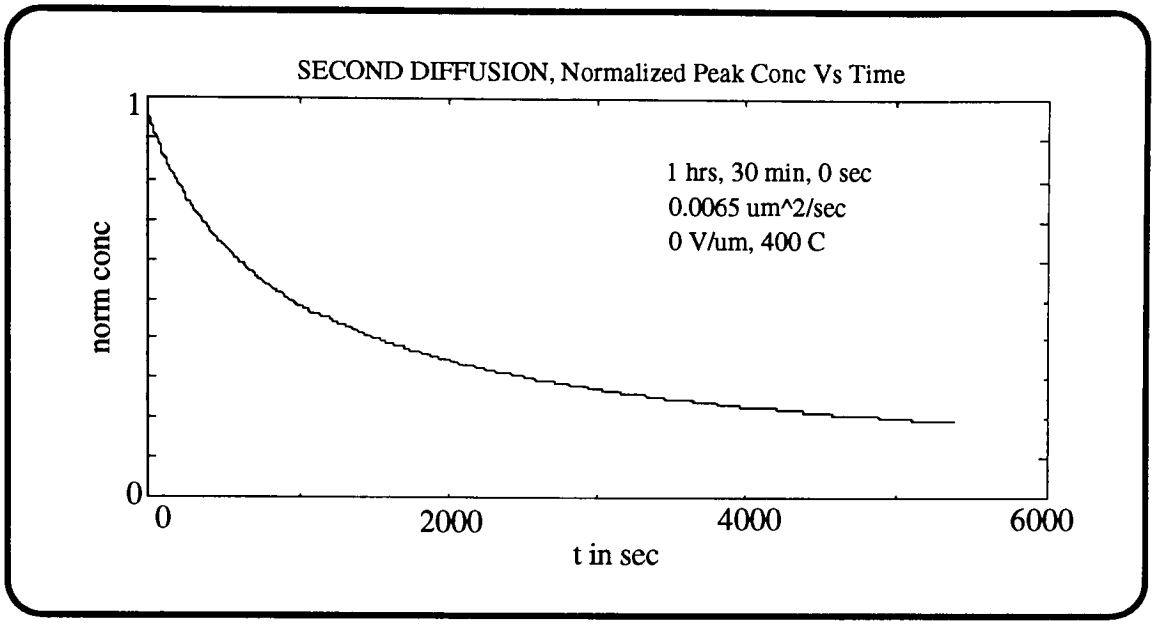

Figure 35: Peak concentration (90min)

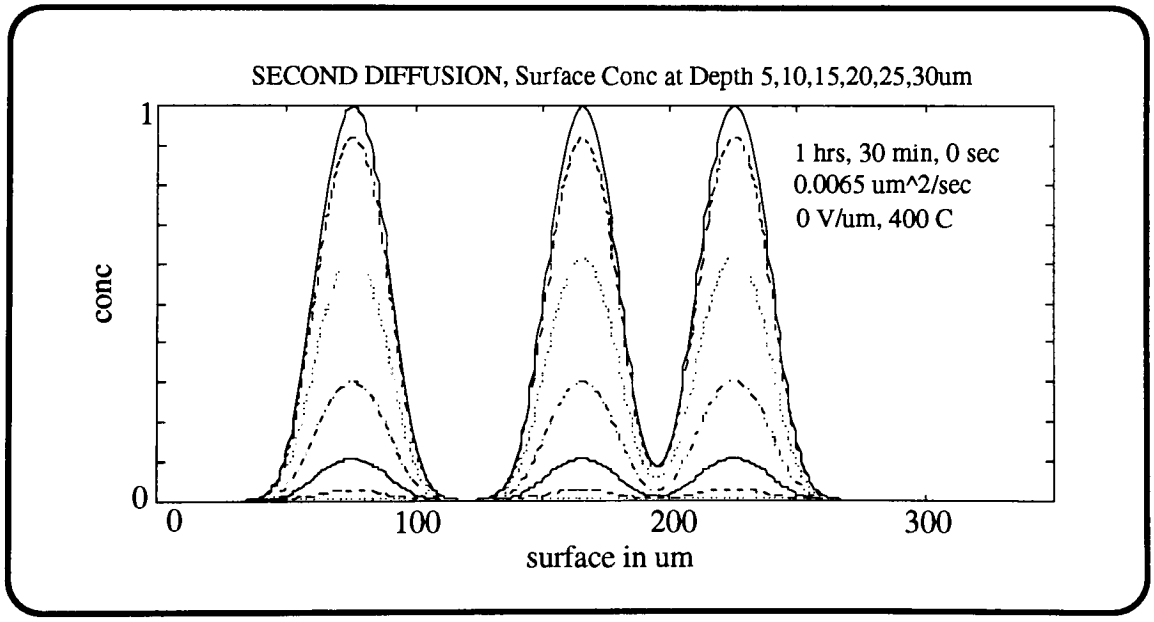

Figure 36: Contour profiles

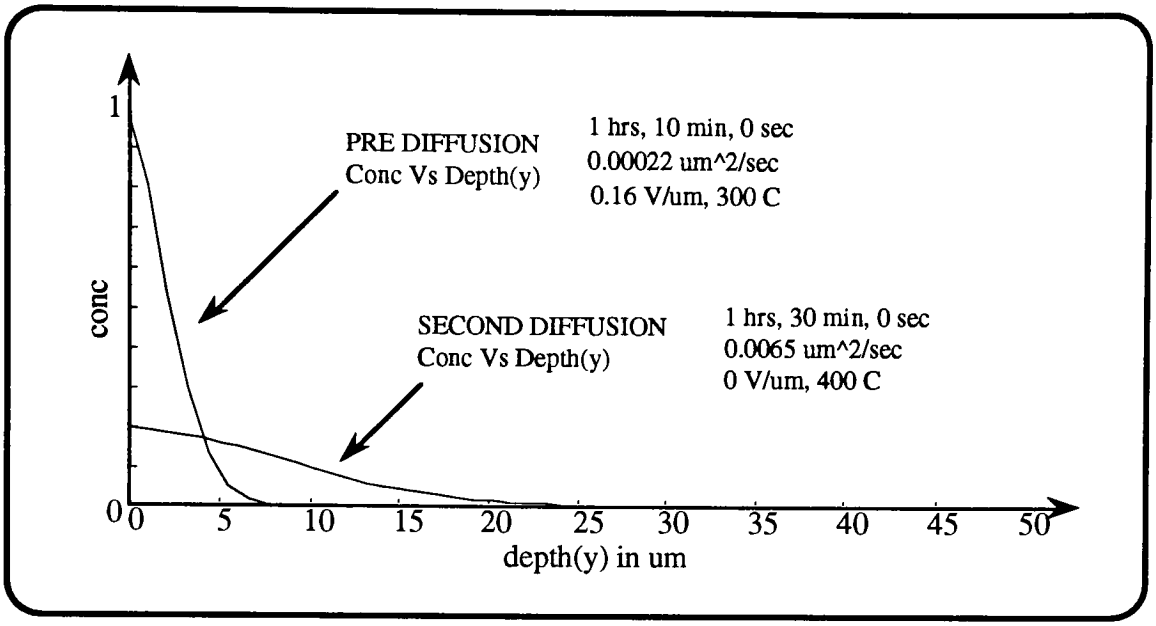

Figure 37: Prediffusion vs. Second diffusion

C. Changes in process parameters

Post electric field aided ion exchange inspection, showed trace amount of silver left in the form of the source film on the surface of the glass in the guide regions. In order to completely drive this film into the glass, the electric field was increased from 100 to 200 volts. This resulted in doubling of the current with shorter diffusion times. However, SEM photos taken during microprobing revealed a well-defined dark band directly below the mask opening:Figure 38.

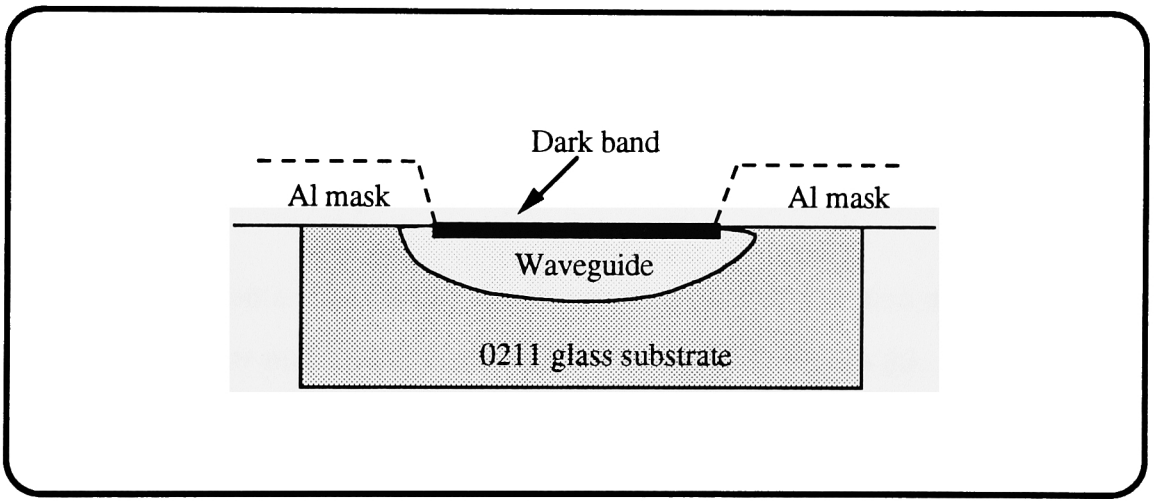

Figure 38: Dark band (drawing of the SEM photo)

When a purely secondary electron signal is displayed, the band does not show up. This indicates that it is not topography related, but rather a concentration related phenomena within the glass. The fact that this disappeared when processing was resumed with the field set back to 100 volts, seemed to suggest a charge related phenomena.

The charge related theory was pursued on the basis of Debby Diffusion length. However, there seemed to be no possible solution in this. Out diffusion theory does not provide an adequate explanation from the concentration point of view. More intriguing was the fact that it appeared to be unique to our specific process, as there were no references made in any of the published literature. The subject was dropped with the note that no further occurrences were detected since the change back to 100 volts.

Another phenomena noted was the saddle shape of wide waveguides (50um). This is typical of field aided ion exchanges and is explained by the differences in field strengths. The field strength is strongest at the edges when compared to the center.[38]

The placement of parallel guides in close proximity, also shapes the field lines in a manner that yields asymmetric waveguides: Figure 39.

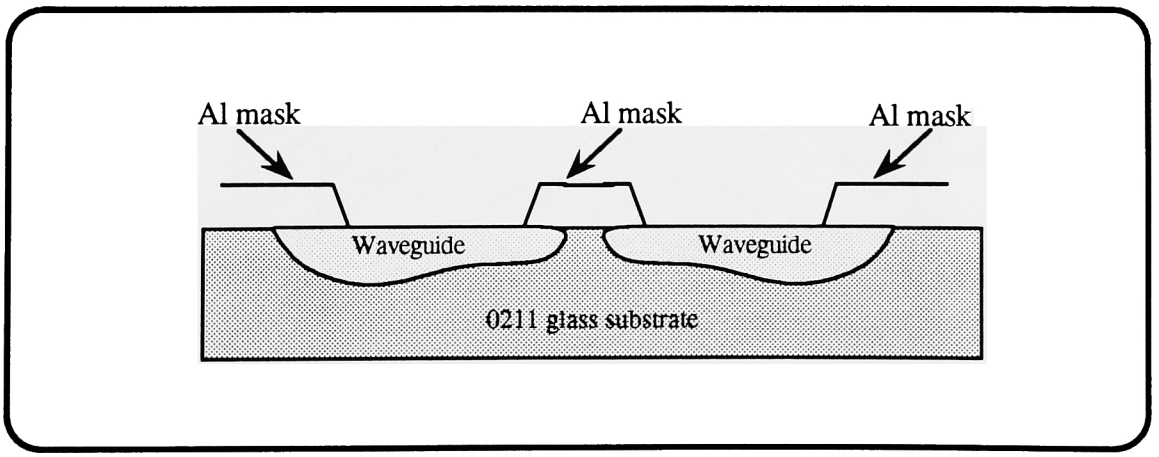

Figure 39: Asymmetric guides (drawing of the SEM photo)

It should be noted that the initial film thickness was the same, and because greater than 95% of the film was diffused into the guides, the total number of ions in each guide is approximately the same. This uneven first diffusion is negligible when compared to the depth of the second diffusion, and is therefore not a cause for alarm. It should be noted that a few minutes of extra diffusion, after the electric field had been turned off during the predeposition step, evened out this saddled shape.

The bubble phenomena which has been referred to periodically, is discussed here in further detail. Bubbles on the surface of the glass were first noted when examining the substrates after the field assisted ion exchange. They appeared to be circular in shape with a well-defined boundary: Figure 40.

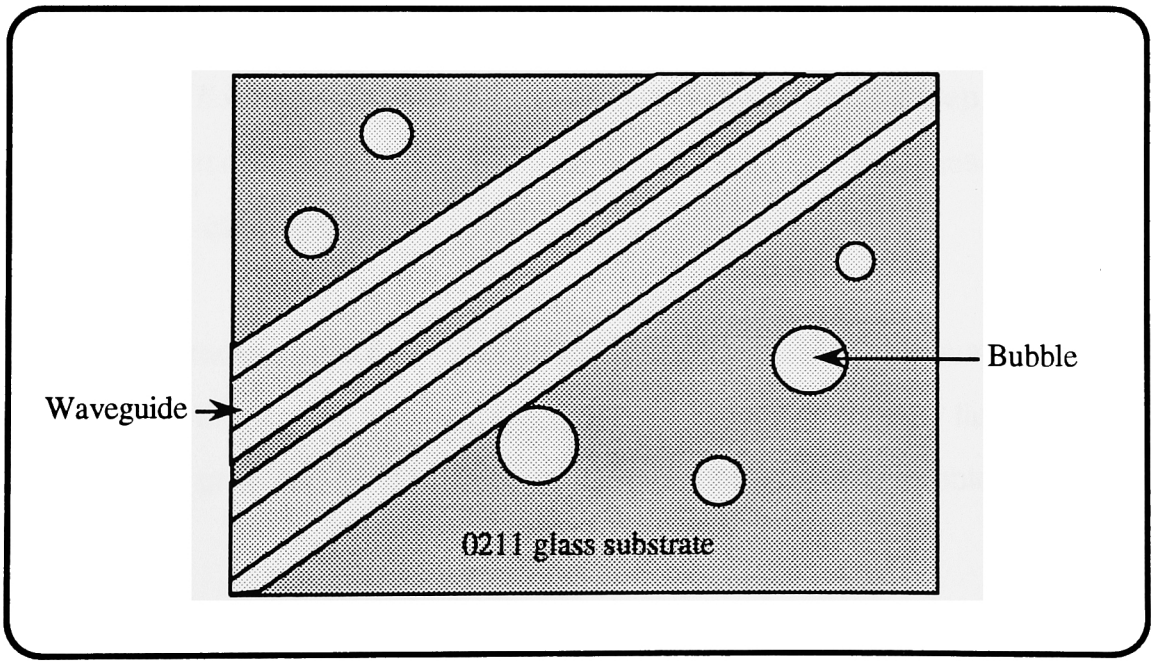

Figure 40: Bubbles (drawing of the SEM photo)

SEM examination of these guides could not detect topography. However, the back scattered signal seemed to indicate the presence of Ag^+ ions in these regions. It was assumed that this was the result of the diffusion process where silver penetrates the aluminum mask. The Al diffusion mask was deposited thicker. Modifications were also made to the diffusion apparatus. While these actions caused some reduction of bubbles, they were still present in numbers enough to cause concern.

Further scrutiny showed the bubble formation on the Al mask just prior to the deposition of silver. It was postulated that these bubbles burst during the exchange process bringing the silver in contact with the glass. The electric field in turn caused the diffusion, which resulted in bubbles in the glass.

The initial process as mentioned, consisted of an O_2 plasma strip of the photoresist. Examination of the Al mask before and after this step, revealed a drastic increase in the number and size of bubbles. The heat associated with this step was causing this.

The process was then changed to a flood exposure removal technique. Adhesion of the Al film seemed adequate to withstand another fluid process. This change provided an adequate solution by reducing the bubble count and size.

In an attempt to determine if it was indeed the heat that was causing the problem, an ion exchange was tried at a reduced temperature; 270°C instead of 300°C. Examination of the Al mask after diffusion and stripping of the remaining silver, revealed a smooth film consisting of only an occasional blister.

The first diffusion was thus changed to a process temperature of 270°C. An important point to note here is that this drop in temperature does not significantly alter the shape or depth of the profile.[25] The lower processing temperature also produced a smooth drop during the later stages of the prediffusion, when compared with the 300°C process which yielded an erratic drop: Figure 41.

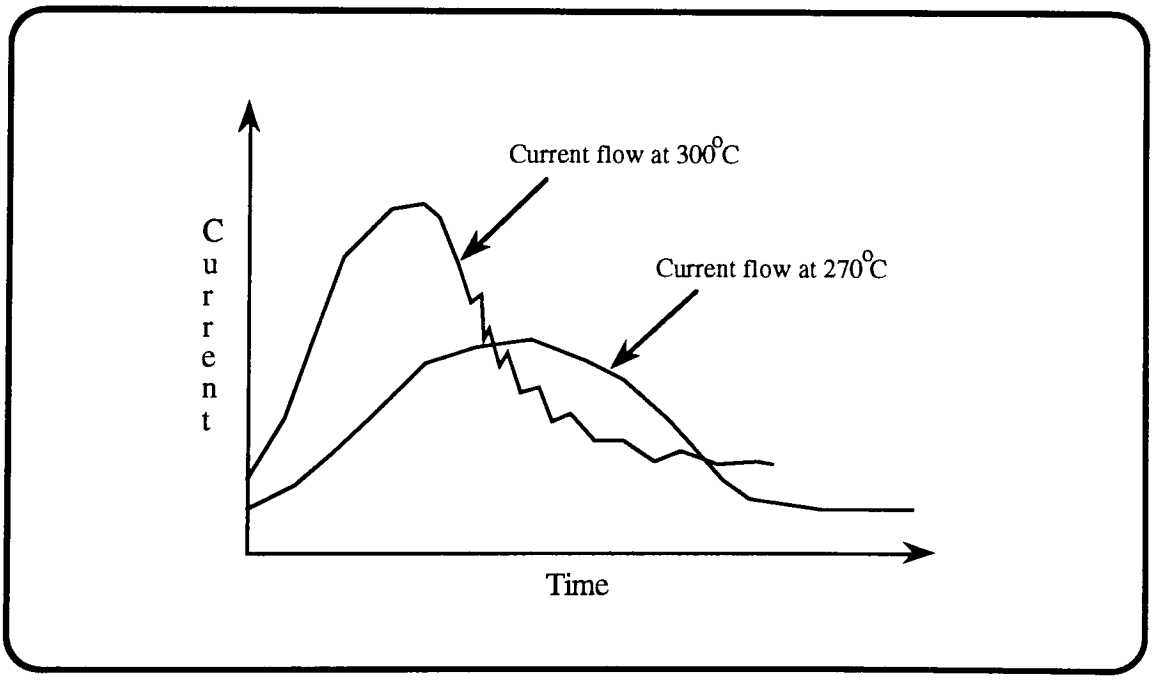

Figure 41: Simulated current flow

Figure 42, is a plot of the actual current flow at processing temperatures of 270°C and 300°C.

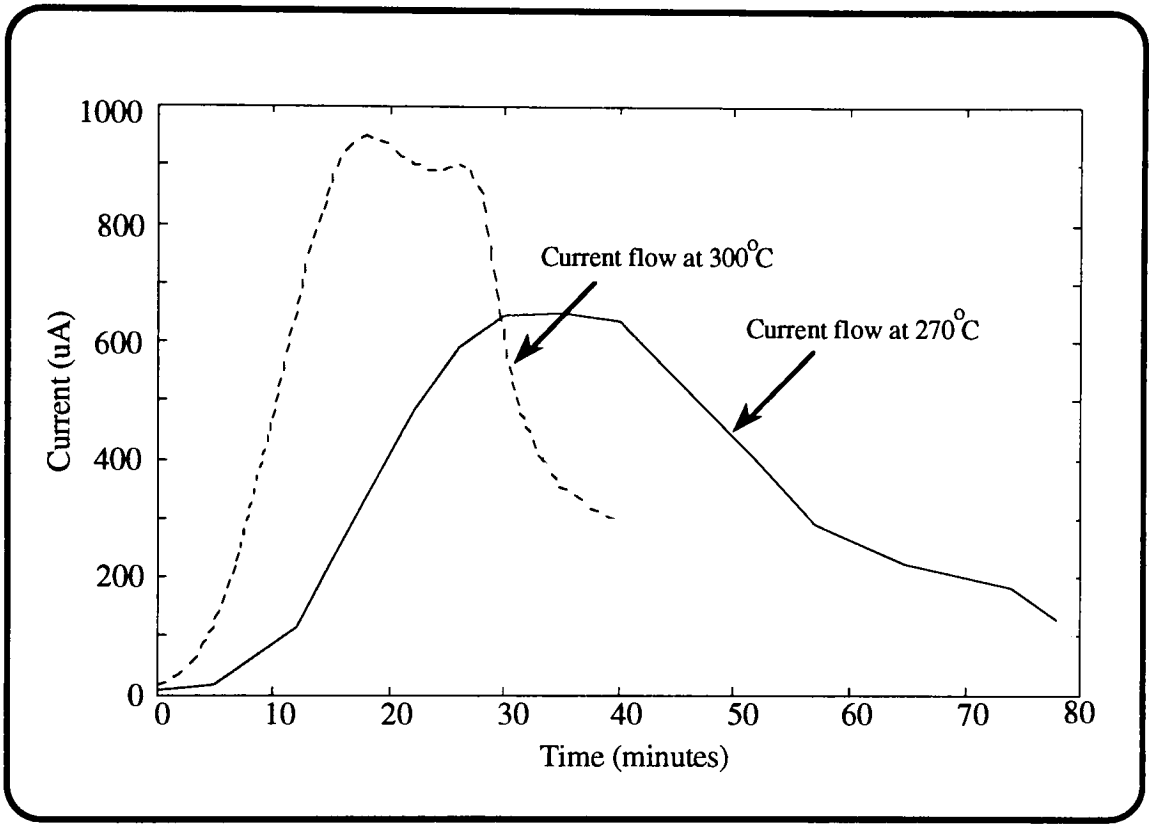

Figure 42: Actual current flow

The process calls for stoppage of the electric field aided ion exchange when the current falls to 1/20th the maximum value. This ensures process consistency.

D. Recommendations

When the Simple Coupler design was first tested, the process consisted of only the prediffusion step. These tests showed no signs of coupling. The initial second diffusion step provided coupling which resulted in flat-bottomed PCR V curves. It seemed that while the profiles were merged, it was inadequate. As a result, only the highest order modes were coupling into the coupled guides. Figure 43, shows a theoretical flat bottomed curve with respect to the input point of excitation.

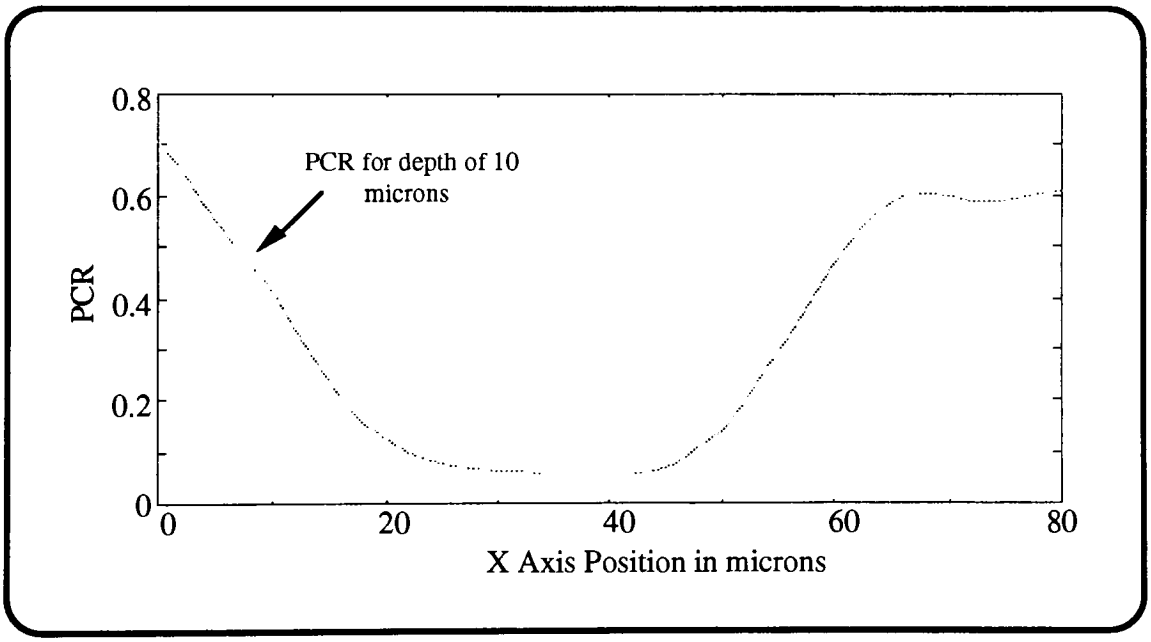

Figure 43: Flat bottom U curve

At this point, an increase in the second diffusion time from 60 to 90 minutes, provided the optimum V curve. The increase in diffusion time, resulted in more outdiffusion of the silver ions, giving a profile with more of a merger.

The profile merging point acts as a filter. An increase in the overlap of the profiles, result in a greater number of low order modes being coupled into the coupled guide: Figure 44.

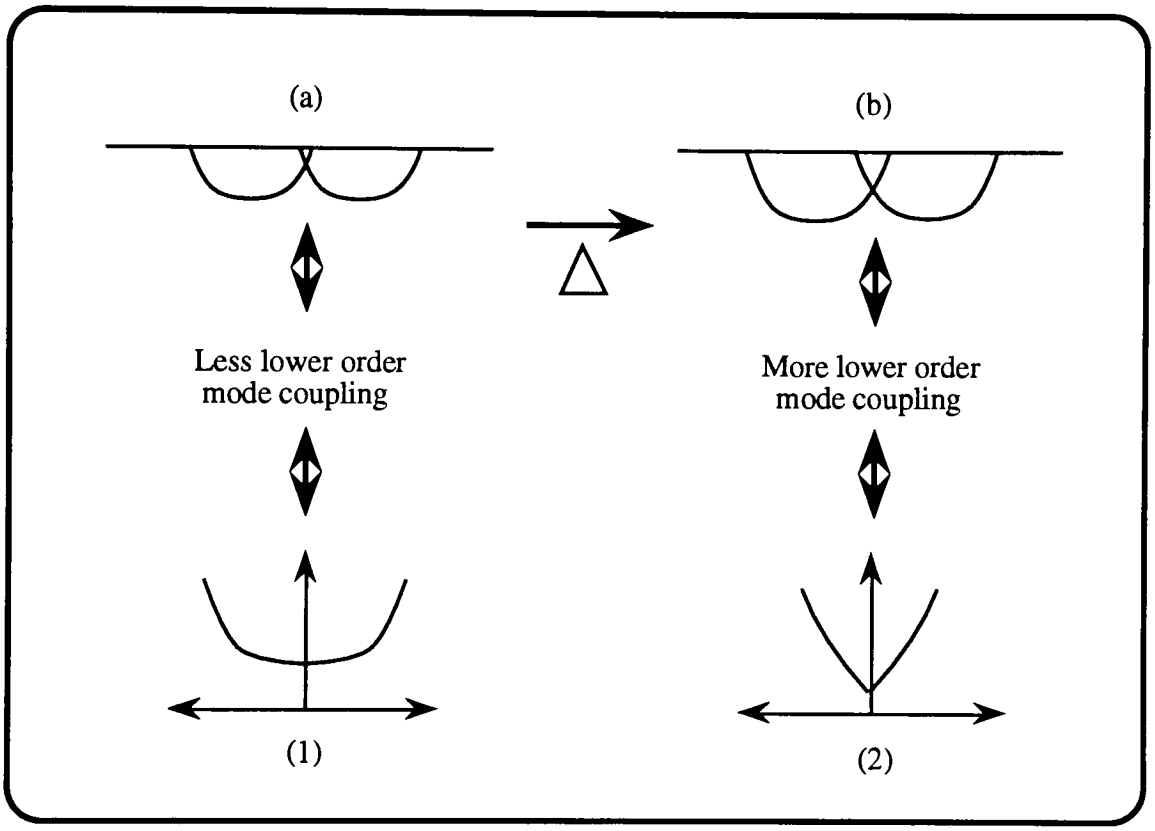

Figure 44: Profile merger

PCR curve (2) was the result of profile (b), which was the cause of thermal energy addition to profile (a), which otherwise produces PCR curve (1).

The compound coupler has been processed using the same parameters which yielded the optimum V curve on the simple coupler. However, this produced a flat bottomed V curve as shown in figure 44a. This discrepancy is due very likely to the design change which utilizes less of a coupling length for each individual coupling leg. Coupling length also affects the coupling property of each mode.

Since the length of the compound coupler cannot be varied significantly, this line of reasoning leads to the obvious solution, an increase in second diffusion time. It is recommended that the existing design be utilized on a compound coupler, with the only process change being in the length of second diffusion time. Experience gained from the optimization phase of the simpler coupler seems to indicate an increase from 90 to a 120 minutes. This should result in a deeper profile with an increase in overlap, resulting in greater coupling of the lower order modes.

An important observation from the simulations, was the drop in peak concentrations. As demonstrated in figure 37, due to the exponential nature of this graph, a significant drop is not expected. However, the increase time, could result in PCR curves that lack sensitivity and give shallow sidewalls: Figure 45.

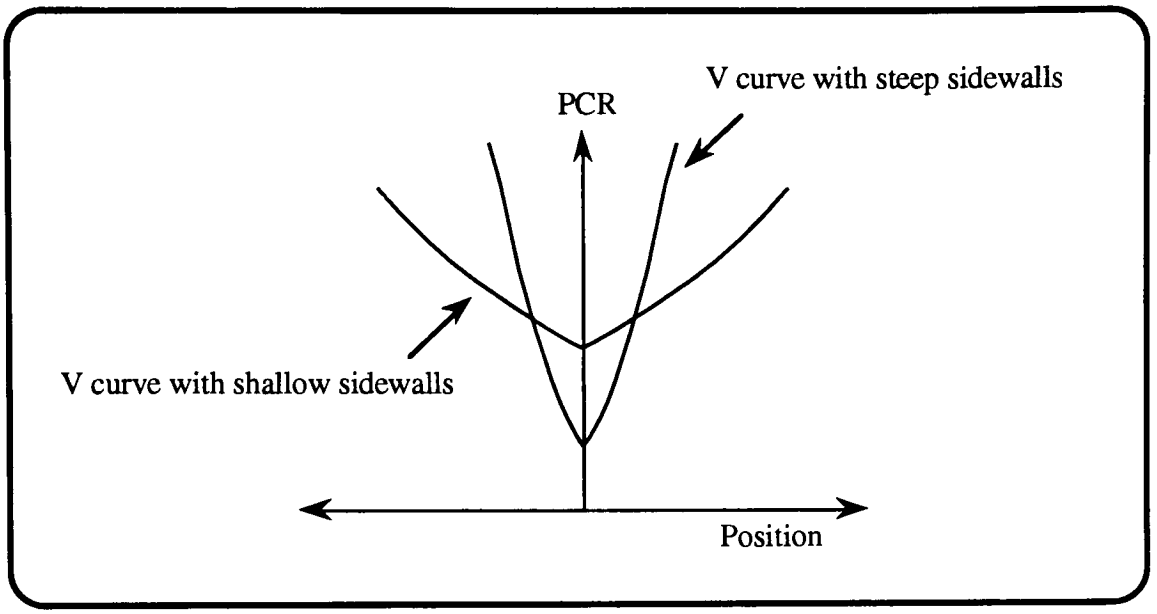

Figure 45: PCR sensitivity

A possible solution for this would be to try an increased silver film thickness prior to prediffusion. This higher peak concentration would result in a correspondingly higher second diffusion profile peak.

As is the case with almost any new process, until all related parameters and their effects are reasonably understood, the yield levels will remain in single digits. The testing process at this point should be exhaustive. With regards to this project, since even the testing process itself is not clearly understood, it is very strongly recommended that every available compound coupler be tested extensively for the two dimensional PCR V curve.

E. Conclusion

In conclusion with regards to the process aspect of Integrated Optics, and specifically the High Precision Laser Radar Tracking device, a high degree of success has been achieved with a two step Solid Silver Ion Exchange process. Success is evident from the simplicity of the process, while the device itself has proved itself through the PCR V curves obtained from the two dimensional tests. The V curve obtained from the fabricated device (figure 32a), demonstrates increased sensitivity when compared to the commercial coupler tests (Appendix A1, A4, A5, A6).

Recommendations have been made with regard to optimizing the compound coupler. The process, while being delicate, is simple and needs no special measures. However, due to the shape, weight and sodium content of the substrates, care should be exercised in the implementation of this process in a Microelectronic cleanroom facility.

References

[1] M.I.Skolnik, *Radar Handbook, McGraw-Hill Book Co.*, Chapter 21-Tracking Radar Performance, p.46, 1970.

[2] Defense Science and Engineering, *Sensors for SDI*, p.36, May 1987

[3] Gerald F. Ross, A Novel Fiber Optic Multimode Feed for Monopulse LIDAR Antenna Application - Phase II, Project Summary, Submitted to Strategic Defense Initiative Organization, 1988.

[4] J.DeLorenzo, Walter K.Kahn, Robert E. Pearson, Gerald F. Ross, David A. Sumberg, Lorraine D. Treacy, Fiber Optic Multimode Feed for Monopulse LIDAR, Phase 1 Final Report, Contract No. DNA 001-87-C-0041, Sept. 1987.

[5] J.E.Gortych and D.G.Hall, Fabrication of Planar Optical Waveguides by K^+ Ion Exchange in BK 7 and Pyrex Glass, *IEEE, J. Quantum Electronics,* Vol. QE-22, p.892, June 1986.

[6] H.Kogellini, Limits in Integrated Optics, *Proceedings of the IEEE,* vol. 69, p.232, Feb.1981

[7] M.Young, Optics and Lasers, Springer-Verlay, N.Y., p.3, 1984.

[8] J.Senior, Prentice-hall International Series in Optoelectronics, Englewood Cliff, N.J., p.22,1985.

[9] V.Suematsu and K. Iga, Introduction to Optical Fiber Communications, John Wiley and Sons, N.Y., p.13, 1985.

[10] P.K.Tien, R.Ulrich and R.J.Martin, Modes of Propagating Lightwaves in Thin Deposited Semiconductor Films, *Appl. Phy,* Vol. 14, No. 9

[11] L.Ross, Heidelberg, R.Th.Kersten and Mainz, Integrated Optics: On the way to future, *Schott Information,* 1987.

[12] J.Albert and G.L.Yip, Stress-induced Index change for K^+-Na^+ Ion Exchange in Glass, *Electron Lett.*, Vol. 23, p.737, 1987.

[13] R.V.Ramaswamy and R.Srivastava, Ion Exchange Glass Waveguides: A Review, *J.Lightwave Techn.* Vol. 6, June 1988.

[14] A.Brandenburg, Stress in Ion Exchange Glass Waveguides, *J.Lightwave Techn.*, Vol. LT-4, p.1580, 1986.

[15] Mahmoud Abou-El-Leil and Fred Leonberger, Model for Ion Exchanged Waveguides in Glass, *Presented at 86th Ann. Meet. American Ceramic Society*, Chicago, Il, Apr. 1986.

[16] Nicholas F.Borrelli, Michael D. Cotter and John C. Luong, Photochemical Method to produce Waveguiding in Glass, *IEEE J.Qua.Elect.*, Vol. QE-22, p.896, June 1986.

[17] A.Tervonen, S.Honkanen and M.Leppihalme, Control of Ion Exchanged Waveguide Profiles with Ag Thin Film Source, *J.Appl. phys.* p.759, Aug. 1987.

[18] Robert G.Hunsperger, Integrated Optics: Theory and Technology, Second Edition, Springer-Verlag Berlin Heidelberg New York Tokyo 1984.

[19] Mahmoud Abou-El-Leil and Fred Leonberger, Model for Ion Exchanged Waveguides in Glass, *J.Am.Ceram. Soc.*, Vol. 71, p.497, June 1988.

[20] S.Honkanen, A.Tervonen, H.von Bagh, A.Salin and M.Leppihalme, Fabrication of Ion Exchanged Channel Waveguides directly into Integrated Circuit Mask Plates, *Appl. phys. Lett.*, p.296, Aug. 1987.

[21] R.G.Walker, C.D.W.Wilkinson and J.A.H.Wilkinson,Integrated Optical Waveguiding Structures made by Silver Ion Exchange in Glass. 1:The propagation Characteristics of Strip Ion Exchanged Waveguides; A Theoretical and Experimental Investigation, *Appl. Opt.,* Vol. 22, p.1923, June 1983.

[22] L.Ross, H.J.Lilienhof and H.W.Holscher, Buried Waveguides for Passive Integrated Optics by Cs^{+}Ion Exchange, *SPIE, Int. Opt. Cir. Eng. III*, Vol. 651, p.32, 1986.

[23] A.Beguin, T.Dumas, M.J.Hackert, R.Jansen and C.Nissim, Fabrication and Performance of Low Loss Optical Components made by Ion Exchange in Glass, *J.Lightwave Tech.*,Vol. 6.p 1483, Oct. 1988.

[24] J.Viljanen and M.Leppihalme, Fabrication of Optical Strip Waveguides with nearly circular cross-section by Silver Ion Migration Technique, *J.Appl.Phys.*,p.3563,July 1980.

[25] S.Honkanen and A. Tervonen, Experimental Analysis of Ag^{+}-Na^{+} Exchange in Glass with Ag film Ion Sources for Planar Optical Waveguide Fabrication, *J.Appl.Phys.*, p 634, Feb. 1988.

[26] Out of plane scattering from ion exchanged optical waveguides.

[27] G.H.Siegel Jr., Optical Absorption of Glasses, *Treatise on Materials Science and Technology*, Vol. 12, 1987.

[28] W.Karthe, R.Goring, Ch. Kaps, G.Schreiter and R.Muller, Multimode Gradient-index Strip Waveguide in Glass Fabricated by Ion exchange, *Spie, Int.Opt.Cir.Eng.III*, Vol. 651, 1986

[29] S.Honkanen, A.Tervonen, H.von Bagh and M.Leppihalme, Ion exchange Process for Fabrication of Waveguide Couplers for Fiber Optic Sensor Applications, *J.Appl. Phys*, p.52 Jan.1987.

[30] R.H.Doremus, Ion exchange in Glasses; Ion exchange-a series of advances, J.A.Marinsky, Chap.1.

[31] T.G.Giallarenzi, E.J.West, R.Kirk, R.Ginther and R.A.Andrew, Optical Waveguides formed by Thermal Migration of Ions in Glass, *Appl. opt.*, Vol. 12, p.1240, 1973.

[32] R.K.Lagu, R.V.Ramaswamy,and S.I.Najafi, Fabrication and Characterization of Buried Glass Waveguides with Symmetric Index Profiles, *Tech. Dig. Third Euro. Conf. Int. Optics,* p.75, May 1985.

[33] P. Chludzinski, R.V.Ramaswamy and T.J. Anderson, Silver-Sodium Ion Exchange in Soda Lime Silicate Glass, *Phys. Chem. Glasses*, Vol.28, p.169, 1987.

[34] J.M.White and P.F.Heidrich, Optical Waveguide Refractive Index Profiles determined from measurement of mode indices: A simple analysis, *Appl. Opt.,* Vol. 15, p.154, 1976.

[35] R.K.Lagu and V.Ramaswamy, Fabrication of Single-mode Glass Waveguides by electrolytic release of silver ions, *Appl. Phy. Lett.*, Vol.45, p.117, 1984.

[36] R.G.Eguchi, E.A.Maunders and I.K.Naik, Fabrication of Low Loss Waveguides in BK-7 by Ion Exchange, *Northrop Research and Technology Center, California.*

[37] Ramu V. Ramaswamy, S. Iraj Najafi, Planar, Buried, Ion-Exchange Glass Waveguides: Diffusion Characteristics, *IEEE J Quantum Electronics.*, Vol. QE 22, No. 6, June 1986.

[38] H.J.Lienhof, E. Voges, D. Ritter, and B. Pantschew, *IEEE J. Quantum Electron.* QE-18, 1877 (1982).

[39] Kathrine Forrest, Stephen J.Pagano and Walter Viehmann, Channel Waveguides in Glass via Silver-Sodium Field- Assisted Ion Exchange, *J. Lightwave Tech.*, Vol. LT-4, p.140, Feb. 1986.

[40] Joseph E. Gortych and Dennis G. Hall, Fabrication of Planar Optical Waveguides by K^+ Ion Exchange in BK 7 and Pyrex Glass, *J. Quantum Electronics*, Vol. QE-22,p.892, June 1986.

[41] R.V. Ramaswamy, H. C. Cheng and Ramakant Srivastava, Process Optimization of Buried Ag^+-Na^+ Ion-Exchange Waveguides: theory and experiment, *Appl. Optics*, Vol. 27, p.1814, May 1988.

Bibliography

Silicon Processing for the VLSI Era, Vol. 1, by S. Wolf & R.N.Tauber, Lattice Press Publication.

An Introduction to Optical Fibers, by Allen H. Cherin, Bell Laboratories, Atlanta Georgia, McGraw-Hill Book Company.

Optical Electronics, 3rd Edition, by Amnon Yariv, California Institute of Tech, CBS College Publishing.

Integrated Optics, Edited by T.Tamir, Dept. of Electrical Engineering, Polytechnic Institute of New York, Second corrected and updated edition, Springer -Verlag Berlin Heidelberg New York 1979.

Integrated Optics: Theory and Technology, Second Edition, Robert G.Hunsperger Springer-Verlag Berlin Heidelberg New York Tokyo 1984.

Electromagnetic Principles of Integrated Optics, by Donald L.Lee, Raytheon Research Division, John Wiley & Sons, New York Chichester Brisbane Toronto Singapore.

Appendices

A1. Old coupler PCR test

A2. Simulated V curve

A3. Simulated V curve

A4. Phase 1 scan

A5. Phase 1 scan

A6. Phase 2 scan

A7.

B1. Manufacturer information on 0211

C1. Lot follower

C2. Source code of the Vax program

C3. Compound coupler design

C4. Al & Ag pallet data from MRC

C5. Silver thickness graph

C6. SEM photos of polished edges

D1. Independent study

Appendix A1

Old coupler test

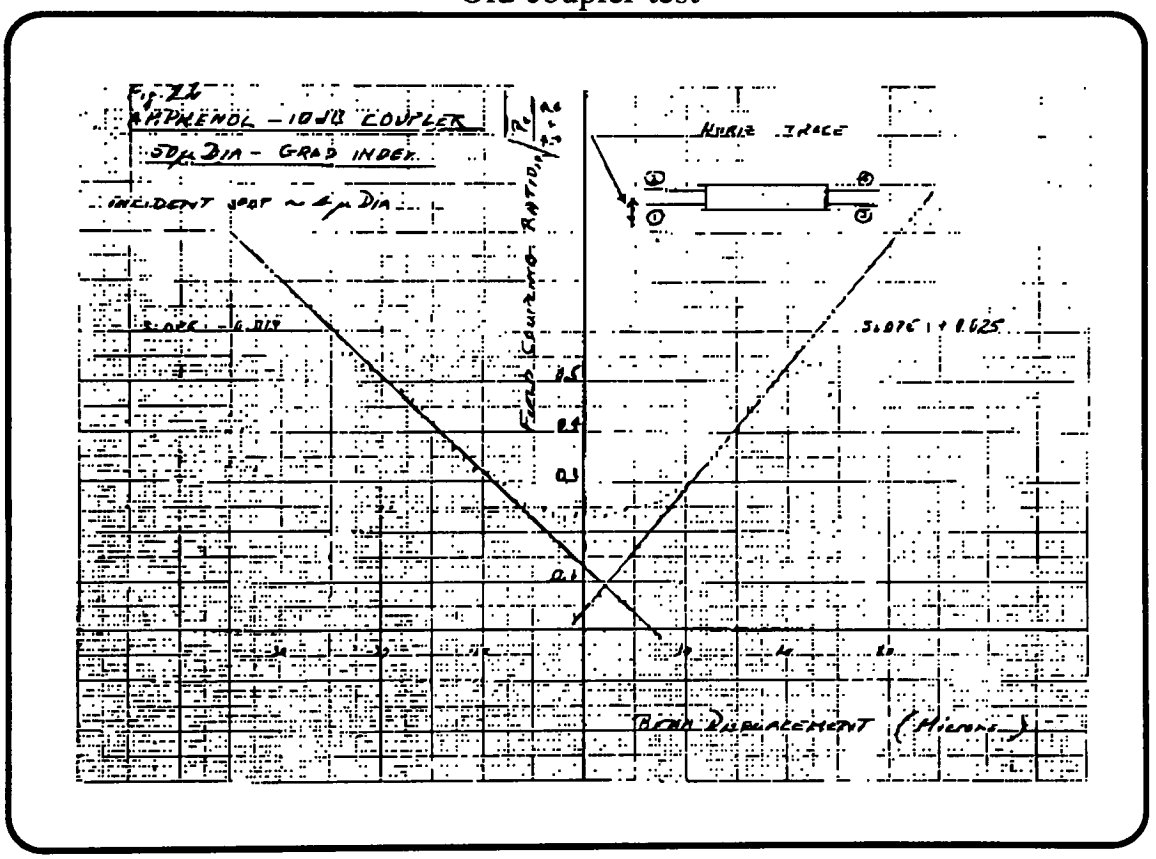

Appendix A2

Simulated V curve

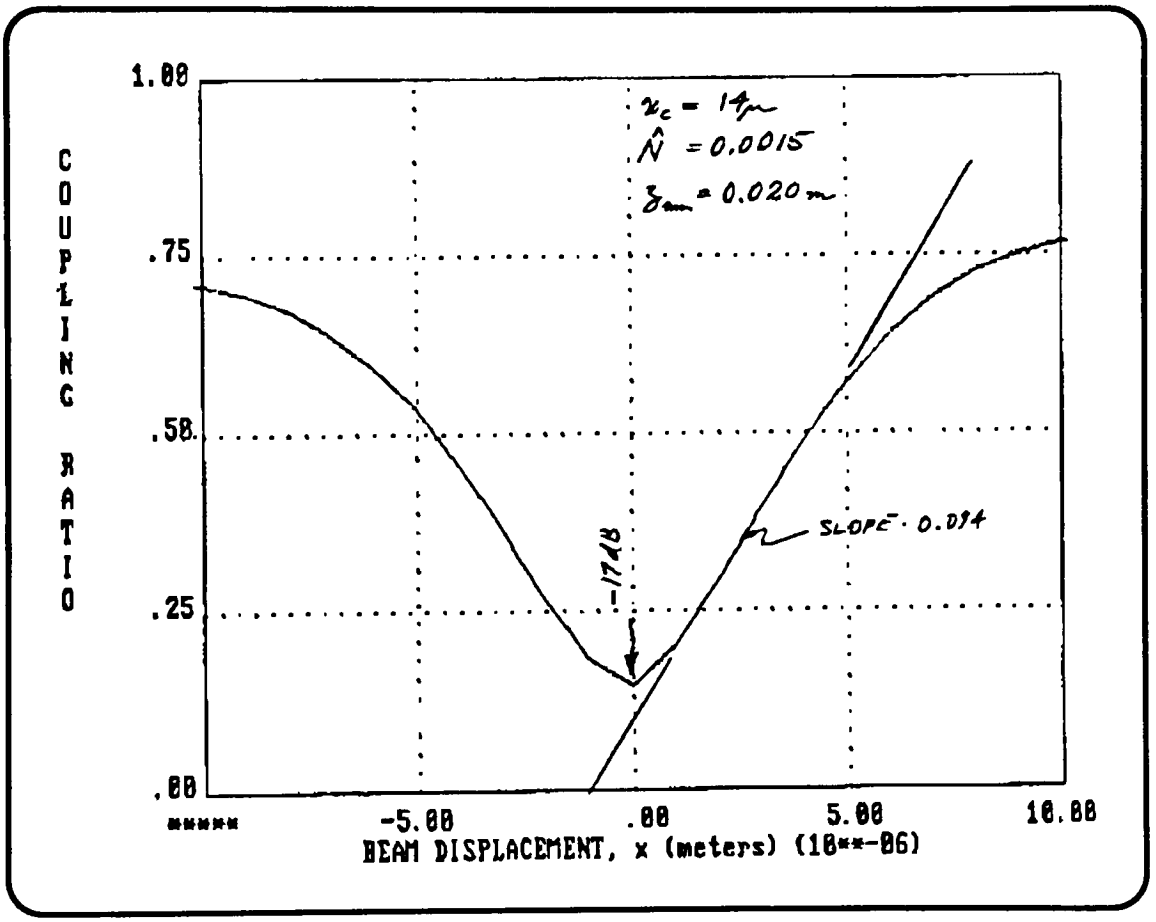

Appendix A3

Simulated V curve

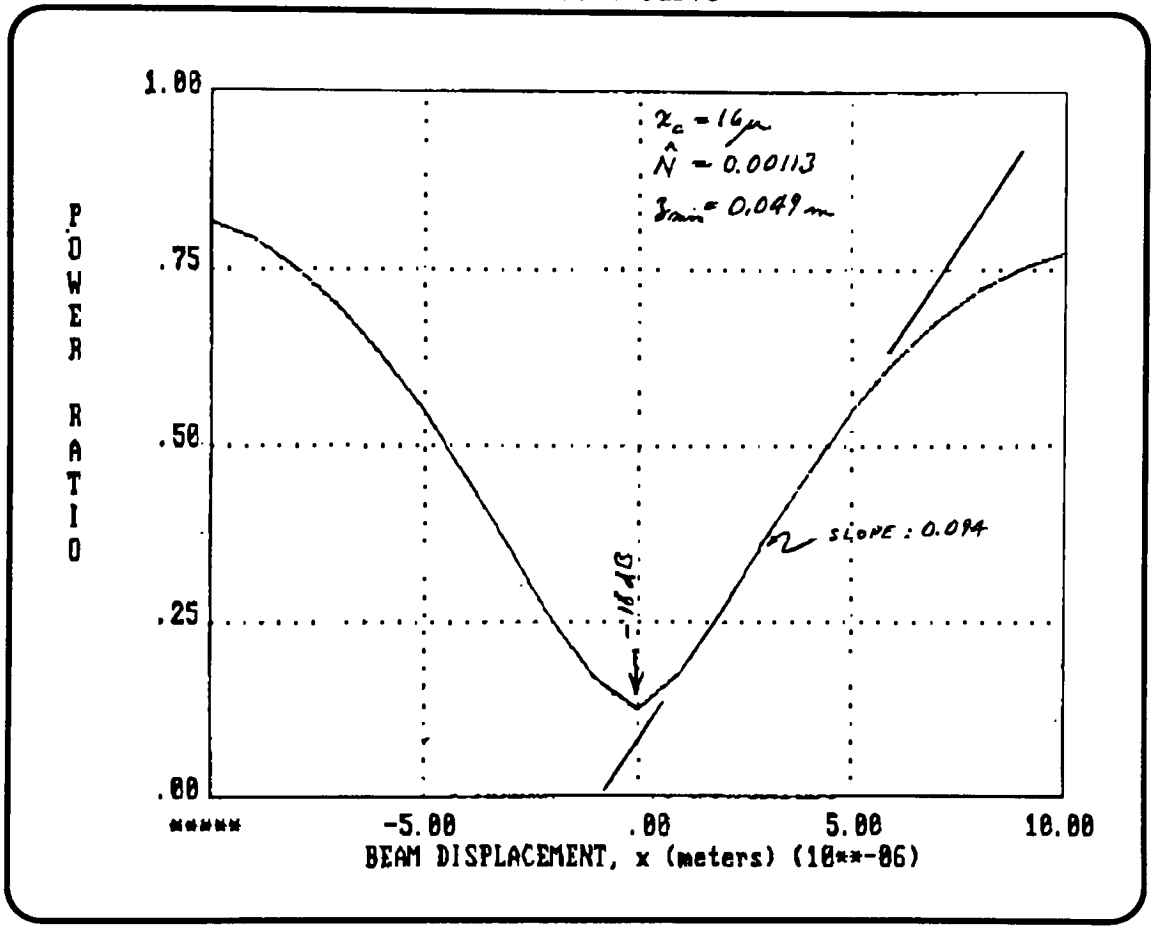

Appendix A4

Phase 1 scan

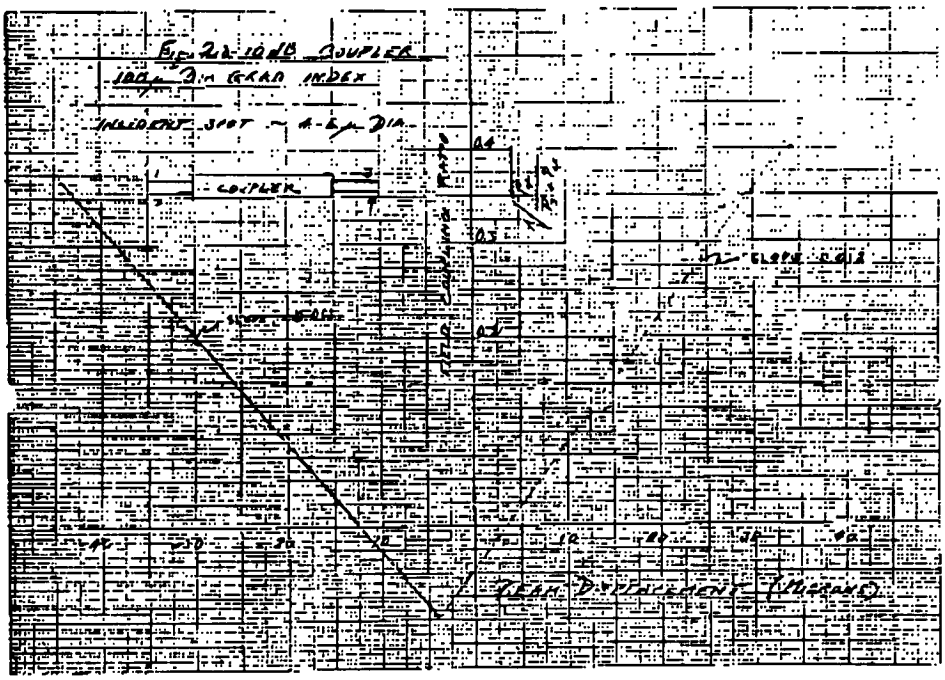

Appendix A5

Phase 1 scan

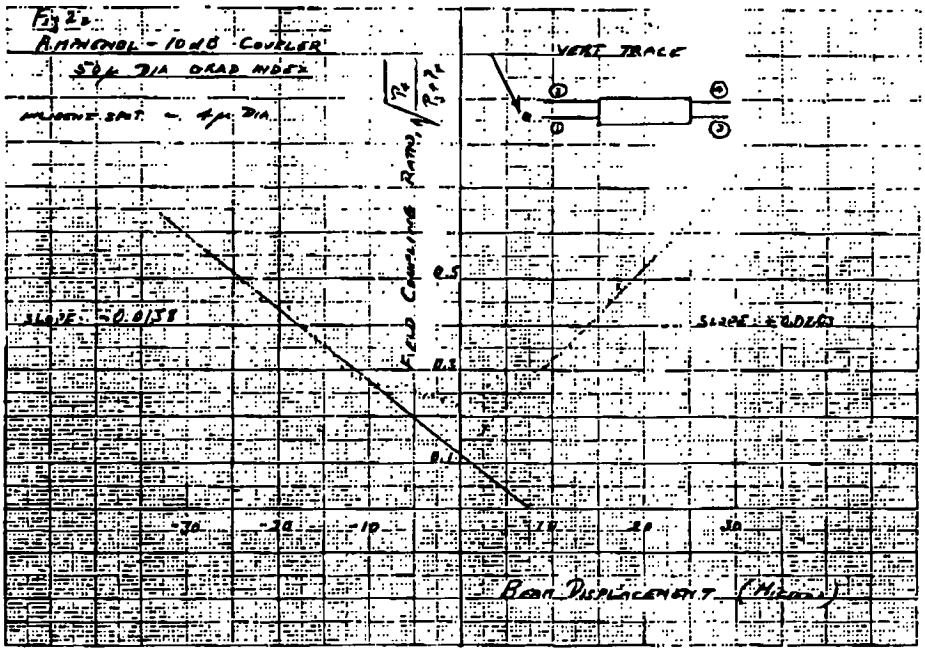

Appendix A6

Phase 2 scan

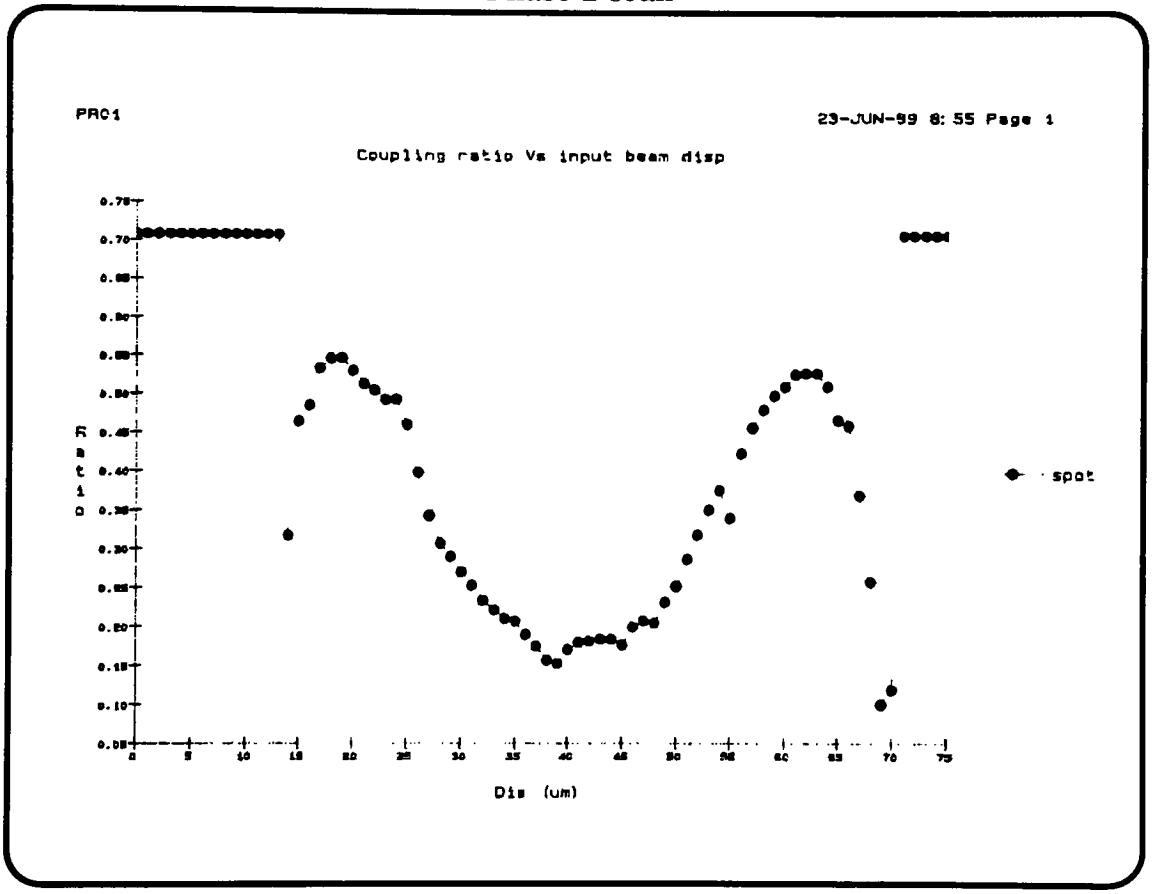

Appendix A7

Balanced output configuration curve

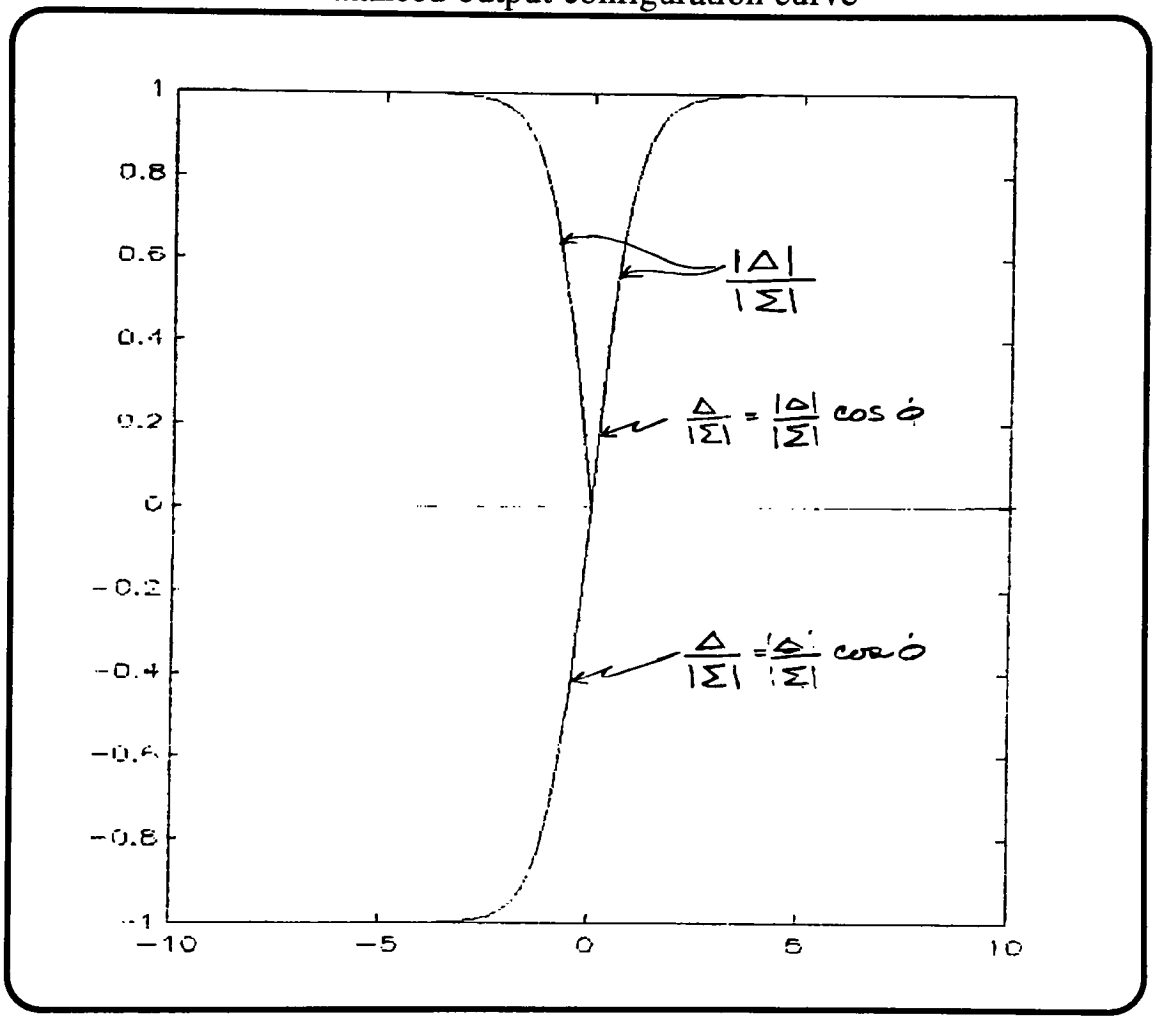

Appendix B1

Manufacturer information on O211

Materials Business
Material Information
14831

Corning Glass Works
Corning, New York

Corning Code: 0211

Description

Glass Type—potash, soda, zinc borosilicate
Color—water-white clear
Forms available—drawn sheet, powder
Principal uses—microscope cover glass, thin film substrate

Properties

Mechanical	**Metric**	**English**
Density	2.53 g/cm3	157.9 lb/ft3
Young's Modulus	7.59 x 103 kg/mm2	10.8 x 1 o6 psi
Poisson's Ratio	0.22	
Shear Modulus	3.09 x 103 kg/mm2	4.4 x 106 psi
Knoop Hardness (KHN,oo)	458	

V~scos~ty

Working Pt. (10' poises)	1 008°C	1 848°F
SofteningPt.(1078poises)	720°C	1328°F
Annealing Pt. (10'3 poises)	550°C	1 022°F
Strain Pt. (10'4 poises)	508°C	946°F

Thermal

Coefficient of Expansion (0-300°C)	73.8x10-7/°C	41.0x10-7/°F
(25°C to Set Point 51 3°C)	84.0 x 10 - 7/°C	48.7 x 10 - 7/°F
Thermal Conductivity, 0°C	.0023 saeC Cm2°C	54 h ft2°F

Optical

Refractive Index (589.3nm)	1.523
Transmission ~a~ 420 nm	92%~
2200 nm	92%-

~Through a sample thickness 1.0 mm

Electrical

Log,O Volume Resistivity @ 250°C	8.3 ohm-cm
(~ 350°C	8.7 ohm-cm
DielectricConstant@20°C;I MHz	8.7
Loss Tangent ~ 20°C; I MHz	.46%

M1-021 1-88

Appendix B1 *contd.*

Coming Code: 0211 Page 2 of 4

Chemical

Weathering # 1
Acid Durability •~ 2

Weathering is def ined as corrosion by atmospheric-borne gases and vapors such as water and carbon dioxide . Glasses rated 1 will almost never show weathering effects; those rated 2 will occasionally be troublesome, par tlcularly if weathering products cannot be removed; those glasses rated 3 require more careful considera bon.

t.~ The Acid Durability column classifies glasses according to their behavior in 5% hydrochloric acid at 95°C (203°F) for 24 hours.

Classification Thickness Loss (in.)

< 104
2 104_105
3 10-5 10J
4 > 10~

Values are listed with four degrees of accuracy. Those that are underscored (e.g. 2) result from recent determina tion and are reliable. Values not underscored are estimates offered with confidence. When two values are listed with one underscored, this indicates the range within which the true value lies: the underscored value is the more probable one (e.g. 2-3). A question mark indicates considerable uncertainty.

Appendix B1 *contd.*

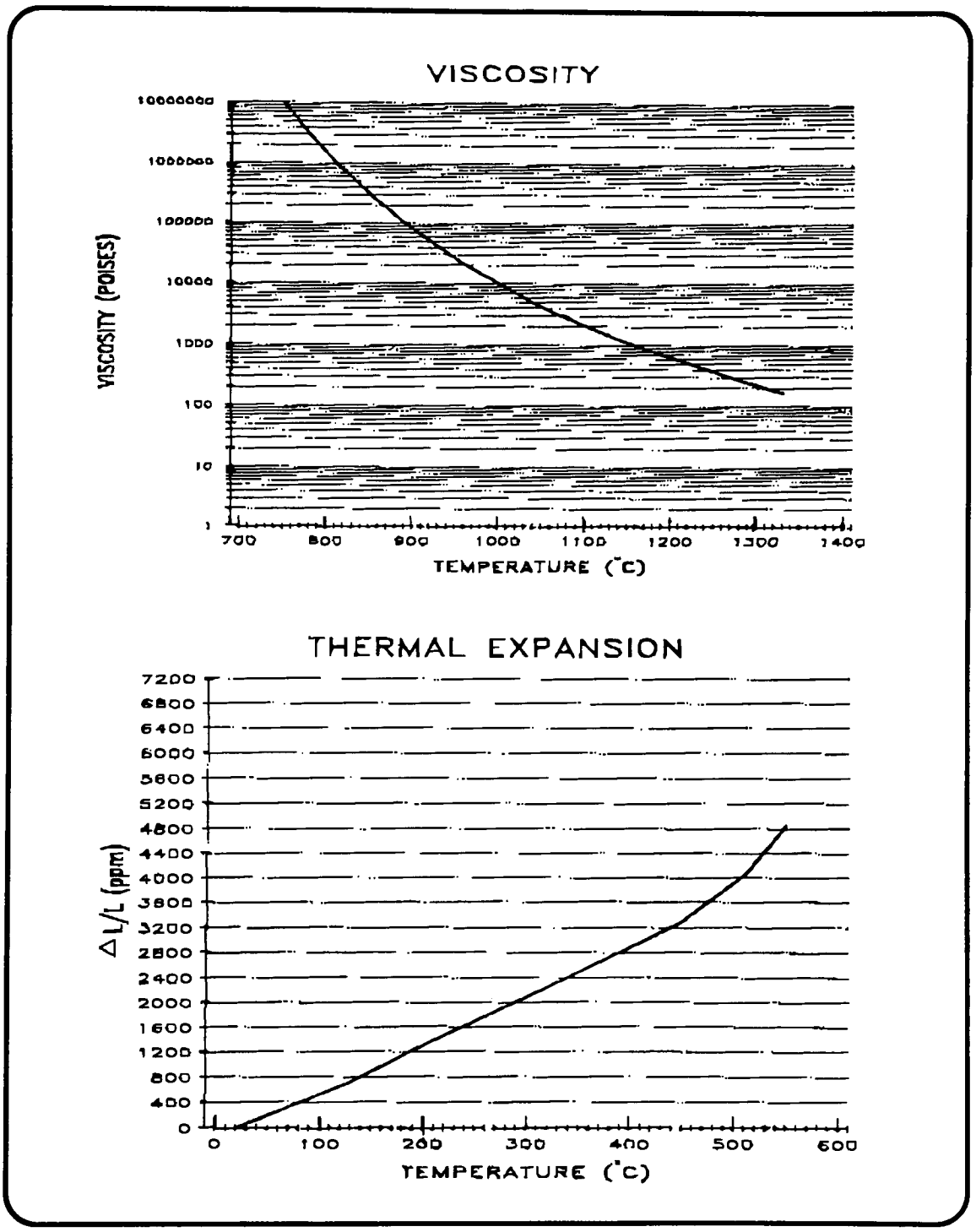

Appendix B1 *contd.*

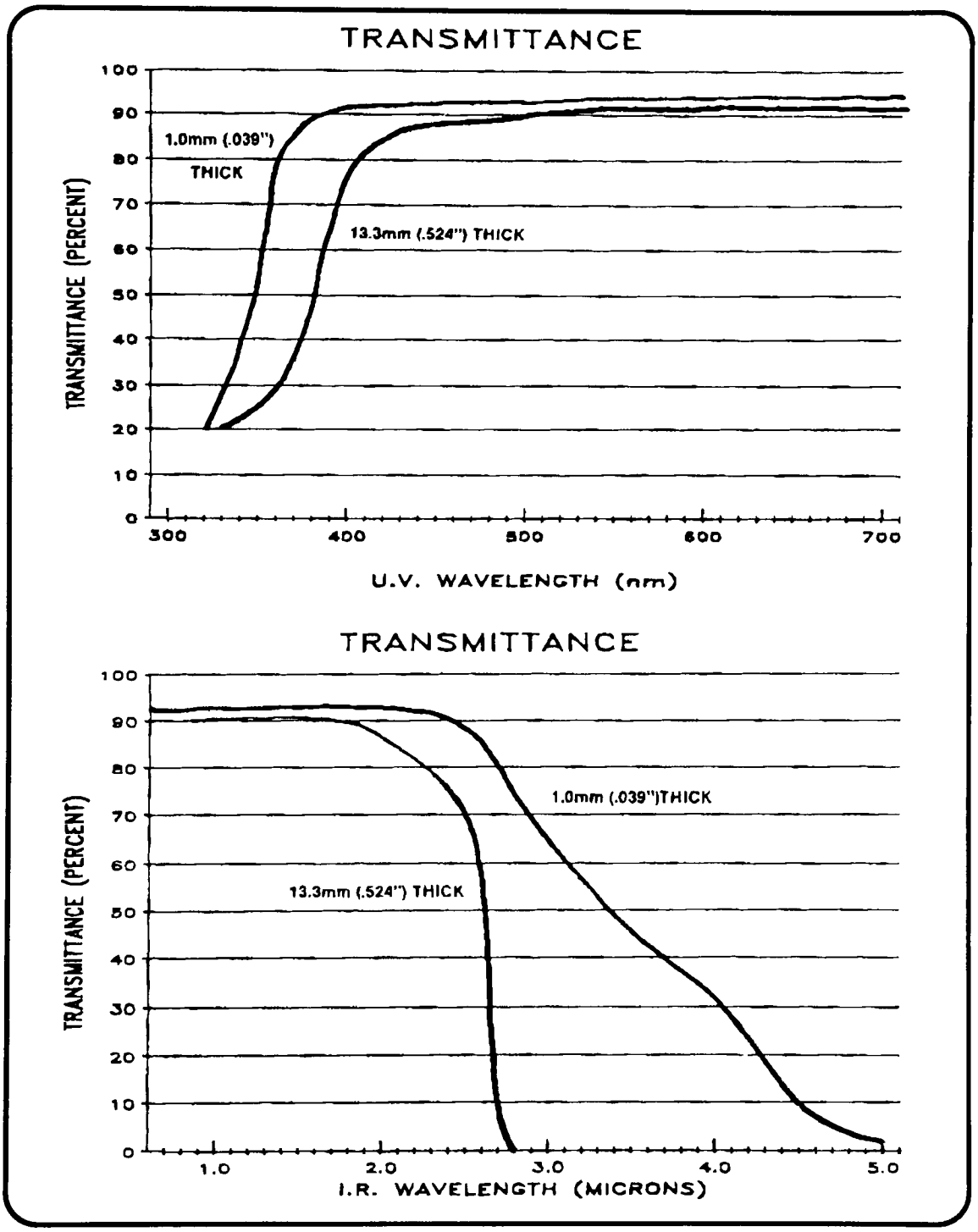

Appendix C1

Lot follower

pages 135 to 145

(To be used during the process)

ROCHESTER INSTITUTE OF TECHNOLOGY

Integrated Optics Lab

Electrical Engineering Department

ANRO Project Process Sheet

Version Date : 03 / 23 / 1991

by : V.P.Raghavan

Glass type : _____

Substrates : __ __ __

Start of process date : ___/___/___

End of clean room process date : ___/___/___

Start of polishing date : ___/___/___

End of polishing date : ___/___/___

Second diffusion date :___/___/___

__ ___/___/___
__ ___/___/___
__ ___/___/___

Microprobe date : ___/___/___

Index profile date : ___/___/___

[ ] Substrate glass type : _____

The process is designed for a 3X3 glass substrate of approximately 2 mm thickness. (Corning 0211, 0317 etc.)

Total number of substrates : ___

[ ] Substrate identification :

Melt wax on the bottom middle surface.(thin coating)
Imprint ID # on the wax surface with steel stamps.

Substrate # ___ ___ ___

Etch the glass with Armour Etch.

Etch time - 5.0 min.

(This surface will be referred to as the top surface.)
note : The LHS and RHS alignment marks will be scratched on the surface after the AL evaporation step.

Top Surface of Substrate

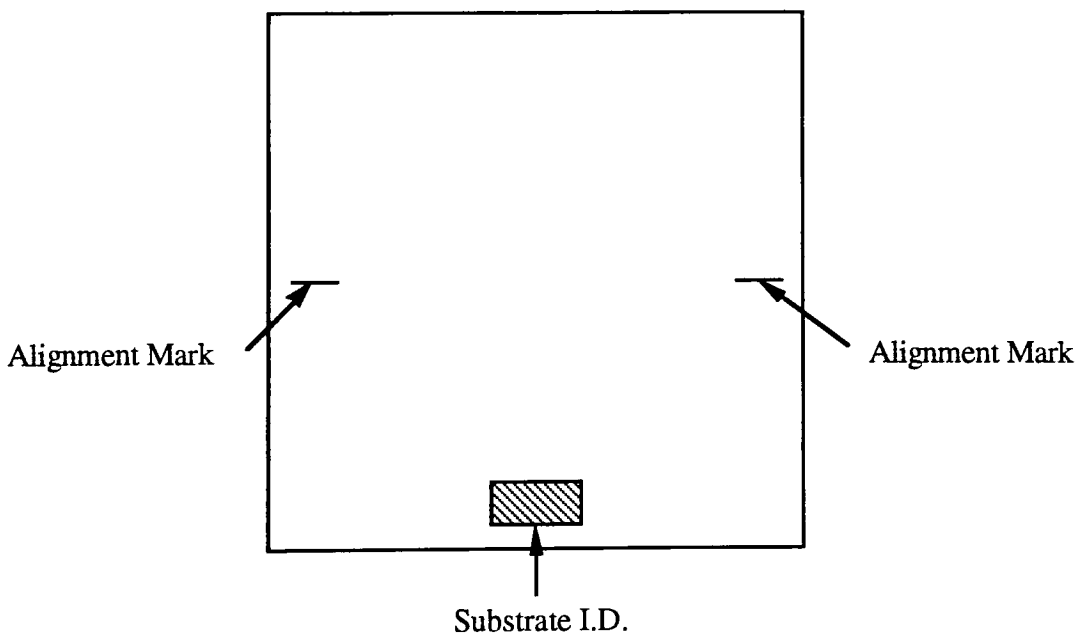

[ ] Cleaning Procedure :

Brush the surface with a clean brush.
Avoid the use of cleaning solutions.

O_2 plasma clean for 20 min.

Follow the operation manual for the Plasma Line.

O_2 pressure: _____
Chamber pressure: _____
Flow rate: _____
Reflected power: _____
Forward power: _____

[ ] Inspect substrates under dark field illumination :

Comments:

[ ] Evaporate Aluminum on the front side :

Use 99.9995% pure Al (VP or MARZ grade from MRC).
Follow the operation manual for the CVC.

Use 3 pallets.
Frequency drop of 4.
Alpha step thickness measurement : _____

[ ] Scratch alignment marks.

Scratch LHS and RHS alignment marks on the Al surface as shown on the previous page.

[ ] Clean with an air brush :

Inspect for particles under dark field.

[ ] Spin on photo resist :

Use KTI 820 and a manual spin process.

Spin coat HMDS: 3000 rpm for 30 sec.
Air dry : 1.0 min.
Spin coat KTI 820 : 4500 rpm for 30 sec.
Soft bake : 85 C for 30 min.

[ ] Exposure process :

Follow the exposure manual.

Mask used : _____
Measured irradiance : _____
Total time of exposure : _____ **(50 mJ or as required.)**
Total exposure : _____

[ ] Development process :

Use AZ 934 developer, 1:1 with DI water.
30 to 40 sec development time.

[ ] Inspect the substrates for completion of development and under cutting :

Comments :

[ ] Aluminum etch process :

Etch temperature : 55°C.
Etch time : less than 2.0 min.

[ ] Photoresist strip - Flood exposure process :

Follow the exposure manual. Flood expose the substrates.

Total time of exposure : _____ **(80 mJ or as required.)**
Total exposure : _____

[ ] Development process :

Use AZ 934 developer, 1:1 with DI water.
60 to 70 sec development time.

[ ] Line width measurement :

[ ] Inspect under dark field illumination :

Comments :

[ ] Evaporation of Silver on the back surface :

Follow the CVC operation manual.
Source - MARZ grade Silver from MRC.

Use the Alumina oxide coated boats for this process.
Use 2 pallets of Silver.
Place a blank slide with substrates to measure final thickness using an Alpha step.
Reset the frequency counter and zero with knobs.
Evaporation voltage on the Variac - 190 volts
Frequency drop - 3.0 on the 10 scale.

[ ] Inspect and measure the film thickness :

Thickness : _____
Comments:

[ ] Evaporation of Silver on the front surface :

Follow the CVC operation manual.
Source - MARZ grade Silver from MRC.

Use the Alumina oxide coated boats for this process.
Load two Silver pallets.
Reset the frequency counter and zero with knobs.
Evaporation voltage on the Variac - 190 volts
Frequency drop - 6.2 on the 10 scale.

[ ] Inspect and measure the film thickness :

Thickness : _____
Comments:

[ ] Prediffusion Process :

Inspect the top and bottom surfaces (dark field) to ensure clean areas for contact with the electrodes.

The substrate (one at a time) should be connected as shown below.

Place an Al foil at the top and bottom of the substrate.

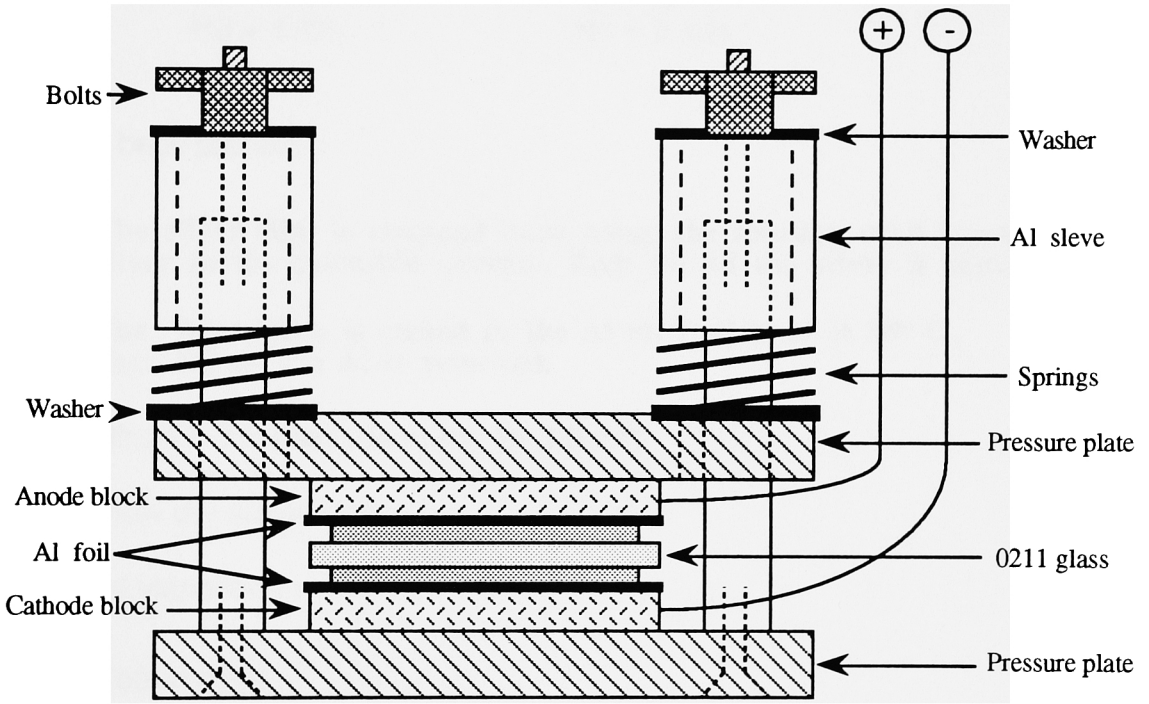

The following prediffusion program should be used in the oven.

Note : After 70 min. of diffusion turn the E field off.

Diffuse using 100 volts across the anode and cathode.

R1 = 20°C / min.	R4 = 25°C / min.
T1 = 260°C	T4 = 100°C
H1 = 5 min.	H4 = 0 min.
R2 = 3°C / min.	R5 = 20°C / min.
T2 = 300°C	T5 = 40°C
H2 = 120 min.	H5 = 1 min.
R3 = 1°C / min.	R6 = 30°C / min.
T3 = 301°C	T6 = 39°C
H3 = 1 min.	H6 = 0 min.

[ ] Strip back process :

The silver film is stripped back using the solution used for etching silver in the photolith process. Etch till all the silver is removed.

The Aluminum is etched in the Al etch solution at 55° C. Etch till all the Al is removed.

Rinse in the cascade rinser for 3.0 min.

Blow dry substrates.

[ ] Visual inspection :

Comments:

Date : ___/___/___ **by : _____**

[ ] Cut and polish process :

Process sheet numbers:

Date : ___/___/___ **by : _____**

[ ] Index profile :

Computer data file numbers:

Date : ___/___/___ **by : _____**

[ ] Microprobe results :

SEM photograph numbers:

Profile data sheet numbers:

[ ] Drive in diffusion process :

The following prediffusion program should be used in the oven.

R1 = 20°C / min.	R4 = 10°C / min.
T1 = 360°C	T4 = 250°C
H1 = 5 min.	H4 = 0 min.
R2 = 3°C / min.	R5 = 20°C / min.
T2 = 400°C	T5 = 40°C
H2 = 90 min.	H5 = 1 min.
R3 = 1°C / min.	R6 = 30°C / min.
T3 = 402°C	T6 = 39°C
H3 = 1 min.	H6 = 0 min.

[ ] Visual inspection :

Comments:

Date : ___/___/___ **by :** _____

[ ] Index profile :

Computer data file numbers:

Date : ___/___/___ **by :** _____

[ ] Microprobe results :

SEM photograph numbers:

Profile data sheet numbers:

Date : ___/___/___ **by :** _____

[ ] Analysis :

Appendix C2

Source code for the Vax program

Appendix C2 *contd.*

```
***** THIS PROGRAM COMPUTES THE INPUT FILE WHICH IS USED BY
***** THE MANN 3000 PATTERN GENERATER, GIVEN THE FOLLOWING:

***** LENGTH in cm, HEIGHT in cm, WIDTH in microns AND THE
***** DEGREE OF INCREMENTS TO BE USED IN THE CALCULATIONS.

***** VARIABLES USED

 REAL LENGTH,HEIGHT,WIDTH,ANGLE
 REAL XI,YI,X2,Y2
 REAL CX,CY,DX,DY,XXI,YYI,XX2,YY2
 REAL RAD
 REAL THETA,DELTA
 REAL PI
 REAL RXXI,RIXXI,R2XXI,REM
 REAL RXX2,RIXX2,R2XX2
 REAL RYYI,RIYYI,R2YYI
 REAL RYY2,RIYY2,R2YY2
 REAL WI,W2,W3,WREM,WTI
 REAL WIB,W2B,W3B,WBREM,BOXL,WB
 REAL YB,LXB,RLB

 INTEGER IXXI,IYYI
 INTEGER IXX2,IYY2
 INTEGER WT,WBT,WTT
 INTEGER N
 INTEGER ALPHA
 INTEGER ILXB,IYB,LXT,YT
 INTEGER LB

 PI = 3.141593

***** DATA FILE T23DAT.DAT -- INPUT FILE FOR THE MANN3000.
***** DATA FILE T22DAT.DAT -- INPUT FILE FOR PLT2D.
***** DATA FILE T21DAT.DAT -- FOR SCREEN DISPLAY.

 OPEN (UNIT=7,FILE='T21DAT',STATUS='NEW')
 OPEN (UNIT=8,FILE='T22DAT',STATUS='NEW')
 OPEN (UNIT=9,FILE='T23DAT',STATUS='NEW',
 1    CARRIAGECONTROL='LIST')

***** INPUT LENGTH,HEIGHT,WIDTH AND DEGREE OF INCREMENTs
***** FROM THE TERMINAL.

      96 WRITE (6,98)
      98 FORMAT (/IX,'LENGTH HAS TO BE BETWEEN 0.0 AND 4.0 cm',$)
 WRITE (6,100)
100 FORMAT (/IX,'LENGTH (in cm) = ',$)
 READ (5,*) LENGTH
 IF ((LENGTH.GT.4.0).OR.(LENGTH.LT.O.O)) THEN
   GOTO 96
 ENDIF
```

Appendix C2 *contd.*

```
196 WRITE (6,198)
198 FORMAT (/1X, HEIGHT HAS TO BE BETWEEN 0.0 AND 4.0 cm ,$)
 WRITE (6,200)
200 FORMAT (/1X, HEIGHT (in cm) = ,$)
 READ (5,*) HEIGHT
 IF ((HEIGHT.GT.4.0).OR.(HEIGHT.LT.O.O)) THEN
   GOTO 196
 ENDIF
296 WRITE (6,298)
298 FORMAT(/1X, WIDTH HAS TO BE BETWEEN 10.0 AND 100.0 microns ,$)
 WRITE (6,250)
250 FORMAT (/1X, WIDTH (in microns) = ,$)
 READ (5,*) WIDTH
 IF ((WIDTH.GT.lOO.O).OR.(WIDTH.LT.10.0)) THEN
   GOTO 296
 ENDIF
 WRITE (6,260)
260 FORMAT (/1X, DEG INCREMENTS (in DEGREES) = ,$)
 READ (5,*) ANGLE
 DO 270 LOOP = 1 , 40
     WRITE(9,265)
265      FORMAT ( )
270 CONTINUE
***** WRITE ID TO D23DAT.DAT (LENGTH,HEIGHT,WIDTH)
 WRITE(9,272)
272 FORMAT ( MANN3000 INPUT FILE TO GENERATE A WAVEGUIDE )
 WRITE(9,274) LENGTH
274 FORMAT ( LENGTH = ,F4.1, cm )
 WRITE(9,276) HEIGHT
276 FORMAT ( HEIGHT = ,F4.1, cm )
 WRITE(9,278) WIDTH
278 FORMAT ( WIDTH = ,F4.1, microns )
 WRITE(9,265)
 WRITE(9,279)
279 FORMAT ( by V.P.RAGHAVAN )
 DO 280 LOOP = 1 , 5
     WRITE(9,265)
280 CONTINUE
***** CALCULATE WIDTH AND ROUNDOFF
       WIDTH = WIDTH * 3.937
       WI = ANINT(WIDTH)
       W2 = AINT(WI)
       W3 = AINT(WI/10.0)
       WREM = W2 - (W3 * 10.0)
          IF (WREM.LT.3) THEN
               WT = INT(W3 * 10)
            ELSEIF ((WREM.GT.2.0).AND.(WREM.LT.8.0)) THEN
               WT = INT((W3 * 10) + 5)
            ELSEIF ((WREM.GT.7.0).AND.(WREM.LT.10.0)) THEN
               WT = INT((W3 * 10) + 10)
```

Appendix C2 *contd.*

```
    ENDIF
 WTI = WT / 3.937
***** CALCULATE THE BOTTOM LEFT POINT OF THE RECTANGLE  YI = 200000 - (HEIGHT *
10000 * 3.937) / 2
 XI = 200000 - (LENGTH * 10000 * 3.937– / 2
 Y2 = 200000 + (HEIGHT * 10000 * 3 937) / 2
 X2 = 200000 + (LENGTH * 10000 * 3 937) / 2
***** CALCULATE THE CENTER POINT OF THE RECTANGLE  CX = (X2 + X1)/2
 CY = (Y2 + Y1)/2
***** CALCULATE THE POINT 1/4 DISTANCE FROM THE BOTTOM LEFT *****
 DX = (XI + CX)/2
 DY = (YI + CY)/2
***** WRITE THESE COORDINATE POINTS TO THE SCREEN  WRITE (6,*) ' '
 WRITE (6,*) 'XI = ',XI,'YI = ',YI
 WRITE (6,*) 'X2 = ',X2,'Y2 = ',Y2
 WRITE (6,*) 'CX = ',CX,'CY = ',–Y
 WRITE (6,*) 'DX = ',DX,'DY = ',DY
***** CALCULATE THE BOTTOM STRAIGHT LINE OF THE WAVEGUIDE  ILXB = INT(50000)
 YB = INT(YI)
 RYYI = ANINT(YB)
 RIYYI = AINT (RYYI)
 R2YYI = AINT (RYYI/10.0)
 REM = RIYYI - (R2YYI * 10.0)
      IF (REM.LT.3) THEN
          IYB = INT(R2YYI * 10)
        ELSEIF ((REM.GT.2.0).AND.(REM.LT.8.0)) THEN
          IYB = INT((R2YYI * 10) + 5)
        ELSEIF ((REM.GT.7.0).AND.(REM.LT.10.0)) THEN
          IYB = INT((R2YYI * 10) + 10)
      ENDIF
 J = O
 ALPHA = O
 300 LXBI = ILXB + 5000
 IF (LXBI.LT.XI) THEN
    LB = 10000 + 10
    WRITE (8,*) ILXB,IYB
    J = J + 1
    IF (J.EQ.I) THEN
        WRITE (9,310) ILXB,IYB,WT,LB,ALPHA
      ELSE
        WRITE (9,315) ILXB
      ENDIF
310     FORMAT ('X',I6,'Y',I6,'H',I5,'W',I5,'A',I3,'-')
315      FORMAT ('X',I6,';')
         ILXB = ILXB + 10000
    GOTO 300
 ENDIF
```

Appendix C2 *contd.*

```
      LXB = ILXB - 5000
      LXB = (XI + LXB)/2
      RXXI = ANINT(LXB~
      RIXXI = AINT (RXXI)
      R2XXI = AINT (RXXI/10.0)
      REM = RIXXI—(R2XXI * 10.0)
          IF (REM.LT.3) THEN
              ILXB = INT(R2XXI * 10)
           ELSEIF ((REM.GT.2.0).AND.(REM.LT.8.0)) THEN
              ILXB = INT((R2XXI * 10) + 5)
           ELSEIF ((REM.GT.7.0).AND.(REM.LT.10.0)) THEN
              ILXB = INT((R2XXI * 10) + 10)
      ENDIF
      RLB = INT((XI - LXB) * 2) + 10
      WIB = ANINT(RLB)
      W2B = AINT(WIB)
      W3B = AINT(WIB/10.0)
      WBREM = W2B - (W3B * 10.0)
        IF (WBREM.LT.3) THEN
            LB = INT(W3B * 10)
          ELSEIF ((WBREM.GT.2.0).AND.(WBREM.LT.8.0)) THEN
            LB = INT((W3B * 10) + 5)
          ELSEIF ((WBREM.GT.7.0).AND.(WBREM.LT.10.0)) THEN
        LB = INT((W3B * 10) + 10)
    ENDIF
 WRITE (8,*) ILXB,IYB
 WRITE (9,310) ILXB,IYB,WT,LB,ALPHA
***** CALCULATE THE RADIOUS OF THE CURV
 RAD = ((XI - X2) * (XI - DX) / (Y2 - YI)) + DY - YI
***** CALCULATE THE LENGTH OF THE BOXES AND ROUNDOFF
      DELTA = ANGLE * PI / 180
      BOXL = (RAD + (WTI / 2)) * DELTA
      WIB = ANINT(BOXL)
      W2B = AINT(WIB)
      W3B = AINT(WIB/10.0)
      WBREM = W2B - (W3B * 10.0)
        IF (WBREM.LT.3) THEN
            WBT = INT(W3B * 10)
          ELSEIF ((WBREM.GT.2.0).AND.(WBREM.LT.8.0)) THEN
            WBT = INT((W3B * 10) + 5)
          ELSEIF ((WBREM.GT.7.0).AND.(WBREM.LT.10.0)) THEN
        WBT = INT((W3B * 10) + 10)
    ENDIF
    WB = WBT / 3.937
***** WRITE RADIOUS, WIDTH AND BOXLENGTH TO THE SCREEN
 WRITE (6,*) ' '
 WRITE (6,*) ' RADIOUS = ',RAD,'units'
 WRITE (6,*) ' '
 WRITE (6,*) ' WIDTH = ',WT,' = ',WTI,'microns'
 WRITE (6,*) ' '
 WRITE (6,*) 'BOXLENGTH = ',WBT,' = ',WB,'microns'
***** CALCULATE THE BOTTOM HALF OF THE CURVE AND ROUNDOFf
```

Appendix C2 *contd.*

```
        J = o
        N = O
        XXI = 0.0
        THETA = 0.0
        DELTA = ANGLE * PI / 180
1000 IF (Xxl.LT.cx) THEN
     XXI = RAD * SIN(THETA) + XI
     YYI = RAD - RAD * COS(THETA) + YI
     RXXI = ANINT(XXI)
     RIXXI = AINT (RXXI)
     R2XXI = AINT (Rxxl/lo.o)
     REM = RIXXI - (R2XXI * 10.0)
      IF (REM.LT.3) THEN
          IXXI = INT(R2XXI * 10)
        ELSEIF ((REM.GT.2.0).AND.(REM.LT.8.0)) THEN
          IXXI = INT((R2XXI * 10) + 5)
        ELSEIF ((REM.GT.7.o).AND.(REM.LT.lO.o)) THEN
          IXXI = INT((R2XXI * 10) + 10)
      ENDIF
     RYYI = ANINT(YYI)
     RIYYI = AINT (RYYI)
     R2YYI = AINT (RYYI/10.0)
     REM = RIYYI - (R2YYI * 10.0)
      IF (REM.LT.3) THEN
          IYYI = INT(R2YY- * 10)
        ELSEIF ((REM.GT.2.0).AND.(REM.LT.8.0)) THEN
          IYYI = INT((R2YYI * 10) + 5)
        ELSEIF ((REM.GT.7.0).AND.(REM.LT.10.0)) THEN
          IYYI = INT((R2YYI * 10) + 10)
      ENDIF
     ALPHA = INT((THETA * 180.0 / PI) * 10)
      IF (ALPHA.EQ.900) THEN
          ALPHA = 000
      ENDIF
     WRITE (7,*) N,')',XXI,IXXI,YYI,IYYI
     WRITE (8,*) IXXI,IYYI
     J = J + 1
     IF (J.EQ.I) THEN
         WRITE (9,310) IXXI,IYYI,WT,WBT,ALPHA
       ELSE
         WRITE (9,1500) IXXI,IYYI,ALPHA
1500       FORMAT ('X',I6,'Y',I6,'A',I3,';')
    ENDIF
    THETA = THETA + DELTA
    N = N + 1
    GOTO 1000
 ENDIF
 THETA = THETA - DELTA
***** CALCULATE THE TOP HALF OF THE CURVE AND ROUNDOFF
2000 IF (XX2.LT.X2) THEN
    THETA = THETA - DELTA
    XX2 = X2 - RAD * SIN(THETA)
    YY2 = Y2 - RAD + RAD * COS(THETA)
    RXX2 = ANINT(XX2)
    RIXX2 = AINT (RXX2)
    R2XX2 = AINT (RXX2/10.0)
    REM = RIXX2 - (R2XX2 * 10.0)
     IF (REM.LT.3) THEN
```

Appendix C2 *contd.*

```
            IXX2 = INT(R2XX2 * 10)
          ELSEIF ((REM.GT.2.0).AND.(REM.LT.8.0)) THEN
            IXX2 = INT((R2XX2 * 10) + 5)
          ELSEIF ((REM.GT.7.0).AND.(REM.LT.10.0)) THEN
            IXX2 = INT((R2XX2 * 10) + 10)
         ENDIF
        RYY2 = ANINT(YY2)
        RIYY2 = AINT (RYY2)
        R2YY2 = AINT (RYY2/10.0)
        REM = RIYY2 - (R2YY2 * 10.0)
         IF (REM.LT.3) THEN
            IYY2 = INT(R2YY2 * 10)
          ELSEIF ((REM.GT.2.0).AND.(REM.LT.8.0)) THEN
            IYY2 = INT((R2YY2 * 10) + 5)
          ELSEIF ((REM.GT.7.0).AND.(REM.LT.10.0)) THEN
            IYY2 = INT((R2YY2 * 10) + 10)
         ENDIF
        ALPHA = INT((THETA * 180.0 / PI) * 10)
         IF (ALPHA.EQ.900) THEN
            ALPHA = 000
         ENDIF
        WRITE (7,*) N,')',XX2,IXX2,YY2,IYY2
        WRITE (8,*) IXX2,IYY2
        WRITE (9,1500) IXX2,IYY2,ALPHA
        N = N + 1
        GOTO 2000
      ENDIF
***** CALCULATE THE TOP STRAIGHT LINE OF THE WAVEGUIDE
      LXT = INT(IXX2 + 5000)
      YT = INT(IYY2)
      J = O
      ALPHA = O
3000  LXTI = LXT + 5000
      IF (LXTI.LT.350000) THEN
        WTT = 10000 + 10
        WRITE (8,*) LXT,YT
        J = J + 1
        IF(J.EQ.I) THEN
          WRITE (9,310) LXT,YT,WT,WTT,ALPHA
         ELSE
          WRITE (9,315) LXT
        ENDIF
        LXT = LXT + 10000
        GOTO 3000
      ENDIF
      LXT = LXT - 10000
      WTT = INT(350000 - LXT - 5000) + 10
      LXT = (350000 + LXT)/2
      WRITE (8,*) LXT,YT
      WRITE (9,310) LXT,YT,WT,WTT,ALPHA
      WRITE (9,3100)
3100  FORMAT ('S')
      END
```

Appendix C3

Compound coupler design

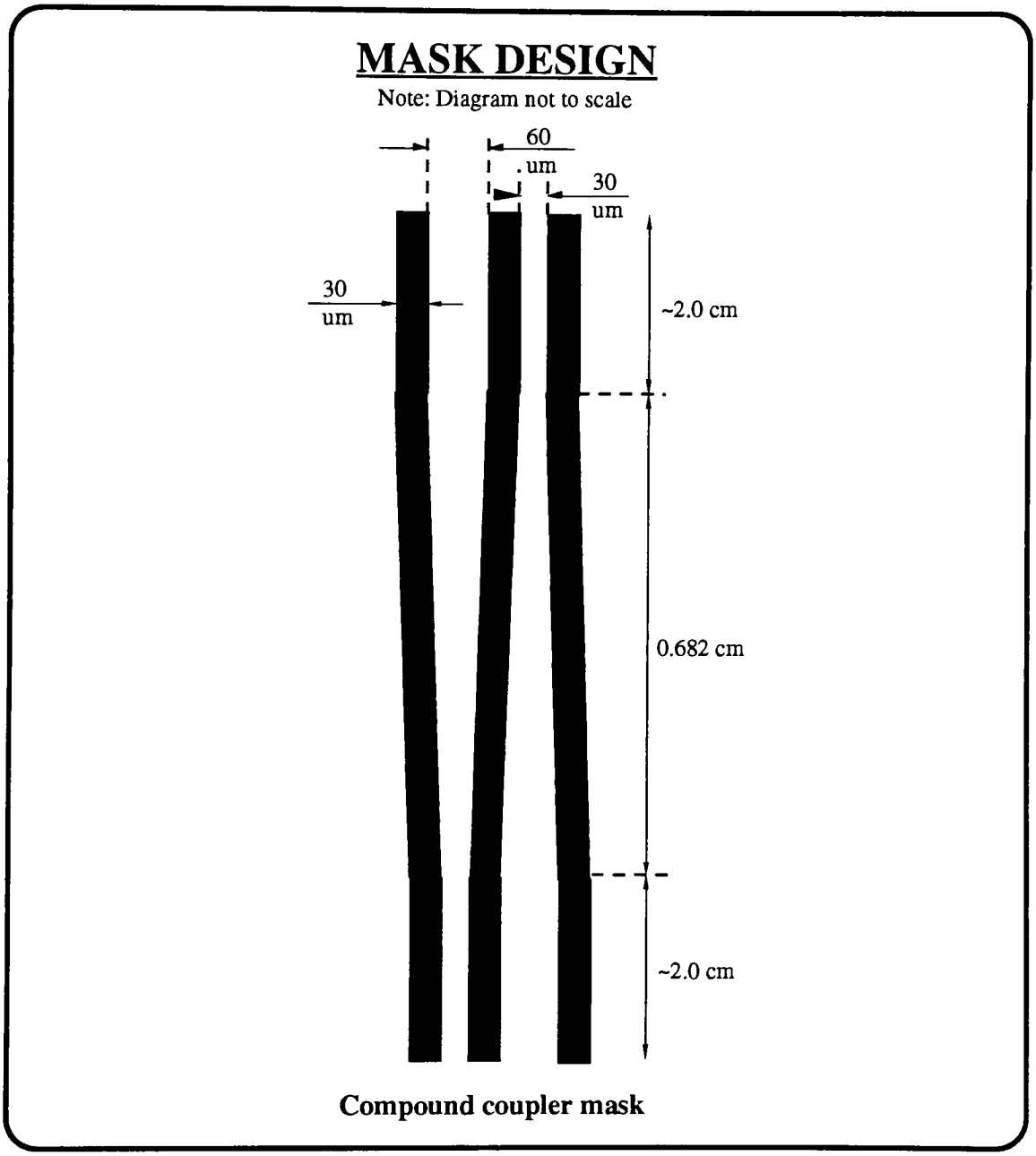

Compound coupler mask

Appendix C4

Al, Ag pallet data from MRC

Aluminum Al

ATOMIC NUMBER	13
ATOMIC WEIGHT	26.97
CRYSTAL STRUCTURE	FCC
MEUING POINT °C	660
DENSITY gm/cc (20°C)	2.70

MARZ~ GRADE lb-/in- 0.0975

TYPICAL MATERIALS ANALYSIS (ppm)

~naysis: E Mass Spectrographic E Vacuum Fusion (Gases) O Emission Sp~rographic ~ Conductometnc (Carbon)

C	20.0	C~	0.30	H~	ND
NI	~ 0.10	Sn	< 0.10	H	3.0
Cd	< 0.10	In	ND	P	ND
T~	ND	0	30.0	CI	< 0.10
K	0.02	Pb	< 0.10	TI	0.10
N	5.00	Co	< 0.10	LI	ND
Pd	ND	V	0.10	Ag	< 0.10
Cr	< 0.10	Mg	0.26	Pt	< 0.10
W	0.10	Al	MAJ	Cu	< 0.10
Mn	< 0.10	Rh	ND	Zn	0.10
A~	< 0.10	Fe	< 0.10	Mo	ND
S	5.0	Zr	0.10	Au	ND
Ga	< 0.10	Na	< 0.10	Sb	< 0.10
BI	< 0.10	Ge	< 0.10	Nb	< 0.10
SI	< 0.10				

METHOD OF PREPARATION: Zone Refined NOMINAL PURITY (TOTAL): 99.9995%

VP GRADE

TYPICAL MATERIALS ANALYSIS (ppm): See pages 132 and 133.

METHOD OF PREPARATION: Chemically re~ined and vacuum melted.

NOMINAL PURITY (TOTAL): 99.999%

Appendix C4 *contd.*

Silver Ag

ATOMIC NUMBER	47
ATOMIC WEIGHT	107.88
CRYSTAL STRUCTURE	FCC
MELTING POINT °C	960.8
DENSITY gm/cc (20°C)	10.49

MARZ~ GRADE lb.lin. o.379

TYPICAL MATERIALS ANALYSIS (ppm)

~nalysis: ~ Mass Spectrographic E Vacuum Fusion (Gases) O Emission Spectrographic ~ Conductometric (Carbon)

C	3.00	C8	0.20	H~	ND
NI	0.10	Sn	0.10	H	1.00
Cd	0.20	In	ND	P	0.40
Ta	0.10	O	5.00	CI	0.10
K	0.30	Pb	0.10	TI	0.10
N	5.00	Co	0.10	LI	ND
Pd	ND	Ag	MAJ	Cr	0.50
M~	0.10	Pt	ND	W	ND
AI	0.40	Cu	0.70	Mn	0.30
Rh	0.10	Zn	0.10	A~	< 0.10
Fo	2.0	Mo	< 0.10	5	0.10
Zr	0.10	Au	< 0.10	Ga	0.10
NI~	0.20	Sb	0.10	el	< 0.10
Ga	0.10	Nb	< 0.10	51	1.0

METHOD OF PREPARATION: Chemically refined and vacuum zone melted

NOMINAL PURITY (TOTAL): 99.999+%

VP GRADE

TYPICAL MATERIALS ANALYSIS (ppm): See pages 132 and 133.

METHOD OF PREPARATION: Chemically refined and vacuum melted.

NOMINAL PURITY (TOTAL): 99.99+ %

Appendix C5

Silver thickness graph

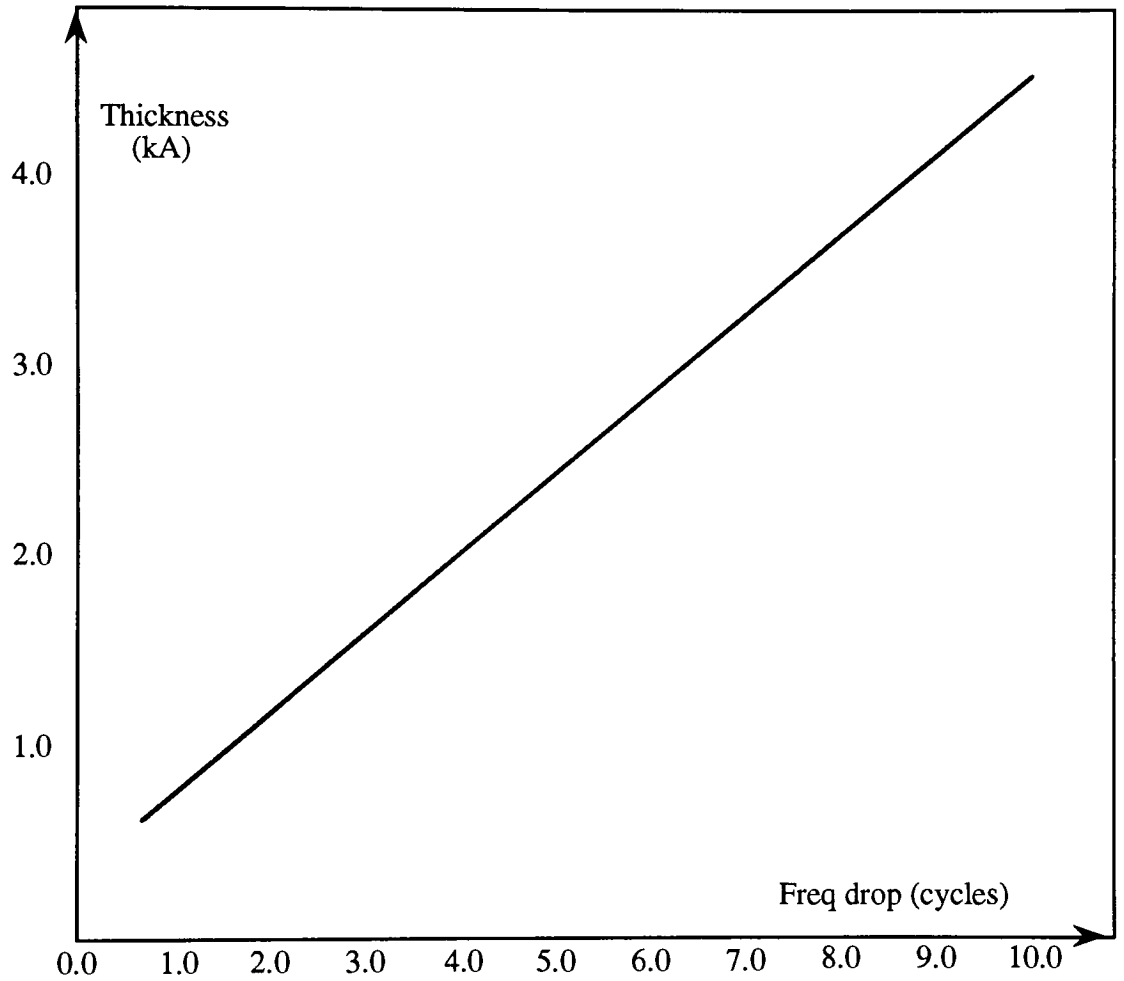

Appendix C6

SEM photos of polished edges (drawings)

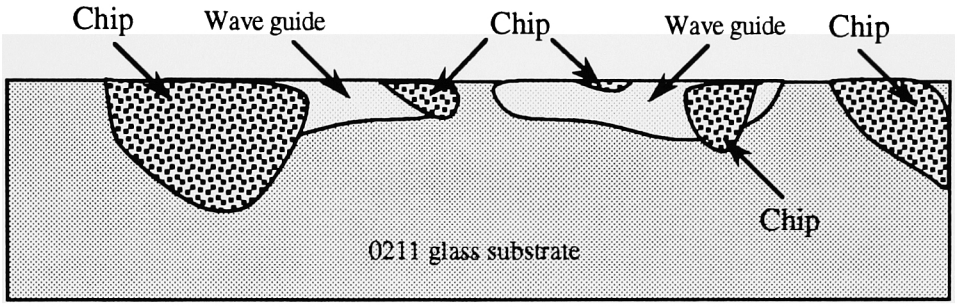

Edge with chips

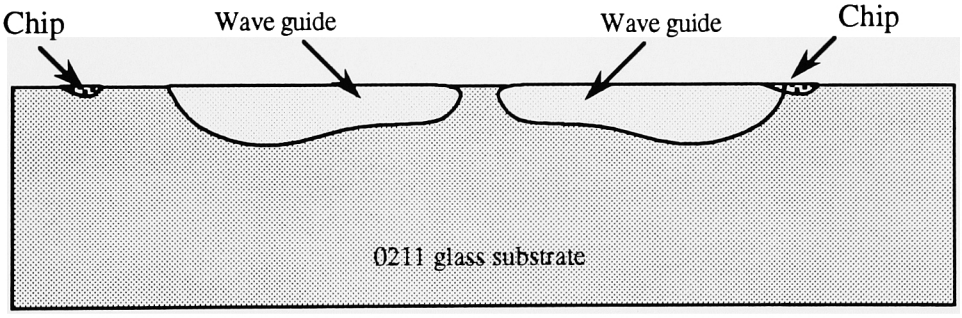

Edge without chips

Appendix D1

Independent study

INDEPENDENT STUDY

by

V.P.Raghavan

Diffusion profiles of ion exchanged waveguides

Prof. Rob Pearson

Microelectronic engineering Dept.

Table of contents

Introduction	page 3
Ion exchange process	page 4
Device design	page 6
Diffusion theory	page 8
Numerical analysis	page 10
Matlab program	page 17
Microprobe profiles	page 20
Analysis of the results	page 22
Matano analysis	page 25
Conclusion	page 29

Introduction

This independent study project is an attempt to understand and model the Ag^+ - Na^+ ion exchange process in 0211 Corning glass substrates.

Ag^+ to Na^+ exchange in optical quality glass, is a process used to selectively increase the refractive index of areas which would function as waveguides, lenses, etc. The optical modes that propagate within structures such as a waveguide require careful tailoring of the two and three dimensional exchange profiles. This study has been done in order to understand and obtain an exchange model, and thus aid in optimizing the process for a high precision laser radar tracking device.

The following has been done in order to achieve this.

a) Processing substrates to form ion exchanged guides.
b) Obtaining concentration data and curve fitting profiles using RS1.
c) Understanding the basic diffusion equations.
d) Converting these equations into MATLAB programs which generate
profiles using numerical methods.
e) Understanding the effects of high concentration on diffusion data using Matano analysis.

Note: All of the steps mentioned above are not necessarily part of this independent study project.

Ion exchange process

Even though the ion exchange process is beyond the scope of this text, the following section attempts to enlighten the reader and help give an understanding of some of the process complexities. A process flowchart is given in Appendix A1

Unlike the diffusion process involved in the microelectronic industry, (impurities are diffused into the silicon wafer where they become a source of holes and electrons) the ion exchange process is one where an ion in the glass substrate is exchanged with another externally introduced ion. This ion would preferably have the same ionic radius while exhibiting a different polarizability. Na^+ and Ag^+ permit this kind of exchange to take place between a sodium rich glass and an external source of silver.

The external source of silver can be obtained either from a melt process or a solid silver film. The process involved in making the high precision laser radar tracking device, uses the solid silver thin film for a Ag^+ source (dictated by other needs of the device). Unlike the melt process where the required Gaussian exchange profile can be obtained in one step, the solid film requires an initial electric field aided predeposit followed by a drivein step. As seen latter, this produces a silver rich layer of about 10um depth, and conforms to a complimentary erf function. A second diffusion or drivein step is then performed. This drives the Ag^+ into the glass about 18um, and gives the required Gaussian profile.

The concentration of silver in the melt is very small. As a result during a long exchange or diffusion, the concentration of the top layer of the substrate equalizes with that of the source. From this point on the profile changes from a complimentary erf to a Gaussian. Since the total number of ions in the melt is a lot greater than that diffusing into the substrate, it can be considered a constant, which means that the peak surface concentration of the substrate will also remain a constant. The total number of ions in the substrate will increase for the entire period of diffusion.

During second diffusion in the solid silver process, all the silver source is stripped off the surface. Since the total number of ions in the substrate remains a constant, (except for out diffusion) the peak surface concentration of silver in the substrate will continue to fall as the ions diffuse deeper.

The profiles are obtained via microbe analysis. An RS1 curve fit is done on the microprobe data and yield the profile with the least square error. A brief explanation of this technique is given in the section on Microprobe profiles.

Device design

The device is a High Precision Laser Radar Tracker, operating at He-Ne wavelengths. Again the theory of operation is beyond the scope of this text. The following section is a brief detail of the operation as required by the reader to understand the device.

The device consists of three waveguides placed in a configuration shown in Appendix A2. When light (a Gaussian beam is focused down by a lens) is butt coupled into the driven guide, modes propagate down its length. The higher order modes couple light proportionally into the second guide. This in turn couples light into the third or coupled guide. The number of modes being excited by the guide is determined by the input position to the driven guide.The least number of modes are propagated when light is injected on bore sight. (Bore sight is defined to be the center point of the waveguide which excites the lowest order mode within the guide.) This in turn couples the least number of modes into the coupled guide, and corresponds to the least power output by the coupled guide.When light is injected into the driven guide off bore sight, (off center) higher order modes propagate down the driven guide, resulting in more power being coupled into the coupled guide. The further off bore sight the input beam, the greater the power output at the coupled guide.

A power coupling ratio in the form of

$$PCR = \sqrt{\frac{P_3}{P_1 + P_2 + P_3}}$$

gives a V curve as shown in appendix B1. The power varies as a function of the input beams position. Y axis represents vertical scan depth.

The sensing information is obtained by performing coherent detection. Left or right of bore sight is dependent on the phase shift of the coupled guide output. As can be seen in appendix B1, the sensitivity of this device is dependent on the lowest null obtainable. Its also highly desirable to have steep side walls on the V . This translates to a greater shift in power for a small shift in position.

The side walls of the V depend on the exchanged profiles. It is understood that the optimum V is obtained if the two Gaussian profiles barely merge on the side where the guides are 30um apart. This ensures optimum coupling. It is also required that the guides (profiles) do not touch on the side where they are 60um apart. Coupling should not take place in this region.

Diffusion theory

Ficks first and second laws are used to obtain the basic equation. The electric field aided term is added on to this equation. It is then manipulated into a form which can be used in a numerical computer program.

Ficks first law states that the flux of matter across a given plane is proportional to the concentration gradients across the plane. The flux J is given by

$$J = - D \frac{\partial C(x,t)}{\partial x} \qquad \text{.....(1)}$$

where D, the constant of proportionality, is the diffusion constant for the material. Dimensions of this equation are

J (mass) / (length^2 x time) = -D (length^2 / time) dC/dx (mass/length^3/length)

In the case of a finite volume, the impurity gradient decreases with time - the concentration changes with time. Consider an element, delta x thick along the x axis. This would have J_1 entering and J_2 leaving.

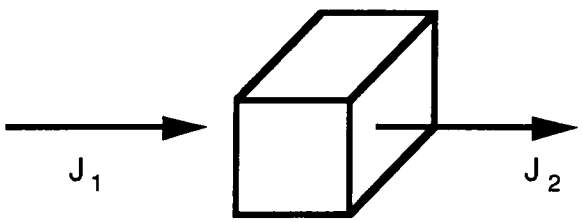

Therefore the net increase in matter in the element per unit time, is given by

$$J_2 - J_2 = \Delta x \left(\frac{\partial C}{\partial t}\right) = - \Delta x \left(\frac{\partial J}{\partial x}\right) \qquad \text{.....(2)}$$

This can be written as

$$\frac{\partial C(x,t)}{\partial t} = -\frac{\partial J}{\partial x} \qquad \text{.....(3)}$$

Substitution from equation (1), yields the prototypical parabolic equation

$$\frac{\partial C(x,t)}{\partial t} = \frac{\partial}{\partial x}\left(D\,\frac{\partial C}{\partial x}\right) \qquad \text{.....(4)}$$

Case 1: When the solute concentration is low the diffusion coefficient is independent of concentration or position.

$$\frac{\partial}{\partial x}\left(D\,\frac{\partial C}{\partial x}\right) = D\,\frac{\partial}{\partial x}\left(\frac{\partial C}{\partial x}\right) = D\left(\frac{\partial^2 C}{\partial x^2}\right) \qquad \text{.....(5)}$$

Therefore the diffusion equation in a single dimension (X axis) is

$$\frac{\partial C(x,t)}{\partial t} = D\left(\frac{\partial^2 C(x,t)}{\partial x^2}\right) \qquad \text{.....(6)}$$

Note: In this study the simplifying assumption of equal Ag^+ and Na^+ mobilities has been made. The diffusion equation for the case of an applied force is

$$\frac{\partial C(x,y,t)}{\partial t} = D\,\nabla^2_{xy}\,C(x,y,t) - \mu\nabla^2_{xy}.\left(C\,\overline{E}(x,y)\right) \qquad \text{.....(7)}$$

where C(x,y,t) is the concentration of Ag^+ as a function of x or lateral dimension (parallel to substrate surface),y, or depth dimension (perpendicular to substrate surface),and t, diffusion time; D is the concentration independent diffusion coefficient; u is the ionic mobility and E(x,y) is the applied electric field.

Numerical analysis

The diffusion equation with the applied force field is manipulated in order to obtain a numerical expression as shown below.The resulting expression can then be used in a computer program to obtain the diffusion profiles. Equation (7)

$$\frac{\partial C(x,y,t)}{\partial t} = D\,\nabla^2_{xy}\,C(x,y,t) - \mu\nabla^2_{xy}.\left(C\,\overline{E}(x,y)\right) \qquad \text{.....(7)}$$

In the above equation the Laplacian is given by

$$\nabla^2_{xy} = \frac{\partial^2}{\partial x^2} + \frac{\partial^2}{\partial y^2} \qquad \text{.....(8)}$$

and the divergence is given by

$$\nabla_{xy} = i\,\frac{\partial}{\partial x} + j\,\frac{\partial}{\partial y} \qquad \text{.....(9)}$$

The analysis follows the axis convention given below.

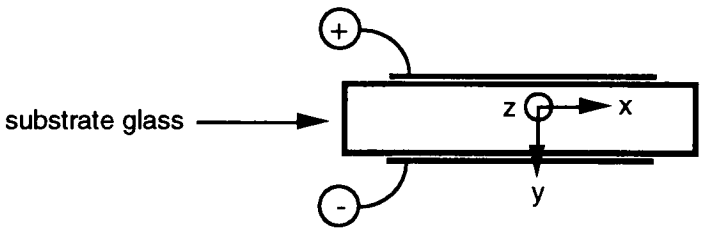

The electric field is assumed to be in the Y direction or

$$\overline{E}(x,y) = j\,E_y \qquad \text{.....(10)}$$

Therefore the field aided term in equation (7) becomes

$$\mu\,\nabla_{xy}.\left(C(x,y,t)\,\overline{E}(x,y)\right) = \mu\,\nabla_{xy}.C(x,y,t)\,j\,E_y = \mu\,E_y\,\nabla_{xy}.\left(j\,C(x,y,t)\right) \qquad \text{.....(11)}$$

Applying the following relationship

$$\nabla^2 C = \nabla.(\nabla C)$$

to the flux conservative term in equation (7), yields the following.

$$D\,\nabla^2_{xy}\,C(x,y,t) = D\nabla_{xy}.(\nabla_{xy}\,C(x,y,t)) \qquad \text{.....(12)}$$

Substituting equation (11) and (12) into equation (7), results in the equation

$$\frac{\partial}{\partial t} C(x,y,t) = D\nabla_{xy}.(\nabla_{xy}\,C(x,y,t)) - \mu\,E_y\,\nabla_{xy}.(j\,C(x,y,t)) \qquad \text{.....(13)}$$

Taking the integral over an incremental volume, dv

$$\int \frac{\partial}{\partial t} C(x,y,t)\,dv = \int D\nabla_{xy}.(\nabla_{xy}\,C(x,y,t))\,dv \quad \int \mu\,E_y\,\nabla_{xy}.(j\,C(x,y,t))\,dv$$

Since D,E_y and mobility are constants

$$\int \frac{\partial}{\partial t} C(x,y,t)\,dv = D\int \nabla_{xy}.(\nabla_{xy}\,C(x,y,t))\,dv - \mu\,E_y\int \nabla_{xy}.(j\,C(x,y,t))\,dv$$

.....(14)

Using the following relationships

$$D\int \nabla_{xy}.(\nabla_{xy}\,C(x,y,t))\,dv = D\oiint \nabla_{xy}\,C(x,y,t).d\bar{s}$$

and

$$\mu\,E_y\int \nabla_{xy}.(j\,C(x,y,t))\,dv = \mu\,E_y\oiint j\,C(x,y,t).d\bar{s}$$

equation (14) becomes

$$\int \frac{\partial}{\partial t} C(x,y,t)\, dv = D \oiint \nabla_{xy}\, C(x,y,t).d\bar{s} - \mu\, E_y \oiint j\, C(x,y,t).d\bar{s}$$

.....(15)

The concentration C(x,y,t) is a continuous variation on x and y. Using the finite difference method, the function C(x,y,t) can be represented by a discrete set of rectangular cubes. The cross sectional area of each cube is delta x. delta y, while the length is 1meter (in the z direction) as shown below.

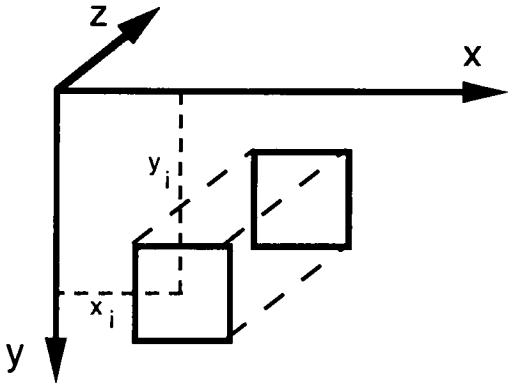

If the axis x and y are considered to be the surface, a matrix grid of m x n x 1 is formed. This checkerboard arrangement of the surface, provides a means of matrix manipulation to obtain the diffusion profile.The analysis continues in a 2 dimensional matrix form since the z axis is fixed at 1m length.The quantization of concentration, results in is a constant C at x_i, y_j and is given by

$$C(x,y,t) = C_{ij}(t)$$

This result has the following impact on equation (15).

$$\int \frac{\partial}{\partial t} C(x,y,t)\, dv \Rightarrow \frac{\partial}{\partial t} C_{ij}(t) \int dv \Rightarrow \frac{\partial}{\partial t} C_{ij}(t)\, \Delta x\, \Delta y$$

.....(16)

From the definition of derivatives

$$\frac{\partial}{\partial t} C_{ij}(t)\,\Delta x\,\Delta y \cong \frac{C_{ij}(t+\Delta t) - C_{ij}(t)}{\Delta t}\,\Delta x\,\Delta y \qquad \text{.....(17)}$$

In the surface integral, ds is depended on the corresponding surfaces.

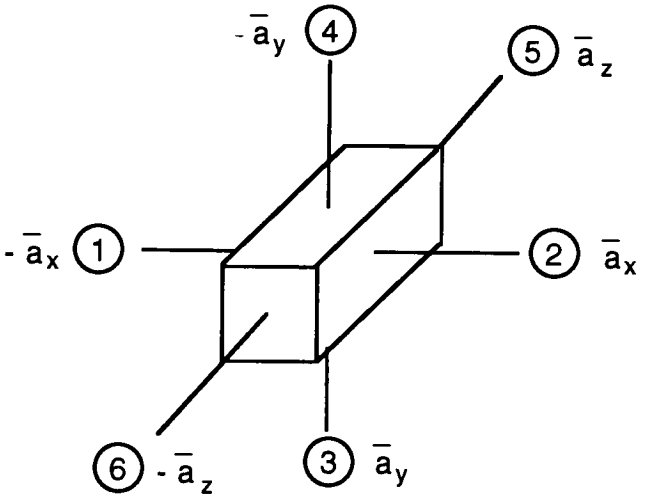

Using

$$\Delta_{xy}\, C_{ij}(t) \simeq \bar{a}_x \frac{\partial C}{\partial x} + \bar{a}_y \frac{\partial C}{\partial y}$$

the second term in equation (15) becomes

$$\begin{aligned}\oiint \nabla_{xy}\left(C_{ij}(t)\right).d\bar{s} \Rightarrow & \oiint_1 \left(\bar{a}_x \frac{\partial C}{\partial x} + \bar{a}_y \frac{\partial C}{\partial y}\right) . (-\bar{a}_x)\, ds + \oiint_2 \left(\bar{a}_x \frac{\partial C}{\partial x} + \bar{a}_y \frac{\partial C}{\partial y}\right) . (\bar{a}_x)\, ds \\ & + \oiint_3 \left(\bar{a}_x \frac{\partial C}{\partial x} + \bar{a}_y \frac{\partial C}{\partial y}\right) . (\bar{a}_y)\, ds + \oiint_4 \left(\bar{a}_x \frac{\partial C}{\partial x} + \bar{a}_y \frac{\partial C}{\partial y}\right) . (-\bar{a}_y)\, ds \\ & + \oiint_5 \left(\bar{a}_x \frac{\partial C}{\partial x} + \bar{a}_y \frac{\partial C}{\partial y}\right) . (\bar{a}_z)\, ds + \oiint_6 \left(\bar{a}_x \frac{\partial C}{\partial x} + \bar{a}_y \frac{\partial C}{\partial y}\right) . (-\bar{a}_z)\, ds\end{aligned}$$

.....(18)

For surface 1 the corresponding term reduces to

$$\oiint_1 \left(\bar{a}_x \frac{\partial C}{\partial x} + \bar{a}_y \frac{\partial C}{\partial y}\right) . (-\bar{a}_x)\, ds = - \oiint_1 \frac{\partial}{\partial x} C_{ij}(t) .ds \Rightarrow - \oiint_1 \frac{C_{ij}(t) - C_{i-1,j}(t)}{\Delta x} ds$$

$$\Rightarrow \frac{C_{ij}(t) - C_{i-1,j}(t)}{\Delta x} \oiint_1 ds \Rightarrow \frac{C_{ij}(t) - C_{i-1,j}(t)}{\Delta x} \Delta y$$

For surface 2 the corresponding term reduces to

$$\oiint_2 \left(\bar{a}_x \frac{\partial C}{\partial x} + \bar{a}_y \frac{\partial C}{\partial y}\right) . (\bar{a}_x)\, ds = \oiint_2 \frac{\partial}{\partial x} C_{ij}(t) .ds \Rightarrow \oiint_2 \frac{C_{i+1,j}(t) - C_{ij}(t)}{\Delta x} ds$$

$$\Rightarrow \frac{C_{i+1,j}(t) - C_{ij}(t)}{\Delta x} \oiint_2 ds \Rightarrow \frac{C_{i+1,j}(t) - C_{ij}(t)}{\Delta x} \Delta y$$

Therefore the sum of surfaces 1 and 2 gives

$$\oiint_1 + \oiint_2 = \frac{C_{i+1,j}(t) - 2C_{ij}(t) + C_{i-1,j}(t)}{\Delta x} \Delta y \qquad \text{.....(19)}$$

Similarly the sum of surfaces 3 and 4 gives

$$\oiint_3 + \oiint_4 = \frac{C_{i,j+1}(t) - 2C_{ij}(t) + C_{i,j-1}(t)}{\Delta y} \Delta x \qquad \text{.....(20)}$$

The dot product reduces the sum of surfaces 5 and 6 to zero.

$$\oiint_5 + \oiint_6 = 0 \qquad \text{.....(21)}$$

The third surface integral in equation (15)

$$\iint j\, C_{ij}(t)\,.d\bar{s} = \iint \bar{a}_y C_{ij}(t)\,.d\bar{s}$$

$$= \iint_3 \bar{a}_y C_{ij}(t)\,.(\bar{a}_y)\,dx + \iint_4 \bar{a}_y C_{ij}(t)\,.(-\bar{a}_y)\,dx$$

$$= \frac{C_{i,j+1}(t) + C_{ij}(t)}{2}\Delta x - \frac{C_{ij}(t) + C_{ij-1}(t)}{2}\Delta x$$

.....(22)

Substituting equations (17), (19), (20) and (22) into equation (15), gives the following result.

$$\frac{C_{ij}(t+\Delta t) - C_{ij}(t)}{\Delta t}\Delta x\,\Delta y = D\left[\frac{C_{i+1,j}(t) - 2C_{ij}(t) + C_{i-1,j}(t)}{\Delta x}\Delta y + \frac{C_{i,j+1}(t) - 2C_{ij}(t) + C_{i,j-1}(t)}{\Delta y}\Delta x\right] - \mu E_y\left[\frac{C_{i,j+1}(t) + C_{ij}(t)}{2}\Delta x - \frac{C_{ij}(t) + C_{ij-1}(t)}{2}\Delta x\right]$$

.....(23)

Multiplying equation (23) by

$$\frac{\Delta t}{\Delta x\,\Delta y}$$

results in the following form.

$$C_{ij}(t+\Delta t) - C_{ij}(t) = D\,\Delta t\left[\frac{C_{i+1,j}(t) - 2C_{ij}(t) + C_{i-1,j}(t)}{\Delta x^2} + \frac{C_{i,j+1}(t) - 2C_{ij}(t) + C_{i,j-1}(t)}{\Delta y^2}\right] - \mu E_y \frac{\Delta t}{\Delta y}\left[\frac{C_{i,j+1}(t) + C_{ij}(t)}{2} - \frac{C_{ij}(t) + C_{ij-1}(t)}{2}\right]$$

.....(24)

Note: The electric field given in equation (24) is in the Y direction.

If we let $\Delta x = 1, \ \Delta y = 1$ equation (24) can be rewritten as

$$C_{ij}(t+\Delta t) = C_{ij}(t) + D\,\Delta t\,[C_{i+1,j}(t) + C_{i-1,j}(t) + C_{i,j+1}(t) + C_{i,j-1}(t) - 4C_{ij}(t)] - \mu E_y \frac{\Delta t}{2}[C_{i,j+1}(t) - C_{ij-1}(t)] \quad \text{.....(25)}$$

For the computer program, the term dc is first calculated as

$$dc = \frac{C_{ij}(t+\Delta t) - C_{ij}(t)}{\Delta t} \quad \text{.....(26)}$$

From this is obtained

$$C_{ij}(t+\Delta t) = \Delta t.dc + C_{ij}(t) \quad \text{.....(27)}$$

In the above equations the term $C_{ij}(t)$ represents the concentration of the i,j th cube at a time t. The LHS term represents the concentration of the same cube at time t + delta t. It should also be noted that the stability criterion for equation (24) is

$$2\,D\,\Delta t \leq 1$$

The physical interpretation of this restriction is that the maximum allowable time step, is the diffusion time to cross a cell of the basic dimension delta x or delta y.

MATLAB Program

Matrix laboratory, better known as MATLAB, is a interactive program whose basic data element is a matrix that does not require dimensioning. A big advantage with MATLAB is that the problem solution is expressed exactly as it is written in the mathematical form. The program is available on many computers.This study utilizes a Macintosh which runs MacMATLAB. Program listing is given in Appendix C1-C4.

The basic program uses a (50 x 300) matrix named C. The first row of this matrix defines waveguides. A one placed on the following cells indicates the deposited silver. The rest of the cells in C are set equal to zero.

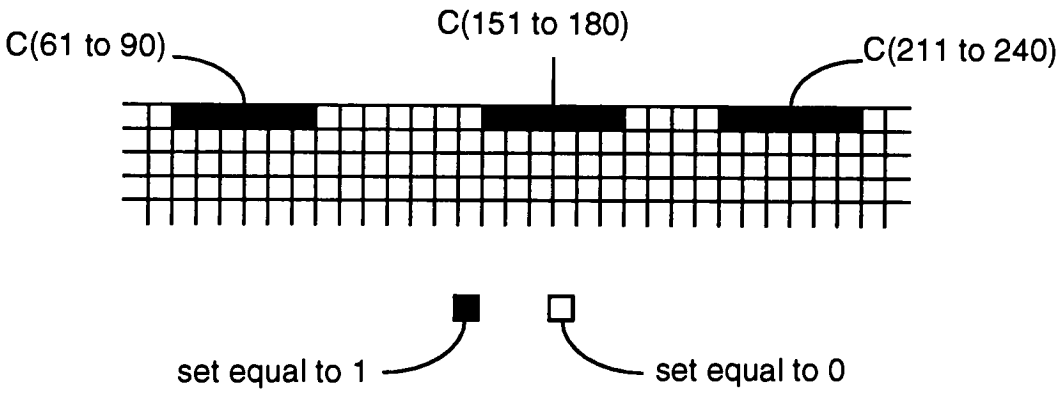

Another matrix dc , (49 x 299), defines the incremental change in concentration. It is calculated using equation (26). Rows 2 through 50 and columns 2 through 300 of the matrix C are then updated to the new value of the concentration. The first row of C, (other than the cells containing the guides) is then set equal to zero. This is needed to prevent out diffusion of silver. The calculations are performed in a loop until the required time limit is reached.

Another matrix , is made up of a single cell concentration as it varies with time. The final C and Y matrix along with diffusivity, temperature and time data are then stored in a file. This file can be accessed by another program to print the following graphs.

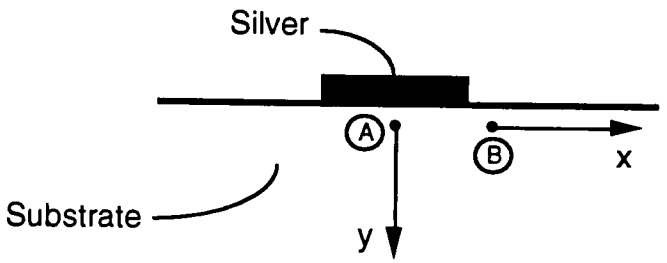

(a) Concentration at point A vs. time.

(b) Concentration at point B vs. time.

(c) Profiles in the X direction. (concentration vs. position)

(d) Profiles in the Y direction. (concentration vs. position)

(e) Three dimensional profile.

(f) X profiles at depths 2,4,6,8..... um into the glass.

From this file its possible to extract almost any data of interest. All the data is generated with respect to the surface solid silver concentration of 1. Each plot can have a maximum concentration value of less than 1.These plots are normalized so that the maximum concentration is always 1.

The entire process is divided into two sections. First is the predeposit. This program operates as described above with the following parameters.

$E = 0.16$ volts/um, $T = 300^{o}C$.

The second part of this process is the second diffusion. This program also operates as described above with a few exceptions. The starting matrix C is set equal to the C matrix of the predeposit. (This matrix was set equal to zero in the previous case.) Unlike the predeposit case which had a constant source of silver, the first row of the second diffusion C matrix, is always set equal to the second row. This implies, no silver source and no out diffusion. The following parameters are set for this section.

$$E = 0 \text{ volts/um}, \qquad T = 400^{o}C.$$

As before the C and Y matrix are saved to be used by the plotting program.

Microprobe profiles

Microprobe was done on the cross sections of the polished samples.The number of back scattered electrons is proportional to the number of Ag^+ in the glass. The main problem with microprobe was that it had to be done at the U of R institute of optics. This involved scheduling the already heavily used SEM. This in combination with the process complexity of the device, permitted only limited aqusition of diffusion profile data. The S E M scanning stage was also a problem. Even though the data points were separated by 2um, the position of the first data point was ambiguous. It could be in the region of 0 to 2 microns into the glass surface. For this study, the first data point was taken to be 2um into the glass.

Microprobe data was obtained from five samples.

Sample 1 - Prediffusion; 100 v; 60 min.; 300^{o}C

Sample 2 - Prediffusion; 100 v; 240 min.; 300^{o}C
+ Second diffusion; 0 v;120 min.; 400^{o}C

Sample 3 - Prediffusion; 100 v; 70 min.; 300^{o}C

Sample 4 - Prediffusion; 100 v; 70 min.; 300^{o}C
+ Second diffusion; 0 v;90 min.; 400^{o}C

Sample 5 - Prediffusion; 100 v; 70 min.; 300^{o}C
+ Second diffusion; 0 v;60 min.; 400^{o}C

All curves are normalized. The data obtained from sample 1 is given in Appendix D1. The RS1 curve fitted polynomial is given by the double line curve. The single line curve is a complimentary erf function. Note the Kink region exhibited by the data at the bottom of the curve.

Sample 2 data is given in appendix D2. RS1 curve fit is given by the double line. Appendix D3 shows this RS1 fitted polynomial along with a Gaussian curve. Note the shift in the tail region.

Sample 3 data is shown in Appendix D4. The curve with the least square error (RS1) is given by the doted lines. Note the absence of the kink.

Sample 4 data is shown in Appendix D5. Best fit is given by the double line curve (RS1). The total depth of this guide is in the region of 18 to 20um. Appendix D6 gives sample 5 data. The depth of this guide is about 20 to 22um.

Analysis of the results

The MATLAB program was run many times with different parameter settings. A Diffusivity of 0.00022 um^2/sec was seen to give the best fitting curves for the prediffusion microprobe data. The following plots show the microprobe data as a solid line. The dashed line shows the program generated profiles.

Appendix E1 is a plot of the 60 min. microprobe data (solid line), and the corresponding simulated profile. Except in the kink region these demonstrate good fit. Appendix E2 gives the 70 min. prediffusion data. The simulated curve fit is not as good as in the previous case.

The absence of the kink region in E2, places doubt on the kink in E1. None of the other microprobe results exhibit this phenomenon either. It is very possible that the microprobe stage did not move by the required 2um as set by the operator. Since the actual position translated by the stage is not printed out, it seems likely that the kink is the result of a mechanical problem rather than a diffusion or exchange related phenomenon. It should be noted that a similar kink phenomenon is seen in the phosphorus diffusion in the microelectronic industry.

Appendix E3, E4 and E5 are plots of the 60, 90 and 240 min. second diffusions. A diffusivity of 0.0065 um^2/sec seems to yield the best fitting simulated profiles.

Note: The second diffusion is at a higher temperature.

As can be seen, E3 and E5 provide a good fit while E4 provides an adequate fit. Appendix E6 is a simulation of the 90 min. second diffusion using a diffusivity value of 0.0045 um^2/sec. While observing a near perfect fit, it should be noted that D is given by

$$D = D_o e^{(-Q/kT)}$$

which means that for a given temperature, D should remain a constant.

All the plots show a definite discrepancy in the tail region. The simulated profile has a tail which is characteristic of a Gaussian. This is not seen in the microprobe data, and could be attributed to the following.

(a) Non linear reflectance of low concentration silver ions or, non linear response of the detector or, some combination of two.

(b) Low diffusivity in the regions with little silver concentrations.

At this point, this phenomenon is not well understood. The latter is studied in greater depth in the next section.

Concentration vs. time plots provide interesting information. Appendix E7 shows the peek concentration as it varies with time for the 60 min. prediffusion sample. The graph indicates that a prediffusion time of at least 50 min. would be required before 90% of the silver is diffused into the sample. Appendix E8 is the peek concentration as it varies with time for the 240 min. second diffused sample. The graph is an indication of time dependence of this diffusion.

Short diffusion indicates greater change in concentration resulting in critical control of second diffusion time. On the other hand, longer diffusion times show less of a gradient, giving rise to a more controlled process. The optimum second diffusion time used in the process is 90 min. (Appendix E9)

As noted before, merger of the two coupling guides is critical for the device performances. This information is obtained from Appendix E10 which is a profile plot at different depths into the guide. The inability to understand or accurately simulate the tail regions of the microprobe profiles is a major draw back. The simulation of the 90 min. profile indicates the merger point to be at a depth of about 30 um. This is due to the Gaussian tail.(extended tail) However, the short tail of the microprobe profiles would indicate a merger at a depth of about 10um.

It should be noted that the simulated profiles do give a good indication as to its shape. Appendix E11 and E12 are three dimensional plots of the concentration matrix of prediffusion and second diffusion.

Appendix E13 and E14 are unnormalized plots of the 240min sample. Peak concentration of the source is taken to be one. Surface concentration after pre deposit is seen to approach this value - Appendix E13. This value is seen to drop as a result of the stripped silver source second diffusion - Appendix E14.

Matano analysis

Equation (4) is stated below. (In the Y direction)

$$\frac{\partial C}{\partial t} = \frac{\partial}{\partial y}\left(D \frac{\partial C}{\partial y}\right) \qquad \text{.....(4)}$$

In case 1, it was assumed that when the solute concentration is low the diffusivity is independent of concentration or position. This results in equation (6).If however the diffusivity is a function of concentration, D = D(C), equation (6) becomes

$$\frac{\partial C}{\partial t} = \frac{\partial D}{\partial y}\frac{\partial C}{\partial y} + D\frac{\partial^2 C}{\partial y^2} \qquad \text{.....(28)}$$

This concentration dependent D makes equation (28) an inhomogeneous differential equation. It should be stated that while its possible to find solutions to equation (5), its difficult to find a closed form solution for equation (28). Using the MATLAB program with some modifications, its possible to incorporate the concentration dependent diffusivity into the simulated profile.To accomplish this, a diffusivity vs. conc profile is needed as an input file. The program would have to read this file as it progresses with concentration calculations from cell to cell.

The program modification is not attempted in this study. However an attempt is made to extract the position related diffusivity profile. The following is a brief explanation of the Matano analysis which is used for this purpose.(For a detail description refer to Silicon Processing for the VLSI era, Volume 1 by S Wolf and R.N.Tauber)

As stated on the previous page Matano analysis allows D(C) to be calculated from an experimentally determined concentration profile such as the microprobe data. Using a change of variables

$$\eta = \frac{x}{\sqrt{t}} \qquad \text{.....(29)}$$

equation (28) becomes

$$\frac{-\eta}{2}\frac{\partial C}{\partial \eta} = \frac{\partial}{\partial \eta}\left(D\frac{\partial C}{\partial \eta}\right) \qquad \text{.....(30)}$$

The surface concentration is taken to be C_o with the concentration elsewhere being equal to zero.Integrating equation (30) between the limits C=0 and $C=C_1$, where C_1 is the concentration at which the diffusion coefficient is desired, gives

$$\frac{-1}{2}\int_0^{C_1} \eta \, dC = \left[D\frac{\partial C}{\partial \eta}\right]_{C=0}^{C=C_1}$$

With the proper boundary conditions the expression for concentration dependent diffusivity is

$$D(C_1) = \frac{-1}{2t}\left(\frac{dx}{dC}\right)_{C_1}\int_0^{C_1} x \, dC \qquad \text{.....(31)}$$

(Note: This equation is in single dimension.)

This means that D as a function of position can be obtained from graphical integration and differentiation of the microprobe profile as shown.

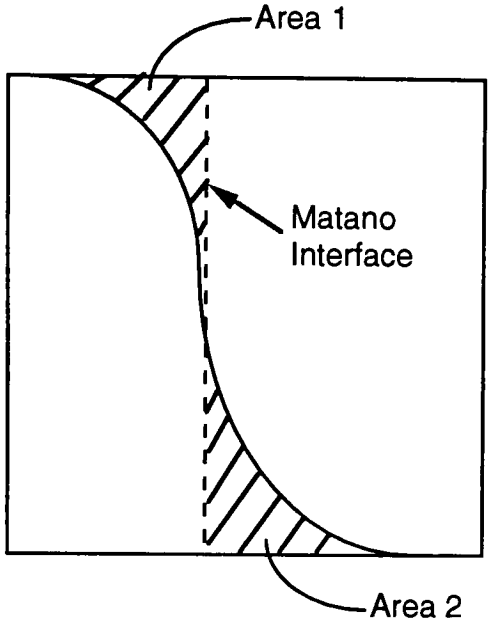

The Matano interface is defined as the line which makes area1 equal to area2.

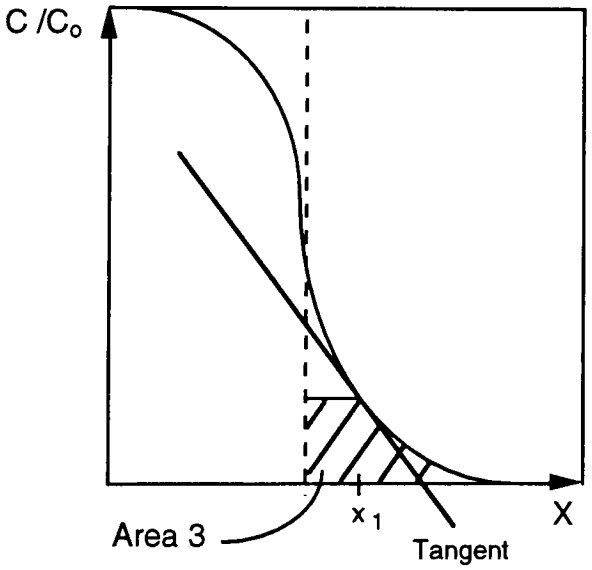

Area3 is equal to the integral term

$$\int_0^{C_1} x \, dC$$

and the reciprocal of the slope at depth x_1 is

$$\left(\frac{dx}{dC}\right)$$

The program used for the Matano analysis is given in Appendix F1. The diffusivity obtained from this program is in the range of the value used in the simulations as shown in Appendix F2 - F6.

The kink region in the 60 min. prediffusion shows up as the peak in F2 and F3. Appendix F4 and F5 are diffusivity data obtained from the 240 min. microprobe sample. Appendix F6 is a Matano analysis of the 240 min. simulation. The interpretation of these plots is unclear. The diffusivity obtained from F6 should be a constant since a constant value was used for the simulation. The diffusivity obtained from F6 does not indicate this. Similarity between F5 and F6 would seem to indicate an error in the Matano program or the input file.

Conclusion

The MATLAB program is seen to give accurate simulations. The fit in the tail region is not as good as that in the main body. The diffusivity which yields the best fitting curve for predeposition is 0.00022um^2/sec. The diffusivity used in the second diffusion simulation is 0.0065um^2/sec. Since only one temperature was used in the tests, (T=300°C - prediffusion and T=400°C - second diffusion) its impossible to obtain the activation energy, Q, or the coefficient of diffusion, D_o. (Its expected that the activation energy and diffusion coefficient will differ for prediffusion and second diffusion) While these numbers are in the region given by other references, the process conditions are different. As a result no comparisons can be made.

With some modification this program could be used with non constant diffusivity. For this to be accurate a two dimensional diffusivity matrix is needed. This would require a two dimensional microprobe profile.The Matano analysis could be used to extract the diffusivity data from this. The Matano analysis is seen to produce diffusivity within two orders of magnitude compared to simulations. However the results are not well understood. It should be stated that the diffusivity could be tailored to produce simulations that fit the body and the tail regions of the microprobe profiles by implementing the scheme described.

Independent study

Appendix

Appendix A1

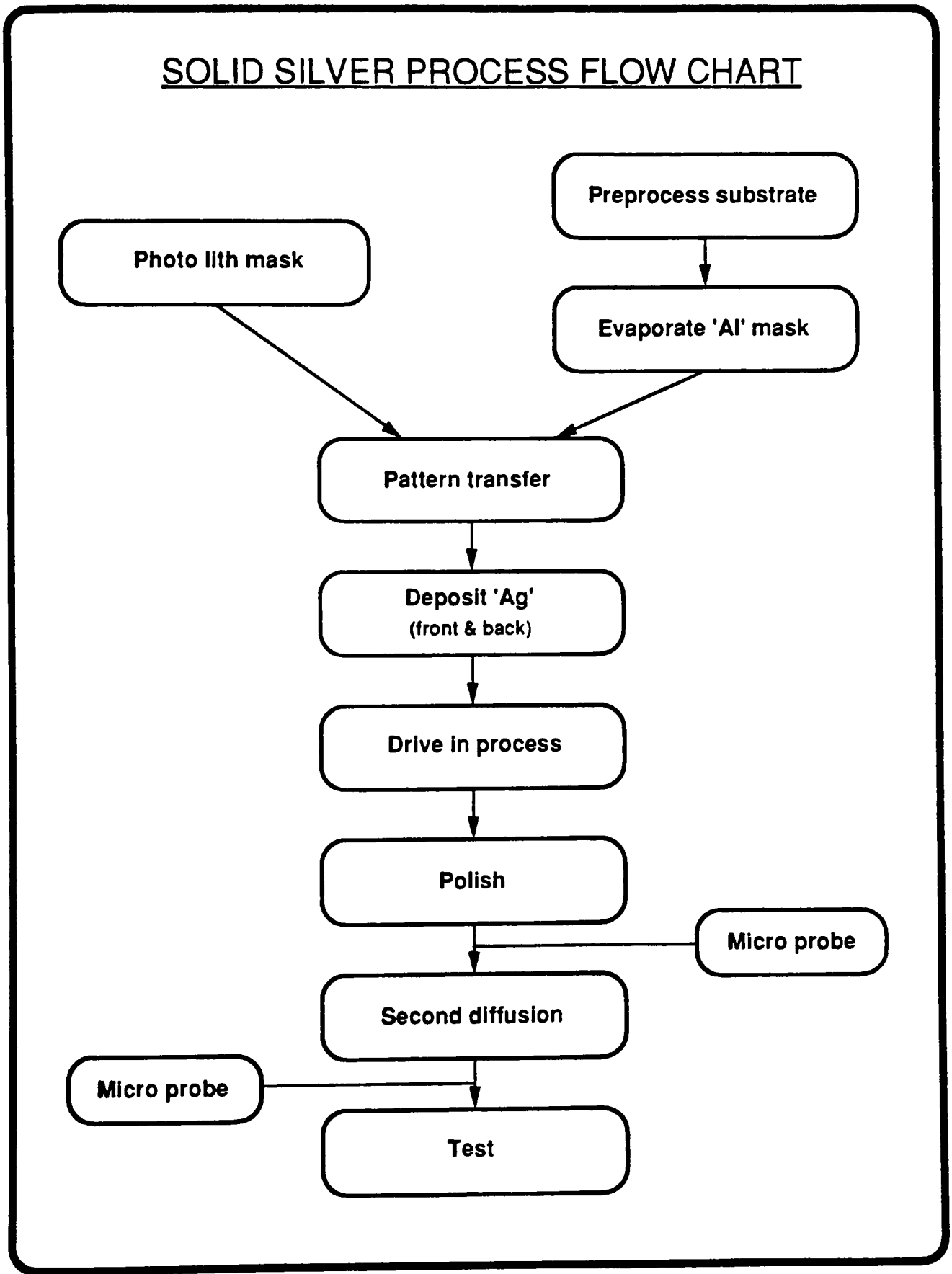
SOLID SILVER PROCESS FLOW CHART
Preprocess substrate
Photo lith mask
Evaporate 'Al' mask
Pattern transfer
Deposit 'Ag'
(front & back)
Drive in process
Polish
Micro probe
Second diffusion
Micro probe
Test

Appendix A2

MASK DESIGN

Note: Diagram not to scale

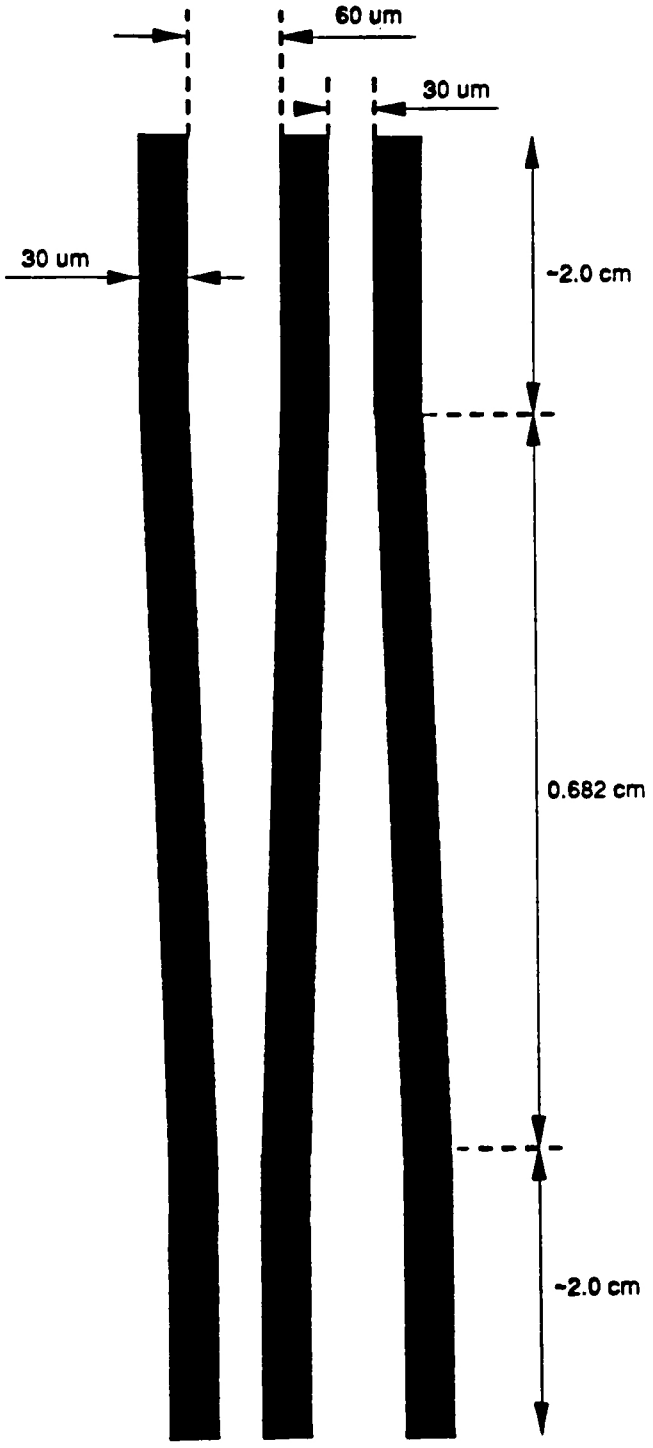

Compound coupler mask

V- Curve

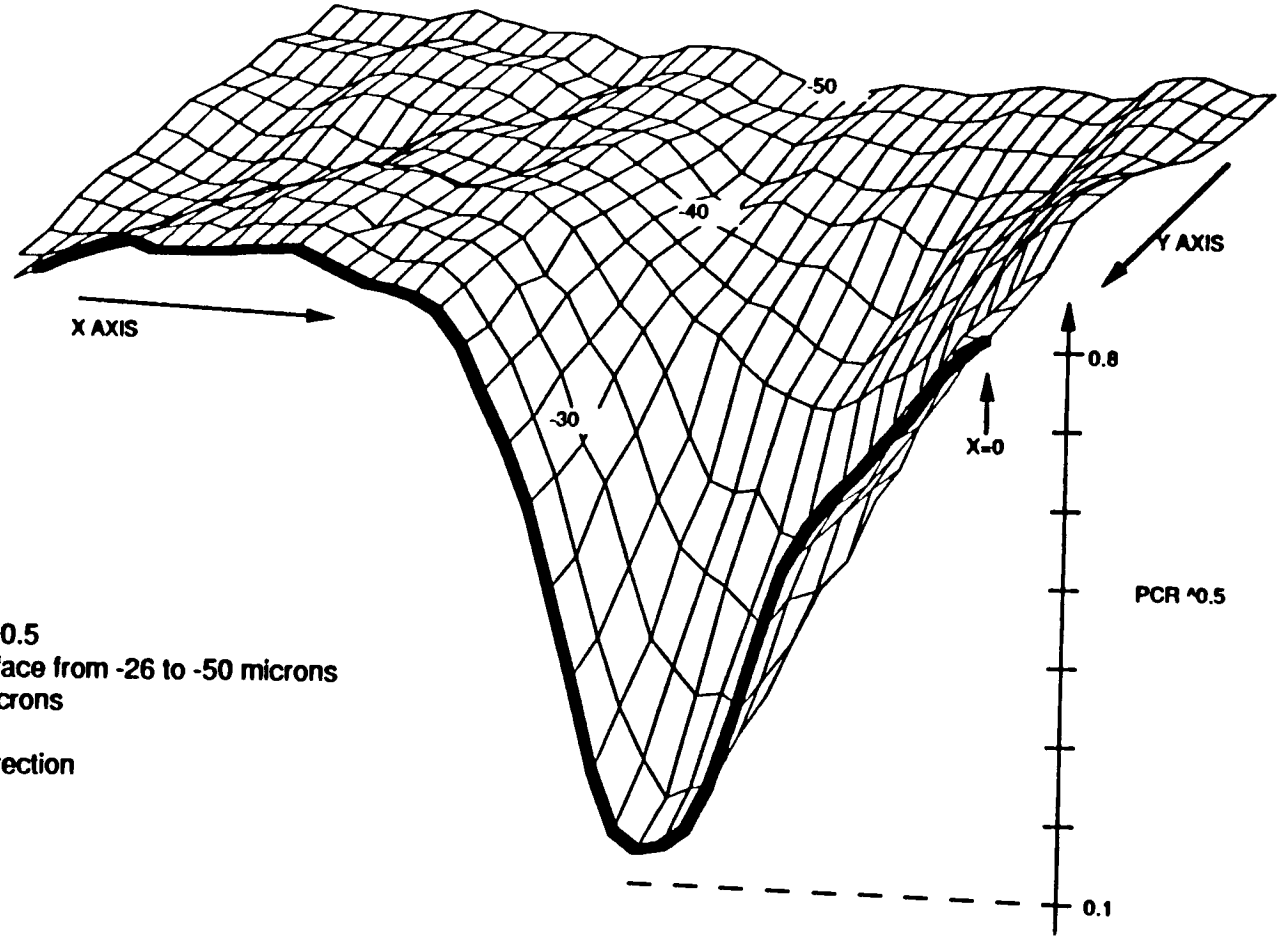

Graph of Power Coupling Ratio ^0.5
At Y Depths below Substrate Surface from -26 to -50 microns
X Position varies from -80 to 0 microns

Steps of 2 microns for X and Y direction
spot size 15 microns diameter

Coupler # 10, Sample # 1
Coupler 15/16 inch long

Appendix B1

```
%                                   Pre diffusion
%
clear                                                   % clear
shg                                                     % show graph screen
axis([1 2 3 4]);axis;                                   % sets auto scaling
t2=60;                                                  % prediff time-steps of 5 min
t2=t2*60;                                               % prediff time in sec
T=300;                                                  % °C
E=.160;                                                 % Volts/micron
Qp=3.6e4;                                               % activation energy - J/mol
R=8.31;                                                 % gas constant - J/mol.K
D=2.2e-4;
m=D*1.6e-19/(1.38e-23*(T+273));                         % microns^2/(Volt*second)
mEd2=m*E/2;                                             % microns/second
%
y=[0];y1=[0];y11=[0];
dt=10;t=0;                                              % calculation every 10 sec
c=zeros(51,301);                                        % set Conc matrix = 0
c1=zeros(51,301);                                       % set Conc matrix = 0
c(1,61:90)=ones(1,30);                                  % width of guide = 30um
c(1,151:180)=ones(1,30);                                % width of guide = 30um
c(1,211:240)=ones(1,30);                                % width of guide = 30um
dc=zeros(49,299);                                       % delta Conc matrix = 0
%
     for j=1:t2/300                                     % plot every 300sec
         for i=1:30,                                    % compute every 10sec
              dc=D*(c(2:50,3:301)-2*c(2:50,2:300)...
                 +c(2:50,1:299)+c(1:49,2:300)...
                 -2*c(2:50,2:300)+c(3:51,2:300))...
                 +mEd2*(c(1:49,2:300)-c(3:51,2:300)); % compute delta Conc
              c(2:50,2:300)=dt*dc+c(2:50,2:300);      % new C=old C + delta C
              c(1,[1:60 91:150 181:210 241:301])=...
              c(2,[1:60 91:150 181:210 241:301]);    % C beyond guide = const
              y=[y;c(2,85)];y1=[y1;[t]];y11=[y11;c(2,240)];
              t=dt+t;                                   % time incr
          end
          z=c(2:20,85);                                 % obtain plot matrix
          clg
          plot(z)                                       % plot conc
%                                                       % compute time and plot
          hr=fix(t/3600);minute=fix((t-hr*3600)/60);sec=(t-hr*3600-minute*60);
          text(.5,.8,[' Pre diffusion '],'sc')
          text(.5,.75,[num2str(hr),' hrs, ',...
               num2str(minute),' min, ',num2str(sec),' sec',],'sc')
          E1=E;T1=T;D1=(D);
          text(.5,.7,[num2str(D1),' um^2/sec ',],'sc')
          text(.5,.65,[num2str(E1),' V/um, ',num2str(T1),' C',],'sc')



          t1=t;
      end
c1=c;
save prediff_temp00022 c1 y y1 y11 t1 E1 T1 D1      % save prediff_temp file
```

Appendix C2

```
 ear                                                    % clear
                                                        % show graph screen
axis([1 2 3 4]);axis;                                   % sets auto scaling
t3=240;                                                 % secdiff time-steps of 5min
t3=t3*60;                                               % secdiff time in sec
T=400;                                                  % °C
E=0.0;                                                  % Volts/micron
R=8.31;                                                 % gas constant - J/mol.K
Qs=3.6e4;                                               % activation energy - J/mol
D=0.0065;
m=D*1.6e-19/(1.38e-23*(T+273));                         % microns^2/(Volt*second)
mEd2=m*E/2;                                             % microns/second
%
load prediff_temp00022;
c=c1;
x=[0];x1=[0];x11=[0];
dt=10;t=0;                                              % calculation every 10sec
%c(1,26:76)=ones(1,51);
c(1,[1:301])=c(2,[1:301]);                              % remove silver from surface
dc=zeros(49,299);                                        % set delta matrix = 0
%
    for j=1:t3/300                                      % plot every 300sec
        for i=1:30,                                     % compute every 10sec
            dc=D*(c(2:50,3:301)-2*c(2:50,2:300)...
               +c(2:50,1:299)+c(1:49,2:300)...
               -2*c(2:50,2:300)+c(3:51,2:300))...
               +mEd2*(c(1:49,2:300)-c(3:51,2:300));  % compute delta matrix
            c(2:50,2:300)=dt*dc+c(2:50,2:300);      % new C=old C + delta C
            c(1,[1:301])=c(2,[1:301]);              % new surf C=old surf C
            x=[x,c(2,65)];x11=[x11;c(2,240)];x1=[x1;[t]];
            t=dt+t;                                 % incr time
        end
        z=c(2:50,65);                               % obtain plot matrix
        clg
        plot(z)                                     % plot conc
                                                    % compute time and plot
        hr=fix(t/3600);minute=fix((t-hr*3600)/60);sec=(t-hr*3600-minute*60);
        text(.5,.8,[' Second diffusion '],'sc')
        text(.5,.75,[num2str(hr),' hrs, ',...
             num2str(minute),' min, ',num2str(sec),' sec',],'sc')
        text(.5,.7,[num2str(D),' um^2/sec ',],'sc')
        text(.5,.65,[num2str(E),' V/um, ',num2str(T),' C',],'sc')
    end
ave secdiff_temp0065 c x x1 x11 t E T D
```

```
 ear                                                    % clear
                                                        % show graph screen
axis([1 2 3 4]);axis;                                   % sets auto scaling
for i=1:5,
load prediff_temp00022
load secdiff_temp0065
fig
plot(y1,y,'-')
        title('PRE DIFFUSION, Peek Surface Conc Vs Time ')
        xlabel('t in sec')
        ylabel('conc ')
        hr1=fix(t1/3600);minute1=fix((t1-hr1*3600)/60);
        sec1=(t1-hr1*3600-minute1*60);
        text(.2,.85,[num2str(hr1),' hrs, ',...
            num2str(minute1),' min, ',num2str(sec1),' sec',],'sc')
        text(.2,.8,[num2str(D1),' um^2/sec ',],'sc')
        text(.2,.75,[num2str(E1),' V/um, ',num2str(T1),' C',],'sc')
ause
fig
        y=y/max(y);
   'y1,y,'-')
        title('PRE DIFFUSION, Normalized Peek Surface Conc Vs Time ')
        xlabel('t in sec')
        ylabel('norm conc ')
        text(.2,.85,[num2str(hr1),' hrs, ',...
            num2str(minute1),' min, ',num2str(sec1),' sec',],'sc')
        text(.2,.8,[num2str(D1),' um^2/sec ',],'sc')
        text(.2,.75,[num2str(E1),' V/um, ',num2str(T1),' C',],'sc')
ause
fig
lot(y1,y11,'-');                                        % plot abs conc - prediff
        title('PRE DIFFUSION, Peek Surface Conc Vs Time ')
        xlabel('t in sec')
        ylabel('conc ')
        text(.2,.85,[num2str(hr1),' hrs, ',...
            num2str(minute1),' min, ',num2str(sec1),' sec',],'sc')
        text(.2,.8,[num2str(D1),' um^2/sec ',],'sc')
        text(.2,.75,[num2str(E1),' V/um, ',num2str(T1),' C',],'sc')
ause
fig
    y11=y11/max(y11);
lot(y1,y11,'-')                                         % plot abs conc - prediff
        title('PRE DIFFUSION, Normalized Peek Surface Conc Vs Time ')
        xlabel('t in sec')
        ylabel('norm conc ')
```

```
 ear                                                    % clear graph screen
                                                        % show graph screen
ixis([1 2 3 4]);axis;                                   % sets auto scaling
oad prediff_temp00022
        z=c1(2:20,65);z=z/z(1);                         % obtain plot matrix
        z1=c1(2,241:300);z1=z1/z1(1);
        z2=c1(2:20,:);
                    z2=z2/z2(65);
lg
or i=1:5,
lot(y1,y,'-')                                           % plot abs conc - prediff
        text(.4,.35,[' PRE DIFFUSION, Peek Conc Vs Time ',],'sc')
        hr1=fix(t1/3600);minute1=fix((t1-hr1*3600)/60);
        sec1=(t1-hr1*3600-minute1*60);
        text(.45,.3,[num2str(hr1),' hrs, ',...
            num2str(minute1),' min, ',num2str(sec1),' sec',],'sc')
        text(.45,.25,[num2str(D1),' um^2/sec ',],'sc')
        text(.45,.2,[num2str(E1),' V/um, ',num2str(T1),' C',],'sc')
ause
lg
l''(y1,y11,'-')                                         % plot abs conc - prediff
        text(.4,.35,[' PRE DIFFUSION, Peek Conc Vs Time ',],'sc')
        hr1=fix(t1/3600);minute1=fix((t1-hr1*3600)/60);
        sec1=(t1-hr1*3600-minute1*60);
        text(.45,.3,[num2str(hr1),' hrs, ',...
            num2str(minute1),' min, ',num2str(sec1),' sec',],'sc')
        text(.45,.25,[num2str(D1),' um^2/sec ',],'sc')
        text(.45,.2,[num2str(E1),' V/um, ',num2str(T1),' C',],'sc')
ause
lg
lot(z)                                                  % plot norm conc - prediff
        text(.35,.85,[' PRE DIFFUSION, Conc Vs Depth(x) ',],'sc')
        hr1=fix(t1/3600);minute1=fix((t1-hr1*3600)/60);
        sec1=(t1-hr1*3600-minute1*60);
        text(.4,.8,[num2str(hr1),' hrs, ',...
            num2str(minute1),' min, ',num2str(sec1),' sec',],'sc')
        text(.4,.75,[num2str(D1),' um^2/sec ',],'sc')
        text(.4,.7,[num2str(E1),' V/um, ',num2str(T1),' C',],'sc')
ause
ig
l   z1)                                                 % plot norm conc - prediff
        text(.35,.85,[' PRE DIFFUSION, Conc Vs Depth(y) ',],'sc')
        hr1=fix(t1/3600);minute1=fix((t1-hr1*3600)/60);
        sec1=(t1-hr1*3600-minute1*60);
        text(.4,.8,[num2str(hr1),' hrs, ',...
```

```
            num2str(minute1),' min, ',num2str(sec1),' sec',],'sc')
        text(.4,.75,[num2str(D1),' um^2/sec ',],'sc')
        text(.4,.7,[num2str(E1),' U/um, ',num2str(T1),' C',],'sc')
c
lg
lot(z2','-')                                          % plot norm conc - prediff
        text(.35,.85,[' PRE DIFFUSION, Conc Vs Depth(y) ',],'sc')
        hr1=fix(t1/3600);minute1=fix((t1-hr1*3600)/60);
        sec1=(t1-hr1*3600-minute1*60);
        text(.4,.8,[num2str(hr1),' hrs, ',...
            num2str(minute1),' min, ',num2str(sec1),' sec',],'sc')
        text(.4,.75,[num2str(D1),' um^2/sec ',],'sc')
        text(.4,.7,[num2str(E1),' U/um, ',num2str(T1),' C',],'sc')
ause
lg
esh(c1(2:50,:),[-10 30],[2 2 1])
        text(.75,.95,[' PRE DIFFUSION',],'sc')
        text(.75,.9,[' Peek Conc Vs Time ',],'sc')
        hr1=fix(t1/3600);minute1=fix((t1-hr1*3600)/60);
        sec1=(t1-hr1*3600-minute1*60);
        text(.75,.85,[num2str(hr1),' hrs, ',...
            num2str(minute1),' min, ',num2str(sec1),' sec',],'sc')
        text(.75,.8,[num2str(D1),' um^2/sec ',],'sc')
        text(.75,.75,[num2str(E1),' U/um, ',num2str(T1),' C',],'sc')
ause
lg
nd
```

```
        text(.2,.85,[num2str(hr1),' hrs, ',...
            num2str(minute1),' min, ',num2str(sec1),' sec',],'sc')
        text(.2,.8,[num2str(D1),' um^2/sec ',],'sc')
        text(.2,.75,[num2str(E1),' V/um, ',num2str(T1),' C',],'sc')
pause
clg
        z=ci(2:20,65);
plot(z)                                          % plot norm conc - prediff
        title('PRE DIFFUSION, Conc Vs Depth(y) ')
        xlabel('depth(y) in um')
        ylabel('conc ')
        text(.7,.85,[num2str(hr1),' hrs, ',...
            num2str(minute1),' min, ',num2str(sec1),' sec',],'sc')
        text(.7,.8,[num2str(D1),' um^2/sec ',],'sc')
        text(.7,.75,[num2str(E1),' V/um, ',num2str(T1),' C',],'sc')
pause
clg
        z=z/z(1);
plot(z)
        title('PRE DIFFUSION, Normalized Conc Vs Depth ')
        xlabel('depth(y) in um')
        ylabel('norm conc ')
        text(.7,.85,[num2str(hr1),' hrs, ',...
            num2str(minute1),' min, ',num2str(sec1),' sec',],'sc')
        text(.7,.8,[num2str(D1),' um^2/sec ',],'sc')
        text(.7,.75,[num2str(E1),' V/um, ',num2str(T1),' C',],'sc')
pause
clg
        z1=ci(2,:);
        z1=[z1;ci(4,:)];
        z1=[z1;ci(6,:)];
        z1=[z1;ci(8,:)];
        plot(z1')
        title('PRE DIFFUSION, Surface Conc at Depth 2um, 4um, 6um, 8um')
        xlabel('surface in um')
        ylabel('conc ')
        text(.7,.85,[num2str(hr1),' hrs, ',...
            num2str(minute1),' min, ',num2str(sec1),' sec',],'sc')
        text(.7,.8,[num2str(D1),' um^2/sec ',],'sc')
        text(.7,.75,[num2str(E1),' V/um, ',num2str(T1),' C',],'sc')
pause
        z1=z1/max(ci(2,:));
        plot(z1')
        title('PRE DIFFUSION, Norm Surface Conc at Depth 2um, 4um, 6um, 8um')
        xlabel('surface in um')
        ylabel('norm conc ')
```

```
        text(.7,.85,[num2str(hr1),' hrs, ',...
            num2str(minute1),' min, ',num2str(sec1),' sec',],'sc')
        text(.7,.8,[num2str(D1),' um^2/sec ',],'sc')
        text(.7,.75,[num2str(E1),' V/um, ',num2str(T1),' C',],'sc')
pause
clg
mesh(c1(2:10,:),[-10 30],[2 2 1])
        title('PRE DIFFUSION')
        xlabel('depth(y) in um')
        ylabel('conc ')
        text(.75,.85,[num2str(hr1),' hrs, ',...
            num2str(minute1),' min, ',num2str(sec1),' sec',],'sc')
        text(.75,.8,[num2str(D1),' um^2/sec ',],'sc')
        text(.75,.75,[num2str(E1),' V/um, ',num2str(T1),' C',],'sc')
pause
clg
plot(x1,x,'-')
        title('SECOND DIFFUSION, Peek Conc Vs Time ')
        xlabel('t in sec')
        ylabel('conc ')
        hr1=fix(t/3600);minute1=fix((t-hr1*3600)/60);
        sec1=(t-hr1*3600-minute1*60);
        text(.7,.85,[num2str(hr1),' hrs, ',...
            num2str(minute1),' min, ',num2str(sec1),' sec',],'sc')
        text(.7,.8,[num2str(D),' um^2/sec ',],'sc')
        text(.7,.75,[num2str(E),' V/um, ',num2str(T),' C',],'sc')
pause
clg
        x=x/max(y);
plot(x1,x,'-')
        title('SECOND DIFFUSION, Normalized Peek Conc Vs Time ')
        xlabel('t in sec')
        ylabel('norm conc ')
        text(.7,.85,[num2str(hr1),' hrs, ',...
            num2str(minute1),' min, ',num2str(sec1),' sec',],'sc')
        text(.7,.8,[num2str(D),' um^2/sec ',],'sc')
        text(.7,.75,[num2str(E),' V/um, ',num2str(T),' C',],'sc')
pause
clg
plot(x1,x11,'-')
        title('SECOND DIFFUSION, Peek Surface Conc Vs Time ')
        xlabel('t in sec')
        ylabel('conc ')
        text(.7,.85,[num2str(hr1),' hrs, ',...
            num2str(minute1),' min, ',num2str(sec1),' sec',],'sc')
        text(.7,.8,[num2str(D),' um^2/sec ',],'sc')
        text(.7,.75,[num2str(E),' V/um, ',num2str(T),' C',],'sc')
```

```
use
g
        x11=x11/max(x11);
   (x1,x11,'-')
        title('SECOND DIFFUSION, Normalized Peek Surface Conc Vs Time ')
        xlabel('t in sec')
        ylabel('norm conc ')
        text(.7,.85,[num2str(hr1),' hrs, ',...
            num2str(minute1),' min, ',num2str(sec1),' sec',],'sc')
        text(.7,.8,[num2str(D),' um^2/sec ',],'sc')
        text(.7,.75,[num2str(E),' V/um, ',num2str(T),' C',],'sc')
pause
clg
        w=c(2:50,85);
plot(w)
        title('SECOND DIFFUSION, Conc Vs Depth(y) ')
        xlabel('depth(y) in sec')
        ylabel('conc ')
        text(.7,.85,[num2str(hr1),' hrs, ',...
            num2str(minute1),' min, ',num2str(sec1),' sec',],'sc')
        text(.7,.8,[num2str(D),' um^2/sec ',],'sc')
        text(.7,.75,[num2str(E),' V/um, ',num2str(T),' C',],'sc')
c
lg
        w=w/w(1);
lot(w)
        title('SECOND DIFFUSION, Normalized Conc Vs Depth(y) ')
        xlabel('depth(y) in sec')
        ylabel('norm conc ')
        text(.7,.85,[num2str(hr1),' hrs, ',...
            num2str(minute1),' min, ',num2str(sec1),' sec',],'sc')
        text(.7,.8,[num2str(D),' um^2/sec ',],'sc')
        text(.7,.75,[num2str(E),' V/um, ',num2str(T),' C',],'sc')
ause
lg
        w1=c(2,:);
        w1=[w1;c(5,:)];
        w1=[w1;c(10,:)];
        w1=[w1;c(15,:)];
        w1=[w1;c(20,:)];
        w1=[w1;c(25,:)];
        w1=[w1;c(30,:)];
l  ,w1')
        title('SECOND DIFFUSION, Surface Conc at Depth 5,10,15,20,25,30um')
        xlabel('surface in um')
        ylabel('conc ')
        text(.7,.85,[num2str(hr1),' hrs, ',...
```

```
            num2str(minute1),' min, ',num2str(sec1),' sec',],'sc')
        text(.7,.6,[num2str(D),' um^2/sec ',],'sc')
        text(.7,.75,[num2str(E),' V/um, ',num2str(T),' C',],'sc')
    e
ig
        w1=w1/max(c(2,:));
plot(w1')
        title('SECOND DIFFUSION, Surface Conc at Depth 5,10,15,20,25,30um')
        xlabel('surface in um')
        ylabel('conc ')
        text(.7,.85,[num2str(hr1),' hrs, ',...
            num2str(minute1),' min, ',num2str(sec1),' sec',],'sc')
        text(.7,.8,[num2str(D),' um^2/sec ',],'sc')
        text(.7,.75,[num2str(E),' V/um, ',num2str(T),' C',],'sc')
ause
ig
esh(c(2:51,:),[-10 30],[2 2 1])
        title('SECOND DIFFUSION')
        xlabel('surface in um')
        ylabel('conc ')
        text(.75,.85,[num2str(hr1),' hrs, ',...
            num2str(minute1),' min, ',num2str(sec1),' sec',],'sc')
        text(.75,.8,[num2str(D),' um^2/sec ',],'sc')
        text(.75,.75,[num2str(E),' V/um, ',num2str(T),' C',],'sc')
ause
ig
nd
```

Appendix D1

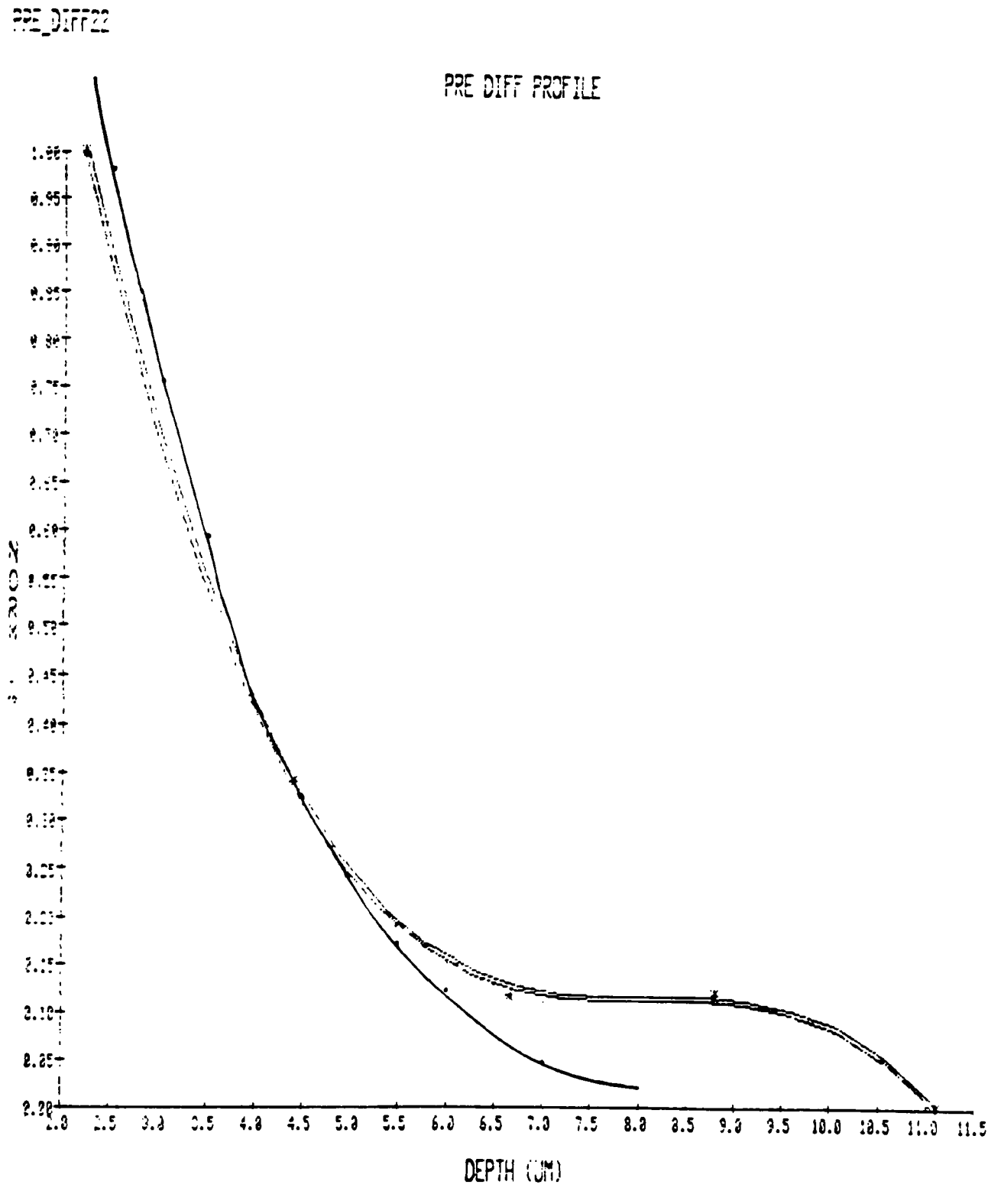
PRE_DIFF22
PRE DIFF PROFILE
DEPTH (UM)
PRE DIFF
-4.308754e-03*X**3 +0.105878*X**2 -0.853938*X +2.426497

Appendix D2

SEC_DIFF22

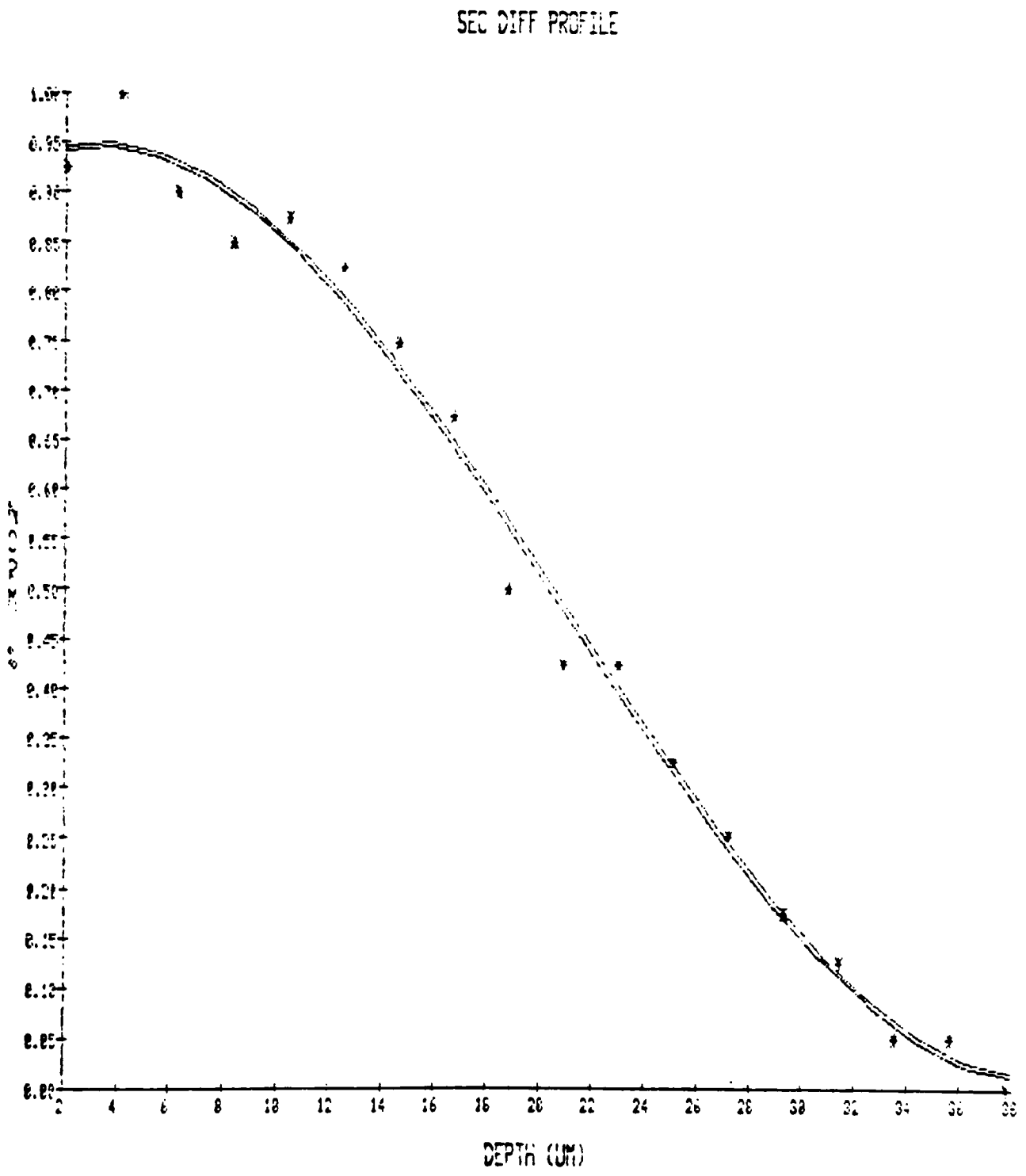

Appendix D3

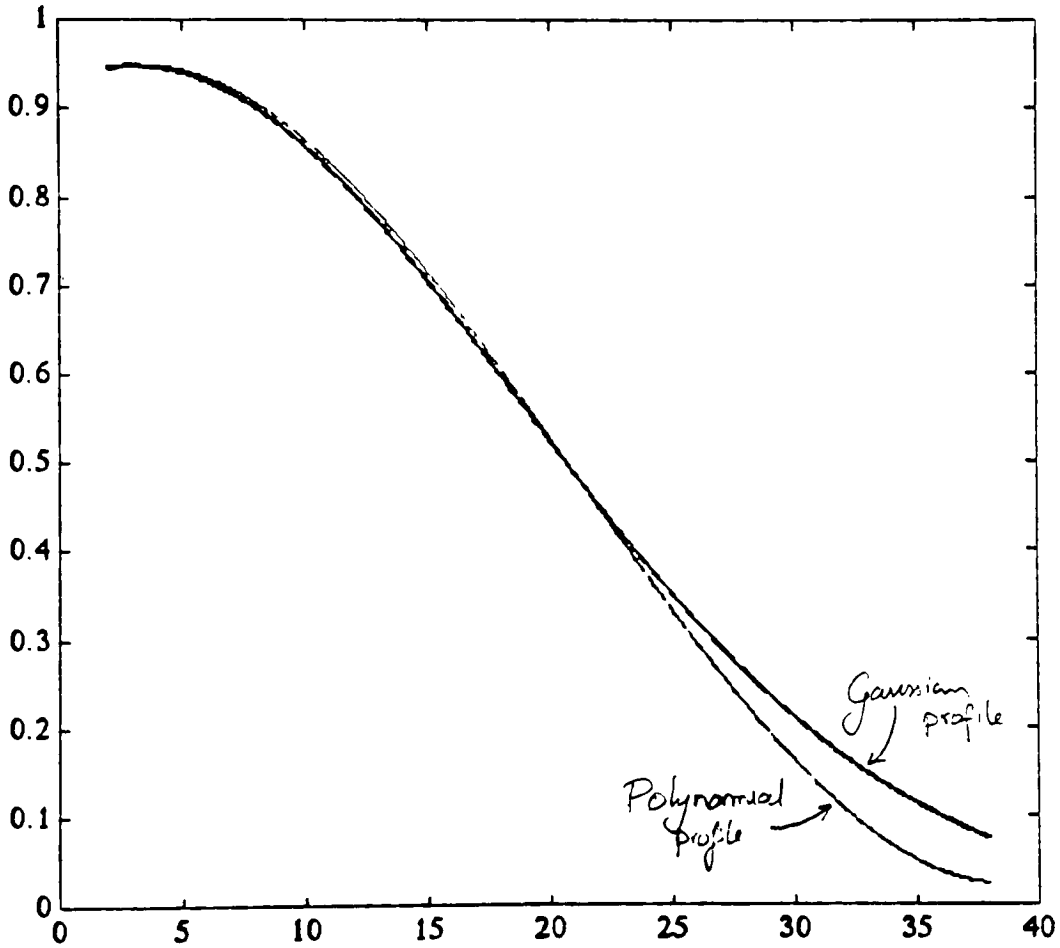
1
0.9
0.8
0.7
0.6
0.5
0.4
0.3
0.2
0.1
0
0
5
10
15
20
25
30
35
40
Gaussian profile
Polynomial profile

Appendix D4

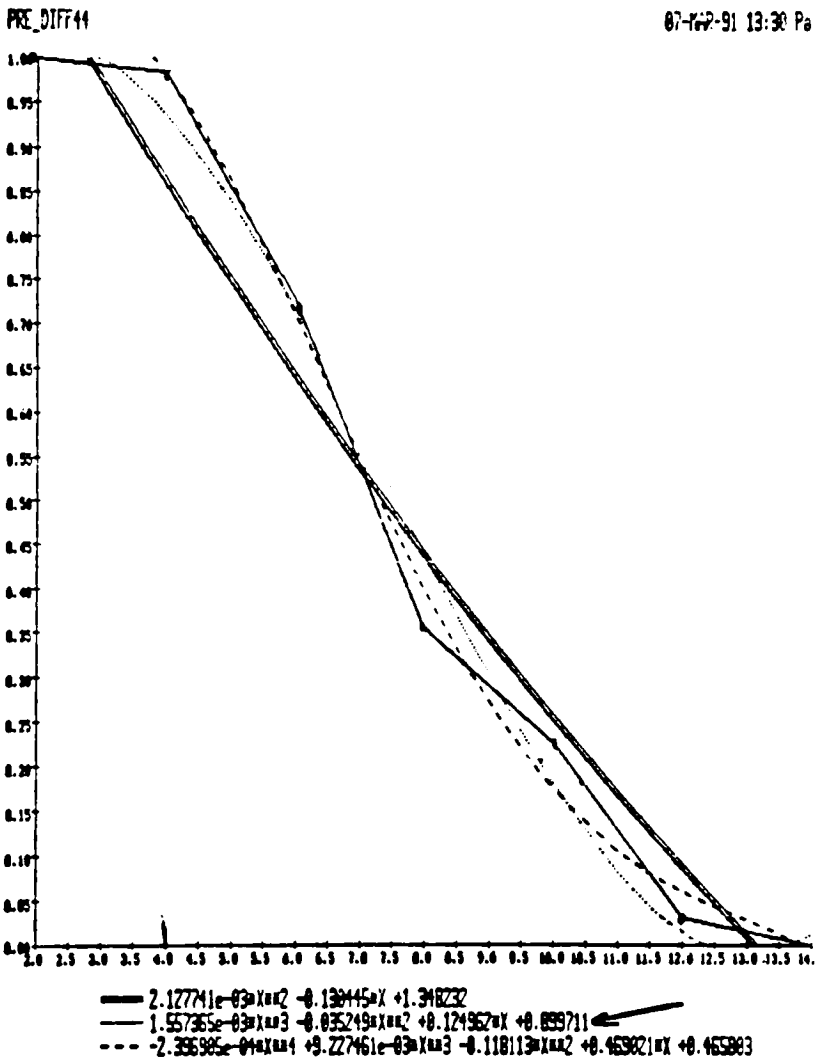
PRE_DIFF44
07-Mar-91 13:30 Pa
2.127741e-03*X**2 -0.138445*X +1.348232
1.557365e-03*X**3 -0.035249*X**2 +0.124962*X +0.859711
-2.355985e-04*X**4 +9.227461e-03*X**3 -0.118113*X**2 +0.465021*X +0.465883

Appendix D5

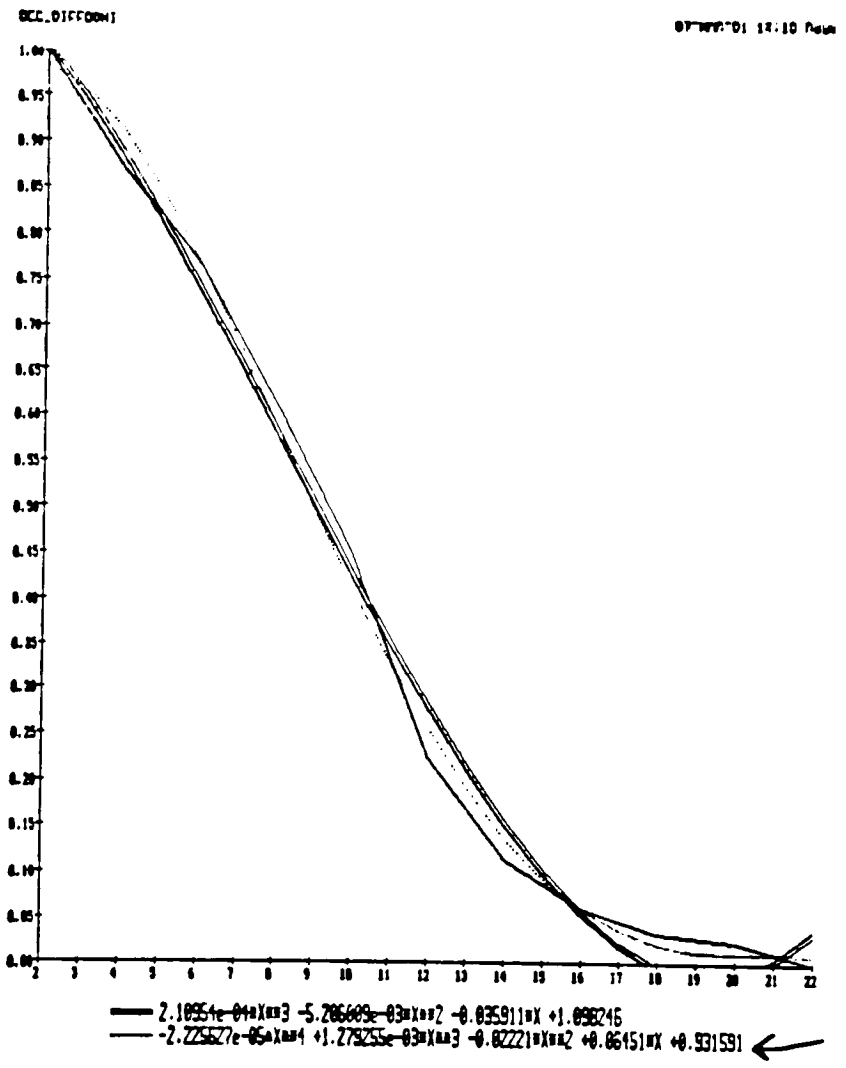
2.10954e-04*x**3 -5.286609e-03*x**2 -0.035911*x +1.058246
-2.225627e-05*x**4 +1.279255e-03*x**3 -0.032221*x**2 +0.864151*x +0.931591

Appendix D6

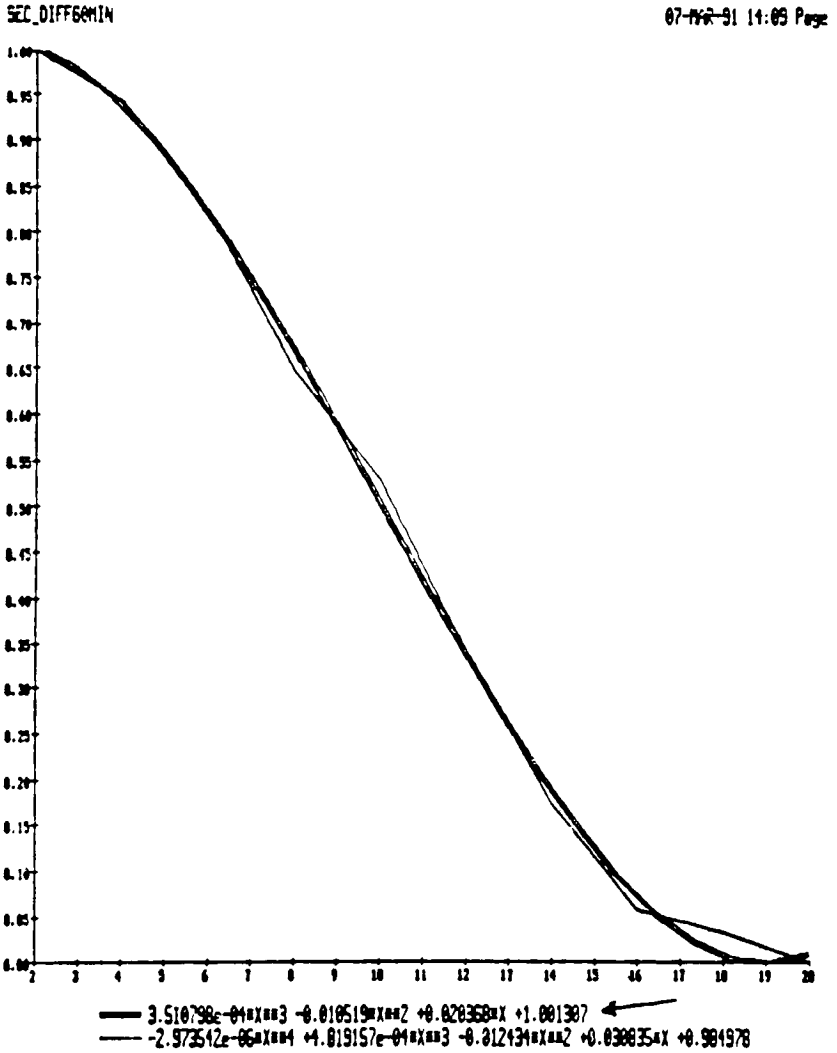
SEC_DIFF60MIN
07-MAR-91 14:09 Page
2 3 4 5 6 7 8 9 10 11 12 13 14 15 16 17 18 19 20
3.510798e-04*X**3 -0.010519*X**2 +0.020358*X +1.001307
-2.973512e-06*X**4 +4.819157e-04*X**3 -0.012134*X**2 +0.030835*X +0.981978

Appendix E1

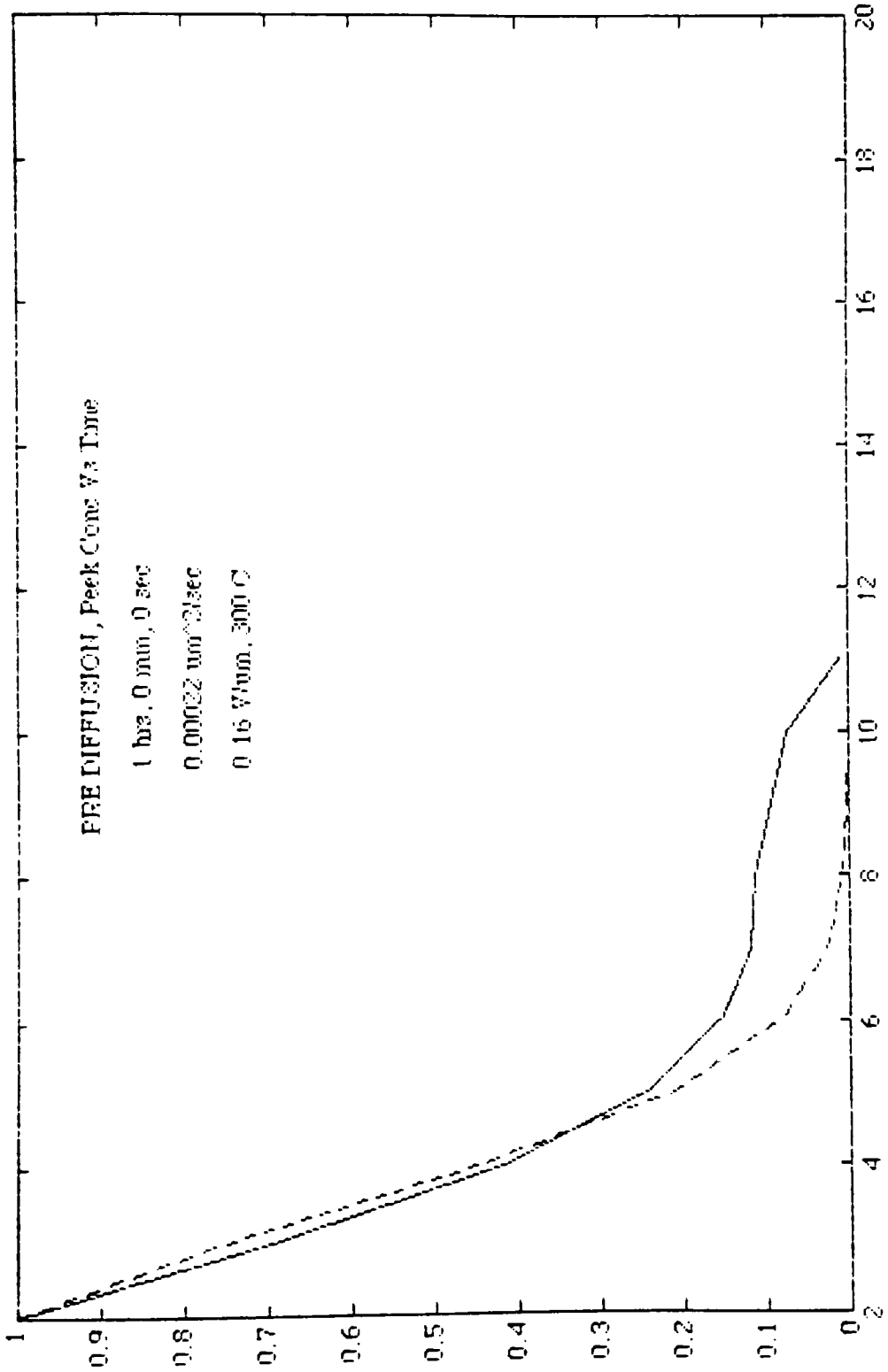
FRE DIFFUSION, Peek Conc Vs Time
1 hrs, 0 min, 0 sec
0.00022 um^2/sec
0.16 Wum, 300 C
0
0.1
0.2
0.3
0.4
0.5
0.6
0.7
0.8
0.9
1
2
4
6
8
10
12
14
16
18
20

Appendix E2

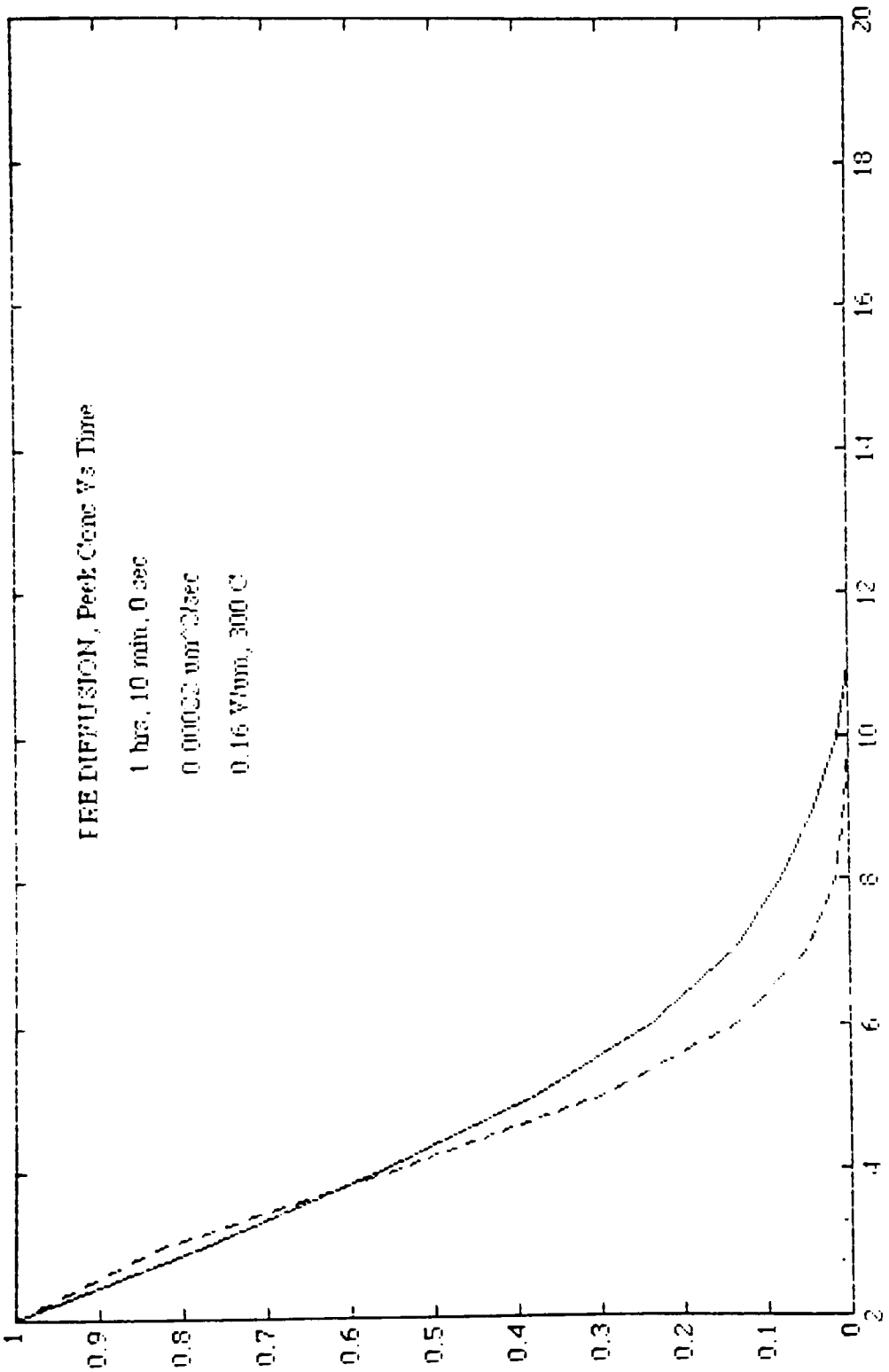
FEE DIFFUSION, Peak Conc Vs Time
1 hrs, 10 min, 0 sec
0.16 Wmm, 300 C
0
0.1
0.2
0.3
0.4
0.5
0.6
0.7
0.8
0.9
1
2
4
6
8
10
12
14
16
18
20

Appendix E3

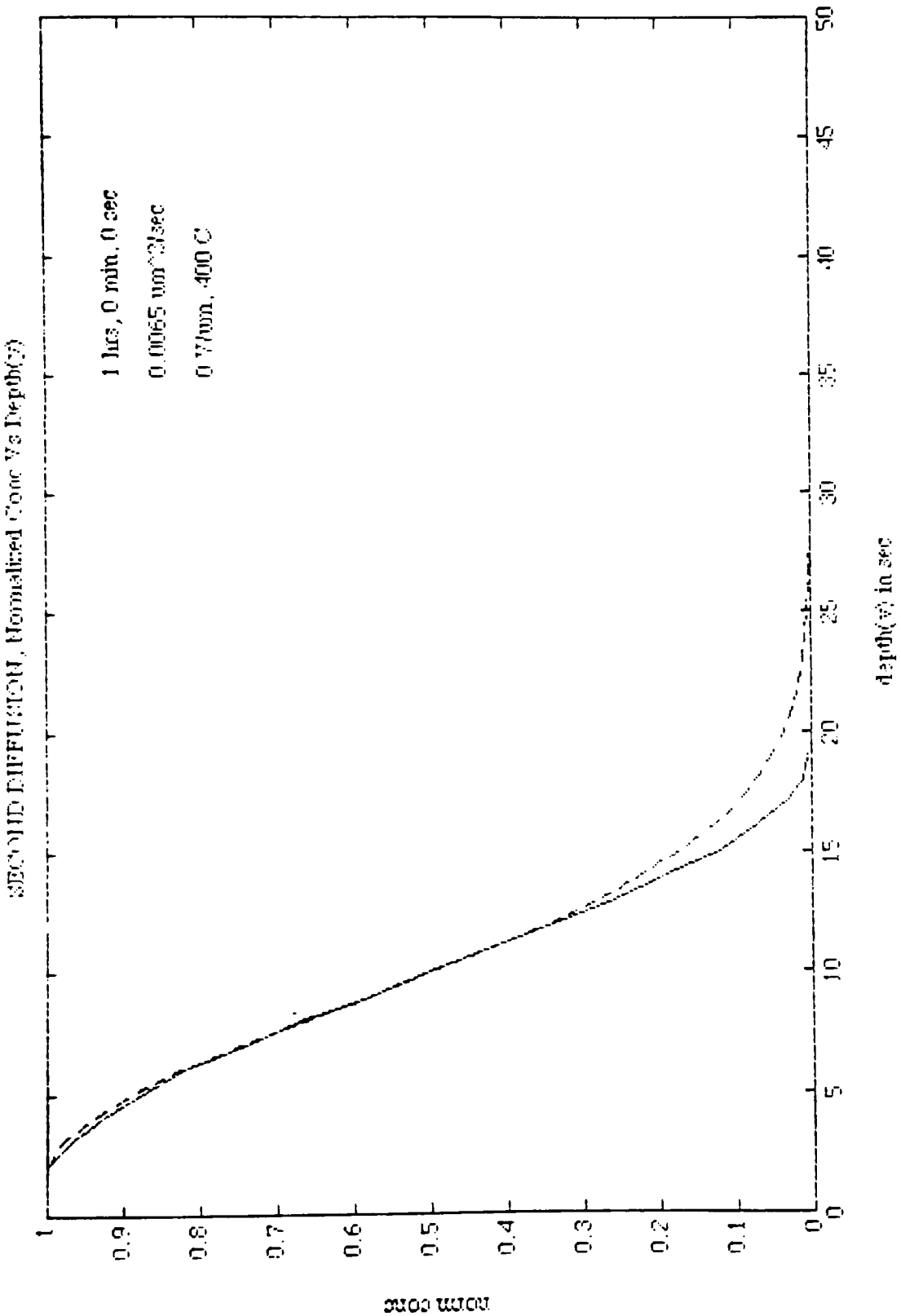
1 hrs, 0 min, 0 sec
0.0065 um^2/sec
0.70um, 400 C
norm conc
depth(z) in sec
0
0.1
0.2
0.3
0.4
0.5
0.6
0.7
0.8
0.9
1
0
5
10
15
20
25
30
35
40
45
50

Appendix E4

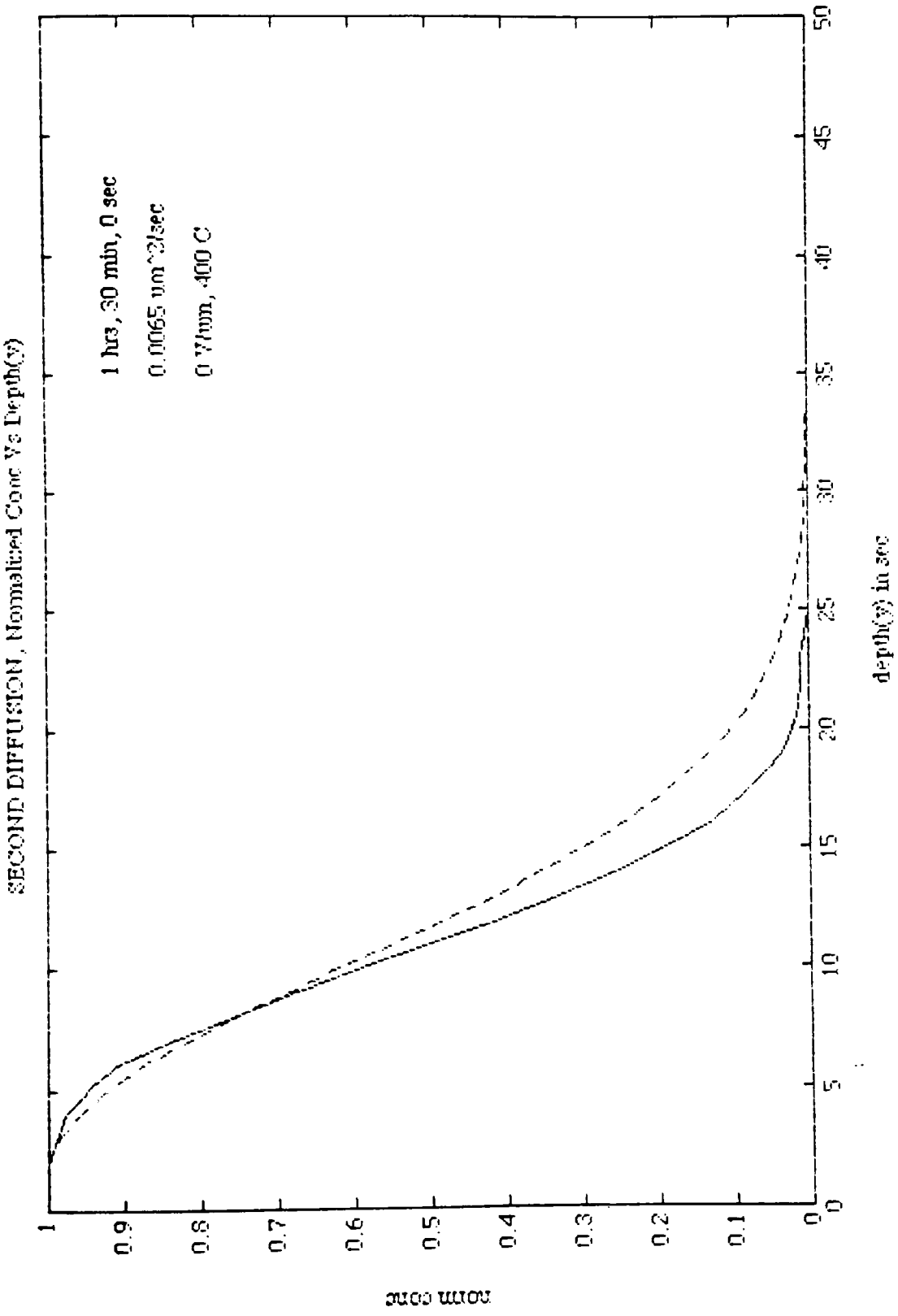
SECOND DIFFUSION, Normalized Conc Vs Depth(y)
1 hrs, 30 min, 0 sec
0.0065 um^2/sec
0 Wmm, 400 C
norm conc
depth(y) in um
0
0.1
0.2
0.3
0.4
0.5
0.6
0.7
0.8
0.9
1
0
5
10
15
20
25
30
35
40
45
50

Appendix E5

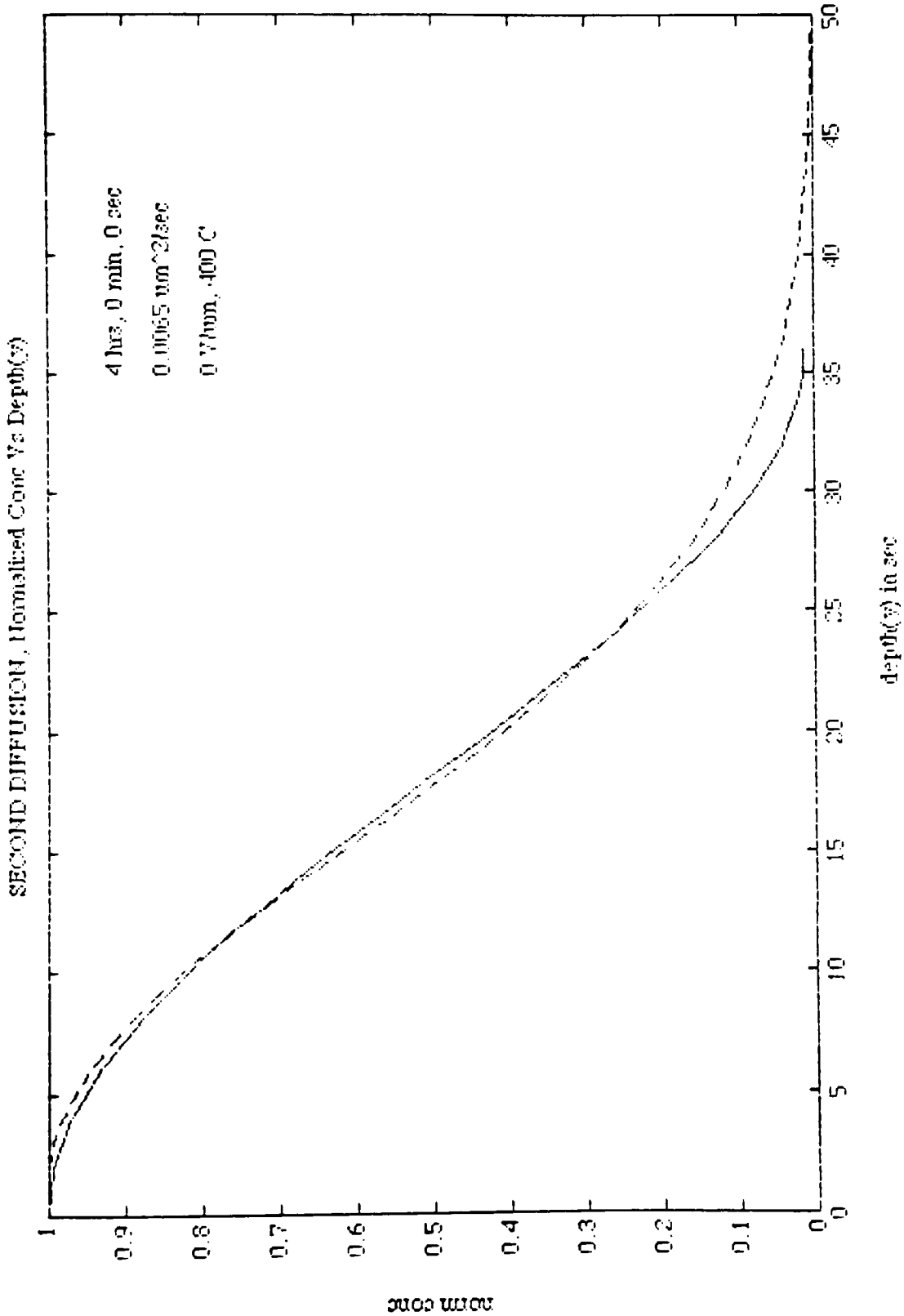
SECOND DIFFUSION, Normalized Conc Vs Depth(y)
4 hrs, 0 min, 0 sec
0.00065 um^2/sec
0.77hrs, 400 C
norm conc
depth(y) in sec
0
0.1
0.2
0.3
0.4
0.5
0.6
0.7
0.8
0.9
1
0
5
10
15
20
25
30
35
40
45
50

Appendix E6

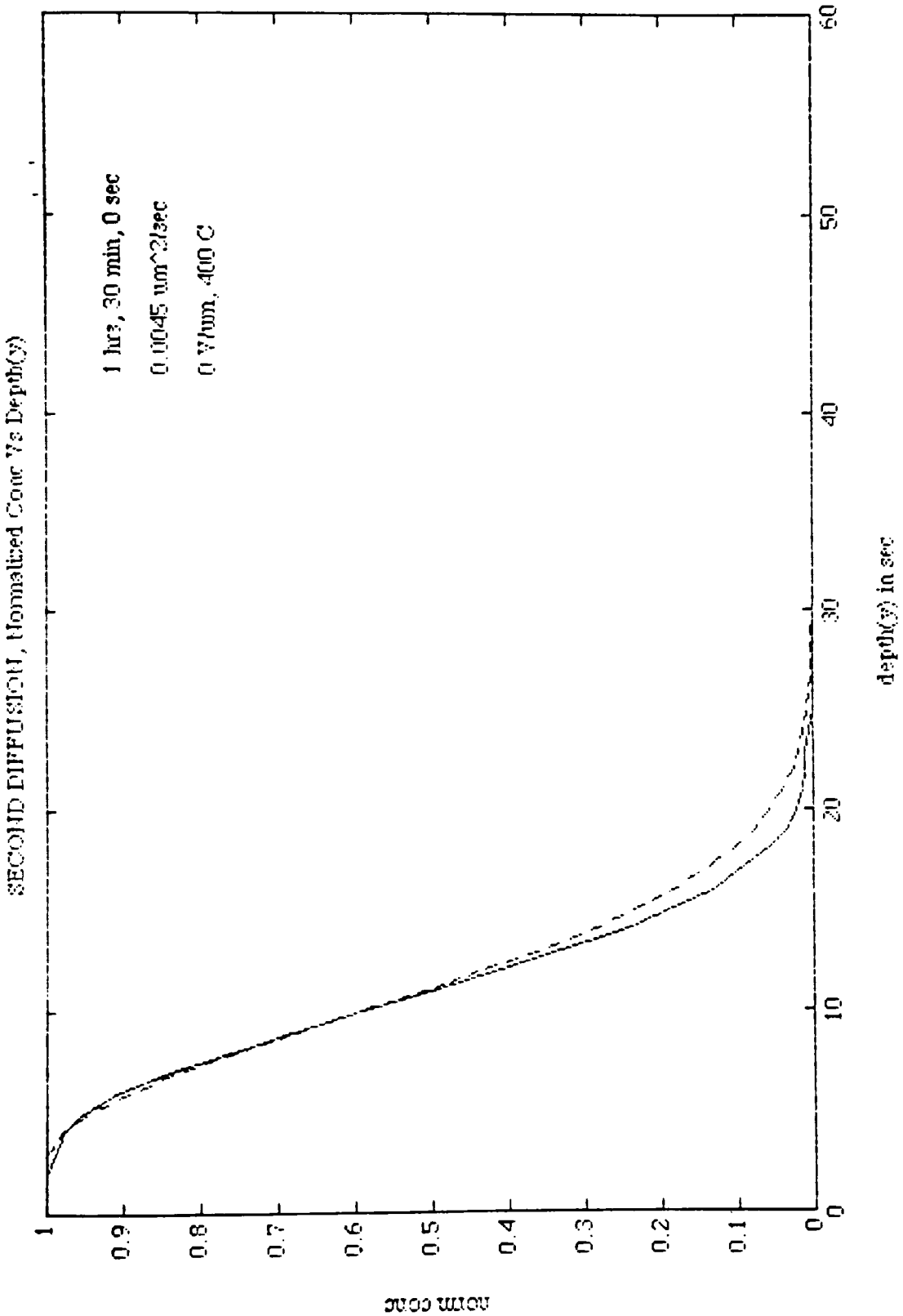
SECOND DIFFUSION, Normalized Conc Vs Depth(y)
1 hr3, 30 min, 0 sec
0.0045 um^2/sec
0 Whm, 400 C
norm conc
depth(y) in sec
0
0.1
0.2
0.3
0.4
0.5
0.6
0.7
0.8
0.9
1
0
10
20
30
40
50
60

Appendix E7

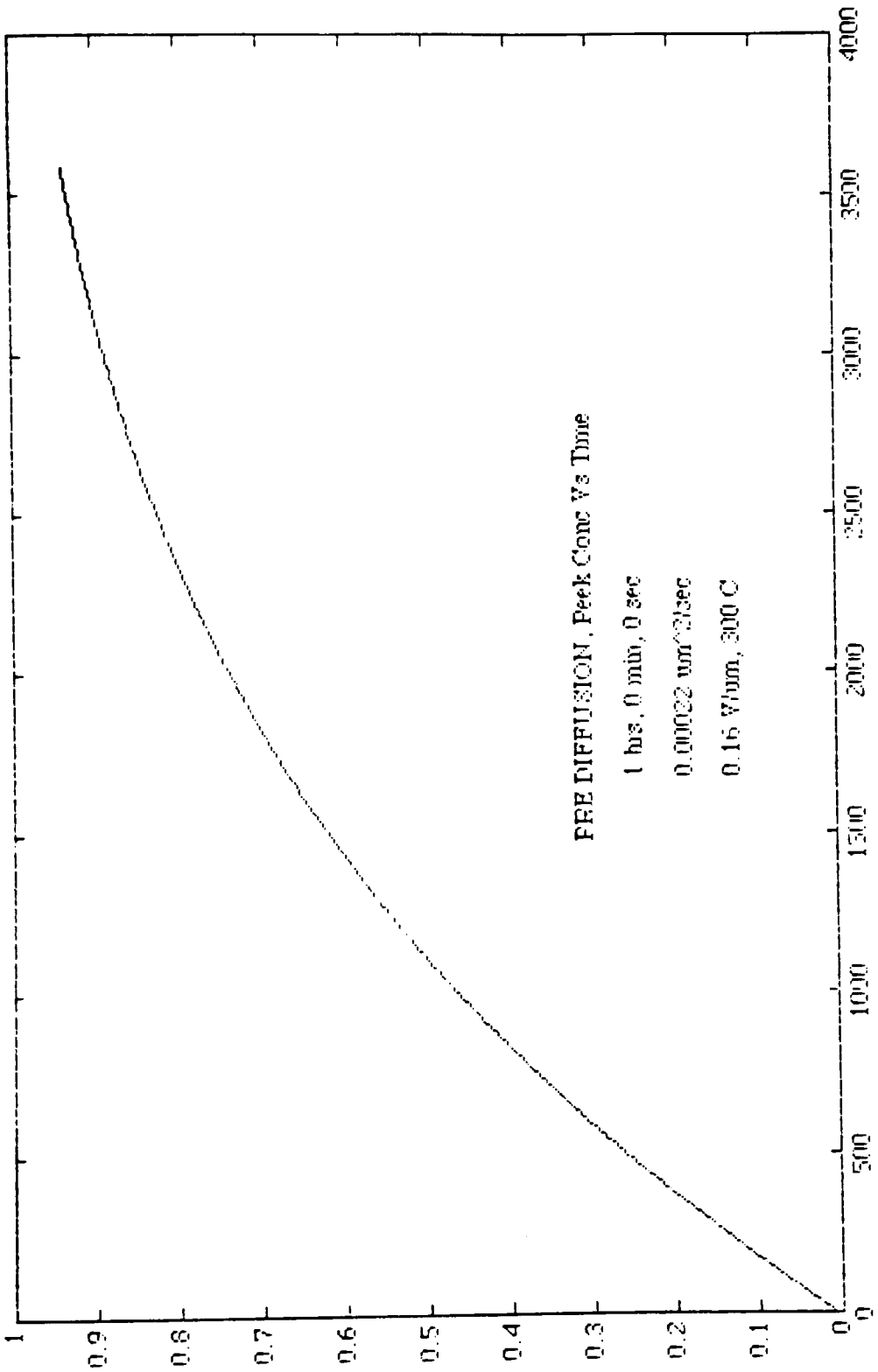
FRE DIFFUSION, Peek Conc Vs Time
1 hr, 0 min, 0 sec
0.00022 cm^2/sec
0.16 Wum, 300 C
1
0.9
0.8
0.7
0.6
0.5
0.4
0.3
0.2
0.1
0
0
500
1000
1500
2000
2500
3000
3500
4000

Appendix E8

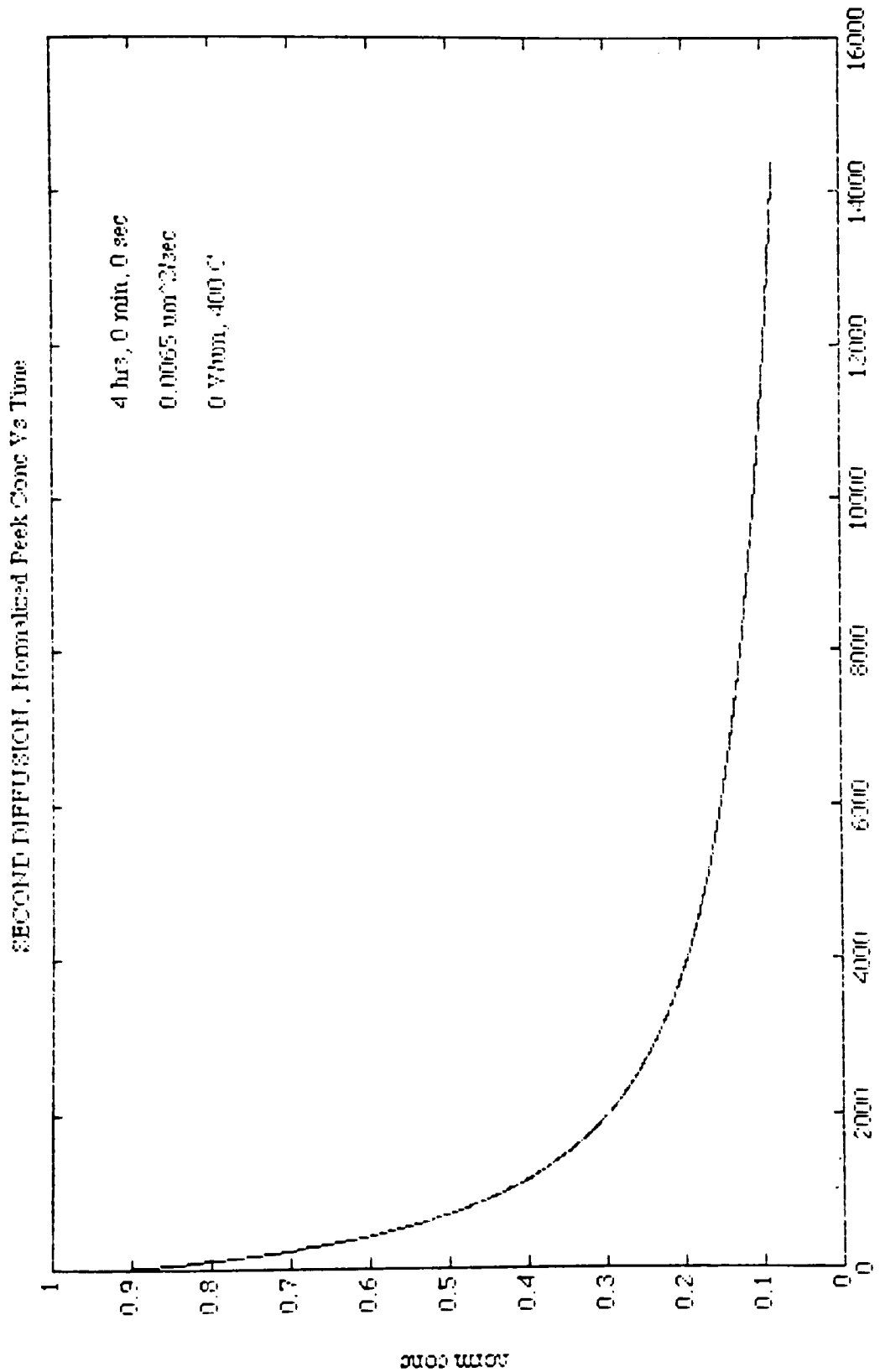
SECOND DIFFUSION, Normalised Peak Conc Vs Time
4 hrs, 0 min, 0 sec
0.0065 um^2/sec
0 V/nm, 400 C
norm conc
t in sec
0
0.1
0.2
0.3
0.4
0.5
0.6
0.7
0.8
0.9
1
0
2000
4000
6000
8000
10000
12000
14000
16000

Appendix E9

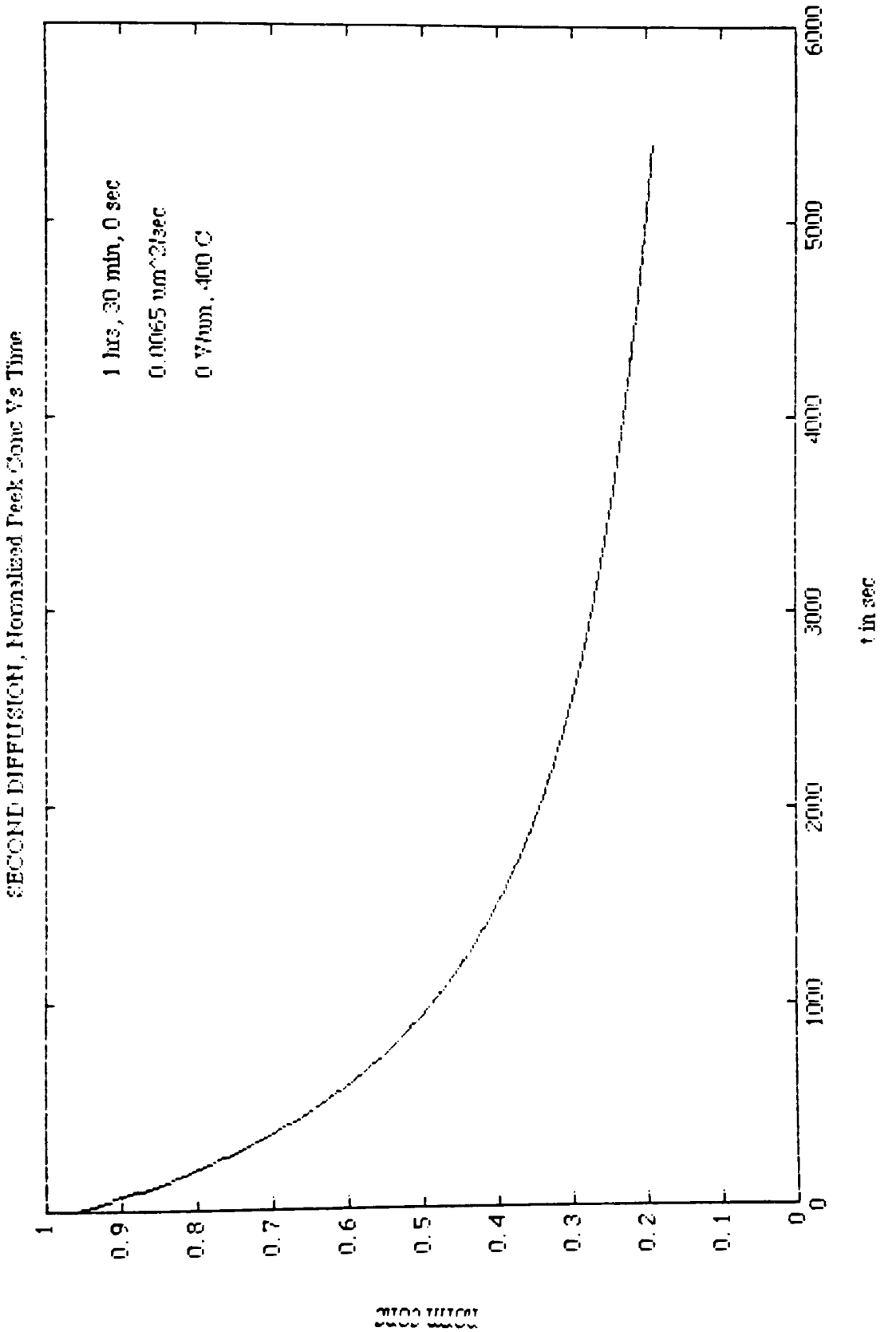
SECOND DIFFUSION, Normalized Peak Conc Vs Time
1 hrs, 30 min, 0 sec
0.0065 um^2/sec
0 Wum, 400 C
NORM CONC
t in sec
0
0.1
0.2
0.3
0.4
0.5
0.6
0.7
0.8
0.9
1
1000
2000
3000
4000
5000
6000

Appendix E10

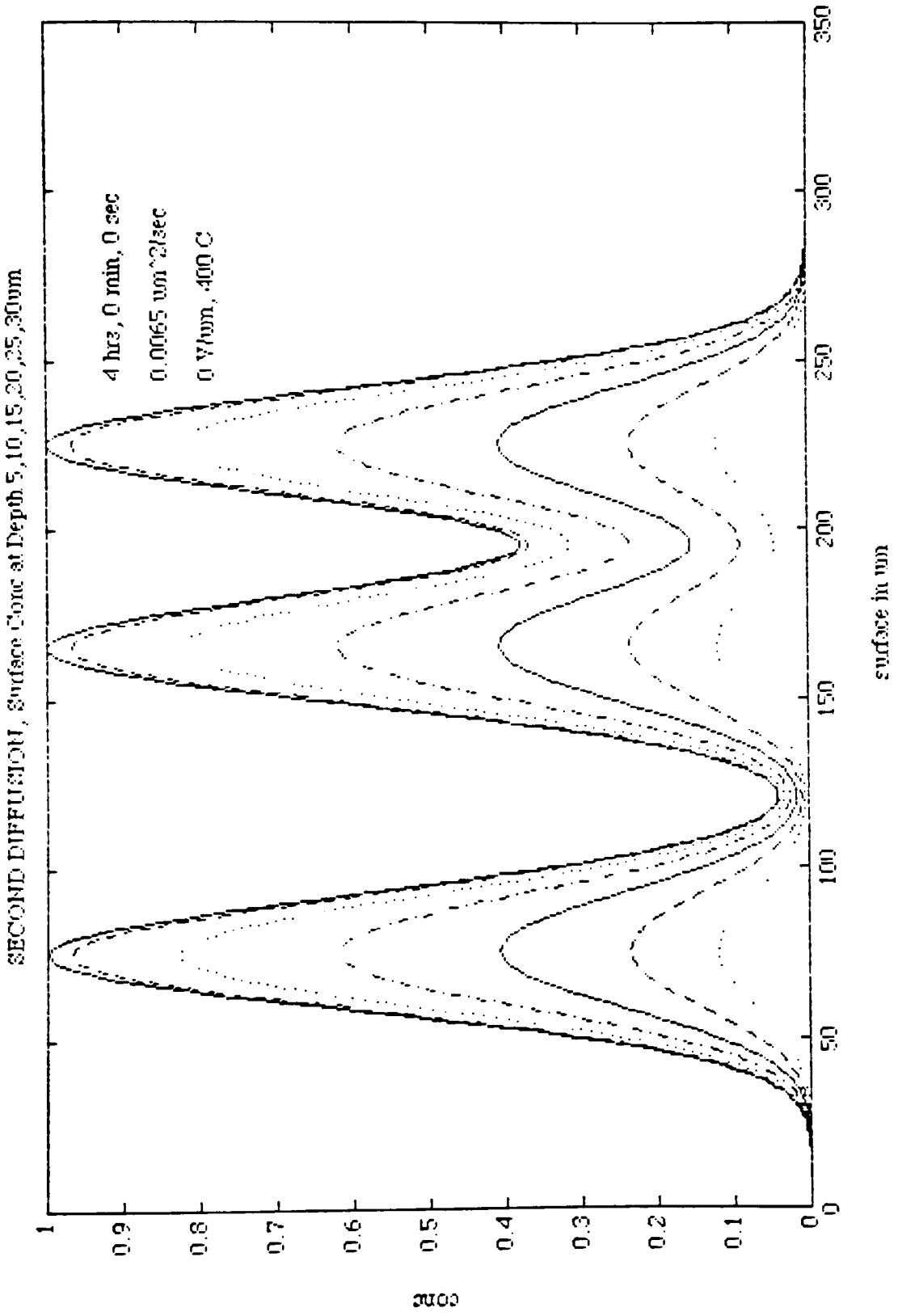

Appendix E11

Appendix E12

Appendix E13

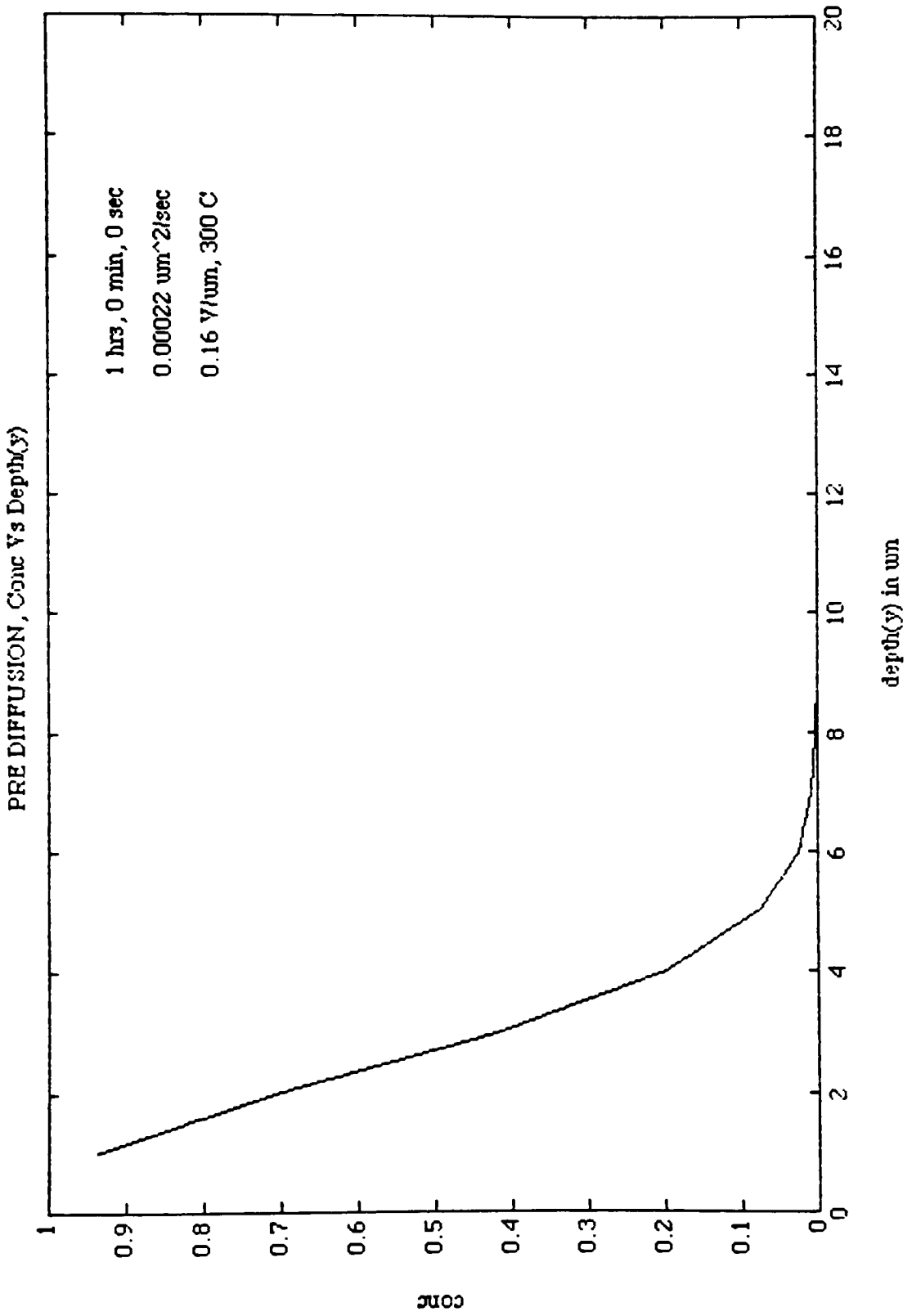

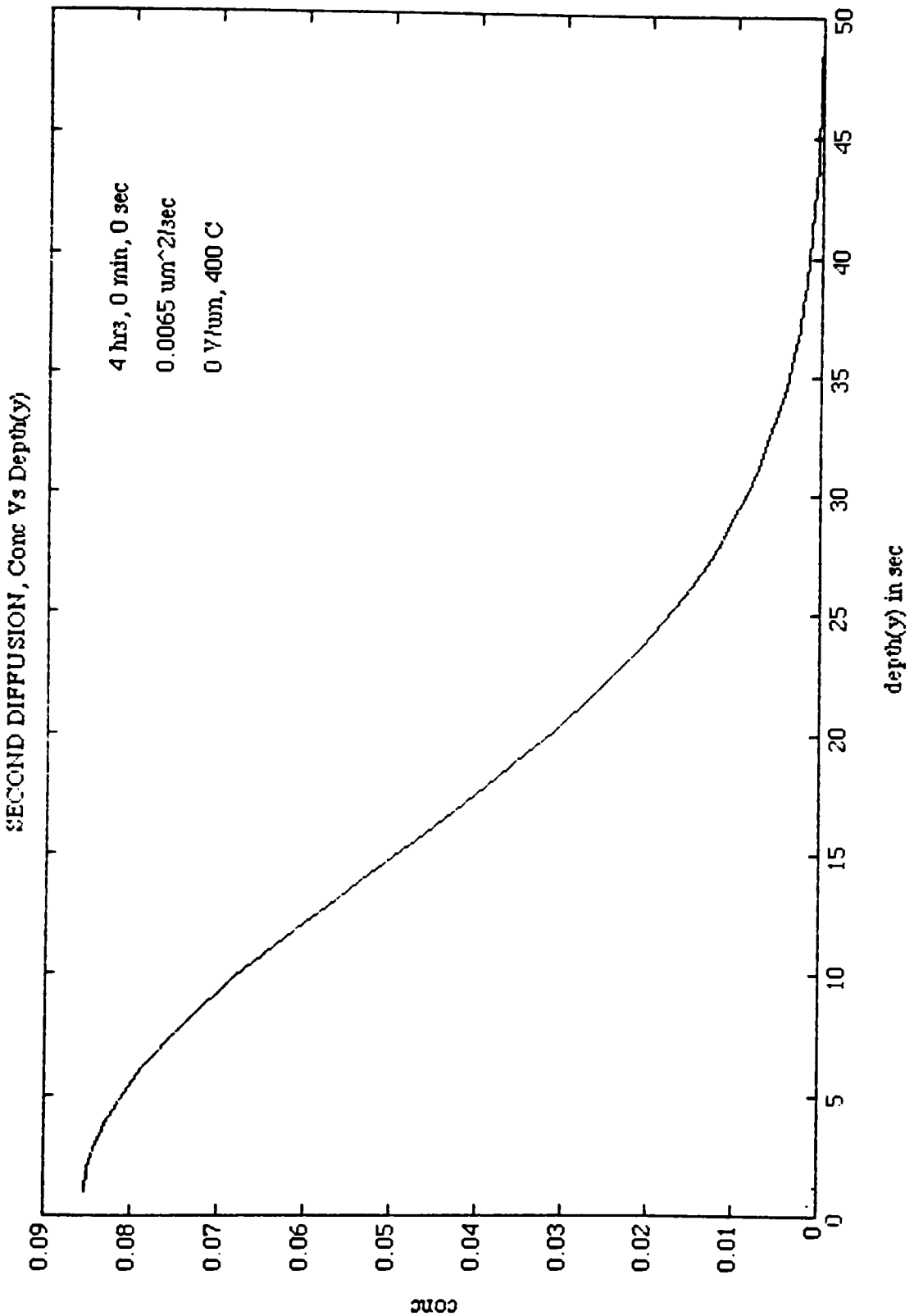
SECOND DIFFUSION, Conc Vs Depth(y)
4 hrs, 0 min, 0 sec
0.0065 um^2/sec
0 V/um, 400 C
conc
depth(y) in sec
0.09
0.08
0.07
0.06
0.05
0.04
0.03
0.02
0.01
0
0
5
10
15
20
25
30
35
40
45
50

Appendix F1

```
C
C  PROGRAM DESCRIPTION:
C
C    THIS PROGRAM IS INTENDED TO ALLOW THE USER TO CALCULATE DIFFUSIVITIES
C  FROM SUPREM CALCULATED DOPANT PROFILES
C-----------------------------------------------------------------------
C
      INTEGER ESC,RTN,CHOICE,ERROR
      REAL N,XINC,COUNT
      REAL INT(200),DEPTH(200),CONC(200)
C
C
C
      DIMENSION DCDX(200),D(200)
C
C
      WRITE(6,1012)
 1012 FORMAT(' ENTER THE DIFFUSION TIME IN SECONDS')
      READ(5,*) T
C
      OPEN(UNIT=10, FILE='MATANO', STATUS='OLD')
      OPEN(UNIT=9,  FILE='OUTPUT', STATUS='NEW')
      OPEN(UNIT=8,  FILE='PLOT1', STATUS='NEW')
      OPEN(UNIT=11, FILE='PLOT2', STATUS='NEW')
C
      READ(10,*)
      READ(10,*)
      READ(10,*)
C
      DO 1014 N2 = 1, 200
                READ(10,*, END = 1014)DEPTH(N2),CONC(N2)
* 5              FORMAT(5X,F6.1,4X,E14.7)
                COUNT = COUNT + 1
1014  CONTINUE
C
      N = COUNT
C
C
C     CALCULATE dC/dX
C     since the increment in SUPREM III is not CONSTANT this must be
C     changed to read the actual increments, xincleft and xincright
      DO 1040 I=2,N-1,1
c       depth has to be in cm.
        DCDX(I)=(CONC(I-1)-CONC(I+1))/((DEPTH(I+1)-DEPTH(I-1))*0.0001)
 1040 CONTINUE
C
C     CALCULATE THE INTEGRAL
C     again the increment may be changing
C
      DO 1060 J=2,(N-1),1
         DO 1050 I=N,J,-1
            INT(J)=INT(J)+CONC(I)*DEPTH(I)*0.0001
 1050    CONTINUE
 1060 CONTINUE
C
C     CALCULATE AND OUTPUT D
C
      DO 1070 I=2,N-1,1
         D(I)=INT(I)/(2.0*T*DCDX(I))
C        CONC IS IN LOG




*          CONC(I) = LOG(CONC(I))
*          D(I) = LOG(D(I))
          WRITE(9,1065) DEPTH(I),D(I),CONC(I)
 1065     FORMAT(' DEPTH = ',E12.4,' DIFFUSIVITIY = ',E12.4,
     +' CONCENTRATION = ',E12.4)
          WRITE(8,*) DEPTH(I),CONC(I)
          WRITE(11,*) DEPTH(I),D(I)
 1070 CONTINUE
C
```

Appendix F2

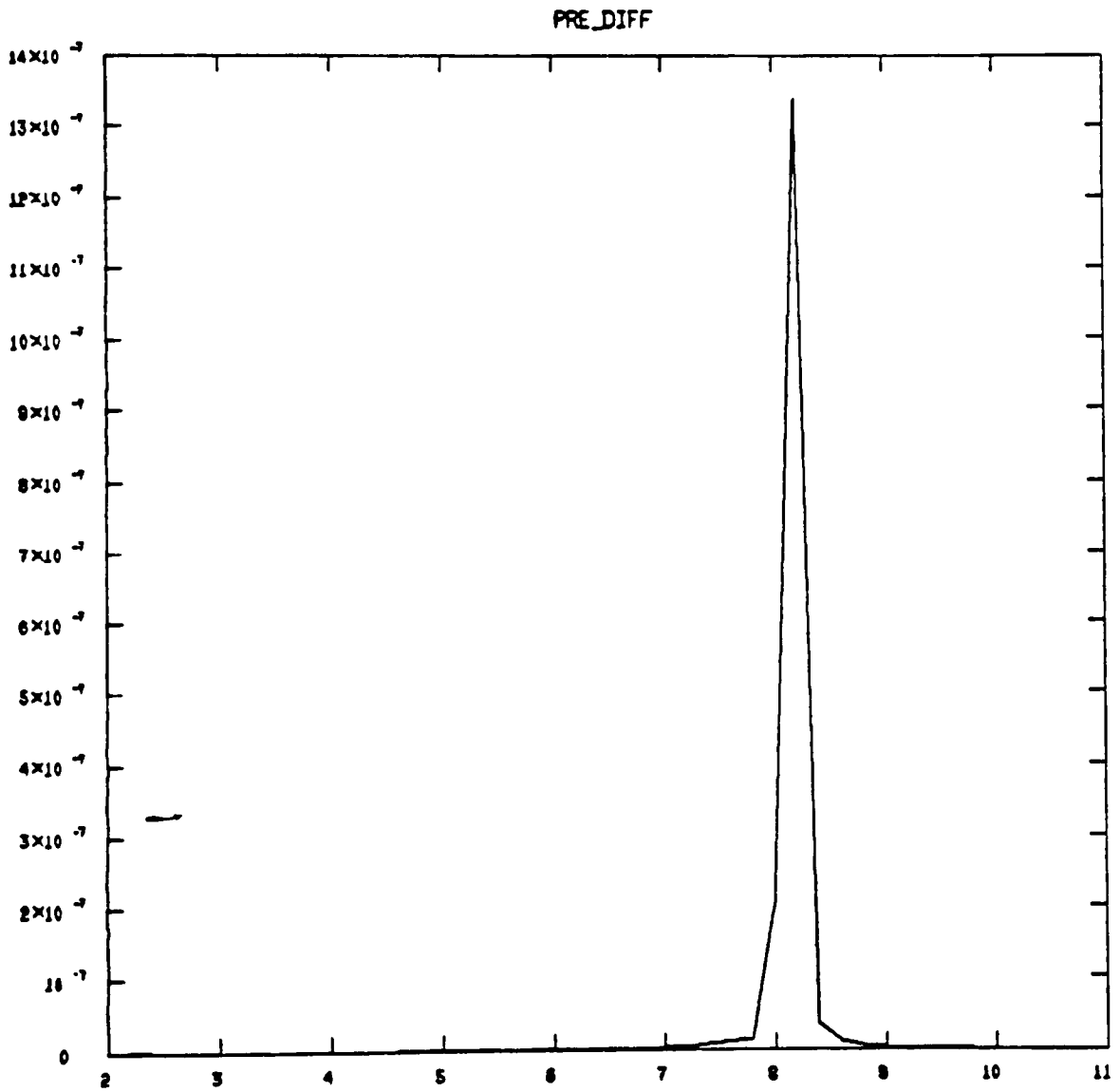
PRE_DIFF
14×10 -7
13×10 -7
12×10 -7
11×10 -7
10×10 -7
9×10 -7
8×10 -7
7×10 -7
6×10 -7
5×10 -7
4×10 -7
3×10 -7
2×10 -7
1×10 -7
0
2
3
4
5
6
7
8
9
10
11

Appendix F3

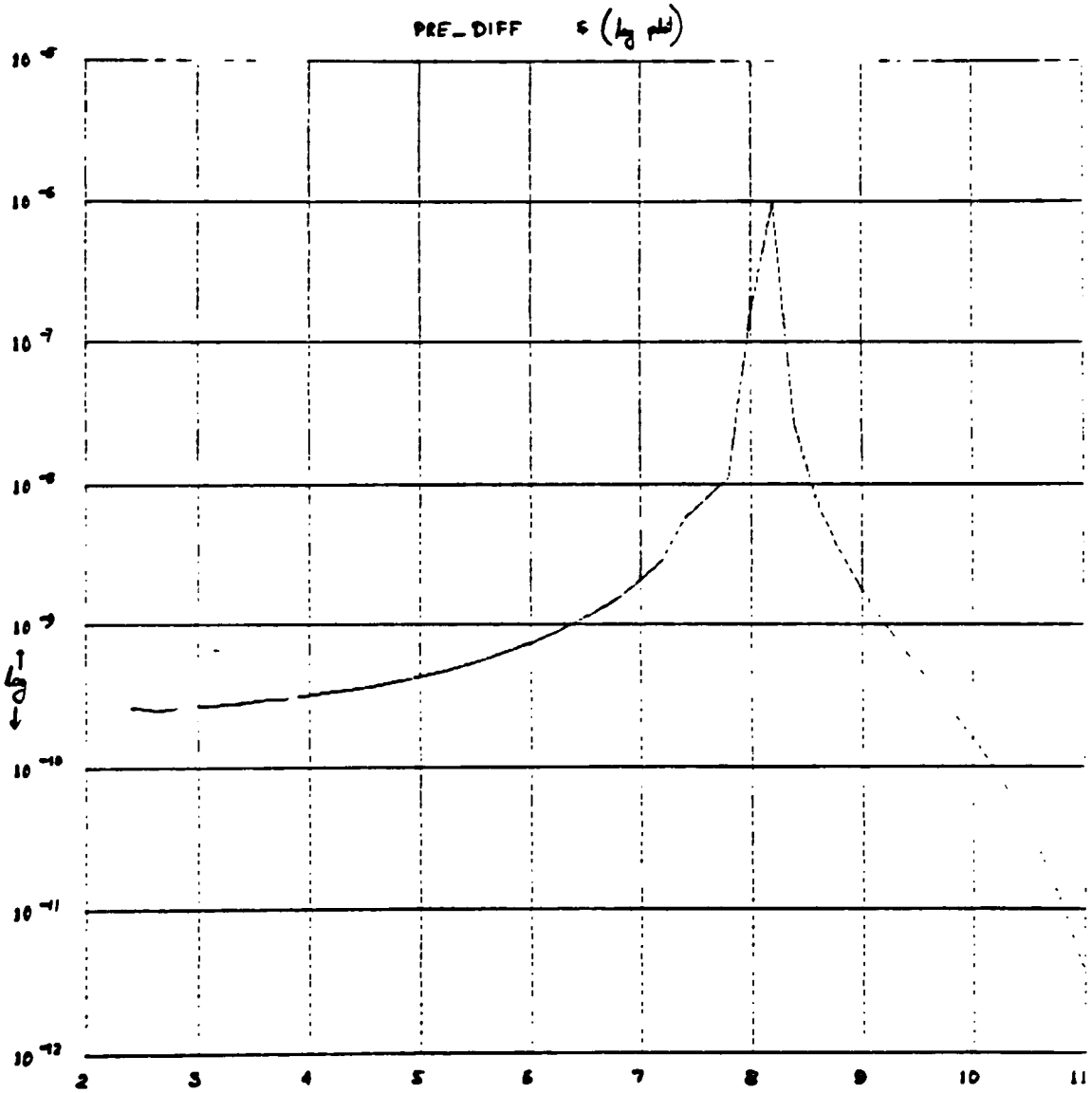

Appendix F4

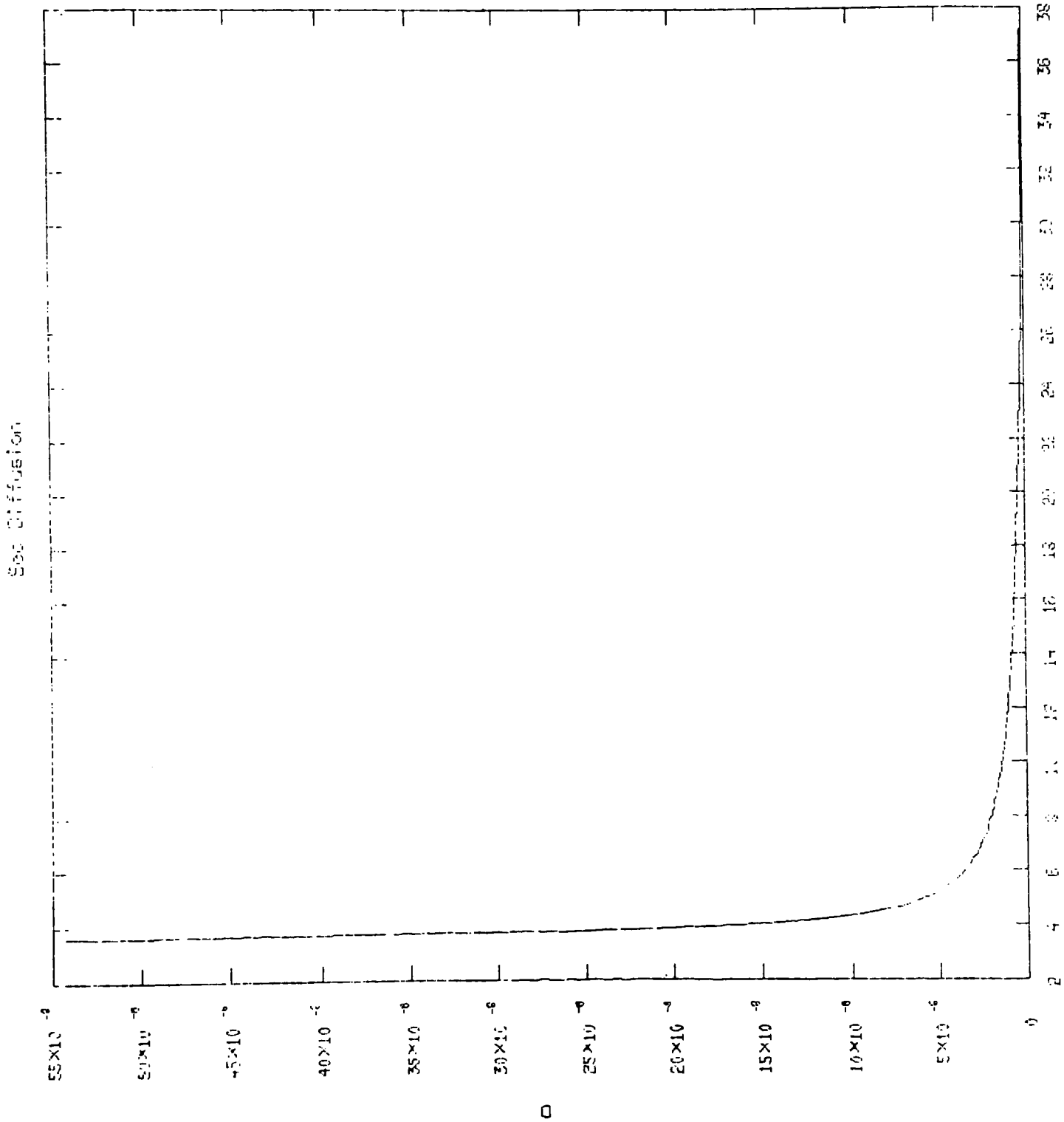
Sb2 Diffusion
D
55×10 -8
50×10 -8
45×10 -8
40×10 -8
35×10 -8
30×10 -8
25×10 -8
20×10 -8
15×10 -8
10×10 -8
5×10 -8
0
2
4
6
8
10
12
14
16
18
20
22
24
26
28
30
32
34
36
38

Appendix F5

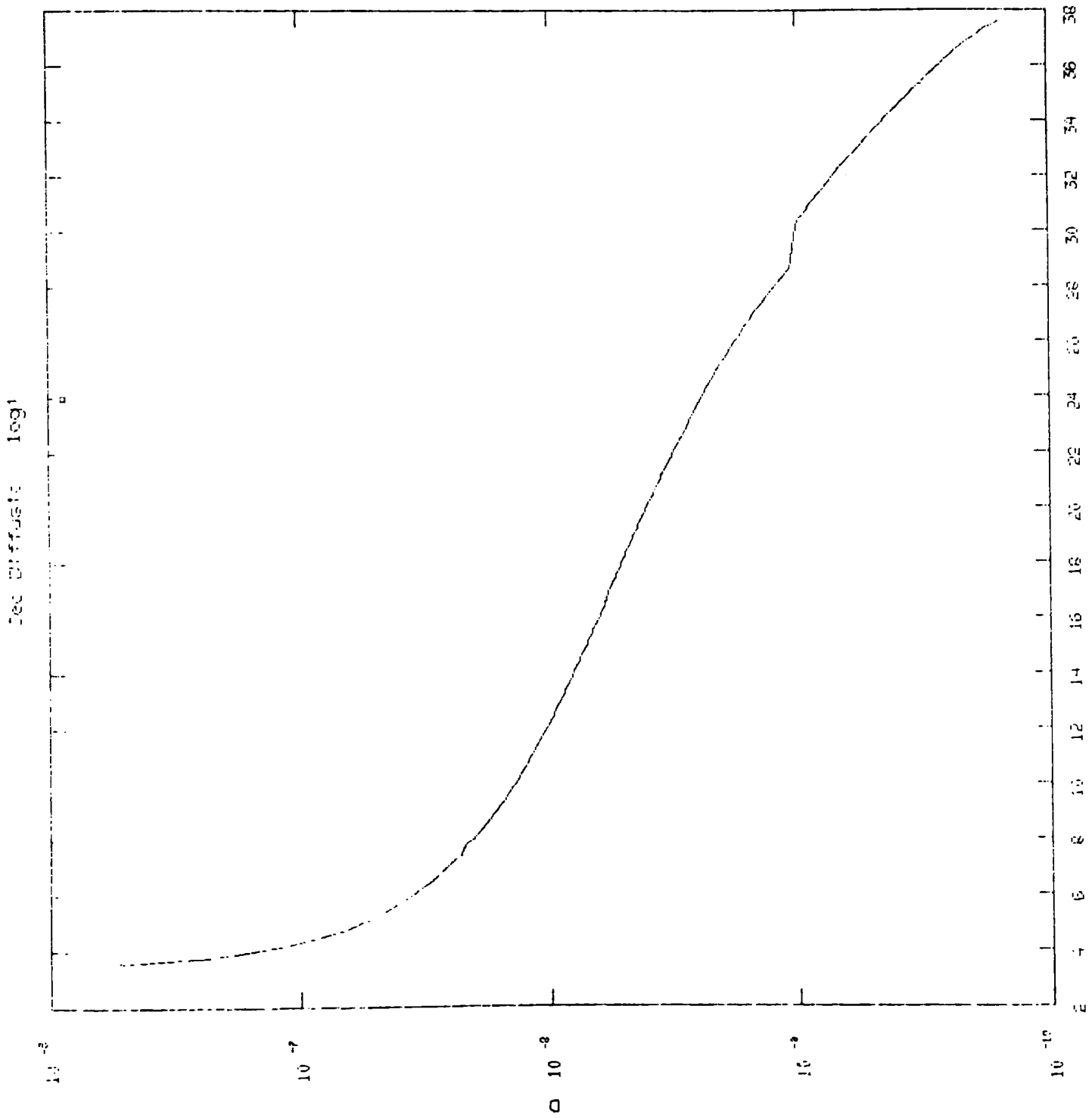

Appendix F6